

**Mass spectrometric analysis, *in situ*  
imaging and preparative tools for the study  
of marine secondary metabolites:  
Chemo-ecological and natural products research on  
the muricid *Dicathais orbita***

A thesis submitted in fulfilment of the  
requirement for the award of the degree

DOCTOR OF PHILOSOPHY

From

FLINDERS UNIVERSITY  
School of Biological Sciences

By

**DAVID ANDRE RUDD, B. Tech. Hons.**

2016

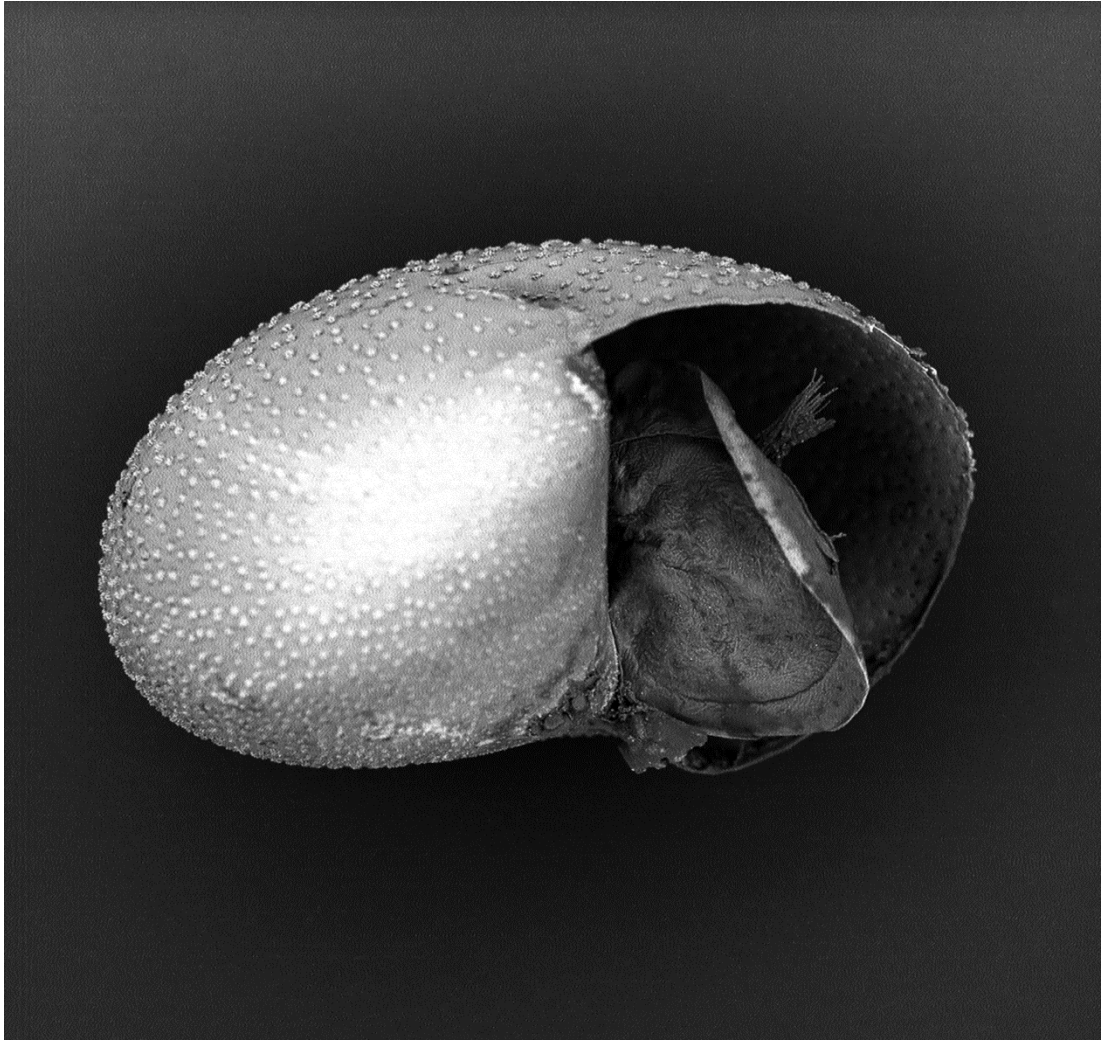


## Table of Contents:

Acknowledgements	ix
Abstract	x
<b>1 Chapter One.....</b>	<b>1</b>
<b>1.1 General introduction .....</b>	<b>1</b>
<b>1.2 Molluscan secondary metabolites – chemical diversity and its relation to natural product discovery .....</b>	<b>4</b>
1.2.1 Mollusc natural product potential.....	5
1.2.2 Biomedical translation of mollusc secondary metabolites .....	6
<b>1.3 Chemical ecology / ecological function of secondary metabolites .....</b>	<b>12</b>
1.3.1 Chemical Defence .....	12
1.3.2 Mate attraction, reproduction and larval survival .....	13
1.3.3 Predation - Hunting innovations of the Neogastropoda .....	14
1.3.4 Molecules of keystone significance .....	26
<b>1.4 Biodistribution and Biosynthetic origin.....</b>	<b>30</b>
1.4.1 Traditional approaches .....	31
<b>1.5 Mass spectrometry imaging as a tool for natural product research and chemical ecology .....</b>	<b>33</b>
1.5.1 LDI-MSI methods .....	38
<b>1.6 Muricidae molluscs as models for MNP research .....</b>	<b>44</b>
1.6.1 Historical resource as a dye.....	45
1.6.2 The Muricidae hypobranchial chromogenic secondary metabolites ...	45
1.6.3 Anatomy of muricid biosynthetic organs .....	48
1.6.4 Muricid intracapsular chemistry.....	49
1.6.5 Biomedical potential of Muricidae molluscs.....	50
1.6.6 Extract preparation for nutraceutical application .....	62
1.6.7 <i>Dicathais orbita</i> as a model muricid species.....	62
<b>1.7 Thesis aims and objectives .....</b>	<b>64</b>
1.7.1 Thesis structure.....	65
1.7.2 Chapter objectives .....	68
<b>2 Chapter Two – Mass spectrometry imaging on porous silicon: investigating the distribution of bioactives in marine mollusc tissues .....</b>	<b>71</b>
<b>2.1 Abstract .....</b>	<b>71</b>
<b>2.2 Introduction.....</b>	<b>72</b>
<b>2.3 Experimental Section.....</b>	<b>75</b>

2.3.1	Materials .....	75
2.3.2	pSi fabrication .....	75
2.3.3	Oxidation and functionalization .....	76
2.3.4	<i>D. orbita</i> collection and dissection.....	76
2.3.5	Tissue preparation .....	76
2.3.6	DIOS-MSI analysis .....	77
2.3.7	Mass spectrometer parameters .....	78
<b>2.4</b>	<b>Results .....</b>	<b>78</b>
2.4.1	SALDI-MSI contact printing.....	78
2.4.2	<i>D. orbita</i> hypobranchial tissue .....	81
2.4.3	DIOS-MSI detection of brominated secondary metabolites .....	82
2.4.4	NALDI-MSI detection of brominated secondary metabolites .....	89
2.4.5	SALDI-MSI for biodistributional studies.....	91
<b>2.5</b>	<b>Conclusion .....</b>	<b>97</b>
<b>2.6</b>	<b>Acknowledgements .....</b>	<b>97</b>
<b>3</b>	<b>Chapter Three - Solvent Separating Secondary Metabolites Directly from Biosynthetic Tissue for Surface-Assisted Laser Desorption Ionisation Mass Spectrometry.....</b>	<b>98</b>
<b>3.1</b>	<b>Abstract .....</b>	<b>98</b>
<b>3.2</b>	<b>Introduction.....</b>	<b>99</b>
<b>3.3</b>	<b>Experimental.....</b>	<b>108</b>
3.3.1	Tissue preparation for extraction and solvent separation on MSI substrates .....	108
3.3.2	Extraction of secondary metabolites for LC-MS .....	109
3.3.3	NALDI and DIOS surface fabrication, oxidation and functionalization 111	
3.3.4	Tissue sectioning, deposition and solvent separation on NALDI and DIOS surfaces.....	112
3.3.5	NALDI and DIOS-MS acquisition.....	112
3.3.6	Mass spectrometry imaging.....	113
3.3.7	Statistical analyses.....	114
<b>3.4</b>	<b>Results and discussion .....</b>	<b>114</b>
3.4.1	Hydrophilic compounds .....	121
3.4.2	Ethanol solvent separation.....	122
3.4.3	CHCl <sub>3</sub> solvent separation.....	124
3.4.4	Lipophilic separation using <i>n</i> -hexane.....	125
3.4.5	Quantification of secondary metabolites using SALDI-MS .....	128

3.5	Conclusions.....	131
3.6	Acknowledgments .....	131
4	<b>Chapter Four - Mass spectrometry imaging reveals new biological roles for choline esters and Tyrian purple precursors in muricid molluscs .....</b>	<b>132</b>
4.1	Abstract .....	132
4.2	Introduction.....	133
4.3	Experimental methods.....	137
4.3.1	Collection and maintenance of whelk breeding population .....	137
4.3.2	Tissue preparation for mass spectrometry imaging (MSI).....	138
4.3.3	MSI pSi substrate fabrication, oxidation and functionalisation .....	138
4.3.4	Tissue sectioning and imprinting for DIOS-MS .....	139
4.3.5	DIOS-MS and MSI.....	140
4.3.6	Extraction and elucidation of brominated indoles.....	142
4.3.7	Extraction and elucidation of murexine structure .....	143
4.3.8	Bioassay of murexine in hatching stage <i>D. orbita</i> larvae.....	144
4.4	<b>Results and discussion .....</b>	<b>145</b>
4.4.1	Detection and identification of secondary metabolite patterns on functionalised pSi.....	145
4.4.2	Biodistribution of secondary metabolites across the reproductive cycle	152
4.4.3	Maternal provisioning and chemical changes during encapsulated larval development .....	155
4.4.4	Biological role for murexine .....	157
4.5	<b>Conclusion .....</b>	<b>159</b>
4.6	<b>Acknowledgements .....</b>	<b>159</b>
5	<b>Chapter Five - Supercritical CO<sub>2</sub> extraction of bioactive Tyrian purple precursors from the hypobranchial gland of a marine gastropod.....</b>	<b>161</b>
5.1	Abstract .....	161
5.2	Introduction.....	162
5.3	Methods .....	168
5.3.1	Raw materials and sample preparation.....	168
5.3.2	Liquid solvent extraction.....	169
5.3.3	Supercritical CO <sub>2</sub> extraction.....	169
5.3.4	Brominated indole analysis by liquid chromatography–mass spectrometry .....	170
5.3.5	Choline ester analyses by thin layer chromatography.....	171
5.4	<b>Results and discussion .....</b>	<b>171</b>
5.4.1	SFE extraction yield .....	171

5.4.2	Extraction composition.....	174
<b>5.5</b>	<b>Conclusion .....</b>	<b>181</b>
<b>5.6</b>	<b>Acknowledgements .....</b>	<b>181</b>
<b>6</b>	<b>Chapter Six – General Discussion.....</b>	<b>182</b>
<b>6.1</b>	<b>Secondary metabolites <i>in situ</i> .....</b>	<b>182</b>
<b>6.2</b>	<b>Tools for biorational drug discovery.....</b>	<b>183</b>
6.2.1	DIOS-MSI as a top-down approach to biodiscovery .....	184
<b>6.3</b>	<b>The ecological significance of choline esters in muricid reproduction and egg capsule development .....</b>	<b>185</b>
<b>6.4</b>	<b>Analysing the ecological significance of the brominated indoles.....</b>	<b>187</b>
<b>6.5</b>	<b>The biomedical potential of the brominated indoles .....</b>	<b>191</b>
<b>6.6</b>	<b>Conclusion .....</b>	<b>193</b>
<b>7</b>	<b>Appendix I.....</b>	<b>194</b>
<b>7.1</b>	<b>Computational binding model of murexine to the ligand-binding domain of acetylcholine-binding protein (AChBP): A model for the nicotinic acetylcholine receptor (nAChR).....</b>	<b>194</b>
7.1.1	<i>In silico</i> docking methods of murexine in AChBP.....	194
7.1.2	<i>In silico</i> results of flexible murexine docking .....	195
<b>8</b>	<b>Appendix II .....</b>	<b>202</b>
<b>8.1</b>	<b>Supplementary results for Chapter 4 .....</b>	<b>202</b>
8.1.1	Detection of brominated indoles .....	202
8.1.2	Detection and structural elucidation of murexine .....	208
<b>9</b>	<b>Appendix III.....</b>	<b>212</b>
<b>9.1</b>	<b>Introduction.....</b>	<b>212</b>
<b>9.2</b>	<b>Methods .....</b>	<b>216</b>
9.2.1	Materials .....	216
9.2.2	<i>In vivo</i> murine model.....	216
9.2.3	AARGC evaluation .....	218
9.2.4	Surface fabrication of pSi.....	219
9.2.5	Tissue preparation and DIOS-MSI.....	219
9.2.6	DIOS-MSI analysis .....	220
9.2.7	Statistical analysis .....	221
<b>9.3</b>	<b>Results .....</b>	<b>222</b>
9.3.1	Brominated metabolite discovery in tissue sections.....	222
9.3.2	DIOS-MSI effectively defines tissue distribution .....	228
9.3.3	Pro-apoptotic effect of 6-bromoisatin .....	230
<b>9.4</b>	<b>Discussion .....</b>	<b>233</b>

<b>10</b>	<b>REFERENCES .....</b>	<b>234</b>
-----------	-------------------------	------------

## Thesis Declaration

I certify that this thesis does not incorporate, without acknowledgement, any material previously submitted for a degree or diploma in any university; and that to the best of my knowledge it does not contain any material previously published or written by another person except where due reference is made in the text.

.....

David Andre Rudd

.....

Date

## Acknowledgements

Firstly I would like to thank my supervisor Associate Professor Kirsten Benkendorff. You have given me the freedom to explore, provided constant support and helped me craft my writing skills over the length of my candidature. It never ceases to amaze me how your assistance and rapid feedback is just what I required when I had mentally stalled. *D. orbita* has always proved such an intriguing species to work with, including its complex and unstable chemistry.

I would also like to thank Dr. James Harris and Associate Professor Cathy Abbott, for providing local support and being a soundboard for ideas and methods. It has been great working in your labs and drawing on your extensive scientific knowledge. Members of both labs, including Lisa Pogson, James Forwood, Babak Esmaeelian and Hanna Krysinska are great company for inspiration. Also, more broadly, members of the School of Biological Sciences have provided genuine support and friendship. A thankyou goes to the Mollusc lab, Marine labs, Landscape Genomics lab, Plant labs, Technical Teaching Group and other lecturers / demonstrators. Special gratitude is extended to Associate Professor Martin Johnston for NMR assistance and Dr. Daniel Jardine and Jason Young from the analytical chemistry facility, who allowed me free reign on the MALDI-TOF.

I am also indebted to Professor Nicolas Voelcker, Dr. Maurizio Ronci and Taryn Guinan from the University of South Australia for initially teaching me about mass spectrometry imaging on nanostructured surfaces and for an invaluable collaboration. Your work has been essential in the success of my project. It has been the perfect combination of analytical chemistry, chemical ecology and biology that has given real insights into the functional ecology of *D. orbita* secondary metabolites.

Finally, I would like to thank Kiel Hummel, my family and friends, who provided unblinding support.

## Abstract

Species in the marine environment interact and thrive based on a language of chemical cues composed of secondary metabolites. Involved at the most basic level of organism to organism interaction, secondary metabolites affect a species ability to feed, fight, thrive and reproduce. Through these mechanisms, highly successful secondary metabolites termed ‘molecules of keystone significance,’ can drive resource allocation and shape ecosystem structures and diversity. Beyond an ecological value, some secondary metabolites have been developed into successful biomedical resources, and the marine environment can be considered a relatively untapped resource. Whether for ecological function or biomedical evaluation, secondary metabolites from the marine environment are poorly understood. Few studies have effectively defined function, in part due to the hurdles in method execution associated with demonstrating *in situ* synthesis, storage and deployment; key pieces of evidence in describing ecological relevance. Recently, analytical tools including mass spectrometry imaging have emerged to enable the spatial detection of chemical entities in biological tissues. Sophisticated approaches, including nanostructured surface-assisted laser desorption/ ionisation mass spectrometry imaging, have enabled the mapping of low molecular weight metabolites directly from tissue or tissue imprints, which is ideal for the analysis of secondary metabolites.

Muricidae molluscs, famed for the production of the historically significant dye Tyrian purple, provide a well characterised model system for application of novel analytical and preparative tools to study secondary metabolite distribution. One Australian species in particular, *Dicathais orbita*, is an extensively studied model organism for muricid chemistry and ecology. *D. orbita* produce two classes of secondary metabolites that originate in the hypobranchial gland, brominated indoles,

which are currently being investigated as chemo-preventative compounds and choline esters, known to be natural muscle relaxants.

To investigate the biodistribution and ecological role of brominated indoles and choline esters in *D. orbita*, novel methods for mass spectrometry imaging were developed. In Chapter 2, a method for tissue imprinting for absorption of small molecular weight compounds onto functionalised porous silicon (pSi) chips was developed, then laser desorption/ionisation on pSi (DIOS) and nanostructure-assisted laser desorption ionisation (NALDI) mass spectrometry imaging were employed to spatially map brominated indoles and choline esters *in situ* within the hypobranchial gland. These methods were successful in detecting a range of secondary metabolites (molecular weights from 72 to 825 Da), across a broad range of polarities (from Log P -3.37 – 4.47) in *D. orbita*. In Chapter 3 this approach was further optimised using “on surface” solvent separation directly from mollusc tissue onto nanostructured surfaces, as a mechanism for simplifying the interpretation, annotation and quantification of MS data acquired from the complex mixtures of secondary metabolites found in natural tissue samples. Water, ethanol, chloroform and hexane selectively extracted compounds of different polarity and key metabolites of interest could be quantified by comparison to standard curves on the nanostructured surfaces.

In Chapter 4, DIOS-MSI was applied to investigate the chemical ecology of *D. orbita* over the reproductive cycle. This confirmed the presence of tranquilising choline esters in the egg capsule gland of an adult female during the egg laying phase, and tracked maternally derived choline esters and brominated indole precursors into the fluid content of egg capsules. The chemical constituents of capsules encasing early stage embryos included hydrophilic tyrindoxyl sulfate and tranquilising murexine, whilst analysis of mature capsules accommodating hatching stage veligers detected hydrophobic Tyrian purple, 6,6'-dibromoindigo and 6,6'-dibromoindirubin. Changes

in the secondary metabolite profile detected using DIOS-MSI demonstrates a slow process of chemical ripening. A change in the distribution and abundance of choline ester murexine suggests an important role in egg laying and larval development. The effect of murexine on larvae was further investigated by developing a larval mobility bioassay. The choline ester murexine was found to temporarily relax veliger larvae, with full recovery after 60mins exposure. These findings, coupled with the MS data showing the loss of polar compounds from the egg capsules over time, indicate that the secondary metabolite murexine relaxes the vulnerable early stage larvae to achieve developmental maturity inside the capsule environment, potentially influencing survival.

Chapter 5 contributes to the potential development of the brominated indoles from *D. orbita* as medicinal products. A novel method for preparative extraction was designed and employed to selectively capture the bioactive fraction from *D. orbita* tissue without the need to use toxic chlorinated solvents. Supercritical CO<sub>2</sub> extraction was successful in separating the bioactive brominated indoles from the polar non-active precursor and potentially toxic choline esters. Changes in the partial pressure enabled selective concentration of the anti-cancer agent 6-bromoisatin, with high yields that were comparable to solvent extraction. This provides a safe and effective extraction method for future *in vivo* bioactive testing of brominated indoles as chemopreventative compounds and for nutraceutical development. Future preclinical studies will analyse the *in vivo* gastrointestinal absorption and metabolism of these brominated indoles employing the novel mass spectrometry imaging methods developed in this study.

The inescapable presence of secondary metabolites in the marine biome is a testament to their value in shaping ecosystems and driving diversity. They are both an ecological resource and a natural product resource, providing humans with chemical

structures of medicinal interest. Tools such as mass spectrometry imaging and supercritical fluid extraction that can aid in these dual pursuits will be of broad value to future marine natural products research.

# 1 Chapter One

## 1.1 General introduction

The marine habitat harbours impressive biological diversity; estimates include approximately ~226,000 described eukaryotic species, 72,000 collected species yet to be described and up to 741,000 yet to be sampled (Appeltans et al., 2012). The phylum Mollusca contributes over one fifth of known marine species diversity, currently estimated at 51,689 described species and up to 164,107 total species (Appeltans et al., 2012). Mollusca can be found thriving in a large range of habitats from alpine regions to deep sea benthic areas, including environmentally extreme locations such as hydrothermal vents. The phylum is not only species rich; Mollusca are also morphologically diverse and exhibit a range of lifestyles including predatory, herbivorous, scavenging, detritivorous, corallivorous, filter-feeding, symbiotic photo- and chemo-autotrophic lifestyles (Benkendorff, 2014, Modica and Holford, 2010). Consequently, studies on molluscs have shown them to be a rich source of biologically active secondary metabolites. *Aplysia dactylomela* alone has yielded 58 isolated compounds alone (Benkendorff, 2010), mostly originating from the diet (Pereira et al., 2016), and members of the *Conus* genus produce an entire repertoire of thousands of structurally varied conotoxins (Hu et al., 2011). Yet surprisingly, secondary metabolites have only been investigated from a small fraction (0.53%) of all named molluscan species, with a bias towards the reduced or non-shelled Heterobranchia (Benkendorff, 2010, Benkendorff, 2014).

Secondary metabolites have been simply defined as organic compounds not directly involved in primary metabolism (Hay and Fenical, 1996), but they play an important role in many species interactions. Secondary metabolites have been detected during a number of mollusc species interactions for predation (Olivera et al., 1990,

Modica and Holford, 2010), released by prey to prevent predation (Kelley et al., 2003, Andersen et al., 2006), expressed during mate selection (Cummins et al., 2005), and can act as a form of communication (Cimino et al., 1991), enhance reproductive success (Zatylny et al., 2002), and reduce fouling in adults (Okino et al., 1996) and offspring (Lim et al., 2007, Paul et al., 2011). Producing secondary metabolites can be metabolically expensive (Rogers et al., 2002, Ivanisevic et al., 2011) and often results in structurally complex compounds. Some molluscs reduce this metabolic cost, albeit incurring other metabolic costs, by obtaining secondary metabolites through the diet and sequestering them within relevant tissues, an activity that requires selective foraging (Pereira et al., 2016, Rogers et al., 2002). The energy and effort in producing or concentrating secondary metabolites has led to the prevailing assumption that they enhance the fitness of the producer (Hay and Fenical, 1996, Williams et al., 1989, Paul et al., 2007). Therefore, secondary metabolites act at the interface between genes and the environment, either directly or indirectly, having formed under intense selective pressures to be potent modulators of basic cellular functions (Williams et al., 1989). Secondary metabolites allow a species to thrive within a particular niche.

The study of structural novelty and function in marine secondary metabolites has been largely based around two fields of research, chemical ecology and marine natural product (NP) research. Chemical ecology seeks to understand the underlying chemical mechanism for ecological interactions (Hay, 1996). This has traditionally focused on species-species interactions, but more recently has been broadened to include the community structure effects of advantageous secondary metabolites (Hay, 2009, Benkendorff, 2014, Derby and Zimmer, 2014). There is also an emerging field of research aimed at translating the mechanisms by which potent secondary metabolites, termed 'keystone molecules', have strong impacts on species interactions at multiple trophic levels. For example, tetrodotoxin occurs within a range of species as an anti-

predation mechanism (Derby and Zimmer, 2014). NP research is a multidisciplinary field, identifying bioactive secondary metabolites with potential to become useful products. Generally NP screening approaches prioritize commercially relevant compounds with biological activity for human benefit (Capon, 2010), either through their development as pharmaceuticals, other medicinal products, agricultural chemicals or as biotechnological tools (Gerwick and Moore, 2012, Benkendorff, 2009, Llewellyn and Burnell, 2000).

By no means are the two approaches to the study of secondary metabolites mutually exclusive; chemical ecology and NP research involves shared methods for understanding how and where metabolites are synthesized, under what conditions and by which taxa. In many cases research into the ecological role and biomedical applications of NPs originate from the same laboratories (Capon, 2010). The initial focus for both fields requires knowledge of the active compound, which is usually found by isolation, either by chemical chromatography or biologically guided fractionation, structural elucidation and bioactivity testing *in vitro* or *in vivo* (Avila, 2006). Both fields of study also have much to gain from the other, for example, ecologically guided natural product discovery may save considerable research effort through de-replication and promote targeted discovery to species likely to harbour novel bioactive compounds (Leal et al., 2012), e.g., sessile chemically defended species, species in extreme environments, and phylogenetic lineages of chemically rich species (Benkendorff, 2010, Benkendorff, 2014).

NP research has, to some degree, enabled an economic value to be attributed to biodiversity (Okino et al., 1996). Many of the tools funded and refined from NP structural elucidation, purification or bioassay-guided fractionation have also advanced the field of chemical ecology. Methods that isolate, activity test and elucidate specific compounds involved in species interactions can both shed light on the function

of the metabolites to the producing organisms and further the development of bioactive compounds (Molinski, 2010).

Highlighted within this thesis introduction is some of the current research into the origin and proposed functional nature of the better characterised marine mollusc secondary metabolites and explore current and emerging methodologies used to assign those functions. Muricidae, and molluscs more generally, have been investigated for the biomedical potential of their secondary metabolites and are well represented in the marine natural product drug discovery pipeline. The biomedical potential and value of muricid metabolites will be examined and the relative overlap between the dual fields of chemical ecology and marine natural product discovery will be discussed.

## **1.2 Molluscan secondary metabolites – chemical diversity and its relation to natural product discovery**

Marine molluscs have been particularly interesting targets for the study of novel secondary metabolites, having attributes that necessitate potent chemical defence, communication, reproduction and specialised predation (Benkendorff, 2010, Benkendorff, 2014). Mollusc is derived from the Latin term “Mollis” meaning soft (Hickman et al., 2008). Despite the secretion of a hard shell in many lineages, molluscs are essentially soft bodied organisms, which are vulnerable to biotic and abiotic pressures by frequent or permanent exposure of the soft body to the external environment (Benkendorff, 2010). Many mollusc groups are found in shallow intertidal environments, where microbial density and diversity are high, and biofilm formation is rapid (Decho, 2000). Molluscs lack an acquired immunity; therefore, they have a well-developed innate immunity relying on the use of anti-microbial compounds as a part of their humoral immunity (Hooper et al., 2007, Dang et al., 2011)

As mentioned, molluscs are exceptionally diverse and produce a diversity of secondary metabolites, of which a small proportion has been examined (Benkendorff,

2014). Despite this, trends are appearing in the choice of species to study and the types of secondary metabolites being investigated (Leal et al., 2012, Benkendorff, 2014). A recent review of molluscan secondary metabolites showed that of the 277 molluscan species reported within natural product reviews, over 100 were in the Nudibranchia (Benkendorff, 2014). Many of these structures may be from dietary sequestration after selective foraging on algae (Kamiya et al., 2006), so a large diversity of secondary metabolites in the group is unsurprising. The bioactivity of the compounds from the Nudibranchia included cytotoxic/anticancer, antimicrobial, antifouling, neurotoxic, ichthyotoxic properties and alarm pheromones. Other prominent taxa were the Caenogastropoda, Pulmonata, Sacoglossa, Anaspidea, Cephalospidea and the Class Bivalvia (Benkendorff, 2014). Within the trends seen for the study of molluscan secondary metabolites, ecological trends that could be useful for targeting future studies on species likely to have potent secondary metabolites can start to be considered.

### **1.2.1 Mollusc natural product potential**

Molluscs possess many of the ancestral forms of biochemical pathways and cell signalling systems seen in vertebrates, despite their lack of an acquired immune system. *Aplysia californica*, for example, has been an exemplary model species for the study of the vertebrate simple nervous system (Oliverio et al., 2009) expanding our knowledge of nerve impulses (Teichert et al., 2005), behaviour (Olivera, 2006), and neuromodulators (Oliverio and Modica, 2010). The crystal structure of the binding domain of the prototypical nicotinic acetylcholine receptor (nAChR) was obtained using a binding protein discovered in the mollusc *Lymnaea stagnalis* (Brejc et al., 2001), providing a tool for the study of muscular and neuronal receptors. Molluscs also have a simplified apoptotic signalling pathway that are comparative to vertebrates, sharing many of the same intrinsic, extrinsic, caspase dependent and independent

cascades leading to apoptosis (Anand et al., 2014). It stands to reason that secondary metabolites that specifically target these signalling pathways would evolve as these features are shared in molluscan predators, prey, fouling organisms, pathogens and parasites.

There is a renewed interest in searching NPs for drug development (Harvey et al., 2015). This interest has been partly based on the unmet expectation of combinatorial chemistry to meet the screening demands for disease targets. Sheer numbers in screening libraries may not be as useful; more targeted approaches are required. There are many advantages to natural products as potential therapeutic agents. As they have evolved by natural selection, they are generally already biologically active towards a biological target and are therefore more likely to be bioavailable. Species that produce bioactive secondary metabolites are likely to also possess a delivery system for the storage and deployment of those secondary metabolites to their intended destination. Particular secondary metabolites may also be substrates for more generalised cellular transporter systems, allowing compounds access to intracellular sites of action (Harvey et al., 2015).

### **1.2.2 Biomedical translation of mollusc secondary metabolites**

The discovery process of NP research includes the aim of finding compounds with biomedical potential. For molluscs, this has been a fruitful exercise considering only a small fraction (<1%) of species has been investigated and the majority of attention has been on one group - the shell-less or reduced-shell opisthobranchs (Benkendorff, 2010, Benkendorff, 2014). Limiting research to the soft bodied exposed groups is unjustified, as shelled species have successfully led to the development of therapeutic agents, e.g., zinconotide (Prialt®). Clinically approved marine natural products, including three from investigations of mollusc secondary metabolites, are summarised in Table 1.1. Molluscs also feature heavily in the marine pharmaceuticals clinical pipeline (Table

1.2), mainly from the contributions of the monomethyl auristatins derived from the dolstatins, initially discovered from investigations of the sea hare species *Dolabella auricularia* (Pettit, 1997). Since the discovery of the dolstatins, it has been established that cyanobacteria possess the biosynthetic capacity to produce dolastatin 10 and a range of structurally similar secondary metabolites (Luesch et al., 2001), a case of molluscs guiding the search for bioactive secondary metabolites.

**Table 1.1** Marine derived pharmaceuticals / ‘over the counter’ products currently or previously approved by the Food and Drug Administration (FDA) and the European Medicines Evaluation Agency (EMA). Compound Name: structure /derivative used in clinical trials.

Compound Name	Trademark	Company / Institution (country)	Therapeutic activity	Natural product	Source	Approval status 2014
Cytarabine	Cytosar-U®; Depocyt®	Bedford Laboratories® (USA)	Leukemia	Spongothymidine	Sponge <i>Cryptotethya crypta</i>	Approved
Vidarabine	Vira-A®	King Pharma (USA)	Anti-viral – Herpes simplex	Spongouridine	Sponge <i>Cryptotethya crypta</i>	US discontinued
Zinconotide	Prialt®	Jazz Pharmaceuticals®	Neuropathic pain	ω-Conotoxin	Marine snail <i>Conus magus</i>	Approved
Omega-3-acid ethyl esters	Lovaza®	GlaxoSmithKline (UK)	Hyper-triglyceridemia	Omega-3-fatty acids	Fish	Approved
Trabectedin (ET-743)	Yondelis®	PharmaMar (Spain)	Soft tissue and ovarian cancer	Ecteinascidin 743	Tunicate <i>Ecteinascidia turbinata</i>	EMA approved
Eribulin mesylate	Halaven®	Eisai (Japan)	Breast cancer	Halichondrin B	Sponge <i>Halichondria okadai</i>	EMA / FDA approved

**Table 1.1** *continued*

Compound Name	Trademark	Company / Institution (country)	Therapeutic activity	Natural product	Source	Approval status 2014
Brentuximab vedotin (SGN-35, ADC)	Adcentris®	Seattle Genetics (USA); Takeda GRDC (Japan)	Lymphoma and Hodgkin's disease	Monomethyl auristatin E (Dolastatin 10 derivative)	Sea hare <i>Dolabella auricularia</i>	EMA / FDA approved
Iota-carrageenan	Carragelose®	Marionmed (Austria); Boehringer Ingelheim (Germany)	Anti-viral nasal spray	Iota-carrageenan	Rhodophyceae algae	Over the counter
PCSO-524 (Eicosatetraenoic acid)	Lyprinol®	Pharmalink International	Anti-inflammatory / anti-arthritis	Non-polar lipid groups and Omega-3-fatty acids	Green-lipped mussels <i>Perna canaliculus</i>	Over the counter

(ADC): Antibody drug conjugate. Source: (Martins et al., 2014, Molinski et al., 2009, Mayer, 2014, Gerwick and Moore, 2012)

**Table 1.2** Clinical pipeline resulting from investigations into molluscs. Compound Name: structure /derivative used in clinical trial

Compound Name	Trademark	Company / Institution (country)	Therapeutic activity	Natural product	Source	Clinical status
Pliditepsin	Aplidin®	PharmaMar (Spain)	Cancer	Aplidine	Tunicate <i>Aplidium albicans</i>	Phase III
Tetrodotoxin	Tectin®	Wex Pharmaceuticals (Canada)	Pain	Tetrodotoxin	Pufferfish	Phase III
DMXBA (GTS-21)		University of Colorado Health Sciences Center (USA)	Schizophrenia	Anabaseine	Carnivorous marine worms (hoplonemertines)	Phase II
PM00104	Zalypsis®	PharmaMar (Spain)	Cancer	Related to ET-743	Mollusc (nudibranch)	Phase II
PM01183		PharmaMar (Spain)	Cancer	Related to ET-743	Tunicate	Phase II
CDX-011		Celldex Therapeutics	Cancer	Dolastatin derivative (MM auristatin E)	Mollusc / cyanobacteria	Phase II
Marizomib		Triphase (Canada, USA)	Cancer	Salinosporamide A	Bacterium	Phase I
PM060184		PharmaMa (Spain)	Cancer	Tubulin binding polyketide	Sponge <i>Lithoplocamia lithistoides</i>	Phase I

**Table 1.2** *Continued*

<b>Compound Name</b>	<b>Trademark</b>	<b>Company / Institution (country)</b>	<b>Therapeutic activity</b>	<b>Natural product</b>	<b>Source</b>	<b>Clinical status</b>
Bryostatin I		National Cancer Institute (USA)	Cancer / Alzheimer's	Bryostatins (Macrolide lactone)	Bryozoan <i>Bugula neritina</i>	Phase I
SGN-75		Seattle Genetics (USA)	Cancer	Dolastatin derivative (MM auristatin F)	Mollusc / cyanobacteria	Phase I
ASG-5ME		Seattle Genetics (USA)	Cancer	Dolastatin derivative (MM auristatin E)	Mollusc / cyanobacteria	Phase I

(ADC): Antibody drug conjugate. Source: (Martins et al., 2014, Molinski et al., 2009, Mayer, 2014, Gerwick and Moore, 2012)

## 1.3 Chemical ecology / ecological function of secondary metabolites

### 1.3.1 Chemical Defence

A well-studied aspect of secondary metabolites in molluscs is anti-predator chemical defence. Much of the ecological research on molluscan chemical defence has been on members of the Heterobranchia (Cimino and Ghiselin, 1998), which have also been a target group for natural product discovery (Cimino and Ghiselin, 1998, Avila, 2006, Benkendorff, 2014). Potent chemical defence in some groups is advertised visually by their array of impressive colour patterns (Benkendorff, 2014). Surprisingly, only a few studies have confirmed the anti-predator role of many of the compounds assumed to be produced for chemical defence (Benkendorff, 2014), mainly through analysis of *in-situ* activity against co-occurring predators (Wagele et al., 2006).

Defensive secondary metabolites in molluscs originate through three main processes: 1) Biotransformation, where dietary derived metabolites are chemically modified and re-used in chemical defence. For example, the nudibranch *Hypselodoris orsini* recycles the sponge derived sesterterpenoid, scalaradial, using four structural modifications to express 6-keto-deoxoscalarin in mantle dermal formations (Cimino et al., 1993). *Thuridilla hopei* take toxic epoxy lactone from their algal diet and secrete thuridillin-A, -B and -C during defensive behavioural displays (Marin and Ros, 2004); 2) Selective sequestration, where dietary derived secondary metabolites are used in defence unchanged in structure. For example, *Elysia rufescens* concentrate kahalalide F on the mantle fringe for chemical protection (Davis et al., 2013). Studies of *Cadilina luteomarginata* have detected 35 dietary derived terpenoids from the skin and egg masses of the species (Andersen et al., 2006); 3) *De novo* synthesis from dietary origins, where the species possess the genes required for biosynthesis and usually

construct chemical defences from primary metabolites. For example, both *Elysia viridis* and *E. timida* synthesize elysione from primary metabolites in their algal diet (Marin and Ros, 2004), whilst nudibranch *Dendrodoris limbata* can biosynthesize multiple sesquiterpenoids from mevalonic acid (Cimino et al., 1983). The utilisation of these multiple approaches to secondary metabolite generation or acquisition has produced a diversity of bioactive NPs within certain mollusc groups. Sequestration and biotransformation could be seen as a NP selective process already undertaken by specific mollusc species, whereas *de novo* synthesis provides a target for potentially novel NPs.

### **1.3.2 Mate attraction, reproduction and larval survival**

Reproductive strategies also have to be more ‘chemically apparent’ in the marine environment, where visual cues are limited. Specific water-borne pheromones control mate attraction in *Aplysia* (Carbone and Lux, 1988, Vidová et al., 2010), allowing individuals to find an otherwise cryptic mate. Similar cues are required for mass spawning of generally solitary or migratory marine species, to enable coordinated spawning events. For example peptide sex pheromones found in cuttlefish *Sepia officinalis* (Olivera et al., 1990) are required for egg release and reciprocal sperm attracting peptides facilitate external fertilisation (Zatylny et al., 2002). Cuttlefish also utilise mate communication to initiate flirtatious behaviour (Caprioli et al., 1997). Many neogastropod participate in communal spawning behaviours for the deposition of aggregated benthic egg masses (Benkendorff and Davis, 2004, D'Asaro, 1992), however no research has been undertaken to establish whether chemical or visual cues are involved.

The embryonic and larval periods of marine invertebrates are considered to be especially vulnerable to predation in the water column, thus requiring chemical defence (Lindquist and Hay, 1996). Newly hatched larvae are vulnerable to predation

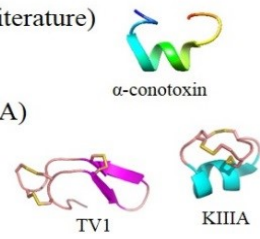
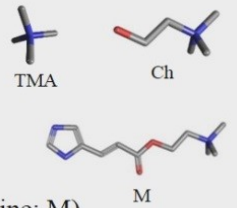
either in the plankton or from direct development, and secondary metabolites could prove to yield particular larvae unpalatable for predation. Benthic egg capsules must also be protected. In molluscs this can involve the encapsulation of developing embryos with anti-microbials and anti-foulants (Benkendorff et al., 2001b, Ramasamy and Murugan, 2005). The chemical ecology of reproduction has only been investigated in a handful of marine molluscs to date, leaving much scope for future research.

### **1.3.3 Predation - Hunting innovations of the Neogastropoda**

The Neogastropoda, an infraorder of the Caenogastropoda (Gastropoda: Mollusca) (Benkendorff, 2014), includes a number of families that have developed specific hunting specializations during their rapid evolutionary radiation in the late cretaceous period (Andersen et al., 2006). The clade includes specialist predatory members including the cone snails (Conidae), mud snails (Nassariidae), olive snails (Olividae), tulip shells (Fascioliariidae), true whelks (Buccinidae) and the oyster drills and purple secreting muricids (Muricidae). Many neogastropods have become dominant members of marine benthic communities, with some at the top of their invertebrate food chain (Andersen et al., 2006). A large part of their success can be attributed to their chemical innovations utilised in a carnivorous diet, ranging from active predation on mobile species, to grazing on immobile/sessile invertebrates and opportunistic scavenging on carrion (Andersen et al., 2006), summarised in Figure 1.1.

Suctorial feeding by haematophagus (bloodsucking) species, e.g. *Cancellaria cooperi*, requires an extended proboscis to consume blood from sleeping vertebrate species, such as the electric ray *Torpedo californica* (Modica and Holford, 2010). These suctorial Cancellariidae species display an unusually long mid oesophagus adapted to the task (Modica and Holford, 2010). Evidence of anticoagulants and anaesthetics, possibly from the salivary glands, during feeding on sleeping vertebrates

indicates a chemical adaptation to the haematophagus lifestyle (Oliverio and Modica, 2010), with secondary metabolites that induce a temporary anaesthetic effect.

		<u>Feeding strategies</u>	<u>Anatomy</u>	<u>Chemistry</u>
CANCELLARIOIDEA		<b>Suctorial feeding:</b> <ul style="list-style-type: none"> <li>• Haematophagy (bloodsucking)</li> <li>• Independently evolved in multiple families</li> </ul>	<ul style="list-style-type: none"> <li>• Extended proboscis</li> <li>• Salivary glands?</li> <li>• Mid-oesophagous? (pre-venom duct)</li> </ul>	<b>Observations suggest:</b> <ul style="list-style-type: none"> <li>• Anaesthetic</li> <li>• Anticoagulant</li> </ul>
CONOIDEA		<b>Harpoon feeding:</b> <ul style="list-style-type: none"> <li>• Predatory ranging from simple molluscs to vertebrates</li> </ul> <b>Paralysis:</b> <ul style="list-style-type: none"> <li>• Mainly targeting a range of ion channels</li> </ul>	<ul style="list-style-type: none"> <li>• Harpoon radula</li> <li>• Venom duct</li> <li>• Muscular venom bulb</li> </ul>	<ul style="list-style-type: none"> <li>• Conotoxins (3000 in literature)</li> <li>• Teretoxins (TV1, KI11A)</li> <li>• Turritoxins</li> </ul> 
MURICOIDEA BUCCINOIDEA OLIVOIDEA		<b>Suctorial feeding:</b> <ul style="list-style-type: none"> <li>• Corallivory (feeding on coral)</li> </ul> <b>Shell drilling:</b> <ul style="list-style-type: none"> <li>• Radula</li> </ul> <b>Shell wedging proboscis:</b> <ul style="list-style-type: none"> <li>• Shell margin as wedge</li> </ul> <b>Paralysis:</b> <ul style="list-style-type: none"> <li>• Anaesthetic via salivary gland</li> </ul>	<ul style="list-style-type: none"> <li>• Primary salivary gland</li> <li>• Accessory salivary glands</li> <li>• Modified radula</li> <li>• Modified shell margin for wedging</li> <li>• Extended muscular proboscis</li> <li>• Hypobranchial gland</li> </ul>	<ul style="list-style-type: none"> <li>• Anticoagulant</li> <li>• Anaesthetics</li> <li>• Tetramine (TMA)</li> <li>• Echotoxin</li> <li>• Biogenic amines</li> <li>• Choline (Ch)</li> <li>• Choline esters (e.g. murexine; M)</li> <li>• Ca<sup>2+</sup> channel inhibitor</li> <li>• Accessory gland saliva causing paralysis, vasodilation, hypotension</li> </ul> 

**Figure 1.1** Summary of specialised feeding strategies seen in the Neogastropoda. Adapted from (Modica and Holford, 2010, Roseghini et al., 1996, Kawashima et al., 2004, Teichert et al., 2005). Shell images courtesy of: Parker R., Delsing J., Schmidt U., Zell H., Hill D., Bould G., Shellnut.

The highly successful Conoidea (or Toxoglossa, meaning “poisoned tongue”) includes the cone snails, terebrids and turrids, which constitute a highly diverse group of hunting snails (Figure 1.1), secreting a mega diverse set of paralysing toxins. These active predators use a highly modified radula tooth, held at the end of the proboscis (Espiritu et al., 2001). Venom injection involves the movement of conotoxin containing mucus from the venom duct to the proboscis via a muscular venom bulb, reaching the piercing tooth used in harpooning prey (Olivera, 2006). The venom duct is the site of biosynthesis of the small toxin peptides (6-40 amino acids in length), which subsequently undergo post translational modification and transport within granules to be secreted into a central lumen, the transport passage to the modified radula (Marshall et al., 2002). Conotoxins are known to target a variety of ion and receptor channels; in particular, the  $\alpha$ -conotoxins are known to block the nicotinic acetylcholine receptor (nAChR; Figure 1.1), adrenergic receptors and voltage gated sodium, potassium and calcium ion channels (Teichert et al., 2005). The variety of target receptors causes paralysis in multiple prey types, allowing prey specialization (Duda and Palumbi, 2004). Ion channel blocking from conotoxins has been shown to range from temporary blockade to more permanent channel inactivation or complete blockage (Carbone and Lux, 1988). Less is known about the targets for toxins secreted by terebrid and turrid snails, but they have similarities in structure to the conotoxins (Anand et al., 2014) and may also target ion and receptor channels.

Chemically induced prey immobilization is also a successful adaptation of members of the Muricoidea, Buccinoidea and Olivoidea (Figure 1.1), with the primary and accessory salivary glands secreting a number of anaesthetizing, narcotizing and anticoagulant secondary metabolites (Modica and Holford, 2010). The primary salivary gland, made up of basal cells with acrocrine secretion and superficial ciliated secreting cells, plays a role in toxin secretion in the absence of accessory salivary

glands or a venom gland (Andrews, 1991). Members of the buccinids, including *Neptunea antiqua*, have large salivary glands that can contain high quantities of the toxin tetramine (tetramethylammonium salt; a quaternary ammonium cation, Figure 1.1), of which a yet unknown counter ion is required for storage (Power et al., 2002, Kawashima et al., 2004). In some cases, the levels of tetramine are so high in edible whelks that they have caused a number of human intoxications (Modica and Holford, 2010). A number of unidentified toxins from the salivary gland have also been encountered in *N. antiqua*, including a neuronal Ca<sup>2+</sup> channel inhibitor (Power et al., 2002), as well as anticoagulants in *Colubraria reticulata* (Modica and Holford, 2010). Given the predatory specialisation of the different neogastropod groups, there is potential for the discovery of novel chemistry or yet unknown secondary metabolites in these predatory molluscs. In particular, secondary metabolites that can target ion channels and ligand gated receptors, are likely to have evolved based on the need for these species to paralyse their prey.

The accessory salivary glands in Muricidae are generally large and well developed, and have been implicated in predation with and without shell drilling. *Nucella lapillus* and *Stramonita haemastoma* are able to secrete mucus that includes a glycoprotein able to elicit flaccid paralysis in *Mytilus edulis* (Andrews, 1991). This mucus decreases cardiac activity and contains a potent vasodilator and hypotensive agent (Huang and Mir, 1972). The anaesthetic metabolites of *N. lapillus* are also delivered with serotonin (5-hydroxytryptamine), with a yet unknown purpose (West et al., 1996). The concentration of predatory toxins seen in the accessory salivary glands of many muricid species requires significant metabolic investment. The glands can make up to 5% of total body weight, and secretions are physiologically able to elicit paralysis in prey (West et al., 1996). Other families within the neogastropods could also possess

interesting secondary metabolites related to muscular paralysis and ion channel activation/inactivation but are yet to be investigated.

Much research effort has gone into the physiological effects of conotoxins, likely due to the development of the pharmaceutical agent ziconotide, and the high diversity of conotoxin structures and their cellular targets. As a consequence of this significant research interest, the *Conus* genus may become the source of the largest and most clinically important pharmacopoeia of any genus (Szekely and Gaillard, 2007). The success of research into conotoxins as natural products has given impetus to the ecological understanding of conotoxin encoding genes and the phylogeny of the entire genus. Based on the hunting behaviours of almost all the neogastropods, research effort should perhaps not be limited to the *Conus* genus.

#### **1.3.3.1 Neogastropod hypobranchial choline esters**

The hypobranchial gland is an anatomical specialization found within gastropods, whose biological function is not well characterised. Many species of the Neogastropoda are known to secrete choline esters (Figure 1.2) from the medial epithelium of the hypobranchial gland (Roseghini et al., 1996). These secondary metabolites are structurally able to elicit paralysis via neuromuscular blocking activity, although some researchers have suggested ecological concentrations do not reach ‘physiologically active’ levels for paralysis in the external environment (West et al., 1996, Modica and Holford, 2010). Concentrations detected vary considerably from species to species (Roseghini et al., 1996), and species found to contain choline esters generally have more than one type (see Roseghini et al., 1996 for a comprehensive list). The repertoire of choline esters includes murexine (urocanylcholine or  $\beta$ [imidazolyl-4(5)acrylcholine]), dihydromurexine, seneciroylcholine ( $\beta,\beta$ -dimethylacryloylcholine), tigloylcholine and acryloylcholine (Roseghini et al., 1996, Shiomi et al., 1998). Tigloylcholine, detected in *Thais clavigera* and *Thais bronni*, is

a structural isomer of seneciylcholine, based on  $^1\text{H}$ - and  $^{13}\text{C}$ -NMR (Shiomi et al., 1998).

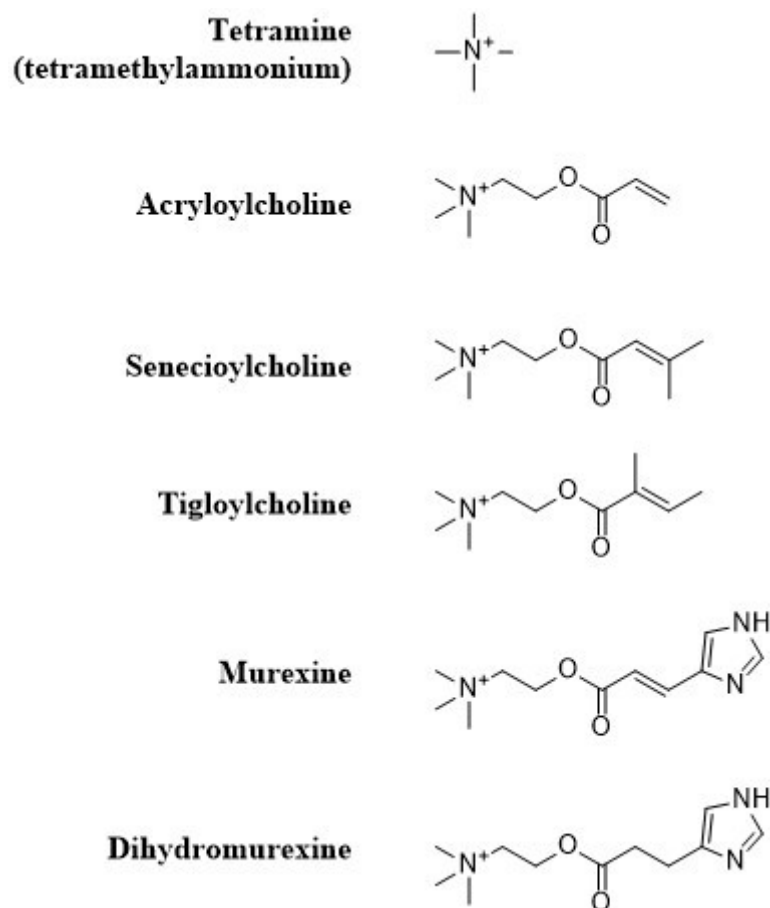


**Figure 1.2** Structure of secondary metabolites of the Muricoidea found to elicit paralysis including tetramine and the choline esters

The most comprehensive study of choline esters in neogastropods found that all species containing the imidazole and acryloyl based choline esters were predatory species (Roseghini et al., 1996). These paralysis inducing choline esters were undetectable when tested in closely related herbivorous or scavenging molluscs (Roseghini et al., 1996), providing evidence for a role in predatory specialization. In addition to choline esters, the hypobranchial gland secretes choline, acetylcholine and biogenic amines including urocanic acid, imidazolepropionic acid, methylimidazolepropionate, tyramine, octopamine, serotonin, histamine, urocanylhistamine and imidazolepropionyl-histamine (Roseghini et al., 1970,

Roseghini et al., 1996, Baker and Duke, 1976). It is plausible that some of these biogenic amines are a result of degradation or precursors required as part of the synthetic pathway for choline esters. For example, histamine and other small imidazole containing compounds could be used for inclusion into imidazole containing murexine. However, the presence of large quantities of histamine and octopamine is interesting, as these compounds have been found to act as neurotransmitters in many molluscan species (Karhunen et al., 1993, LaFleur et al., 2014). The presence of serotonin is also worth further investigation; as mentioned, it has been found in both the secretions of the accessory salivary glands of *N. lapillus* (West et al., 1996) and cone snail *Conus imperialis* toxins (Roseghini et al., 1996) in addition to hypobranchial gland / venom duct secretions. The specific mixture of compounds present in these secretions may contribute to the potency or bioavailability during paralysis and thus may shed light on perceived concentration deficiencies of choline esters for external effects during predation. Alternatively, these neurotransmitters may simply be required to regulate control over the secretion of other bioactive secondary metabolites.

Bioactive testing of the chemical weaponry of the Neogastropoda seems to show a consistent pattern of containing at least one paralyzing agent that potentially targets the nAChR (Roseghini et al., 1996, Teichert et al., 2005, Kawashima et al., 2004). To induce paralysis, secondary metabolites would presumably show affinity to the muscle type nAChR (Figure 1.3).  $\alpha$ -Conotoxin shows strong binding affinity to this receptor, demonstrated by a conotoxin ligand bound nAChR crystal structure (Teichert et al., 2005). The pentameric ligand gated channel is normally activated by acetylcholine binding to the receptor pocket between two subunits (Figure 1.3) on the extracellular ligand binding domain, eliciting conformational change and opening the channel (Brejc et al., 2001, Karlin, 2002). Murexine has been suggested as a ligand to the

nAChR muscle type receptor based on the pharmacological actions tested *in vivo*, where scanning electrode experiments measured depolarizing actions on the muscle motor endplate (Roseghini et al., 1996, Erspamer and Glasser, 1957). *In silico* modelling could be used to determine if murexine and the other choline esters bind to the same region of the nAChR receptor.

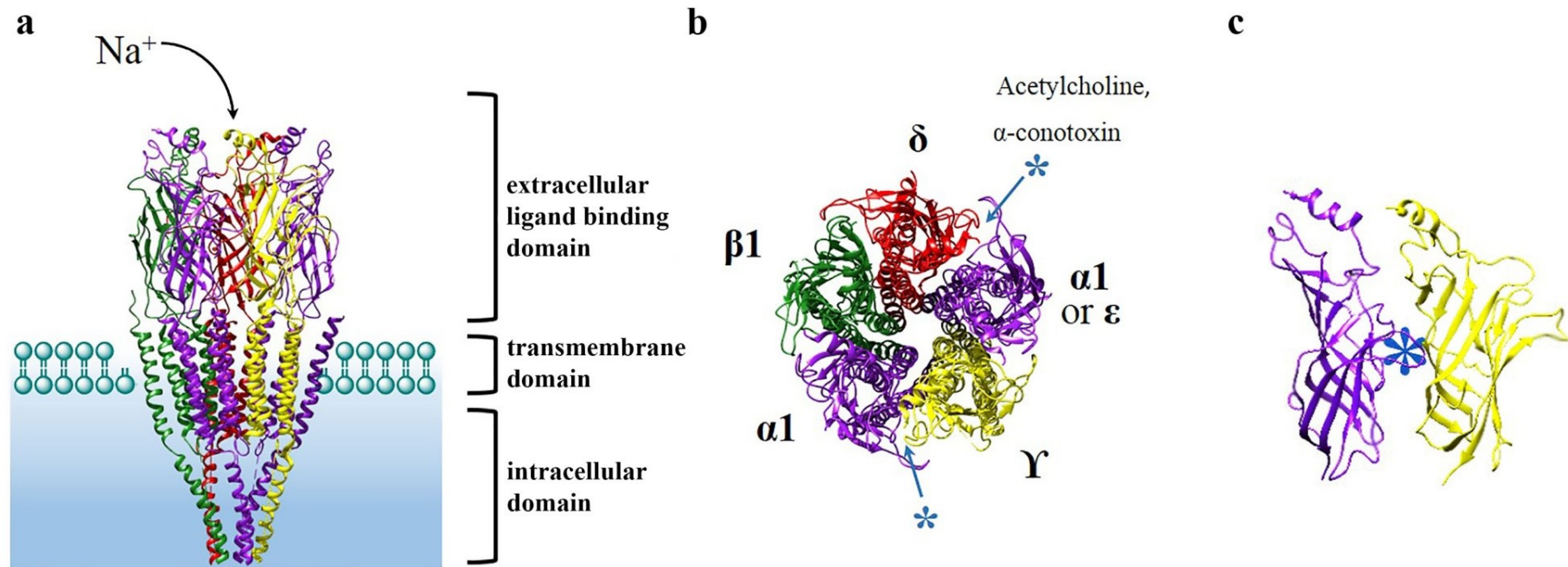


**Figure 1.3** The nicotinic acetylcholine receptor structure within the cell membrane: a) ribbon diagram of the refined structure model of pentameric nAChR from *Torpedo marmorata* positioned within the cell membrane (lateral view); b) top view of nAChR with muscle type subunit labelling and indication of binding site for acetylcholine and  $\alpha$ -conotoxin; and c) ligand binding domain of two subunits where \* indicates ACh binding pocket location in the space between the subunits behind the overlapping Cys-loop structure. Structure was accessed and modified in Chimera (1.9rc) from RCSB Protein Data Base accession 2GB9.

Due to their highly hydrophilic cationic head, choline, acetylcholine, tetramine and the choline esters, require a form of storage prior to secretion (Kawashima et al., 2004). This involves either uptake into storage vesicles in the intracellular environment via the vesicular acetylcholine transporter, e.g., for neuronal synaptic effect (de Castro et al., 2009); or in the case of the hypobranchial gland, the choline esters are held as a salt by a counterion (Baker and Sutherland, 1968, Baker and Duke, 1976) prior to liberation into the external environment. The counterion for choline esters detected in the Australian muricid *Dicathais orbita*, was found to be a salt of tyrindoxyl sulfate (Baker and Duke, 1976), a brominated indole precursor to the natural dye Tyrian purple. Four other prochromogens (Figure 1.4), that act as choline ester counterions have been identified in the hypobranchial gland from different Muricidae species, including brominated and non-brominated indoxyl sulfates (Fouquet and Bielig, 1971). The indoxyl sulfates and their enzymatic products have been investigated for their bioactive properties and for their historical significance, but the exact ecological role is somewhat elusive. Their role in the release of paralysing choline esters may not be the only advantage these unique chromogenic secondary metabolites impart, particularly due to their detection in the egg masses of multiple Muricidae (Palma et al., 1999, Benkendorff et al., 2000, Benkendorff et al., 2001a, Benkendorff et al., 2001b) and the reproductive organs of *D. orbita* showing sex specific differences (Westley and Benkendorff, 2008). Histochemical analysis of the reproductive structures has also detected the tryptophan and tyrindoxyl sulfate precursors as well as bromoperoxidase activity in the hypobranchial gland and reproductive organs (Westley and Benkendorff, 2009a). These findings indicate that the choline esters and/or brominated indole counter ions may also play an essential role in the reproduction of Muricidae.

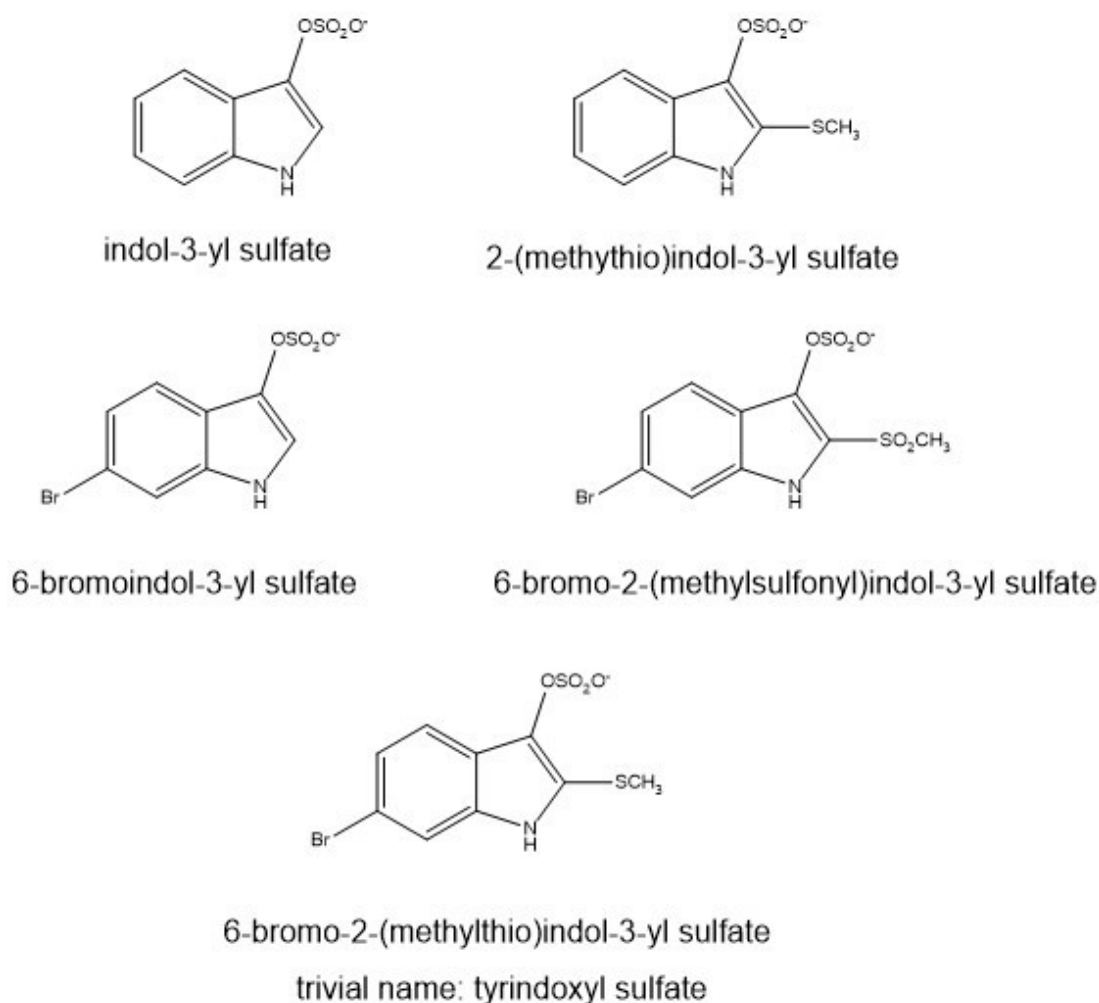


**Figure 1.4** Sulfate esters of indoxyl found as precursors to Tyrian purple and indigos detected in Muricidae molluscs, including tyrindoxyl sulfate (6-bromo-2-(methylthio)indolin-3-yl sulfate) (Baker, 1974, Cooksey, 2001)

### 1.3.4 Molecules of keystone significance

As secondary metabolites influence species interactions, acting as chemical cues, sedatives or deterrents, they can affect large scale foraging patterns, drive resource allocation and influence energy exchange across geographical scales (Hay, 2009, Pohnert et al., 2007, Amsler et al., 2001). Defining function for secondary metabolites can therefore have very wide implications for understanding how some marine communities are structured. When specific secondary metabolites exert wide

ecological effects beyond simple species/species interactions, they can be considered “keystone molecules” (Derby and Zimmer, 2014).

The most studied functional aspect of marine invertebrate secondary metabolites at the community level, where the active compound has been identified, has been field and laboratory assays demonstrating defence against consumers (Hay, 1996). Field work has mostly focussed on sessile or less mobile chemically defended species under predation by generalist consumers, e.g. consumption of sponges, ascidians and bryozoans by common reef fish species (Pawlik et al., 2013, Paul et al., 2007, Lindquist and Hay, 1996). Knowledge of the *in situ* ecological advantages of anti-predator metabolites can be integrated into broader and more complex questions about the effect of secondary metabolites on consumer physiology and fitness (Hay, 1996), and consequently, on the way they shape community structure and diversity. For example, within Caribbean coral reef communities, higher abundances of predatory fish correlated with higher abundances of chemically defended sponge species, whilst lower numbers of predatory fish species appear to be associated with the proliferation of undefended sponge species (Loh and Pawlik, 2014). Chemically defended sponges exposed to predation also had lower growth rates than undefended sponges (Loh and Pawlik, 2014), demonstrating a resource trade-off between chemical defence and growth. These evolutionary trade-offs could greatly affect community sponge diversity under different levels of predation.

Designing experiments around the community wide effects of specific molluscan secondary metabolites could prove difficult. The diversity of molluscs across many environments and the role molluscs have as keystone species in some locations, e.g. reef forming bivalves (Hall-Spencer and Moore, 2000), highlight the potential for some molluscan compounds to act as molecules of keystone significance. The evolution of the conotoxins, facilitated by a hyper-mutation of particular regions of the

conotoxin gene sequence (Espiritu et al., 2001), has co-occurred with the rapid speciation of the genus. *Conus* make up the largest known single genus of venomous animals, with more than 500 *Conus* species, adapting into multiple ecological niches (Espiritu et al., 2001). Both the phylogeny of conotoxin genes and the predatory specificity of a species conotoxin repertoire show adaptive evolution to specialised diets. Phylogenetic clades of *Conus* species have adapted to molluscivory and piscivory from an otherwise vermivorous ancestral clade (Duda and Palumbi, 2004). Conotoxins could therefore be one example of keystone secondary metabolites.

Cephalopod ink, almost ubiquitous to the Coleoidea, is another example of a complex mixture of secondary metabolites likely to have significant influence on community structure and contribute to the success of the highly mobile predators that secrete them (Derby, 2014). Ecosystem modelling of pelagic squid, *Loligo plei*, has found it to be a keystone species in the Southern Brazil Bight, as it exerts a strong effect on community structure yet maintains a relatively low biomass (Gasalla et al., 2010). The squid provide a link between pelagic and demersal energy pathways, where presumably inking influences the success of the species in pelagic environments. Observational studies suggest the ink acts as an immediate anti-predator deterrent through a visual mechanism but has been hypothesized to also have chemical deterrent mechanisms, being exceptionally rich in free amino acids (Wood et al., 2008). Experiments with ink on conspecifics have shown it to also act as a signalling molecule, demonstrating alarm and escape behaviours from the visual stimulus of ink. Melatonin free ink fails to elicit a significant alarm response suggesting a chemical stimulus is involved (Wood et al., 2008). Like many complex molluscan secretions, establishing the chemical composition and ecologically relevant concentrations for cephalopod ink in the pelagic environment, or *in situ*, is difficult to conduct, but would be ecologically informative (Derby, 2014).

Keystone secondary metabolites may also indirectly shape community structure. Specific secondary metabolites that enhance embryonic and larval survival in highly fecund species could contribute to increased recruitment and species distribution. Additionally, secondary metabolites that act as settlement/metamorphic cues can determine species recruitment onto intertidal reefs, as many molluscs have a pelagic (planktotrophic or lecithotrophic) larval phase (Romero et al., 2004). Substances from prey, conspecifics and suitable substrates (biofilms, coralline algae) are known to induce settlement behaviour in bivalves (Hadfield, 2011) and gastropods (Williams et al., 2009). Pelagic larvae may require different cues to induce settlement behaviour from those inducing metamorphosis (Hadfield, 2011), whilst some larvae require only a single metabolite for both. The effect of histamine, leaching from seagrasses, on sea urchin *Holopneustes purpurascens* (Swanson et al., 2004) induces both settlement and metamorphosis of larvae. The identification of settlement inducing secondary metabolites may explain site selection for pelagic larvae, and even associated predatory fish species (Dixson et al., 2014), which has an influence on community structure through recruitment. This has been experimentally shown through the selective settlement of corals and movement of juvenile reef fishes onto healthy protected coral covered reefs with settlement inducing cues, as opposed to unhealthy seaweed dominated reefs that lack coral associated cues (Dixson et al., 2014)

Many examples of dominant invertebrate predators within ecological biomes possess potent secondary metabolites (Pawlik, 1993). These specific keystone molecules could be contributing to community structure and diversity by exerting top-down control on prey populations, whilst maintaining their own chemical defence. Concurrently, keystone molecules may be contributing to bottom up control over community structure by influencing which species actually settle in benthic habitats. Studying the mechanism by which keystone molecules exert an influence on

community structure does requires knowledge of the deployment of these compounds at ecologically relevant concentrations, which starts with knowledge of the *in situ* mechanics surrounding their production.

#### **1.4 Biodistribution and Biosynthetic origin**

Assigning ecological function to secondary metabolites relies on demonstrating *in situ* activity in an ecologically relevant way, which can have considerable hurdles in experimental design (Avila, 2006, Wagele et al., 2006, Paul et al., 2007). *In situ* detection is also valuable for understanding the biosynthesis of NPs within specific tissues, an important step in developing supply strategies for sustainable production. Initially understanding how, when and why a natural product is assembled requires extensive knowledge of the anatomical distribution of metabolites, precursor supply networks, metabolic pathways and genetic and ontogenic traits associated with its biosynthesis (Simmons et al., 2008, Gerwick and Moore, 2012, Garson, 1993, Avila, 2006, Wagele et al., 2006, Paul et al., 2007, Hay, 1996). This becomes more of a complex question for marine gastropods, because they can exhibit *de novo* biosynthesis, bio-transformation and sequestration of potent secondary metabolites. Molluscs often form secondary metabolites from dietary origins and exhibit highly diverse lifestyles where secondary metabolites may be utilised, further complicating the initial discovery of the ‘active’ structure (Garson, 1993).

To answer the question of ‘where’ secondary metabolites are produced requires molecular precision, as secondary metabolites are often stored and secreted in a different cellular environment to the site of biosynthesis (Garson, 1993). Initially, focusing on tissues associated with biosynthesis involves anatomical investigations to identify specialised biosynthetic organs such as the salivary glands in cephalopods (Derby and Zimmer, 2014), hypobranchial glands in Muricidae (Benkendorff, 2013,

Roseghini et al., 1996), the conotoxin producing venom duct in the Conidae (Lewis et al., 2012), and the mantle dermal formations in chromodorid nudibranchs (opisthobranchs) (Carbone et al., 2013, Somerville et al., 2006). To identify sequestration of natural products, anatomical approaches may also help by finding similarities in compounds between prey, digestive glands and specific defensive glands (Garson, 1993, Somerville et al., 2006, Suciati et al., 2011). Focussing on individual cells can even provide evidence for *de novo* synthesis, such as the biosynthesis of lignarenones (aromatic polyketides) in Blochmann's gland cells found in the mantle tissue of opisthobranch mollusc *Scaphander lignarius* (Cutignano et al., 2012a), a synthetic pathway not seen in animals before (Cutignano et al., 2012b).

#### **1.4.1 Traditional approaches**

Detecting unique biodistribution and biosynthesis pathways has commonly been achieved through the use of stable isotope labelling ( $^2\text{H}$ - $^{13}\text{C}$ - incorporation) and NMR of incorporated precursors. For example, stable isotope-labelling was used to identify lignarenones in the cephalaspidean *Scaphander lignarius* (Cutignano et al., 2012a), using  $^2\text{H}$ - and  $^{13}\text{C}$ -labelled precursors within feeding experiments. This approach was combined with fluorescent imaging of the polyketide lignarenones, using confocal laser scanning microscopy, where secondary metabolites were localised to Blochmann's gland cells in the mantle epithelial tissue (Cutignano et al., 2012a). Labelled isotope feeding experiments were also effective in determining the synthesis of the secondary metabolite elysione, from *Elysia viridis* (Cutignano et al., 2009), a mollusc capable of phototrophic  $\text{CO}_2$  fixation through dietary kleptoplasty. Labelling in this case was combined with a direct sunlight irradiation assay to determine the role of elysione in photoprotection by rearrangement of the propionate skeleton, thought to act in preventing light overexposure (Cutignano et al., 2009).

Isotope labelling is certainly effective in detecting biosynthetic pathways, but species must be amenable to feeding experiments where effective amounts of labelled material can be incorporated at a time when synthesis occurs, e.g. in some cases low enrichment prevented recording of  $^{13}\text{C}$ -NMR spectra in molluscan studies (Cimino et al., 2004, Cutignano et al., 2012a). In addition to low incorporation rates of isotopes, integration into extraneous pathways or incorporating enough labelled precursors for NMR can produce misleading results (Garson, 1993, Cimino et al., 2004). Labelling is also rarely used in a holistic manner; additional assay and histochemical analysis are combined for a better view of secondary metabolite distribution and the combination of these approaches make them difficult to adapt distributional / biosynthetic studies to biological events (Garson, 1993).

Histochemical and fluorescent labelling approaches have demonstrated sites of secondary metabolite synthesis, storage and secretion in molluscs (Westley et al., 2010b, Cutignano et al., 2012a, Cutignano et al., 2012b, Westley and Benkendorff, 2009a), although these are generally better directed to the biosynthetic enzymes responsible for production. Histochemical approaches are adaptable to biological events, such as reproductive activities, and specific tissues including reproductive structures. Westley and Benkendorff (2009) employed histochemical staining to examine the distribution of Tyrian purple precursors in the reproductive tissues of the muricid *D. orbita*. Carefully selected stains demonstrated the presence of precursors within secretory cell types via staining reactions from spherules localised to the mucus rich hypobranchial gland (Westley, 2008). Distributions of the precursors in *D. orbita* could then be compared to histochemical staining for biosynthetic enzymes, such as bromoperoxidase and aryl sulfatase, providing evidence for a biosynthetic pathway for Tyrian purple precursors (Westley, 2008). Unfortunately, unless secondary metabolites have some chromophore properties, few labels are available for low

molecular weight secondary metabolites and precursors. Direct labelling with immunocytological probes and oligonucleotide aptamers has been generally ineffective (Wagele et al., 2006). Many marine secondary metabolites possess novel structures, so generating specific labelling can require considerable preparation, and labelling efforts target one or a few secondary metabolites, which do not encompass the full chemo-diversity involved in secondary metabolite biosynthesis.

## **1.5 Mass spectrometry imaging as a tool for natural product research and chemical ecology**

Mass spectrometry (MS) has become an integral part of NP research and is a growing technology base for the field of chemical ecology. Modern mass spectrometry is highly complementary to other methods for structural elucidation and NP detection, including 1D and 2D NMR, X-ray crystallography, UV/Vis detection (Klitgaard et al., 2014) and, in some cases, is predicted to surpass these techniques (Dorrestein, 2014). One of the major advantages of mass spectrometry is the small sample requirement for analysis and the ever improving mass accuracy for analytes detected. Sophisticated equipment can resolve peaks at 24 million ( $\Delta M$ ) with sub parts per billion (ppb) mass accuracy (Bousslimani et al., 2014), highly suitable for low *in situ* concentrations of secondary metabolites. As new technologies have broadened the mass range and compound classes open to mass spectrometry, some ionisation methods have opened the possibility to apply mass spectrometry to the 2D analysis of tissues, providing a molecular snapshot across tissue surfaces.

Mass spectrometry imaging (MSI) relies on the laser raster scanning across the sample at selected sampling points in a defined *xy* geometry at a particular spatial resolution and laser focus diameter. Adduct ions are generated by the ionisation source (Table 1.3) and introduced into a mass analyser, e.g. quadrupole mass analyser, magnetic sector, linear ion trap, time of flight (TOF) analyser. Typically for MALDI,

DESI and variations to LDI-MS, charged adducts include proton  $[M+H]^+$ , sodium  $[M+Na]^+$ , potassium  $[M+K]^+$  and ammonium  $[M+NH_4]^+$ , although molecular ions can also be detected  $[M]^+$ . A mass spectrum for each spot is acquired, with the intensity for each ion generated and summed together for spatial analysis (Pacholski and Winograd, 1999). Raster scanning therefore requires the sample to be controlled, usually by a program controlled  $xy$  stage. Therefore MSI is generally done from a solid platform and methods that are amenable to this design have been adopted, with exceptions for  $xyz$  controlled methods such as nanoDESI, which can be done directly from the petri dish or sample surface (Laskin et al., 2012). Each of the broad groups used in MSI has specific advantages (Table 1.3), mostly based on the type of analyte being sampled, the spatial resolution, and how the sample preparation may affect the target compounds.

For practical considerations of adequate spatial resolution, sensitivity, and the integration of ionisation methods with mass analysers, three broad areas for MSI have been considered useful for biological material / tissue analysis (Watrous and Dorrestein, 2011, Bouslimani et al., 2014), (Table 1.3): 1) Laser desorption ionisation (LDI) group of methods, including direct LDI, ultra violet-matrix assisted laser desorption ionisation (UV-MALDI) and infra-red (IR-MALDI), and more recently the alternative surface assisted methods including desorption/ionisation on organic silicon (DIOS), nanostructure initiated mass spectrometry (NIMS) and nanostructured (or nanowire) assisted laser desorption/ionisation (NALDI) (Figure 1.5); 2) Desorption electrospray ionisation (DESI) and the ambient group of methods including direct DESI, thin film assisted DESI, nano-DESI, the combined laser ablation electrospray ionisation (LAESI) and alternative ambient ESI methods such as liquid extraction surface analysis (LESA) (Figure 1.6); 3) Secondary ion mass spectrometry (SIMS) group of methods including both dynamic (high intensity) electron beam and static

(lower intensity) electron beam, (Figure 1.7). Table 1.3 is not an exhaustive list of possible approaches to MSI; new methods are constantly being added with advances in ionisation, analyte capture, MS infusion methods, depth sampling and targeted approaches. The choice of method is also dependent on the metabolite/s of interest, tissue type and access to available equipment/facilities. Each of the three broad areas of LDI (Figure 1.5), DESI (Figure 1.6), and SIMS (Figure 1.7) has been utilised in the spatial analysis of natural products or chemo-ecological studies (Bouslimani et al., 2014, Vaidyanathan et al., 2008).

Although NPs and secondary metabolites vary significantly in structure and complexity, a large proportion of interesting NPs fall within the low mass range (<700 Da) in the region where matrix difficulties occur. Feher and Schmidt (2002), when reviewing the property distributions between drugs of natural and synthetic origin, found that of the total natural products assessed ( $n = 3287$ ) the mean/median MW was 414/362 Da (Feher and Schmidt, 2002). MSI methods that are sensitive enough to detect low abundance compounds and are adaptable to the low mass range are likely to have the greatest utility in NP and chemo-ecological research involving secondary metabolites.

**Table 1.3** Mass spectrometry methods used in the analysis of NP or chemical ecology with examples of MSI usage

Method	Matrix	Ionisation method	Application	Lateral resolution ( $\mu\text{m}$ ) / depth ( $\mu\text{m}$ )	Mass range (Da)	Notes	Examples for MSI
<b>UV-MALDI</b>	Organic crystalline MALDI matrix	UV -laser (337, 366 nm)	Wide applications from inorganic ions. Small metabolites, peptides, proteins, nucleic acids (~150 base pairs intact), polymers.	50 - 500 / 0.1-20	300-50,000	Excellent for proteins, Cornett, et al. 2007; Franck et al. has been used in many 2009 biological samples	
<b>IR-MALDI</b>	Water irradiation in sample	Infra-red laser (2800-3100 nm)	Carbohydrates, lipids, RNA and DNA (some examples up to more than 500 base pairs intact).	105-200 (although able to focus) / greater depths than UV-MALDI	100-50,000	Softer ionization than Berkenkamp et al. 1998 UV-MALDI and less interference in the low mass range, tuneable wavelength conditions	
<b>LDI</b>	None - target molecule absorbs laser energy	UV -laser (337, 366 nm) direct desorption	Only effective with UV-absorbing molecule (e.g. conjugated double bonds, aromatic compounds).	$\geq 10$ (Bruker SmartBeam <sup>TM</sup> and oversampling), single cell scale resolution / 0.1 – 50	100-5000	High repetition rate Kroiss et al. 2010; Holscher et al. 2013 for imaging UV-absorbing metabolites	
<b>DIOS (Surface assisted-LDI and NIMS)</b>	None - porous silicon (or wire) substrate or embedded initiator absorbs laser energy	UV -laser (337, 366 nm) direct desorption	Effective in the low mass range. Able to be functionalized to suit different classes of compounds (inc. non-volatile). Low fragmentation vs SIMS.	0.15 - 500 / surface or imprint	1-1500	Highly sensitive and functionalize to suit target metabolite, useable at the single cell level, can image imprint of highly soft and un-handleable tissue Kruse et al. 2001; Lowe et al. 2009; Guinan et al. 2012	

**Table 1.3** *continued*

Method	Matrix	Ionisation method	Application	Lateral resolution ( $\mu\text{m}$ ) / depth ( $\mu\text{m}$ )	Mass range (Da)	Notes	Examples for MSI
<b>NALDI</b> (Surface assisted-LDI)	None - nanowire,nano-structure fabricated substrate absorbs laser energy	UV -laser (337, 366 nm) direct desorption	Small metabolites, drugs and highly effective with lipids	0.15 - 500 / surface or imprint	1-1500	Now commercially available Bruker Nanosys NALDI®, developed from SALDI based technology	Vidova et al. 2010; Tata et al. 2012
<b>DESI</b>	None - charged $\text{N}_2$ / solvent spray to eject analyte	Modified ESI source using solvent spray with high-pressure gas flow onto sample surface	Excellent for compounds at the sample surface/spray interface. Can achieve depth desorption from porous tissue.	100 -1000 / based on ESI jet focusing	100-5000	Modified ESI source applied directly to sample at ambient pressure, solvent can be selective, spray pressure can destroy samples	Watrous et al. 2010 ; Lane et al. 2009
<b>nanoDESI</b>	None - solvent droplet bridge rather than pressurised spray	Very soft ionisation via solvent bridge to MS source	Direct imaging of tissue without sample prep. Bacterial colonies, small metabolites to peptides.	10-1000 / 0.1-10	100-10000	Minute sample sizes, almost no sample preparation, target analysis using reactive compounds	Watrous et al. 2013 ; Laskin et al. 2012
<b>LESA</b>	None – robot controlled pipette surface extraction with solvent	nanoESI-MS	Pipette solvent extraction for nanoESI-MS but robot controlled for imaging. Complimentary to DESI for large tissue sections.	Approx. 1mm / surface extraction	100-10000	Controlled infusion into nanoESI using pore etched silicon chip but large lateral resolution	Eikel et al. 2011
<b>SIMS</b> (Static / Dynamic)	None - Charged primary ion beam (e.g. $\text{C}_{60}^+$ or $\text{Au}^+$ ) sputters sample surface to eject secondary analyte ions	Ionisation by collision of primary energised ion beam with analyte, at low energy (static) or high energy (dynamic)	Single elements (cations), lipids, small metabolites. Can be combined as a pre MSI-imaging before MALDI due to minimal sample destruction.	0.3-0.5 (dynamic), 0.5-50 (static) / surface mostly up to 10	1-300 (dynamic), 100-1500 (static)	Mostly to image single cells as imaging area is few $\text{mm}^2$ , e.g. ionic changes in cell signalling, but can be up-scaled (at high cost) and used pre-MALDI, must be clean and flat	Ostrowski et al. 2004; Vaidyanathan et al. 2008; Debois et al. 2008

### 1.5.1 LDI-MSI methods

LDI involves using pulsed laser energy for desorption /ionisation, absorbing laser energy either by direct irradiation, surface absorption, matrix or a combination of these (Svatos, 2010). Ionization for MSI can be achieved using ultraviolet (UV) or infrared (IR) wavelength laser light (Berkenkamp et al., 1998). Examples of lasers used for LDI-MS include nitrogen lasers (337 nm) operating at 2 – 20 Hz, Nd: yttrium aluminium garnet (YAG) pumped optical parametric oscillator laser operating at 2.94 microns (for IR) or high spatial resolution solid-state Nd:YAG lasers (355 nm) at 20 – 2kHz (Goodwin et al., 2008, Niu et al., 1998). LDI is generally coupled to a TOF mass analyser but can be combined with other mass spectrometers (Niu et al., 1998). The pulsed laser creates an expanding plume of ionised molecules that is allowed to expand and equilibrate (delayed extraction) before an electric field is applied to accelerate ions down the flight tube to a detector, via either linear or reflectron TOF (Hillenkamp and Karas, 2007), as outlined in the simple schematic in Figure 1.5. Modern commercial equipment, dedicated to MSI, can achieve laser spot focusing down to 20 µm diameter (SmartBeam-II, Bruker), allowing spatial resolution to better match histological sections (Ronci et al., 2012). Additional improvements include TOF/TOF analysis, where precursor ions can be selected for additional high energy collision induced fragmentation (CID) in a collision cell allowing structural data to be added to TOF analysis, e.g. CID MALDI-TOF/TOF (Vestal and Campbell, 2005). Commercial and open-source software and equipment packages have made MA/LDI-MSI increasingly accessible.

The mass range for the suite of LDI methods is very broad and this has allowed multiple methods to be combined for dual overlay imaging. MALDI is heavily utilised in the analysis of protein distributions, originally emerging in the 2D detection of disease markers and a complementary method to histo-pathology. MALDI-MSI has

become a descriptive tool for cancer pathologies (Schone et al., 2013), neuropsychopharmacology (Shariatgorji et al., 2014) and drug development (Castellino et al., 2011). Refinement of the methods and equipment used in the above applications, on known tissues with somewhat predictable / searchable mass spectra, has also made MALDI and alternate methods applicable to NP discovery (Esquenazi et al., 2009) and chemical ecology. For example MALDI-MSI has been used in the description of antibiotic coatings on leaf cutter ants, used to protect the cultivation of their fungal food source (Schoenian et al., 2011); the epidermal distribution of marine alkaloids in zooanthids, as a potential UV damage protecting mechanism using collagen formation (Genji et al., 2010); and the temporal biosynthesis and distribution of potent secondary metabolites, jamaicamide A and B, in cyanobacteria (Esquenazi et al., 2011).

As MSI has expanded for the analysis of low molecular weight (LMW) metabolites, alternative strategies have been included into LDI to eliminate interference from matrix ions in the low mass range. Direct LDI relies on the UV absorbing nature of target compounds and has been successfully used in the MSI analysis of natural antibiotic distributions on beewolf digger wasp cocoons, protecting larvae from fouling via symbiotic inoculation (Kroiss et al., 2010). It has also been utilised in the analysis of LMW anti-nematode compounds in banana cultivars (Hölscher et al., 2013).

For compounds that are not amenable to direct absorption of UV laser energy, surface assisted (SALDI) methods have been employed for MSI. Desorption / ionisation on organic silicon (DIOS) utilises chemical etching and functionalization of silicon wafers to create a highly porous surface capable of mimicking the attributes of a matrix. The porosity and surface chemistry trap analyte molecules whilst maintaining their distribution and absorb laser energy for desorption/ionisation without

fragmenting analyte structures (Lewis et al., 2003). Although not yet employed in the MSI analysis of natural products, DIOS could provide considerable advantages for natural product MSI, in that the porous layer has the capacity to be functionalized, altering the surface chemistry for the specific capture of target analytes (Trauger et al., 2004). Natural products are often in low abundance, so their selective capture may prevent target ions being suppressed in the abundance of material being imaged. Similar advantages are also seen for nanostructure initiated mass spectrometry (NIMS), nanostructure assisted LDI (NALDI) and alternate surface assisted LDI, which have shown effective distributional analysis of chemical entities (Vidová et al., 2010).

There is a wide range of available approaches to MSI NPs and biosynthetic tissues. LDI-MSI has particular advantages for neogastropod biosynthetic tissues as there is a range of strategies to cope with high salt content, mucus rich tissue whilst still targeting the LMW mass range. In particular, the SALDI suite of methods is able to chemically attract LMW metabolites in their spatial distribution but still allows washing steps that result in a 'cleaner' sample.

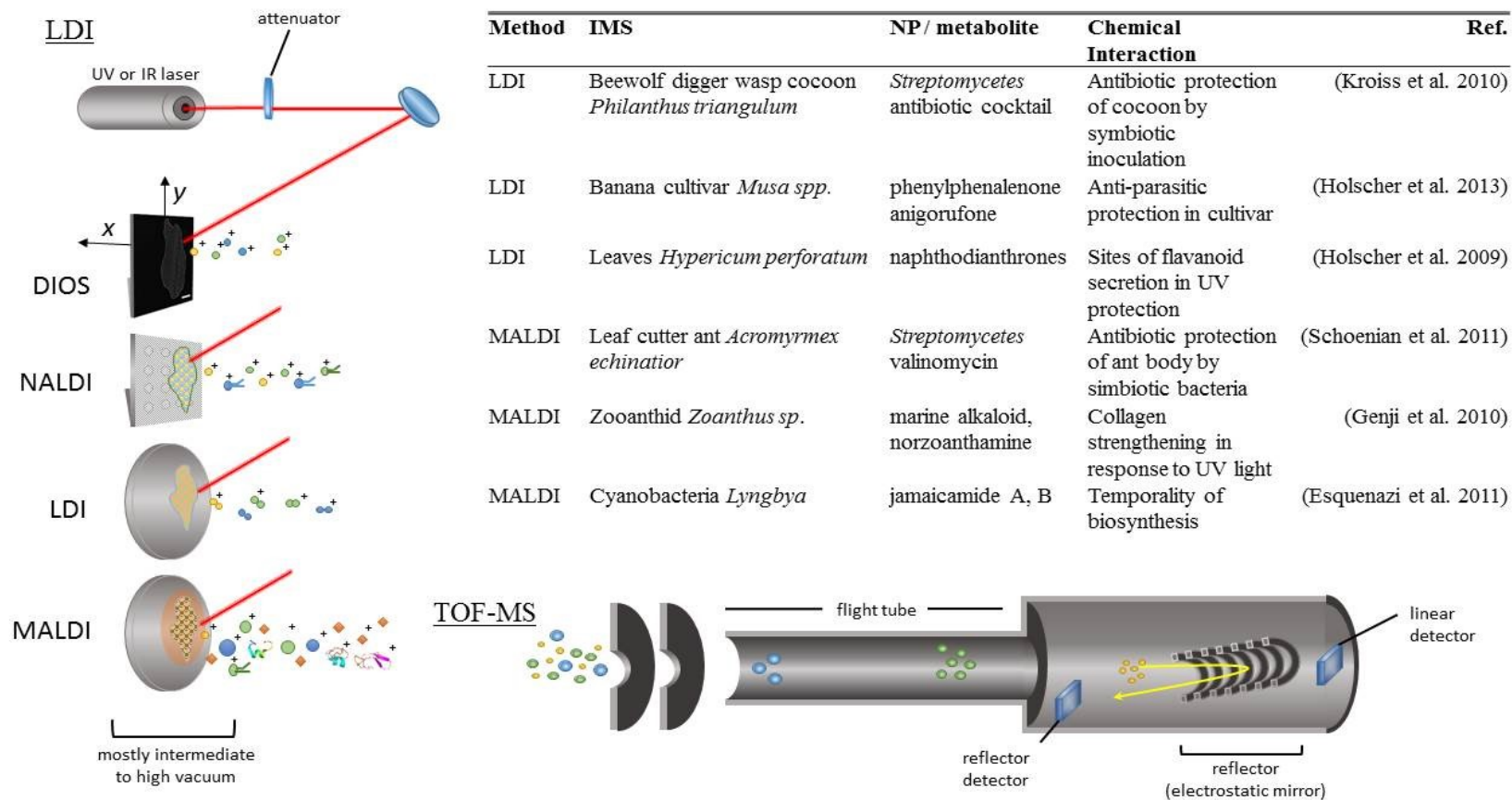
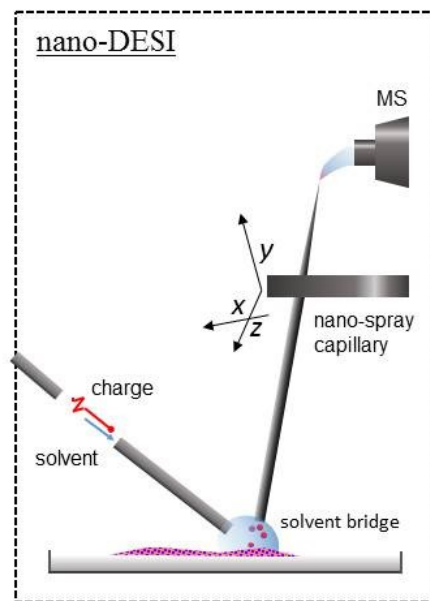
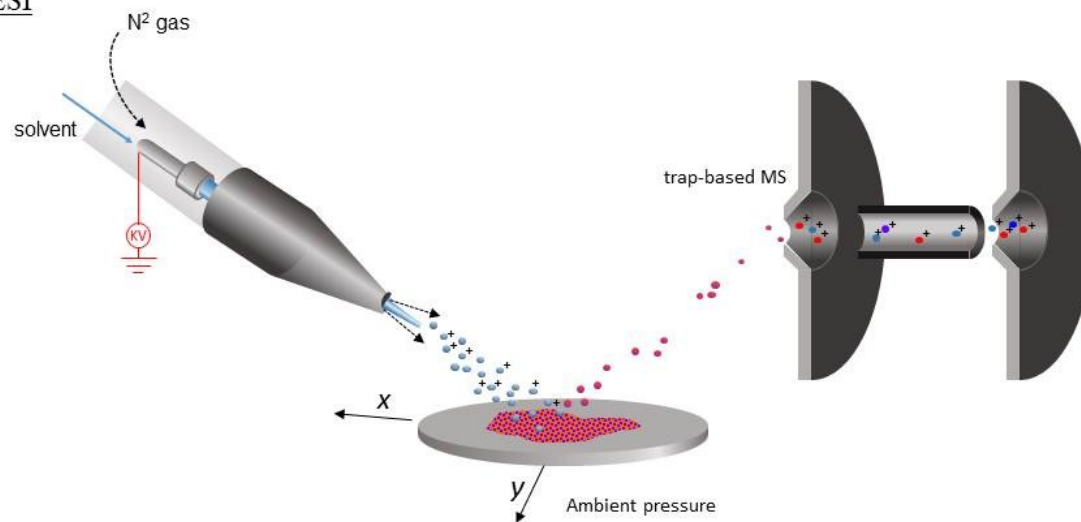


**Figure 1.5** Laser desorption ionisation (LDI) and matrix assisted-LDI (MALDI) mass spectrometry (MS) imaging methods and schematic of time of flight (TOF) analysis with example natural product and chemo-ecological studies (adapted from (Bergman et al., 2014, Watrous and Dorrestein, 2011, Esquenazi et al., 2009, Bouslimani et al., 2014)



DESI



IMS	NP/ metabolite	Chemical Interaction	Ref.
Tropical seaweed	bromophycolides	anti-foulant	(Lane et al. 2009)
Competing bacterial colonies	surfactin plipastatin actinohodin	antibacterial exchange and competition	(Watrous et al. 2010)
<i>In situ</i> bacterial colonies	broad range of secondary metabolites	diverse molecular networks of secondary metabolites	(Watrous et al. 2013)

**Figure 1.6** Ambient desorption electrospray ionisation (DESI) and nanoDESI mass spectrometry imaging methods with example natural product and chemo-ecological studies (adapted from (Bouslimani et al., 2014, Bergman et al., 2014, Watrous and Dorrestein, 2011, Esquenazi et al., 2009).

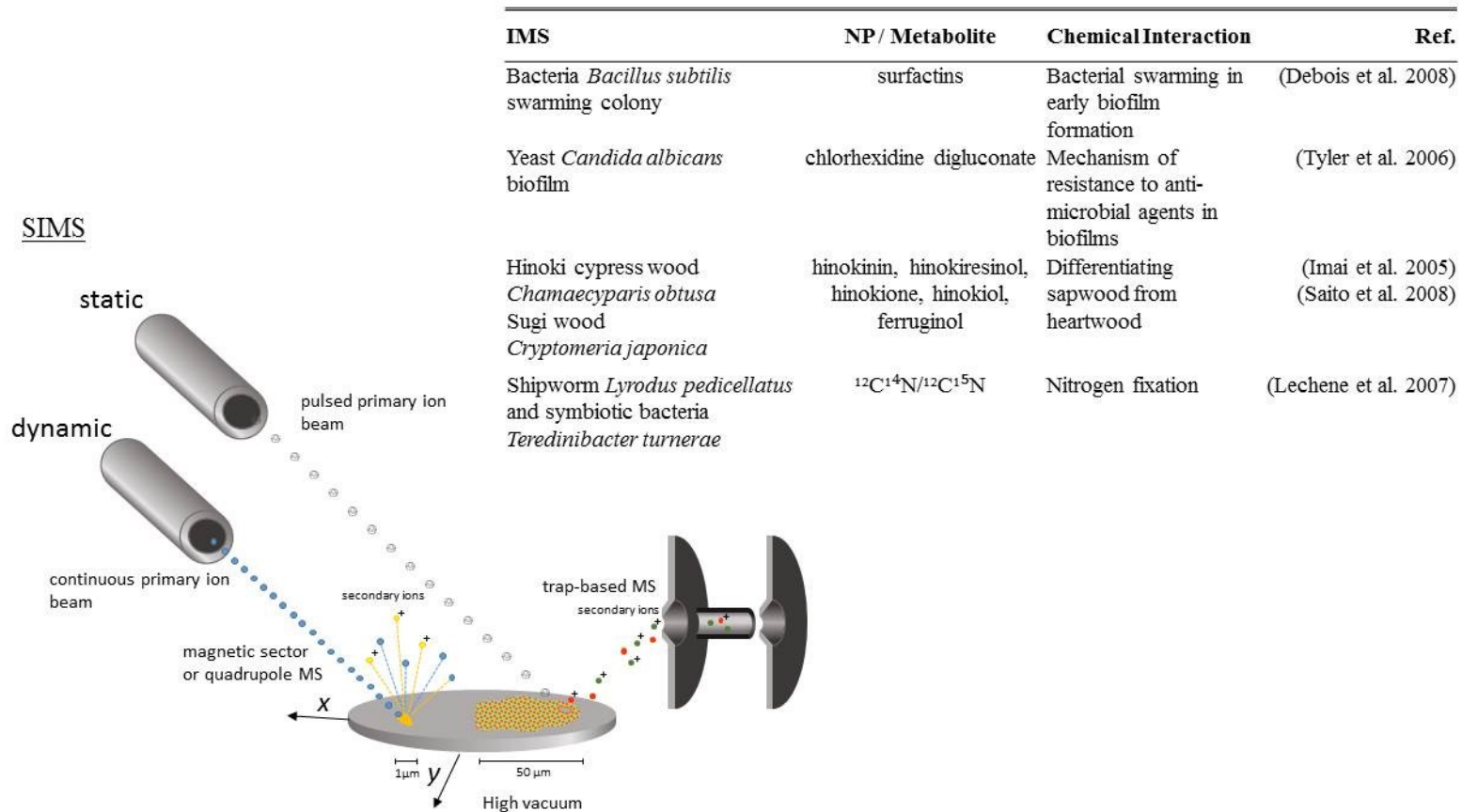


**Figure 1.7** Secondary mass spectrometry (SIMS) imaging methods with examples of natural product and chemo-ecological studies (adapted from (Bouslimani et al., 2014, Bergman et al., 2014, Watrous and Dorrestein, 2011, Esquenazi et al., 2009, Saito et al., 2008).

## **1.6 Muricidae molluscs as models for MNP research**

Developing new MSI techniques for NPs requires a model system in which the NP chemistry is well established and there is available knowledge of the biosynthetic tissues involved. Due to the historical significance of Tyrian purple dye, the utilisation of muricids as a resource and the current research into the bioactive properties of muricid brominated indoles (Benkendorff, 2013) there is a wealth of knowledge on muricid chemical and biological characteristics.

The Muricidae are a highly diverse family of the neogastropods with over 1600 extant describe species (Barco et al., 2010) and a worldwide distribution. Muricid species are typically found on shallow rocky intertidal areas distributed from tropical to polar regions (Ponder, 1998), although particular species have specific habitats, found at depths of >1500m (Barco et al., 2010, Pastorino and Scarabino, 2008). Muricids, like most of the neogastropods, are predators and commonly have a generalist diet, feeding on a range of prey including barnacles, bivalves, limpets, gastropods, polychaetes, small crustaceans and sipunculids (Ponder, 1998). Some studies have found certain species will feed on carrion when available (Ponder, 1998). The generalist diet of muricids makes captive husbandry for experimental purposes possible, with some species able to be maintained on frozen bait (Woodcock and Benkendorff, 2008). Individual sizes range from 6 to 300 mm in length (Ponder, 1998), and due to their predatory nature, muricids are considered important species for structuring intertidal communities (Fairweather, 1988b, Fairweather, 1985).

Muricids are dioecious, although imposex has been recorded in some individuals mainly as a consequence to xenobiotic contaminants (Ramon and Amor, 2001). Females lay large leathery egg masses (D'Asaro, 1992), sometimes communally, which are also amenable to captive holding and experimentation (Benkendorff et al., 2004b). Muricidae egg capsules also contain specific secondary metabolites; the indole

precursors of Tyrian purple (Benkendorff et al., 2004b, Benkendorff et al., 2000, Benkendorff et al., 2001a, Palma et al., 1999). As a consequence, muricids make an excellent model for natural product / chemo-ecological research because they are amenable to observation and experimentation and produce a complex series of halogenated and non-halogenated indole secondary metabolites with uncertain functions.

### **1.6.1 Historical resource as a dye**

The Muricidae family has gained recognition for the production of Tyrian purple, a well described highly valuable dye whose use dates back to 1800 BC in Crete (Cooksey, 2013). This pigmented secondary metabolite is derived from chromogenic secretions originating in the hypobranchial gland (Benkendorff, 2013, Cooksey, 2001, Naegel and Cooksey, 2002). Tyrian purple (6,6 dibromoindigo) is the result of enzymatic, photocatalytic and oxidative reactions from the precursors stored in the hypobranchial gland, (e.g., Figure 1.8), and is only detected in the environment once liberated from the gland (Cooksey, 2001). Tyrian purple was the first marine natural product to be structurally elucidated (Friedlander et al., 1912) and has been the subject of much chemical research due to its historical value (Cooksey, 2013, Baker and Sutherland, 1968, Benkendorff, 2013). The identification of Tyrian purple predates the identification of the associated choline esters, and their presumed ecological function (Erspamer and Benati, 1953, Roseghini et al., 1996) by approximately 60 years.

### **1.6.2 The Muricidae hypobranchial chromogenic secondary metabolites**

The reaction resulting in Tyrian purple is initiated by cleavage of the indoxyl sulfate precursor with an aryl sulfatase enzyme (Figure 1.8), which is also produced and stored in the mollusc hypobranchial gland (Baker and Sutherland, 1968, Laffy et

al., 2013). Baker and Sutherland (1968) were the first to isolate the ultimate precursor, tyrindoxyl sulfate from *D. orbita*, and the sulfatase enzyme capable of hydrolysing tyrindoxyl sulfate, initiating the photocatalytic, oxidative reaction. Intermediate brominated indoles were then identified including the unstable tyrindoxyl, tyrindoleninone (6-bromo-2-methylthio-3*H*-indol-3-one) and tyrindolinone, a methane thiol adduct of tyrindoleninone (Baker and Duke, 1973, Baker and Duke, 1974, Baker and Duke, 1976). A further two intermediates were identified by Baker and Sutherland (1968); the yellow light insensitive 6-bromoisatin, an oxidative product that is the immediate precursor to 6,6'-dibromoindirubin (an isomer to 6,6'-dibromoindigo and minor constituent of Tyrian purple) and the green light sensitive tyriverdin. The structure of tyriverdin was subsequently resolved and shown to be the indole dimer that forms from the reaction of tyrindoxyl and tyrindoleninone (Christophersen et al., 1978). The reaction that forms Tyrian purple in *D. orbita* is one of the more simplified pathways, involving only a single ultimate precursor. The suite of reactions becomes more complex when considering all the possible dye precursors in the Muricidae (Baker, 1974) and the five potential ultimate precursors (Cooksey, 2001), leading to brominated and non-brominated indole dyes.

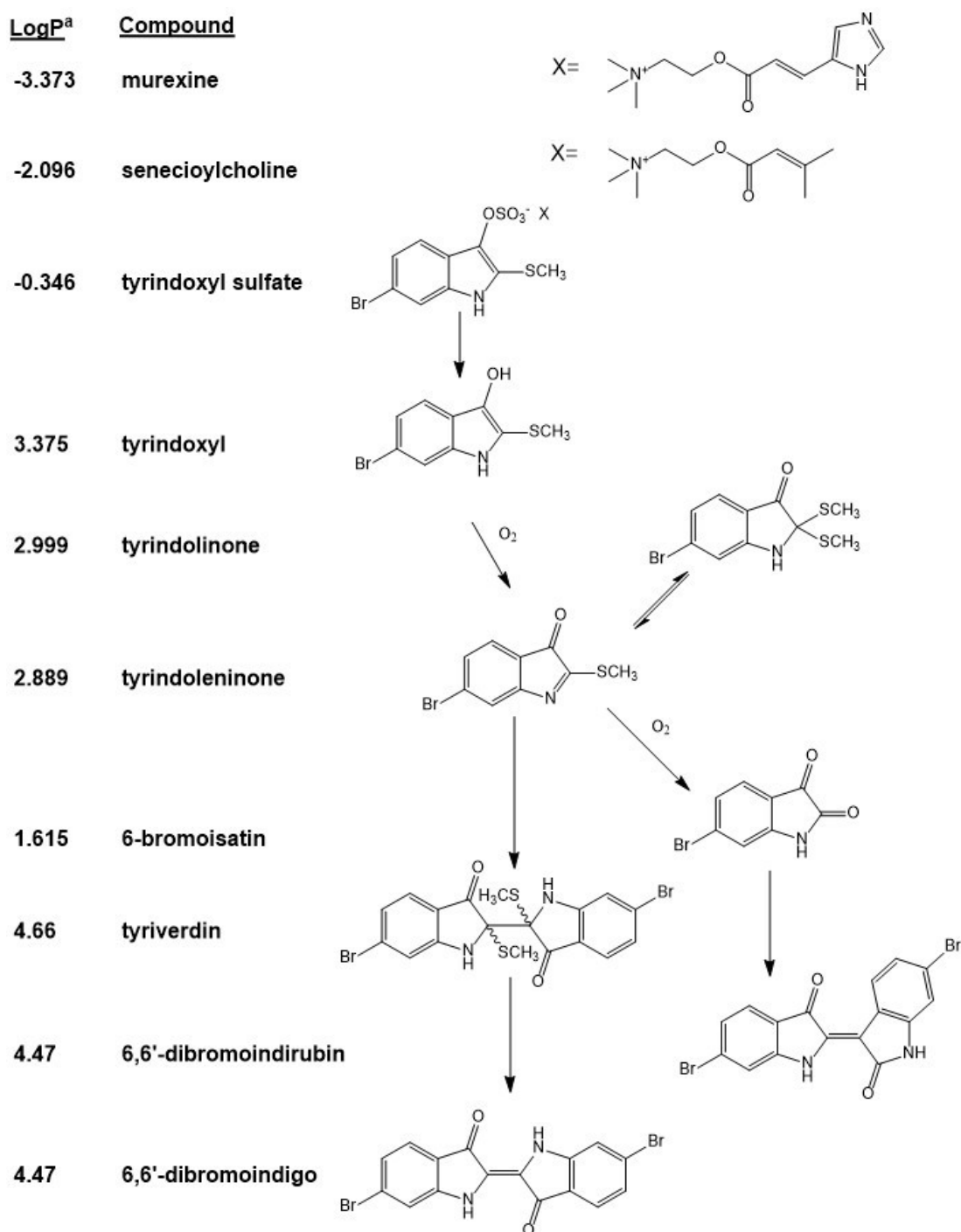


**Figure 1.8** Enzymatic, oxidative and photolytic reaction of bioactive compounds found in *Dicathais orbita* (Muricidae, Mollusca) hypobranchial glands with corresponding solubility indicator and trivial names. <sup>a</sup>LogP is based on octanol-water partition coefficient calculated using the cheminformatics software ChemBioDraw Ultra (v. 13.0, PerkinElmer Informatics, Waltham, MA, USA).

### 1.6.3 Anatomy of muricid biosynthetic organs

The hypobranchial gland in muricids, responsible for the expulsion of choline esters and Tyrian purple precursors, is an antero-posteriorly elongated gland positioned in the dorsal mantle region, extending from the ctenidium. The gland wraps around the rectum on the left dorsal side, with the pallial gonoduct on the opposing side of the rectal gland, together creating a folded secretory region that expels mucus into the mantle cavity (Westley et al., 2010b). Generally, the hypobranchial gland is divided into the branchial, medial and rectal regions, with each region distinguishable by gross morphology and cell type. The tissue is characterised by tall ciliated and non-ciliated columnar epithelial cells, separated from the surrounding tissue by a vascular sinus (Hunt, 1973, Aguilar-Cruz, 2006, Westley et al., 2010a). The secretory regions are situated on sub-epithelial smooth muscle, able to control the expulsion of mucus and bioactive compounds (Westley et al., 2010b, Roller et al., 1995), although some studies have suggested neurological control over expulsion (Srilakshmi, 1991, Hunt, 1973). In the Australian species, *D. orbita*, the hypobranchial tissue is made up of seven different secretory cell types, two of which are unique to Muricidae (Westley et al., 2010a), and therefore likely to be responsible for the synthesis and secretion of Tyrian purple precursors and arylsulfatase enzymes. The presence of goblet cells, abundant in the secretory tissues, also indicates the role of the gland in producing mucus for capture of particulate or fouling matter for periodic cleansing, a feature of all neogastropods (Fretter, 1994).

In females the pallial gonoduct is a contiguous region comprised of the capsule gland (divided into two lateral lobes, a dorsal and a posterior lobe), ingesting gland and albumen gland (Westley et al., 2010b). The pallial gonoduct complex has a central lumen which is responsible for the movement of eggs from the ovaries down the oviduct, into the albumin gland area for the secretion of yolk material, then into the

capsule gland for capsule formation and, finally, shaping in the pedal gland during which fertilisation occurs (Westley et al., 2010b). The detection of tyrindoxyl sulfate in the capsule gland and associated reproductive structures suggests maternal investment of secondary metabolites into reproduction (Benkendorff et al., 2004b, Westley and Benkendorff, 2008). Egg capsule formation also involves the addition of tyrindoxyl sulfate into the capsular fluid, but the exact anatomical feature that facilitates this is unclear (Benkendorff et al., 2000, Westley and Benkendorff, 2009a). Biodistributional studies using MSI on the hypobranchial gland and the reproductive structures, pallial gonoduct and egg capsules, are likely to provide more insight into the biosynthesis and ecological function of specific muricid secondary metabolites.

#### **1.6.4 Muricid intracapsular chemistry**

Both brominated and non-brominated indoles have been detected in muricid egg masses of Australian, Mediterranean and South American species (Benkendorff et al., 2001a). The brominated indoles have been putatively inferred to provide antimicrobial defence to the developing larvae, based on the potent bacteriostatic activity demonstrated for tyriverdin and the milder activity of tyrindoleninone and 6-bromoisatin (Benkendorff et al., 2000). The antimicrobial activity was tested against a range of marine microbes that could act as molluscan pathogens (Benkendorff, 1999). In addition to the indole derivatives in egg masses, other antibacterial compounds, including brominated imidazoles, quinolones and quinoxalines have been detected in muricid capsules (Benkendorff et al., 2004a, Benkendorff, 1999, Benkendorff et al., 2001a), along with some as yet unidentified brominated constituents (Benkendorff, 2013). The anti-microbial role of the brominated indoles is also consistent with the low levels of microbial surface fouling seen on the egg masses of *D. orbita* compared to other molluscan egg masses, such as the cephalopod *Sepioteuthis australis* (Lim et al., 2007).

In addition to anti-microbial brominated indoles, muricid capsules are also protected by mycosporine-like amino acids (MAAs). The MAAs, predominantly mycosporine-glycine, shinorine, porphyra-334 and mycosporine-2-glycine (Przeslawski et al., 2005) can act as sun-screening compounds within the capsular environment (Bandaranayake, 1998). Characterising the secondary metabolite content of the capsular environment warrants further investigation, in particular to identify any unknown constituents. Unknown metabolites in the capsule may be contributing to the perceived anti-microbial role of capsular secondary metabolites, or provide evidence for a new biological purpose, such as the UVA and UVB absorbing abilities of the MAAs. Even the brominated indoles may impart other functional advantages during encapsulated development.

### **1.6.5 Biomedical potential of Muricidae molluscs**

Some of the assumed ecological functions of muricid molluscs have been supported by investigations into the potential bioactivity of the secondary metabolites. In particular, previous research has been conducted on the pharmacological properties of the choline esters (Erspamer and Glasser, 1957), the apoptosis inducing and potential chemo-preventative properties of some of the brominated indoles (Westley et al., 2010c, Edwards et al., 2012, Esmaelian et al., 2013b, Esmaelian et al., 2014), and antimicrobial properties of brominated indoles from egg masses (Benkendorff, 1999, Ramasamy and Murugan, 2005, Benkendorff et al., 2000). Muricid extracts and whole animals have also been used in some traditional medicines (Benkendorff, 2013), and are currently being investigated for further development as a nutraceutical and / or functional food (Benkendorff, 2009, Benkendorff, 2013).

### 1.6.5.1 Anti-cancer properties of brominated indoles

Crude extracts from hypobranchial glands, egg masses and mucus from the Australian species *D. orbita*, are able to induce apoptosis in a range of cancer cell lines (Edwards, 2012, Vine et al., 2007, Edwards et al., 2012, Westley et al., 2010c). Purified brominated indole extracts (tyrindoleninone and 6-bromoisatin) are effective against a range of reproductive cancers cell lines, including cancers of the placenta (Jar cells), granulosa-like cells (steroid production; KGN cells) and ovarian cancer (OVCAR-3 cells), whilst healthy primary granulosa cells and monocytes remained relatively unaffected (Edwards, 2012, Edwards et al., 2012). Brominated indoles were also found to induce apoptosis in colon adenocarcinoma cells (HT29 cells) and colon epithelial cancer cells (CaCo-2 cells) (Esmaelian et al., 2013b). Purified extracts were also tested against a range of other cancer cell lines showing promise against the non-Hodgkin lymphoma cell line (U937 cells), whilst having no effect on freshly isolated mononuclear cells (Vine et al., 2007, Vine, 2002)

Crude chloroform extracts that concentrate the brominated indoles have also demonstrated similar activity *in vivo* to that seen in cell based studies, stimulating an acute apoptotic response to azoxymethane (AOM) induced DNA damage in the distal colon of mice at concentrations of 1 mg/g (Westley et al., 2010c). More specifically, the anticancer activity of 6-bromoisatin, and its potential for the prevention of early stage tumour formation, is further supported by the apoptotic effect of the chemically synthesized compound in a short term colorectal cancer rodent model (Esmaelian et al., 2014). These studies on the anticancer properties of Muricidae extracts and brominated indoles have led to interest in the development of a new nutraceutical (Benkendorff, 2013). Future research into the purification, absorption, biodistribution and the pharmacokinetics/pharmacodynamics of both the crude extract and isolated

brominated indoles is required to promote muricid extracts as a natural medicinal product.

#### **1.6.5.2 Muscle relaxing and nicotinic activity of choline esters**

The choline esters, found in muricid hypobranchial glands, have been tested *in vivo* as muscle relaxants and for inducing short term paralysis (Table 1.4). They have been compared against other approved depolarizing type muscle relaxants (Erspamer and Glasser, 1957, Keyl and Whittaker, 1958, Roseghini et al., 1996). Similarities in the pharmacological properties of the gland extracts and choline esters were demonstrated *in vitro* using the frog rectus abdominis muscle assay (Table 1.4). The choline esters elicited neuromuscular blocking at the motor endplate (Roseghini et al., 1996) on the nicotinic acetylcholine receptor (nAChR) rich muscle. These compounds show a lack of muscarinic activity, mainly seen through no effect on the parasympathetic nerve system. The pharmacological effects suggest specific affinity to the neuro-muscular type (subunits  $\alpha_1$ ,  $\beta_1$ ,  $\delta$ ,  $\gamma$ ,  $\epsilon$ ) nicotinic acetylcholine ligand-gated ion channels (Keyl and Whittaker, 1958), mainly responsible for transmission of nerve impulses from motor nerves to muscle fibres during fast synaptic excitation of voluntary muscle. Keyl and Whittaker (1958) were also able to confirm the neuromuscular blocking activity by detecting depolarization on the endplate region of rat gracilis muscle at concentrations of 3mg/kg (Table 1.4). Murexine binds to post synaptic nAChRs causing an opening of the monovalent cation channel eliciting an endplate potential (Keyl and Whittaker, 1958). Muscle fasciculations measured on the rat gracilis indicate activation of the nAChR for an action potential, but with no immediate elimination of murexine, suggesting murexine to be a nAChR agonist that is not immediately hydrolysed by acetylcholinesterase.

The concentration dependent effect of murexine on twitch reduction has also been tested *in vitro* on cat, dog and rabbit gastro-cnemius, summarised in Table 1.4

(Erspamer and Glasser, 1957). *In vivo* studies using murexine, dihydromurexine and seneciylcholine support the neuromuscular blocking activity seen in the frog rectus assays, where all three choline esters produced head drop in rabbits and paralysis of the back legs in dogs (Erspamer and Glasser, 1957). Further clinical trials on 160 human patients after intravenous (i.v.) administration of murexine demonstrated temporary relaxation (Erspamer and Glasser, 1957) consistent with an nAChR agonist (Table 1.4). *In vivo* nicotinic activity is dose dependant, with low doses having little effect on respiration and blood pressure (Roseghini et al., 1996), whilst high doses above 100-200mg/kg increase blood pressure and respiration in both anaesthetized cats and dogs (Keyl and Whittaker, 1958), indicating sympathetic ganglion stimulation in addition to neuromuscular blocking activity.

There are a number of features of the structure of murexine and other muricid choline esters that influence the potency of their activity as muscle relaxants. When compared to other muscle relaxants, including decamethonium, suxamethonium, gallamine and tubocurarine, the muricid choline esters show greatest similarity in dose and effect to suxamethonium, another depolarizing type of neuromuscular blocker that acts as an nAChR agonist (Erspamer and Glasser, 1957). Hey (1952) outlines the structural characteristics of potent choline esters, including the electron density of the 'ether' oxygen atom and nicotinic activity, possibly related to the affinity for choline esters to fit the ACh receptor site and elicit ion conductance (Hey, 1952, Karlin, 2002). The other major structural feature of the muricid choline esters is the trimethyl ammonium cation ( $O(CH_2)_2N^+(CH_3)_3$ ), as seen on acetylcholine, where it is involved in binding to the receptor via pi-cation interactions. The combination of the ether oxygen and the methyl ammonium could explain some of the similarity between the agonist effect of the two and the action of cholinesterases on reducing the effect in different *in vivo* models (Hey, 1952).

Only a small subset of muricids has been investigated for choline esters (Roseghini et al., 1996). Species in the Muricidae known to contain murexine (M), dihydromurexine (DHM), seneciylcholine (SCH) or tigloylcholine (T) include *Acanthina spirata* (M), *Bolinus brandaris* (M), *Chicoreus brunneus* (M, DHM), *Chicoreus florifer* (DHM), *Chicoreus ramosus* (DHM), *Chicoreus torrefactus* (M, DHM), *Concholepus concholepas* (M, SCH), *D. orbita*, *Hexaplex trunculus* (M), *Murex trapa* (M, DHM), *Murex tribulus* (DHM), *Muricanthus fulvescens* (M), *Nucella emarginata* (nM), *Ocenebra erinacea* (M), *Thais clavigera* (T), *Thais bronni* (T), *Urosalpinx cinerea* (M), and *Urosalpinx heptagonalis* (DHM) (Roseghini et al., 1996, Bender et al., 1974, Shiomi et al., 1998, Duke et al., 1978, Baker and Duke, 1976). Thin layer chromatography (TLC) detection was used to detect the different types of choline esters in various tissue samples of muricid species. Choline ester type was distinguished by spot *R<sub>f</sub>* values on aluminium backed silica or aluminium cellulose plates visualized using Dragendorff reagent or silica gel plates visualized using Pauly's reagent (Roseghini et al., 1996). Identification by TLC alone is rather limited and future investigations using modern analytical methods such as NMR and LC-MS fingerprinting would help confirm the diversity and distribution of choline esters in the Muricidae.

**Table 1.4** Neuromuscular and pain signalling effects of Muricidae extracts and compounds, choline ester & hypobranchial gland (HG) muscle relaxing and nicotinic activity

Effect / origin	Assay / <i>in vivo</i> model	Compound	Conc.	Target
<b>Neuromuscular block</b> HG extract or synthetic murexine	Frog rectus abdominis muscle assay <sup>1,2,3</sup>	M, MCH, DHM, SCH	various	Paralysis of the skeletal musculature after intravenous (i.v.) administration. Murexine binds to nicotinic acetylcholine receptors opening the monovalent cation channel for depolarization of the motor endplate. Mild or no muscarine like activity was detected in guinea-pig and rabbit intestine, rabbit atrium and isolated frog heart assays.
	Neuromuscular block in rat diaphragm assay <sup>1</sup>	M, MCH	0.75mg / assay	
	% Twitch reduction assays on cat, dog and rabbit gastro-cnemius calculated concentration effect <sup>1</sup>	M, MCH	100 - 2,000µg/kg	
	50% rabbit head drop after i.v. injection <sup>3</sup>	M, MCH DHM	0.65mg/kg 0.52mg/kg	
	50% dog paralyzing dose after i.v. injection <sup>1</sup>	M, MCH DHM	0.35mg/kg 0.022mg/kg	
	Relaxing effect in human preliminary clinical trial on 160 patients after a single i.v. injection <sup>1</sup>	M, MCH	1.0 - 1.2mg/kg	
<b>Nicotinic activity</b> HG extract or synthetic murexine	Nicotinic effects of murexine showed a dose dependant rise in blood pressure whilst inducing neuromuscular block in anaesthetised cats and dogs <sup>1,3,4</sup>	M	60µg/kg/min (no effect)	Murexine i.v. at high dose is likely to have nicotinic effects on sympathetic ganglia and adrenal medulla
		M	300µ/kg	

M – murexine was extracted from *Murex trunculus*, *Murex brandaris* and *Tritonalia erinacea*. MCH – murexine chloride hydrochloride (synthetic). DHM – dihydromurexine; and SCH – seneciylcholine are from hypobranchial gland extracts of the above species. Source of data: <sup>1</sup>(Erspamer & Glasser, 1957); <sup>2</sup>(Bender et al., 1974); <sup>3</sup>(Roseghini et al., 1996); <sup>4</sup>(Keyl & Whittaker, 1958).

### 1.6.5.3 Neuromodulatory activity of isatins

Synthetic and natural isatins and their derivatives have structural similarity to endogenous mammalian isatin, the oxidised indole-2,3-dione. Endogenous isatin has a wide range of effects in mammalian systems including behavioural and metabolic functions (Medvedev et al., 2007, Bhattacharya and Chakrabarti, 1998, Bhattacharya et al., 1991). Isatin derivatives (synthetic and naturally derived) therefore exhibit a wide range of effects including anxiogenic, anticonvulsant, sedative, analgesic activity and ion channel activation (Table 1.5). Endogenous isatins have their greatest potency as antagonists of atrial natriuretic peptide (ANP) function and nitric oxide (NO) signalling, both of which are potent vasodilators (Medvedev et al., 2007). Endogenous isatin is known to increase during stress, inhibit monoamine oxidase B, and improve bradykinesia and striatal dopamine levels in rat models of Parkinson disease (Igosheva et al., 2005). After administering labelled [<sup>3</sup>H]isatin *in vivo*, binding can be found in the brain in the hypothalamic nuclei, cortex and hippocampus (Medvedev et al., 2007). Therefore, potential therapeutic agents containing isatins should be carefully administered, as exogenous isatin and derivatives may influence the many endogenous isatin targets (Medvedev et al., 1998). One particular muricid bioactive compound, 6-bromoisatin, is an isomer of synthetic 5-bromoisatin, which has analgesic effects at high doses (Debat, 1972), similar to synthetic isatin (Abel, 1995). Further investigation of 6-bromoisatin in comparison to synthetic isatin may show whether the pharmacological action of 6-bromoisatin is due to the structural similarity, and its interaction with endogenous isatin targets, or whether its effect occurs via another pathway. If the former, 6-bromoisatin may show potential as a neuromodulator (Table 1.5). MSI would be an effective analytical tool for the detection of administered isatin in brain sections.

**Table 1.5** Neuromodulatory activities of isatins, isatin derivatives and 5-bromoisatin

Synthetic / bioactive	Assay / <i>in vivo</i> model	Compound	Conc.	Target
<b>Isatin</b>				
Anxiogenic at low dose	Mice and rats showed axiogenic behaviour in the open-field and elevated plus maze test and the social interaction test via intraperitoneal (i.p.) injection <sup>1</sup>	2,3 dioxoindoline	15-20mg/kg	Monoamine oxidase B inhibition as a contribution to stress related tribulin activity
Sedative at high dose	Mice showed immobility in the forced swim test via i.p. injection <sup>2</sup>	2,3 dioxoindoline	<50mg/kg	Inhibits monoamine oxidase affecting monoamine levels
Proconvulsant at low dose	Isatin i.v. administered after PTZ and 3MPA induced seizures in rats via i.p. injection <sup>2</sup>	indole-2,3-dione	20mg/kg	Atagonise natriuretic peptide receptor A (NPR-A) and NPR-C signalling at low dose due to the metabolite 5-hydroxyisatin
Anticonvulsant at high dose	Effective against PTZ and 3MPA induced clonic convulsions via i.p. injection <sup>3</sup>	indole-2,3-dione	60-80mg/kg	
<b>5-Bromoisatin</b>				
Analgesic	Phenylquinone test i.p. for analgesia in mice showing 90% inhibition after 30mins <sup>4</sup>	5-bromoisatin	200mg/kg	5-bromoisatin was compared to acetylsalicylic and showed comparable analgesia with fewer side effects
	Randall and Selitto test for analgesic comparison given orally to rats <sup>4</sup>	5-bromoisatin	400mg/kg	
	Overall ED50 after 30min reaction time <sup>4</sup>	5-bromoisatin	90mg/kg	

**Table 1.5 continued**

Synthetic / bioactive	Assay / <i>in vivo</i> model	Compound	Conc.	Target
<b>Isatin derivatives</b>				
Skca and IKca ion channel activation	Skca activation in a 15ul cell chamber on human embryonic kidney 293 cell line <sup>5</sup>	indole-2,3-dione-3-oxime or as salt, oxide or hydrate derivative	10uM	SKca and Ikca ion channel associated conditions including respiratory conditions, muscle spasms, convulsive conditions, mood disorders and dementia
Anticonvulsant for ATPA, quisqualate, NMDA seizures and cocaine hypermotility	Administered i.v. to NMRI mice for ATPA rigidity, i.v. to DAB/2 mice for quisqualate seizures, i.v. to NMRI mice for NMDA seizures and orally to NMRI mice for cocaine hypermotility <sup>6</sup>	5,7-dinitro-1-methyl-1H-indole-2,3-dione-3-(0-methyloxime)	0.1-10mg/kg	Excitatory amino acid antagonist blocking glycine and glutamate on the quisqualate, ATPA, AMPA, kainate and NMDA receptors

Source data: <sup>1</sup> Bhattacharya et al. 1991; <sup>2</sup> Abel, 1995; <sup>3</sup> Bhattacharya & Chakrabarti, 1998; <sup>4</sup> Debat, 1972; <sup>5</sup> Jensen et al. 1998; <sup>6</sup> Watjen et al. 1995.

#### 1.6.5.4 *In vivo* toxicity

As muricid choline esters show potent neuromuscular blocking activity, extracts from their hypobranchial glands are likely to have a certain level of toxicity associated with their administration. Table 1.6 compares the *in vivo* toxicity of the various muricid choline esters. The lethal effect of muricid choline esters appears to be attributed to the combination of neuromuscular blocking activity and the effects on the sympathetic nervous system via nicotinic activity. Tigloylcholine (0.92mg/kg) administered i.v. to mice produced tonic tremors, convulsion and jumping, symptomatic of nAChR stimulation, with eventual death after two minutes due to respiratory arrest, possibly from neuromuscular blocking of muscles associated with respiration (Shiomi et al., 1998). Tigloylcholine shows a higher toxicity compared to murexine and dihydromurexine (Shiomi et al., 1998).

Recent studies have also been undertaken on the gastrointestinal and hepatotoxicity of brominated indole extracts from *D. orbita*. In response to two weeks' oral gavage with *D. orbita* crude lipophilic extracts, some minor idiosyncratic effects were seen in histopathological assessment of the gastrointestinal tract and liver samples from <40% of mice (Westley et al., 2013). Synthetic 6-bromoisatin administered daily for two weeks *in vivo* using an AOM colorectal cancer model was used to confirm the anticancer activity seen from the *in vivo* model using crude extracts and in this model 6-bromoisatin showed no effect on mouse weight, blood biochemistry or blood cell morphology, except a reduced K/Na ratio in the blood suggesting a diuretic effect (Esmaelian et al., 2014). Otherwise, the *D. orbita* extract and associated brominated indoles were well tolerated with no weight loss or other indications of ill health (Westley et al., 2013, Esmaelian et al., 2014, Esmaelian, 2014), summarised in Table 1.6.

**Table 1.6** *In vivo* toxicity of muricid natural products and synthetic 6-bromoisatin

Compound (Extract)/Model	Method of administration	Concentration (mg/kg)	Model species	General side effects
<b>Murexine</b>				
LD50	i.v.	6.45	mouse	Paralysis of the skeletal musculature preceded by transient stimulation including muscle tension and fasciculation. Death is caused by anoxia after peripheral respiratory arrest <sup>1</sup>
LD50	s.c.	50	mouse	
LD50 (ineffective)	oral	<1000 ineffective	mouse	
GE	i.v.	0.27	dog	For dogs murexine additionally caused increased saliva and evacuation of urine and faeces but handled 200 times dose with artificial respiration <sup>1</sup>
GE	s.c.	1.35 - 2.16	dog	
GE	i.v.	0.05	pigeon	Birds developed contracture, leg cramp and opisthotonus instead of muscular paralysis <sup>1</sup>
LD	i.v.	0.2 - 0.3	pigeon	
GE	i.b.h.	30-40	octopus	<i>Eledone moschata</i> showed brief stimulation and motor agitation with deep respiratory behaviour <sup>1</sup>
GE	i.v.	1 - 1.2	humans	Muscle relaxation with mild nicotinic effects <sup>2</sup>
<b>Dihydromurexine</b>				
LD50	i.v.	5.57	mouse	Similar to murexine but more potent for mice. 12 times more potent for frog rectus abdominis <sup>1</sup>
<b>Seneciolcholine</b>				
na				Similar to murexine but 1.2 - 2 times more potent for frog rectus abdominis <sup>1</sup>
<b>Tigloylcholine</b>				
LD50	i.v.	0.92	mouse	Considerably more potent than murexine <sup>3</sup>

**Table 1.6 continued**

<b>Compound (Extract)/Model</b>	<b>Method of administration</b>	<b>Concentration (mg/kg)</b>	<b>Model species</b>	<b>General side effects</b>
<b><i>D. orbita</i> brominated indole extracts</b>				
GE	oral	>1	mouse	No mortality after 4 weeks daily oral gavage, no effects on behaviour or any signs of ill health <sup>4</sup>
		>1	rat	No mortality after 1 week daily oral gavage, no effects on behaviour or any signs of ill health <sup>5</sup>
GE	oral	0.5	mouse	Idiosyncratic effects on hepatocytes incl. nonsteroidal fatty change and necrosis <sup>4</sup>
		0.5	mouse	Idiosyncratic gastrointestinal inflammation and ulcers <sup>4</sup>
		1	rat	No mucositic, inflammation, or negative effects of gastric epithelium or blood cells <sup>5</sup>
<b>6 Bromoisatin (syn)</b>				
GE	oral	>1	mouse	No mortality after 2 weeks daily oral gavage, no effects on behaviour or any signs of ill health <sup>6</sup>
		0.25	mouse	Diuretic effects evidenced by reduced K/Na ratio in blood
		1		no negative effects on blood cells, haemoglobin or serum liver enzymes <sup>6</sup>

LD50 – lethal dose for 50% of group; GE – general effects; LD – lethal dose. i.v. – intravenous injection; s.c. – subcutaneous injection. Source data:

<sup>1</sup> Roseghini et al., 1996; <sup>2</sup> Erspamer & Glasser, 1957; <sup>3</sup> Shiomi et al., 1998; <sup>4</sup> Westley et al., 2013; <sup>5</sup> Yazback, Submitted 2015;

<sup>6</sup> Esmaeelian et al., 2014.

### **1.6.6 Extract preparation for nutraceutical application**

The cancer preventative properties of the brominated indoles make them suitable candidates for nutraceutical development but the delivery and formulation of the extract/purified compounds are yet to be resolved. Separation of the choline esters during the extraction process is essential, due to the relative toxicity of the choline esters at higher concentrations and the serious side effects associated with their administration (Table 1.6). The brominated indole *in vivo* models that demonstrate efficacy and show no toxicity (Table 1.6), have relied on a chloroform/methanol extraction process that effectively removes the more polar choline esters into the methanol fraction and retains the brominated indoles in the chloroform fraction (Westley et al., 2013, Yazback et al., 2015, Esmaeelian, 2014). Chlorinated solvents are considered inappropriate for nutraceutical preparations (Administration, 2009). Solvents that are less toxic, such as ethanol and acetone, are more polar and will therefore extract more of the choline esters. Therefore, alternative methods, such as supercritical fluid extraction should be evaluated. CO<sub>2</sub> supercritical fluid extraction has previously been used successfully to extract a range of natural products and organic extracts for nutraceutical preparations (Reverchon and De Marco, 2006).

### **1.6.7 *Dicathais orbita* as a model muricid species**

Commonly known as the Australian dogwhelk or Cartrut shell, *D. orbita* has a wide continuous subtropical/temperate distribution from Fraser Island, Queensland, to North West Cape, Western Australia including Tasmania, as well as New Zealand and Lord Howe Island (Gowlett-Holmes, 2008, Benkendorff, 2013). Found on rocky intertidal and shallow subtidal reefs, *D. orbita* is long lived, with some specimens aged to 19 years, and large, up to 120 mm in length (Phillips and Campbell, 1974, Phillips, 1969, Gowlett-Holmes, 2008). *D. orbita* are common within their habitats and play an

important role in shaping invertebrate community structures, as predatory carnivores mostly preying on sessile bivalves (Fairweather, 1985, Fairweather, 1988a). In fact, *D. orbita* are such effective predators that they are pest predators on molluscan aquaculture farms (Benkendorff, 2009). There has been a considerable amount of ecological field research on the species (Benkendorff, 2013), the phylogeny and systematics are well resolved (Barco et al., 2010), and a wealth biological data are available for these organisms, making them amenable to captive holding and breeding (Benkendorff, 2013). There is also considerable literature on the chemistry of Tyrian purple formation specifically from *D. orbita*, and the associated biosynthetic glands are well studied (Westley, 2008, Benkendorff, 2013). One specific attribute making *D. orbita* a particularly useful model species over other muricids, is the presence of a single dye prochromogen, tyrindoxyl sulfate (Baker and Sutherland, 1968), providing a simplified biosynthetic pathway and dye development to Tyrian purple.



**Figure 1.9** Adult *Dicathais orbita* on the rocky intertidal platform of Ballina Flat Rock beach, New South Wales, Australia.

## **1.7 Thesis aims and objectives**

The aims of this thesis are to develop new analytical and preparative tools for investigating the chemo-ecological relevance and aid the nutraceutical development of muricid choline esters and brominated indole secondary metabolites. To achieve these aims, a new approach to MSI involving tissue imprinting on nanosurfaces, that is more sensitive to the analysis of low molecular weight metabolites, will be developed for biodistributional investigations of muricid tissues. The MSI method will then be applied to the investigation of secondary metabolites over the reproductive cycle of *D. orbita*, and will be followed up with a larval bioassay to test a new hypothesis on the functional role of murexine generated by the MSI data. Finally, a new method for selective extraction of the bioactive brominated indoles will be tested using supercritical CO<sub>2</sub>. These technological innovations will aid the further development of the brominated indoles or extracts from Muricidae as therapeutic agents, specifically

by providing: 1) a method that can be applied to future biodistributional studies in animal models; 2) information on the spatial and temporal changes in the abundance of the bioactive compounds to maximise extraction efficiency; and 3) a safe targeted extraction method for future drug formulation.

### 1.7.1 Thesis structure

This thesis is presented in manuscript format, where each research chapter has been published or submitted for publication in suitable peer reviewed journals. Although there may be some overlap in introduction content, each chapter has built on the thesis aim and comprises a progressive body of research. The thesis has been formatted in a consistent style and references have been compiled into a single list at the end. I am first author on all chapters except the publication / submitted work resulting from parts of the introduction and work in chapter 2, which required a collaborative effort involving specific technical knowledge related to the surface chemistry and mass spectrometry imaging.

The literature review in **Chapter 1** has been included into two articles planned for publication as follows:-

Benkendorff, K., **Rudd, D.**, Nongmaithem, B.D., Liu, L., Young, F., Edwards, V., Avila, C., Abbott, C.A. Are the Traditional Medical Uses of Muricidae Molluscs Substantiated by Their Pharmacological Properties and Bioactive Compounds? *Marine Drugs* **2015**, *13*, 5237-5275

**Rudd, D.**, Roach, M., Harris, J., and Benkendorff, K. 2015. Versatile marine venoms: *In situ* analysis and functional ecology. This manuscript will outline effective analytical methods used to describe functional ecology in marine organism interactions. A suitable ecology and evolutionary journal.

**Chapter 2** has been published as follows:-

Ronci, M., **Rudd, D.**, Guinan, T., Benkendorff, K. and Voelcker, N.H. 2012. Mass spectrometry imaging on porous silicon: Investigating the distribution of bioactives in marine mollusc tissues. *Analytical Chemistry* **84** (21): 8996 - 9001

Within **Chapter 2**, I prepared the histological and cryostat sections of molluscan tissue, developed the new method for tissue imprinting on the nanosurfaces, received training in MSI imaging from the first author, (postdoctoral research fellow Dr Maurizio Ronci), and participated in the MSI data collection and interpretation. For the manuscript, I also prepared Figure 1 and contributed to Figures 2 and 3 (selecting intensity maps), and drafted substantial sections of text, including background information on *D. orbita* and Muricidae chemistry for the Introduction and “Tissue preparation” for the experimental section, as well as contributing to the Results and Discussion. The first author Ronci optimised the parameters for MSI imaging on NALDI and pSI surfaces and was principally responsible for the data acquisition, as well as drafting the other technological sections of the manuscript. Co-author Guinan fabricated the pSI surfaces and assisted with some of the data acquisition. Guinan worked under the supervision of co-author Voelcker who facilitated the study and provided further technological input. Co-author Benkendorff is my supervisor who originally initiated the collaboration and provided background knowledge that contributed to the interpretation of mass spec data for Muricidae brominated indoles, as well as contributing to the draft manuscript.

The LDI-MSI training gained during the research for Chapter 2 enabled me to undertake data acquisition and interpretations independently in subsequent Chapters 3 & 4.

**Chapter 3** is published in *Marine Drugs* as follows:-

**Rudd, D.**, Benkendorff, K. and Voelcker, N.H. 2015. Solvent separating secondary metabolites directly from biosynthetic tissue for surface-assisted laser desorption ionisation mass spectrometry. *Marine Drugs* Special Issue - Advances in Separation, Characterisation and Chemical Profiling Methodologies, **13** (3), 1410-1431; doi:10.3390/md13031410

Within the Chapter 3 manuscript, I conceived and designed the study and conducted the data collection and analysis with guidance from my supervisor and co-author Benkendorff. Co-author Voelcker provided the nanosurfaces and technical input on the surface chemistry. I wrote the draft of the manuscript with some input from Benkendorff and editorial comments from Voelcker.

**Chapter 4** is published in *Nature Scientific Reports*, as follows:-

**Rudd, D.**, Ronci, M., Johnston, M. R., Guinan, T., Voelcker, N. H., and Benkendorff, K. 2015. Mass spectrometry imaging reveals new biological roles for choline esters and Tyrian purple precursors in muricid molluscs. *Scientific Reports*, vol. 5, art. 13408.

For the manuscript in Chapter 4, I designed the study with advice from my supervisor co-author Benkendorff and undertook all of the sample preparation, the MS analyses, MSI data acquisition and larval bioassays. Ronci provided technical input for the MSI data acquisition and interpretation, whereas co-author Johnston assisted with the NMR analyses. Guinan fabricated the pSI surfaces and assisted me in the acquisition of data for the MSI co-localisation. Voelckner facilitated the study and provided the technical input for the nanosurface chemistry. I prepared the draft manuscript with some input from Benkendorff and edits from the other co-authors.

**Chapter 5** has been published as follows:-

**Rudd, D.**, Benkendorff, K. 2014 Supercritical CO<sub>2</sub> extraction of bioactive Tyrian purple precursors from the hypobranchial gland of a marine gastropod. *Journal of Supercritical Fluids*, **94**:1-7

I designed, conducted, analysed the data and prepared the draft manuscript for Chapter 5 with guidance from my supervisor and co-author Benkendorff.

**Appendix III** results are planned for publication as follows:-

**Rudd, D.**, Guinan, T., Gustafsson, J., Krysinska, H., Pogson, L., Esmaelien, B., Voelcker, N. H., Abbott, C. A., and Benkendorff, K. 2015. Mass spectrometry imaging the absorption, distribution, metabolism and excretion of a halogenated marine natural indole. A suitable biochemistry journal.

## **1.7.2 Chapter objectives**

**Chapter 2:** Mass spectrometry imaging on porous silicon: investigating the distribution of bioactives in marine mollusc tissues.

*Objectives:* The aims of Chapter 2 are to demonstrate the application of SALDI-MSI, including DIOS-MSI and NALDI-MSI, for detecting the distribution of the brominated indoles from *D. orbita* hypobranchial tissue. My primary objective was to develop an imprinting method onto the nanostructured surfaces, which could allow the low molecular weight brominated indoles to desorb/ionise without significant signal suppression and maintain spatial distribution. A secondary objective was to compare the attributes of the two surface chemistries; silanized porous silicon and NALDI silane vapour-grown silicon nanowires. Data generated from the DIOS-MSI allow for surface chemistry alterations, specifically functionalization, of the subsequent porous silicon surfaces as MSI substrates for chapter 3 and 4.

**Chapter 3:** Solvent separating secondary metabolites directly from biosynthetic tissue for surface-assisted laser desorption ionisation mass spectrometry

*Objectives:* The methods of Chapter 3 utilise the surface chemistry of DIOS and NALDI as a chromatographic tool for elucidating region specific spectral signals from hypobranchial tissue. As annotation is one of the major hurdles when using MSI, the surface assisted MS and the chemical properties of the secondary metabolites (polarity, solubility and halogenation) can be used in the identification of secondary metabolite signals. The primary objective was to validate and annotate the spectral signals detected in Chapter 2 based on the polarity of each specific secondary metabolite in different solvents. The secondary objective was to determine if SALDI-MSI can be used for the relative quantification of secondary metabolites from tissue sections by calibrating the LDI-MS signal intensities from standard dose curves.

**Chapter 4:** Mass spectrometry imaging reveals new biological roles for choline esters and Tyrian purple precursors in muricid molluscs

*Objectives:* Chapter 4 builds on the methods developed in Chapter 2 and the capacity of the surfaces to be used for annotation of muricid MSI data, specifically using DIOS-MSI based on how effective porous silicon is in desorbing/ionising brominated indoles. In Chapter 4, DIOS-MSI is used as a descriptive tool for tracking the movement of brominated indoles and choline esters during the female reproductive cycle, including capsular development of the larvae. The primary objective was to determine the potential role of specific secondary metabolites within the tissue based on their location, the bioactive properties and our knowledge of the anatomy and behaviour of the species. The secondary objective was to test a new putative role for the choline ester murexine using a larval activity bioassay.

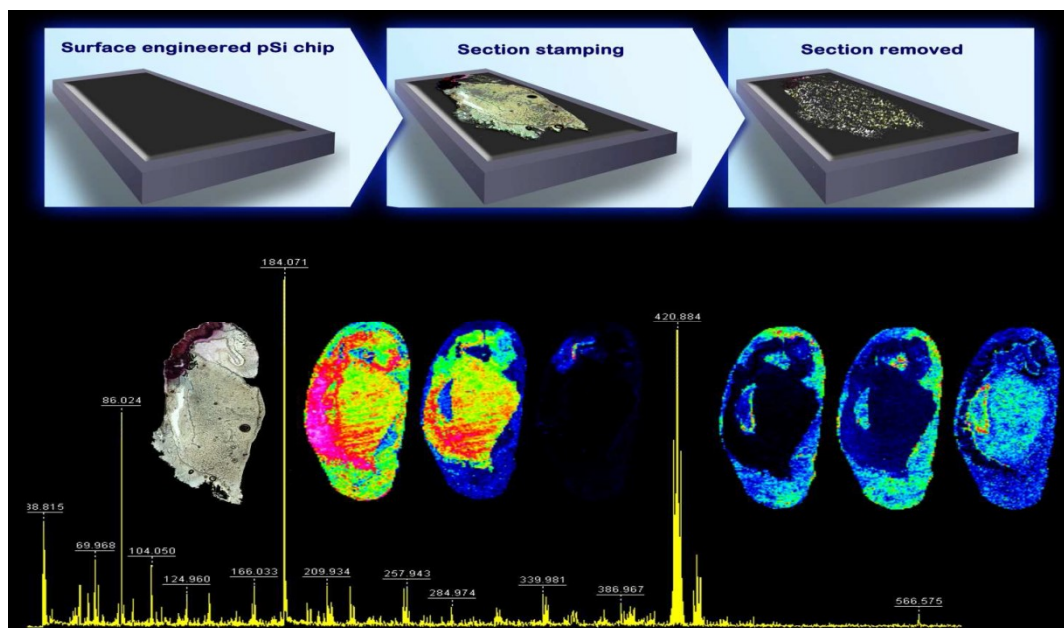
**Chapter 5:** Supercritical CO<sub>2</sub> extraction of bioactive Tyrian purple precursors from the hypobranchial gland of a marine gastropod

*Objectives:* The methods of Chapter 5 utilise the chemical properties and solvent characteristics determined in Chapter 3 to develop a new method for the targeted extraction of intermediate brominated indoles from hypobranchial tissue using supercritical CO<sub>2</sub>. The primary objective of this chapter was to establish an alternative method for the extraction of the bioactive brominated indoles that eliminates the use of chlorinated solvents. The secondary objective was to refine this method for the selective extraction of tyrindoleninone and 6-bromoisatin, the main bioactive fraction, using different pressure regimes.

**Chapter 6:** General Discussion -MSI as a descriptive tool in the chemo-ecological study of Muricidae secondary metabolites and future directions in mollusc natural product research.

*Objectives:* A summary of the research findings are outlined in Chapter 6, which also aims to explore the methodological innovations and resulting findings in the broader context of chemical ecology and natural product research. The chapter includes aims to promote MSI as a sophisticated top-down analytical tool for chemo-ecology and recommends future investigations utilising similar MS methodologies. The future direction of research into muricid secondary metabolite biosynthesis will be explored. Specifically, the use of MSI on porous silicon for the evaluation of administered crude extracts and 6-bromoisatin in a colorectal cancer rodent model is discussed. The effectiveness of the pSi in detecting the brominated indole spatial distribution is ideal for *in vivo* tissue studies. The use of supercritical CO<sub>2</sub> as an extraction medium will also be discussed in light of future formulation and purification efforts.

## 2 Chapter Two – Mass spectrometry imaging on porous silicon: investigating the distribution of bioactives in marine mollusc tissues



### 2.1 Abstract

Desorption/ionisation on porous silicon-mass spectrometry (DIOS-MS) is an effective alternative to conventional matrix-assisted laser desorption/ionisation mass spectrometry (MALDI-MS) for the analysis of low molecular weight compounds, including primary and secondary metabolites. Porous silicon (pSi) chips act as suitable supports for mass spectrometry imaging (MSI). Here, we describe the implementation of DIOS-MSI using the biosynthetic hypobranchial gland of a marine mollusc as proof of principle. Tissue sections were stamped onto a fluorocarbon-functionalized pSi chip, which extracts and traps small hydrophobic metabolites from the tissue whilst retaining the relative spatial distribution. The sections were subsequently removed and the pSi was imaged without the layer of remaining tissue. We applied this novel tissue contacting approach to investigate the distribution of biologically active brominated precursors to Tyrian purple from the hypobranchial gland of marine mollusc, *Dicathais*

*orbita*, with DIOS-MSI. The tissue contact printing is also viable with other types of desorption/ionisation surfaces, such as nanoassisted laser desorption/ionisation (NALDI) target.

## 2.2 Introduction

MSI of biological tissue is becoming a popular tool within the scientific community, mainly as a routine complementary method of proteomic workflows, but also as a valuable source of information in drug development, metabolomics, and pharmacokinetics studies (Franck et al., 2009, Hsieh et al., 2010). In particular, small molecule MSI can dramatically speed up the drug development phase for novel drugs, through the ability to rapidly and efficiently collect valuable information about the distribution of drugs and metabolites in various organs after *in vivo* administration. However, standard MALDI-MSI in the low mass range (less than 1kDa) is challenging due to the interference of intense matrix signals suppressing signals from the less abundant target compounds.

Recently, Yanes et al. (2009) introduced a novel matrix-free tissue MSI approach using pSi functionalized with perfluorinated siloxane [bis(heptadecafluoro-1,1,2,2-tetrahydrodecyl) tetramethyldisiloxane] which was coined nanostructured initiator mass spectrometry (NIMS) (Yanes et al., 2009, Patti et al., 2010). NIMS is a further development of DIOS, which was initially described in 1999 by Siuzdak and collaborators (Wei et al., 1999) as a technique that is extremely well suited for small molecule analysis since it does not require conventional MALDI matrices for desorption/ionisation to occur (Go et al., 2003, Shen et al., 2001, Kruse et al., 2001, Thomas et al., 2001). DIOS employs a pSi layer as an effective medium for trapping and desorbing analyte molecules (Stewart and Buriak, 2000). The porous substrate features a high surface area ( $\sim 600 \text{ m}^2 \text{ cm}^{-3}$ ) in combination with high ultraviolet

absorptivity and substantial thermal and electrical conductivity, allowing the silicon structure to act as a laser energy receptacle and achieving efficient analyte ionisation and sensitive detection (Hu et al., 2007, Lowe et al., 2010). Furthermore, chemical modifiers can be covalently bonded to the pSi surface, thus enhancing or modulating the affinity for target compounds in an analogous fashion to conventional solid-liquid extraction (Trauger et al., 2004, Lowe et al., 2009, Go et al., 2007). Therefore, the pSi acts simultaneously as a support, an absorption substrate, and an ionising agent thereby facilitating extraction, enrichment, and detection in a single step.

However, surprisingly, the potential of NIMS imaging for the detection of small molecules in biological tissue has not been thoroughly evaluated (Calavia et al., 2012). This may be related to the need for extremely thin tissue sections of  $<5\ \mu\text{m}$  which are difficult to prepare and require special cryosectioning skills (Yanes et al., 2009). Furthermore, a major challenge for effective implementation of MSI on pSi is the development of a suitable mechanism for transferring the small molecules from biological tissues sections onto the pSi surface, without significant contamination from large biological molecules. We conjecture that contact printing of the tissue would allow extraction of small molecules into the porous layer. Indeed, Vidova and co-workers (2010) and, very recently, Tata and co-workers (2012) reported a tissue printing approach for the MSI analysis using a NALDI target plate (Vidová et al., 2010, Tata et al., 2012), but their applications were limited to the imaging of lipids.

In order to test extraction properties and mass imaging capabilities of surface-engineered pSi, we selected as model tissue the hypobranchial gland of a marine mollusc known for the production of bioactive brominated indoles. The Muricidae family of predatory marine molluscs is well-known for the production of Tyrian purple (Cooksey, 2001, Westley et al., 2006, Westley and Benkendorff, 2008), a historically important colour-fast natural dye. The main pigment in Tyrian purple, 6,6'-

dibromoindigo, was the first marine natural product ever to be structurally elucidated (Friedlander et al., 1912), and yet, over a century later, still very little information is available regarding the biosynthesis of this compound and its bioactive precursors. Preclinical studies have revealed that extracts from *Dicathais orbita* containing the precursor tyrindoleninone and the oxidation product 6-bromoisatin specifically induce apoptosis in cancer cells *in vitro* (Edwards et al., 2012, Benkendorff et al., 2011) and in DNA-damaged cells *in vivo* (Westley et al., 2010c), thus generating renewed interest in the biosynthesis of these unique brominated indoles. The hypobranchial gland is the main biosynthetic organ responsible for the production of brominated indoles in the Muricidae family (Westley and Benkendorff, 2009a). Histological studies on *D. orbita* have revealed seven secretory cell types across three distinct regions: the medial, branchial, and rectal hypobranchial gland (Westley et al., 2010b), simply defined by their anatomical location.

Here, we describe a novel application of DIOS-MSI and NALDI-MSI, using contact printing of tissue sections to study the distribution of biologically active low molecular weight compounds in the hypobranchial gland of *D. orbita*. Our method combines the advantage of generating “clean” spectra in the low mass range with very limited analyte diffusion across the pSi surface. This could ultimately lead to an improvement in the achievable lateral resolution compared to conventional MALDI-MSI. Furthermore, the possibility to selectively extract different classes of compounds by changing the surface chemistry of the substrate, together with fast sample preparation, acquisition times, high sensitivity, and longer source cleaning intervals, make DIOS-MSI an attractive alternative for metabolomics and drug-development studies.

## 2.3 Experimental Section

### 2.3.1 Materials

Methanol (99.9%) and hydrofluoric acid (HF, 48%) were obtained from Merck (VIC, Australia). Ethanol (EtOH, 100% undenatured) was purchased from Chem Supply (SA, Australia). (Pentafluorophenyl) dimethylchlorosilane (F5PhPr) was purchased from Gelest Inc. (Morrisville, PA, USA).  $\alpha$ -Cyano-4-hydroxycinnamic acid (CHCA) used for calibration, peptide calibration standard mix, and NALDI targets were from Bruker-Daltonics. All buffers and solutions were freshly prepared in Milli-Q grade water.

### 2.3.2 pSi fabrication

Monocrystalline (0.008–0.02  $\Omega$  cm) antimony doped n-type Si (100) wafers from Silicon Quest International (Santa Clara, CA) were cut with a diamond cutter into 3.5 cm  $\times$  3.5 cm squares. The cleaning process was carried out by sonicating the wafers in 99.9% methanol and drying under a stream of nitrogen. The pSi arrays were fabricated by light-assisted anodic etching of cut Si wafers (Lowe et al., 2009). Photopatterned pSi arrays were clamped into a custom-built Teflon cell contacting a gold foil anode (Space Products International, CA, USA). A 0.5 mm diameter platinum wire (99.9 %, Aldrich, WI, USA) formed into a ring was used as a cathode. A 1:1 HF:EtOH electrolyte solution was filled into the Teflon well. The Si surface was illuminated using a fiber optic light source which passed through a set of two aspheric lens,  $f = 80$  mm (OptoSigma, CA, USA) for collimation. A constant current of 20 mA was then applied across the cell for 2 min using a source meter program, created in LabView 6.1 to control a 2425 current source meter (Keithley, Ohio, U.S.A). The pSi surfaces were then subjected to several methanol washes, before being dried under a stream of nitrogen gas.

### **2.3.3 Oxidation and functionalization**

The freshly-etched pSi was ozone-oxidized at a flow rate of 3.25 g/hr using an Ozone-Generator 500 (Fischer, Germany). Following oxidation, the wafer was subjected to a second pore broadening etch using 5 % HF/H<sub>2</sub>O for 30 s. Subsequently, the double etched surface was ozone oxidized (as above) for a second time. The hydroxyl-terminated surface was then silanized via the addition of 80 µl of neat silane (F5PhPr) for 15 min at 90 °C. After silanization, the pSi arrays were washed with methanol, dried under a stream of nitrogen gas and then stored in a desiccator until required.

### **2.3.4 *D. orbita* collection and dissection**

Live *D. orbita* specimens were collected from rocky intertidal shorelines along Southern Metropolitan beaches in South Australia. Samples were prepared by cracking the junction of the primary body whorl and spire with a small vice. The body was removed from the shell by cutting the columnar muscle and the whole soft body was rinsed in MilliQ water to remove excess salt. The dorsal mantle and pallial gonoduct were separated from body and soaked in MilliQ water for 60 min to reduce salt content in the gland section, which would lead to ionization suppression. The hypobranchial gland and pallial gonoduct were removed by an incision along the connection between the ctenidium and the branchial hypobranchial and the posterior gonoduct and S-3 digestive gland. The hypobranchial was then placed in a 5 ml cryovial and snap frozen in liquid nitrogen.

### **2.3.5 Tissue preparation**

Hypobranchial glands were mounted onto cryosectioning specimen holders and held down with a minimal amount of embedding medium (OCT Compound, Tissue-

Tek), ensuring against the transfer of any medium onto the section to be used for the MSI analysis. Glands were cryosectioned, using a cryostat (Leica 1800), onto glass slides to a 10–15  $\mu\text{m}$  thickness for the optical image acquisition or to 30  $\mu\text{m}$  thickness onto the target (either functionalized pSi chip or NALDI plate). In the latter case, the sections were kept for at least 30 min in a desiccator in order to promote tissue–surface interactions leading to the extraction of the small molecules by affinity. The target was subsequently immersed in Milli-Q water at 90 °C for 10 min. A stream of hot water from a pipette was used to help wash the tissue off the surface. The target was then rinsed twice with Milli-Q water and once with methanol and mounted on a customized ground steel target plate (pSi chip) or on the NALDI adaptor (NALDI target). Optical images of the sections on the glass slides were acquired using a Zeiss Axio Imager microscope with Axio imaging software. Images of the sections on pSi or NALDI surfaces were acquired with a conventional desktop scanner (Epson V700 Photo Scanner) before washing off the tissue.

### **2.3.6 DIOS-MSI analysis**

MSI analysis was performed using an Autoflex III TOF/TOF mass spectrometer (Bruker-Daltonics GmbH, Bremen, Germany) equipped with a SmartBeam 200 Hz laser in reflectron positive (RP) mode, in the range of 20–1000 Da with a spatial resolution of 100  $\mu\text{m}$  and the laser focus set to medium, corresponding to a diameter of about 50  $\mu\text{m}$ . Fleximaging 2.1 (build 25, Bruker-Daltonics) was used to control Flexcontrol 3.3 (build 85) during the acquisition and to extract the ion intensity map images after processing the data sets by baseline subtraction, normalization, and data reduction.

### 2.3.7 Mass spectrometer parameters

Quadratic external calibration of the TOF tube was performed, before each acquisition, using CHCA adducts together with Bradykinin (1-7) and Angiotensin II. In particular, the following monoisotopic masses were used for calibration:  $K^+$  38.9637, CHCA  $[M+HH_2O]^+$  172.0399, CHCA  $[M+H]^+$  190.0504, CHCA  $[M+Na]^+$  212.0324, CHCA  $[2M+H-CO_2]^+$  335.1032, CHCA  $[2M+H]^+$  379.0930, Bradykinin (1-7)  $[M+H]^+$  757.3991 and Angiotensin II  $[M+H]^+$  1046.5418. Instrumental parameters were set as follows: 19.00 kV and 16.80 kV for the ion source 1 and 2, respectively, 8.25 kV for the lens and 21.00 kV and 9.40 kV for reflector 1 and 2, respectively. Fleximaging 2.1 (build 25) (Bruker-Daltonics) was used to control Flexcontrol 3.3 (build 85) during the acquisition and to extract the ion intensity map images, after processing the datasets by baseline subtraction, normalization and data reduction.

## 2.4 Results

### 2.4.1 SALDI-MSI contact printing

The hypobranchial gland of the marine mollusc *D. orbita* provides a good tissue model to investigate the ability of pSi to act as a support for tissue imaging in the low mass range, since it produces brominated metabolites easy to identify from their mass spectra based on the molecular ions with isotopic clusters for mono- and dibrominated compounds (Westley and Benkendorff, 2008)

Yanes and collaborators demonstrated the concept of tissue imaging with NIMS on mouse brain sections of 2–4  $\mu\text{m}$  thickness (Yanes et al., 2009). The preparation of such thin tissue sections was necessary in order to obtain good quality mass spectra since ionization occurs only after the tissue has been ablated by several laser shots. In fact, ionization only occurs when the laser light reaches and is absorbed by the

underlying pSi surface. However, histologically different regions may well behave differently when irradiated with laser light, potentially leading to a non-uniform ablation of the tissue and, hence, imaging artefacts. In fact, our preliminary experiments on the hypobranchial gland tissue from *D. orbita* following Yanes' protocol did not show acceptable results (data not shown). It is possible that the abundance of mucus in this tissue prevented ablation even at high laser fluency.

Previous work, including that from our own lab (Thomas et al., 2001, Lowe et al., 2009), has shown that hydrophobic pSi surfaces allow effective extraction of analytes from biological matrices. Hence, we decided to take a different approach (Vidová et al., 2010) and stamp the target tissue onto the pSi surface, allowing time for molecule extraction and MSI analysis of the pSi surface after section removal. By using this contact printing technique on pSi and NALDI targets, the tissue is removed prior to imaging acquisition, and there is no need to use extremely thin sections as required for NIMS. In fact, 20–30  $\mu\text{m}$  thick sections are suitable, which are straightforward to prepare. First, we tested different thickness, from 10 to 60  $\mu\text{m}$ . Our results suggest that the thickness of the section has little effect on the acquisition because the tissue is removed before the analysis (Figure 2.1). We selected 30  $\mu\text{m}$  since this section thickness can be achieved by an operator without particular sectioning skills.

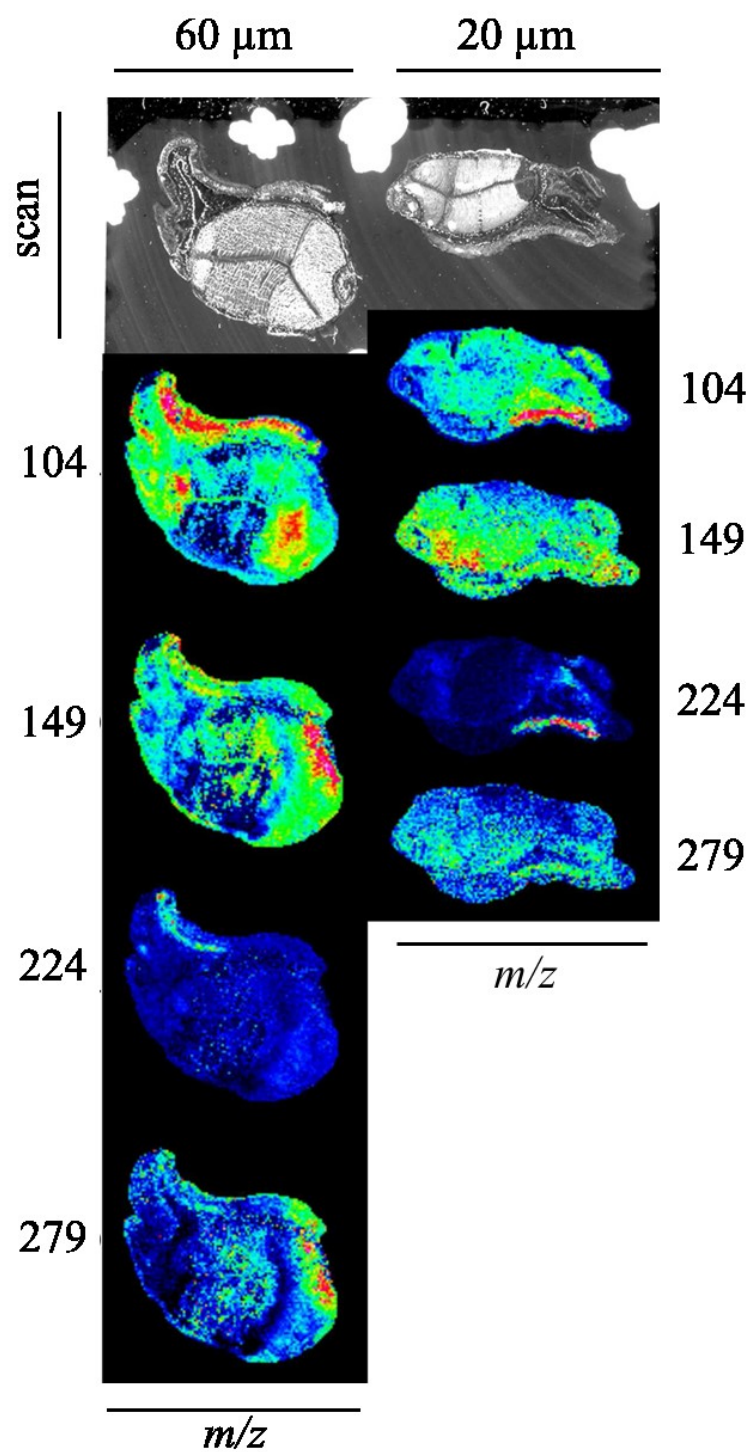


**Figure 2.1** Serial sections of hypobranchial gland of a female sea snail, *D. orbita* of 20 and 60  $\mu\text{m}$  thicknesses. The area under the sections have been analysed by DIOS-MSI after the removal of the tissue in order to evaluate the optimal thickness. Four signals are shown as ion intensity maps and show similar distribution. The effect of the thickness on the imaging performances is negligible.

### **2.4.2 *D. orbita* hypobranchial tissue**

Figure 2.2 shows two optical microscopy images of cryosections of the hypobranchial gland extracted from two males of *D. orbita* sea snail. Panel A shows a 15  $\mu\text{m}$  thick section of the gland used for the experiments on pSi. Panel B shows a 10  $\mu\text{m}$  thick section of the gland used for the experiments on the NALDI target). The different histological regions are labelled in both pictures: branchial hypobranchial gland, medial hypobranchial gland where secretion of prochromogen-containing mucus occurs, rectal hypobranchial gland, vascular sinus, rectal gland, and rectum.

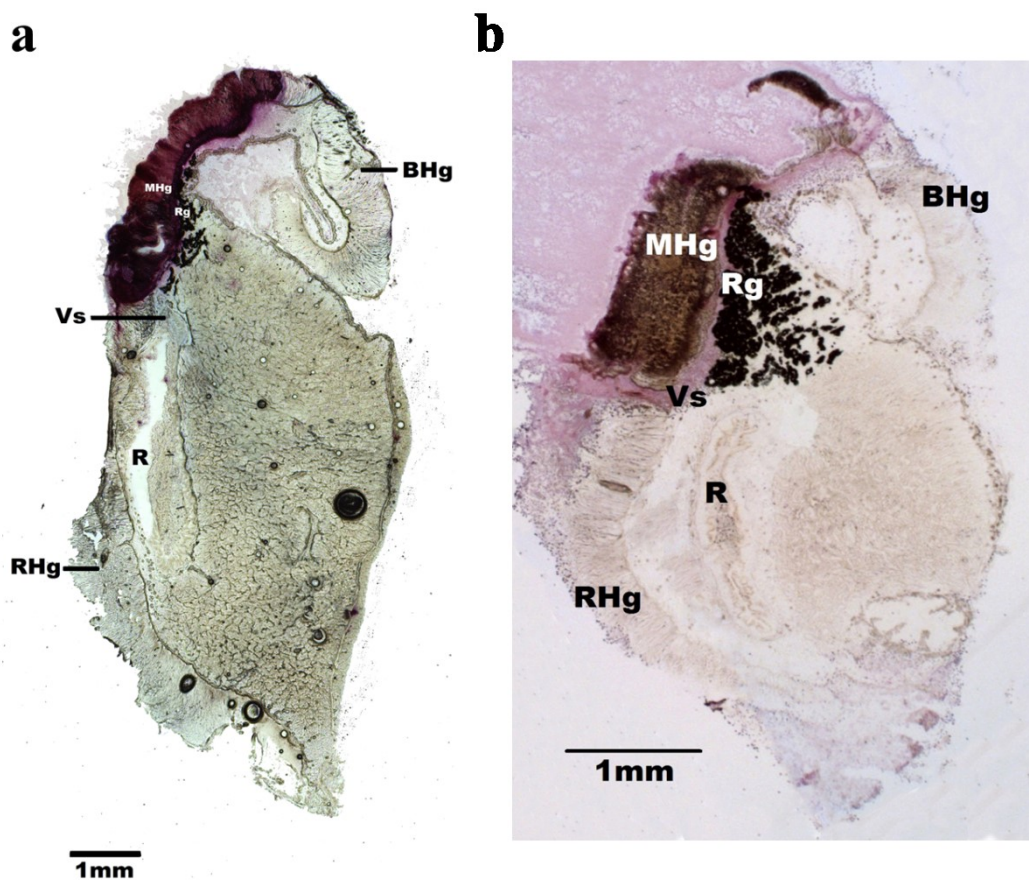


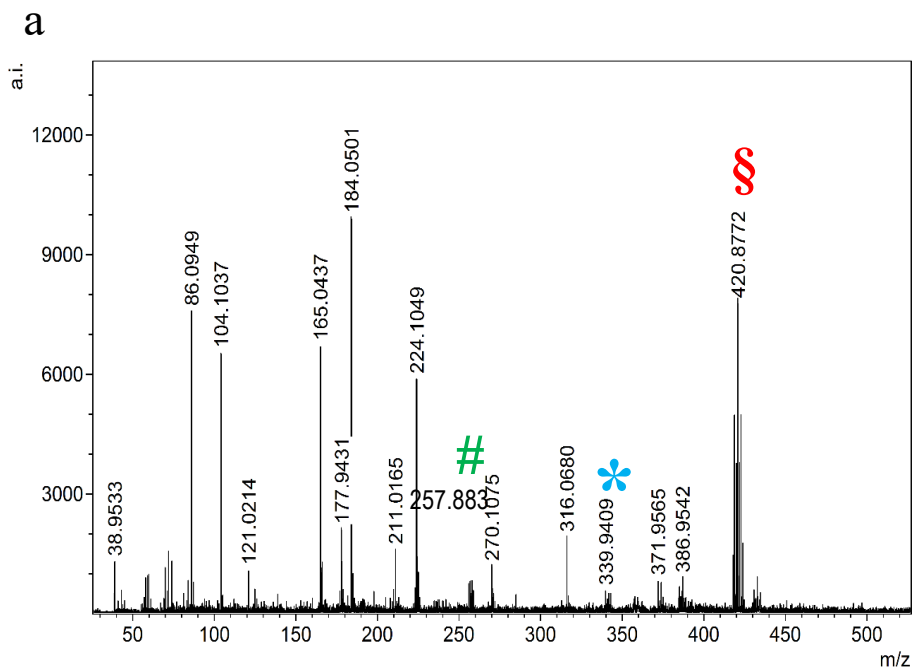
**Figure 2.2** Optical microscopy images of (a) a 15 µm thick transverse cryosection of the hypobranchial gland of a male sea snail, *D. orbita* and (b) a 10 µm thick cryosection of the hypobranchial gland from a different subject (40× magnification). BHg, branchial hypobranchial gland; MHg, medial hypobranchial gland where secretion of prochromogen containing mucus occurs; RHg, rectal hypobranchial gland; Vs, vascular sinus; Rg, rectal gland; R, rectum.

### 2.4.3 DIOS-MSI detection of brominated secondary metabolites

An example of a DIOS mass spectrum acquired in the low mass range after the printing and removal of a 30 µm section from the pSi surface is shown in Figure 2.3a. Signals of particular interest are the masses tentatively attributed to compounds known to be synthesized in the hypobranchial gland: 6,6'-dibromoindigo ( $C_{16}H_8Br_2N_2O_2$ ;  $[M+H]^+_{\text{monoisotopic}} = 418.9037$ ,  $M_{\text{measured}} [M + H]^+ = 418.8777$ , mass shown as an ion

intensity map =  $m/z$  420.8772 for major peak of combined  $^{79}\text{Br}^{81}\text{Br}$  isomers), tyrindoleninone ( $\text{C}_9\text{H}_6\text{BrNOS}$ ;  $[\text{M}+\text{H}]^+$ <sub>monoisotopic</sub> = 255.9438 Da,  $M_{\text{measured}} [\text{M}+\text{H}]^+$  = 255.9030; MSI not shown due to distributional overlap) and a mono-brominated peak tentatively identified as tyrindoxyl sulfate ( $\text{C}_9\text{H}_7\text{BrNO}_4\text{S}_2^-$ ) reduced to tyrindoxyl sulfonic acid ( $\text{C}_9\text{H}_8\text{BrNO}_4\text{S}_2$ ;  $[\text{M}+3\text{H}]^+$ <sub>monoisotopic</sub> =  $M_{\text{measured}} [\text{M} + 3\text{H}]^+$  =  $m/z$  339.9409, mass shown on ion intensity map =  $m/z$  339.94) (Cooksey, 2001). Selected  $m/z$  for distribution maps may not be presented when the distribution overlaps with other unidentified metabolites, for example  $m/z$  255.9030 distribution was not representative when checking spot spectra. Maps were manually verified by checking individual spot spectra from a random selection of locations across the highlighted region and adjusted till a representative map was created. 6,6'-Dibromoindigo is routinely found in extracts from the hypobranchial glands of *D. orbita* with consistent mass spectral data (Westley and Benkendorff, 2008). The ultimate precursor, tyrindoxyl sulfate is typically detected in extracts from the *D. orbita* hypobranchial glands using negative ion electrospray mass spectrometry (see Appendix II). Note that DIOS is able to detect both compounds, even though they show completely different polarity. 6,6'-dibromoindigo is highly insoluble in water where  $\log P = 4.264$ , whereas tyrindoxyl sulfate is a highly polar salt where  $\log P = -0.35$  (calculated using the interactive online  $\log P$  calculator, <http://www.molinspiration.com>). Magnification of the mass signals of tyrindoxyl sulfate, tyrindoleninone and 6,6'-dibromoindigo are shown in Figure 2.3b,c and d. The doublet and triplet typical of mono- and dibrominated compounds can be noted. Figure 2.4 shows virtual ion density maps after the printing of a 30  $\mu\text{m}$  section of the hypobranchial gland of a male *D. orbita* sea snail for the signals at  $m/z$  72.10, 100.13, 112.05, 132.13, 178.13, 184.10, 198.12, 224.16, 339.94, and 420.88 obtained on a pSi surface, together with the scanned image of the gland section before

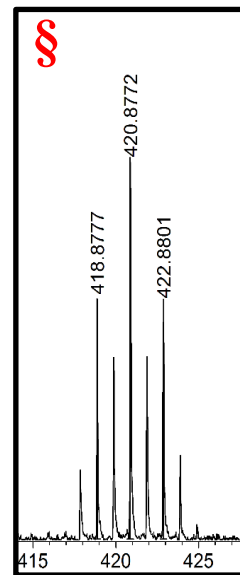
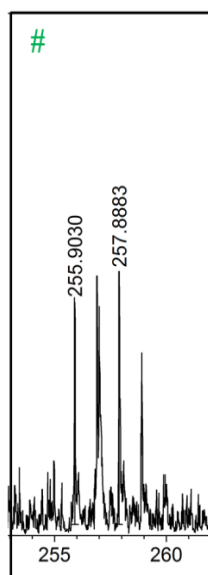
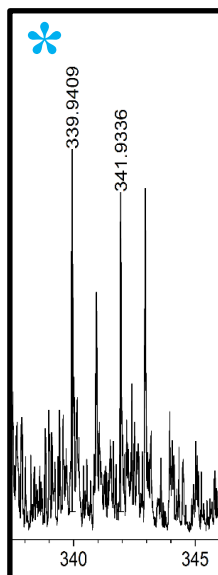
its removal from the pSi substrate and the corresponding brightfield microscopy image.



**b** tyrindoxyl sulfate  
(reduced form,  
tentatively tyrindoxyl  
sulfonic acid)  
[M+3H]<sup>+</sup>=339.9234

**c** tyrindoleninone  
[M+H]<sup>+</sup>=255.9030

**d** 6,6'-dibromoindigo /  
6,6'-dibromoindirubin  
[M+H]<sup>+</sup>=418.8777



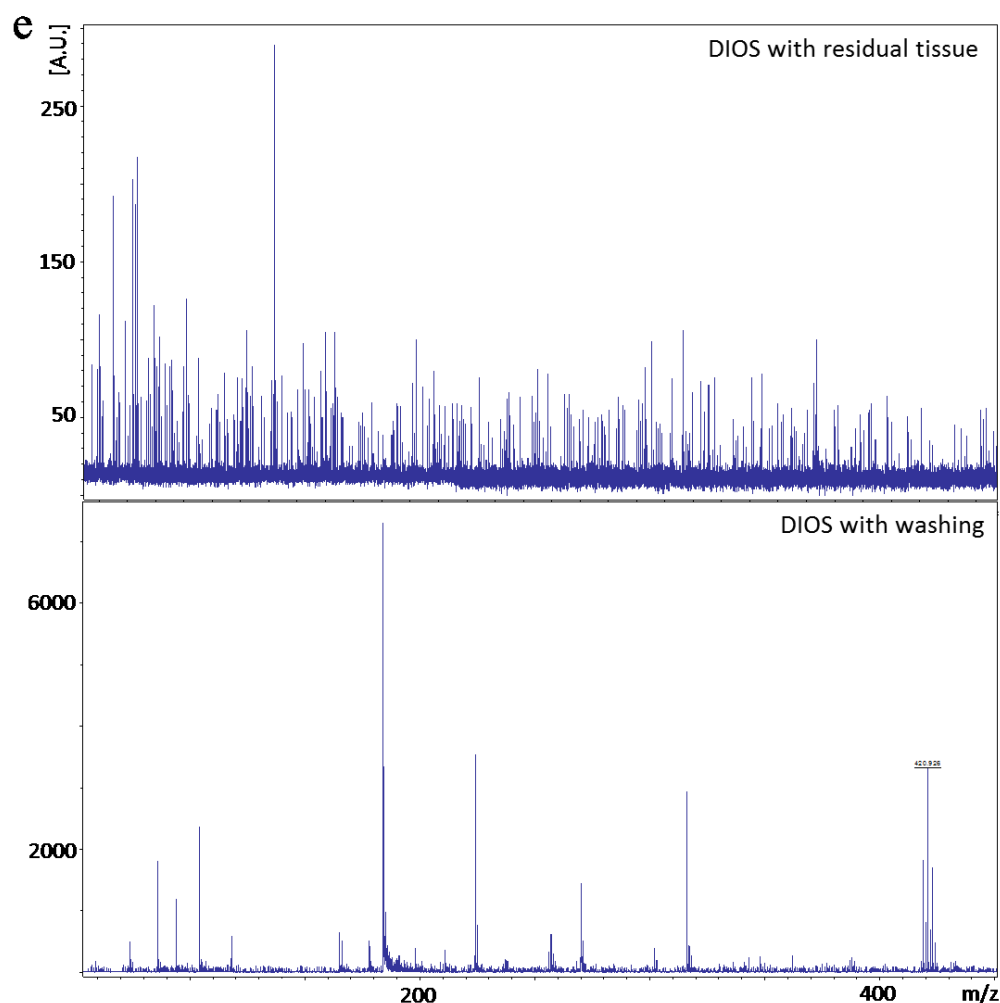


**Figure 2.3** (a) DIOS mass spectrum acquired on pSi in the low mass range after printing and removal of the tissue. (b),(c) and (d) magnification of the signals of tyrindoxyl sulfate reduced form (tentatively tyrindoxyl sulfonic acid; indicated with the symbol \*), tyrindoleninone (indicated with the symbol #) and 6,6'-dibromoindigo (indicated with the symbol §) with their masses respectively. (e) Spectra from tissue before (signal to noise <1) and after washing (signal to noise = 92) off the residual tissue. Note the doublet and triplet mass signals typical of mono- and dibrominated compounds.

The signal at  $m/z$  224.16 co-localized distinctly with the medial section of the hypobranchial gland, with particular intensity along the epithelial surface adjacent to the vascular sinus (Figure 2.4). Another unknown non-brominated compound with  $m/z$  178.13 also appeared in this region. Conversely, tyrindoxyl sulfate, the original

precursor, was concentrated throughout the medial hypobranchial tissue and extended up into the branchial section of the hypobranchial gland. The distribution of the major pigment 6,6'-dibromoindigo partially overlapped with tyrindoxyl sulfate (Figure 2.4), suggesting co-localization of the aryl sulfatase enzyme as previously observed using histochemistry (Westley and Benkendorff, 2009a). Some, 6,6'-dibromoindigo was also strongly concentrated in the rectal gland region and adjacent vascular sinus, leading more diffusely into the rectum (Figure 2.4). Dietary tryptophan from the rectal gland is thought to be the principle biosynthetic origin of indoles in the Muricidae (Westley et al., 2006, Westley et al., 2010b). Unfortunately no signals relating to the molecular mass of tryptophan ( $m/z$  204) were detected by means of MSI suggesting, if this is the case, that it is rapidly converted to brominated indole precursors in tissue.

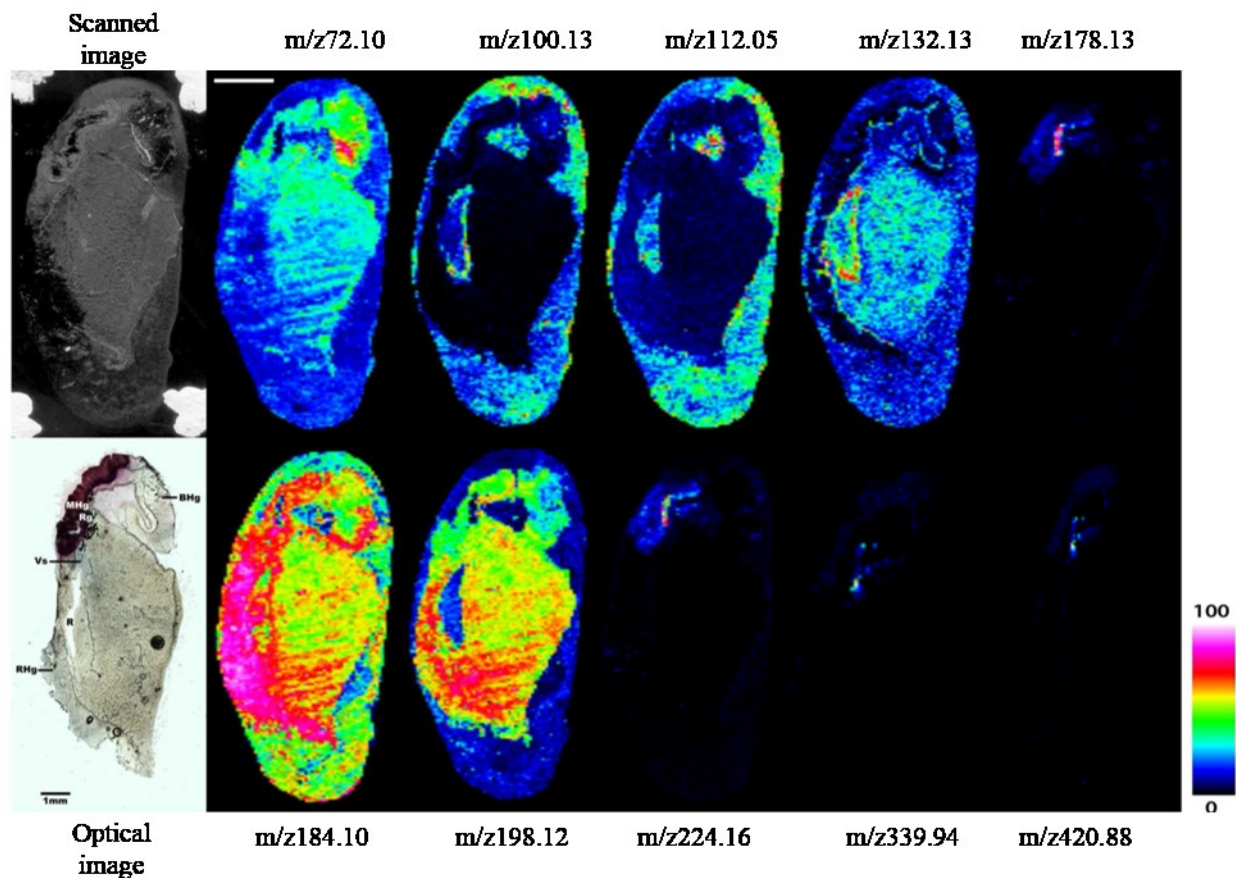


**Figure 2.4** Ion intensity maps for the selected signals on a 30  $\mu\text{m}$  thick section of the hypobranchial gland of a male *D. orbita* snail on pSi. The scanned image of the section before the removal from the pSi surface and the brightfield microscopy image are also shown. The signal at  $m/z$  339.94 was assigned to the reduced tyrindoxyl sulfate and the one at  $m/z$  420.88 to 6,6'-dibromoindigo.

#### **2.4.4 NALDI-MSI detection of brominated secondary metabolites**

We were also curious if the tissue contact printing technique worked for other laser desorption/ionization surfaces such as NALDI and how the performance of DIOS and NALDI-MSI compared. Figure 3 shows the imaging results for the analysis of a section of the hypobranchial gland of a male sea snail specimen on a NALDI target. The ion intensity maps for the same masses selected for the acquisition on pSi together with the scanned image of the section before tissue removal and the brightfield microscopy image are shown. In this case, the signal at  $m/z$  224.16 showed the same distribution as for the specimen on pSi. However, the signals at  $m/z$  339.98 (tyrindoxyl sulfate reduced form) and  $m/z$  420.08 (6,6'- dibromoindigo) were not detected on the NALDI plate. In contrast, a few other signals that were not present in the sections acquired on pSi were detected on the NALDI target including  $m/z$  98.11 (ion intensity strongly associated with the position of the rectal gland),  $m/z$  118.16 (associated with the rectal hypobranchial gland),  $m/z$  538.80 (associated with the rectum), and  $m/z$  825.47.

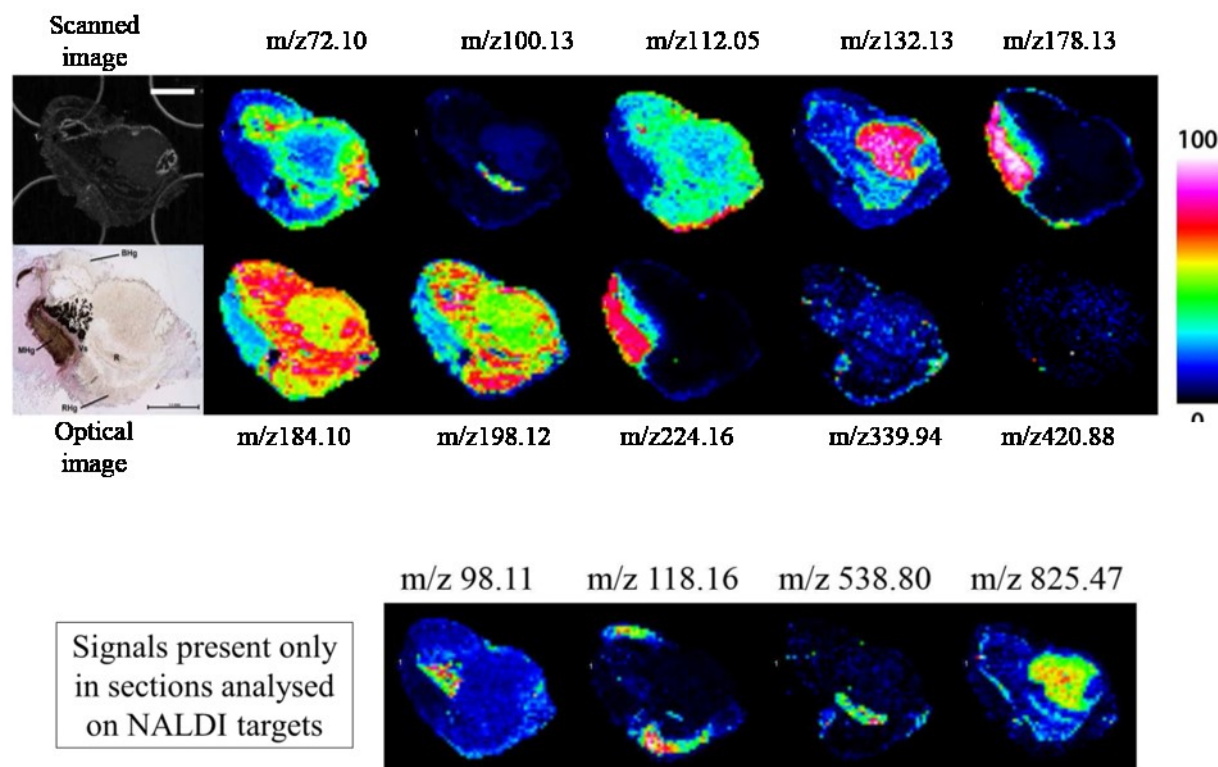


**Figure 2.5** Ion intensity maps for the selected signals on a 30  $\mu\text{m}$  thick section of the hypobranchial gland of a male sea snail specimen on a NALDI target. The scanned image of the section prior to the removal from the target and the brightfield microscopy image are also shown. In this case, the signal at  $m/z$  224.16 showed the same distribution as seen for the section on pSi, whilst signals at  $m/z$  339.94 (tyrindoxyl sulfate reduced form, tentatively tyrindoxyl sulfonic acid) and  $m/z$  420.88 (6,6'-dibromoindigo) were outside the expected MHg distribution.

NALDI-MSI confirmed the localization of the compound at  $m/z$  224.16 around the medial region of the hypobranchial gland (Figure 2.5). Conversely, the compound localized at  $m/z$  198.12 was associated with the branchial and rectal regions of the hypobranchial gland, but not the medial region. As seen using DIOS (Figure 2.4), the compound at  $m/z$  72.10 only appeared to be extracted on the NALDI target (Figure 2.5) and was most prominent in the vascular sinus and mantle tissue. From the NALDI results, the compound at  $m/z$  98.11 was very strongly associated with the rectal gland, whereas the one at  $m/z$  538.80 was concentrated in the rectum (Figure 2.5). A larger molecular weight compound at  $m/z$  825.47, in the typical mass range of biological lipids, was detected in the mantle tissue and in the vascular sinus.

#### **2.4.5 SALDI-MSI for biodistributional studies**

In the DIOS-MSI map for 6,6'-dibromoindigo and tyrindoxyl sulfate, as well as several of the non-brominated compounds shown in Figure 2.4, diffuse signals were observed around the edge of the tissue section, particularly around the bottom and lower right-hand side. This may correspond to mucus secreted from the tissue since the hypobranchial gland is known to be a site of copious mucus production (Fretter, 1994), with secretory cells containing highly sulfated mucopolysaccharides (Westley et al., 2010b). The compounds with  $m/z$  100.13 and 112.05 appeared to be strongly associated with this sticky mucus (Figure 2.4), whereas compounds with  $m/z$  72, 184, and 198 dominate in specific tissue regions and are less associated with the mucus. The compounds at  $m/z$  184.10 and 198.12 were mainly concentrated in the rectal hypobranchial gland region, but the compound at  $m/z$  184.10 also appeared to be distributed within the rectum and dispersed via the vascular sinus, whereas the compound at  $m/z$  198.12 was clearly not present in these areas. The compound at  $m/z$  72.10 was most prominent in the vascular sinus adjacent to the branchial region, but did not appear in the hypobranchial gland tissue.

Low molecular weight compounds present in the tissue sections were extracted by the surface through hydrophobic affinity interaction while retaining their relative spatial distribution. DIOS and NALDI were both suitable for the contact printing technique, and they also showed similar analytical performances, Figure 2.6, 2.7 and 2.8. However, a significant advantage of DIOS over NALDI is the ability to extract molecules in a wider polarity range. Furthermore, the surface chemistry of the pSi can be modified during the fabrication step in order to extract different classes of compounds, hence providing a more targeted investigation. Another crucial difference between pSi and NALDI was observed during the tissue printing process. Sections tended to curl once deposited on the NALDI surface, probably due to the extreme hydrophobicity of that surface. In contrast, the tissue could be easily deposited onto and removed from the pSi.

The thorough evaluation of the highest lateral resolution achievable and the extraction properties of the chemically modified pSi surface will be the focus of future work. Since molecular mass imaging is very appealing for many medical and pharmaceutical research fields, there is a strong interest in solving the key problems connected with conventional MALDI-MSI. In particular, for the low mass range, a key advantage of DIOS over MALDI is related to the matrix-free approach. In terms of MSI, the matrix-free approach combined with the extraction properties of pSi potentially yields higher lateral resolution for DIOS-MSI than for MALDI-MSI, since no liquid step is involved in the sample preparation (e.g., matrix coating). Furthermore, given that background noise from matrix fragments is limited for DIOS and NALDI, a few laser shots are usually sufficient to obtain good signal-to-noise ratios, resulting in shorter acquisition times. It is also known that instruments dedicated to MALDI-MSI analysis of biological tissues produce thousands of laser shots per run, and in order to maintain high performance, it is mandatory to regularly remove sample and

matrix debris from the MALDI source. This brings about significant downtime of the instrument. The limited number of laser shots required to obtain good mass spectra and the avoidance of matrix help keep the source clean longer in DIOS-MS

6,6'-dibromoindigo ([M+H] <sup>+</sup> ) $m_a$ = 418.9026 Da				
$i$ (DIOS-MSI)	$m_i$	$\Delta m_i$ (Da)	$\Delta m_i$ (mDa)	$\Delta m/m_i \times 10^6$ (ppm)
1	418.8620	-0.0405	-40.5500	-96.8006
2	418.8610	-0.0416	-41.5500	-99.1877
3	418.8800	-0.0226	-22.5500	-53.8311
4	418.8800	-0.0226	-22.5500	-53.8311
5	418.8800	-0.0226	-22.5500	-53.8311
6	418.8800	-0.0226	-22.5500	-53.8311
7	418.8800	-0.0226	-22.5500	-53.8311
8	418.8800	-0.0226	-22.5500	-53.8311
9	418.8800	-0.0226	-22.5500	-53.8311
Mean	418.8759	-0.0267	-26.6611	-63.6451
Standard error of the mean	0.0027	0.0027	2.7205	6.4944
Median	418.8800	-0.0226	-22.5500	-53.8311
Mode	418.8800	-0.0226	-22.5500	-53.8311
Standard deviation	0.0082	0.0082	8.1616	19.4832
Sample variance	6.7E-05	6.7E-05	66.6111	379.5952
Count	9	9	9	9
Confidence limits of the mean	0.0053	0.0053	5.3321	12.7288

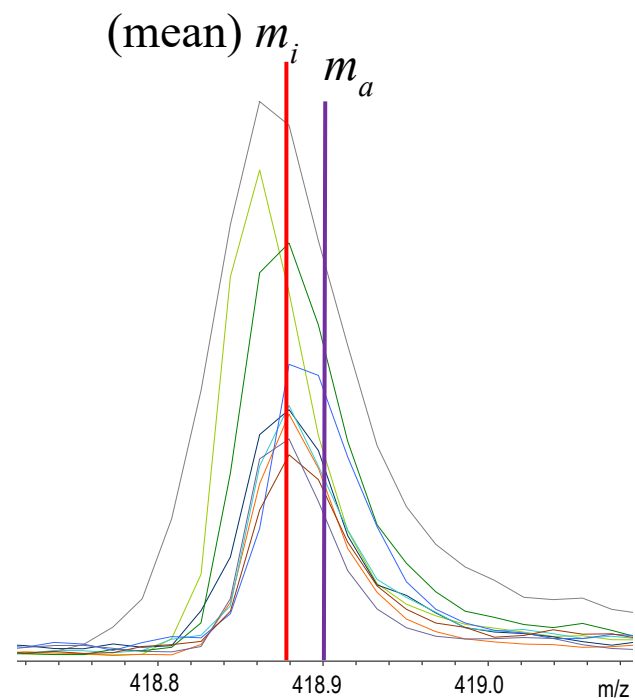


**Figure 2.6** Descriptive statistics of the repeated measurement of 6,6'-dibromoindigo  $[M+H]^+$  across the DIOS-MSI data set taken from 9 individual points showing ( $m_a$ ) calculated exact mass, ( $m_i$ ) measured mass, ( $\Delta m_i$  (Da)) shift from the exact mass in Daltons, ( $\Delta m_i$  (mDa)) shift in milliDaltons, and ( $\Delta m/m_i \times 10^6$  (ppm)) mass error in parts per million. The corresponding spectra are indicated.

6,6'-dibromoindigo ( $[M+H]^+$ ) $m_a = 418.9026$ Da				
$i$ (NALDI-MSI)	$m_i$	$\Delta m_i$ (Da)	$\Delta m_i$ (mDa)	$\Delta m/m_i \times 10^6$ (ppm)
1	418.9150	0.0125	12.4500	29.7205
2	418.9330	0.0304	30.4500	72.6899
3	418.9330	0.0304	30.4500	72.6899
4	418.9330	0.0304	30.4500	72.6899
Mean	418.9285	0.0259	25.9500	61.9476
Standard error of the mean	0.0030	0.0030	3.0000	7.1616
Median	418.9330	0.0304	30.4500	72.6899
Mode	418.9330	0.0304	30.4500	72.6899
Standard deviation	0.0090	0.0090	9.0000	21.4847
Sample variance	8.1E-05	8.1E-05	81.0000	461.5928
Count	4	4	4	4
Confidence limits of the mean	0.0088	0.0088	8.8198	21.0546

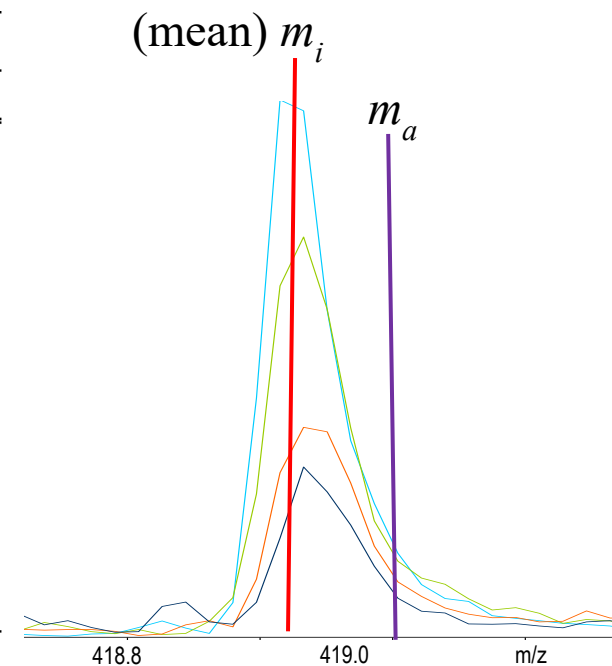


**Figure 2.7** Descriptive statistics of the repeated measurement of 6,6'-dibromoindigo  $[M+H]^+$  across the DIOS-MSI data set taken from 9 individual points showing ( $m_a$ ) calculated exact mass, ( $m_i$ ) measured mass, ( $\Delta m_i$  (Da)) shift from the exact mass in Daltons, ( $\Delta m_i$  (mDa)) shift in milliDaltons, and ( $\Delta m/m_i \times 10^6$  (ppm)) mass error in parts per million. The corresponding spectra are indicated (Note: spectra not scaled proportionally to Figure 2.6).

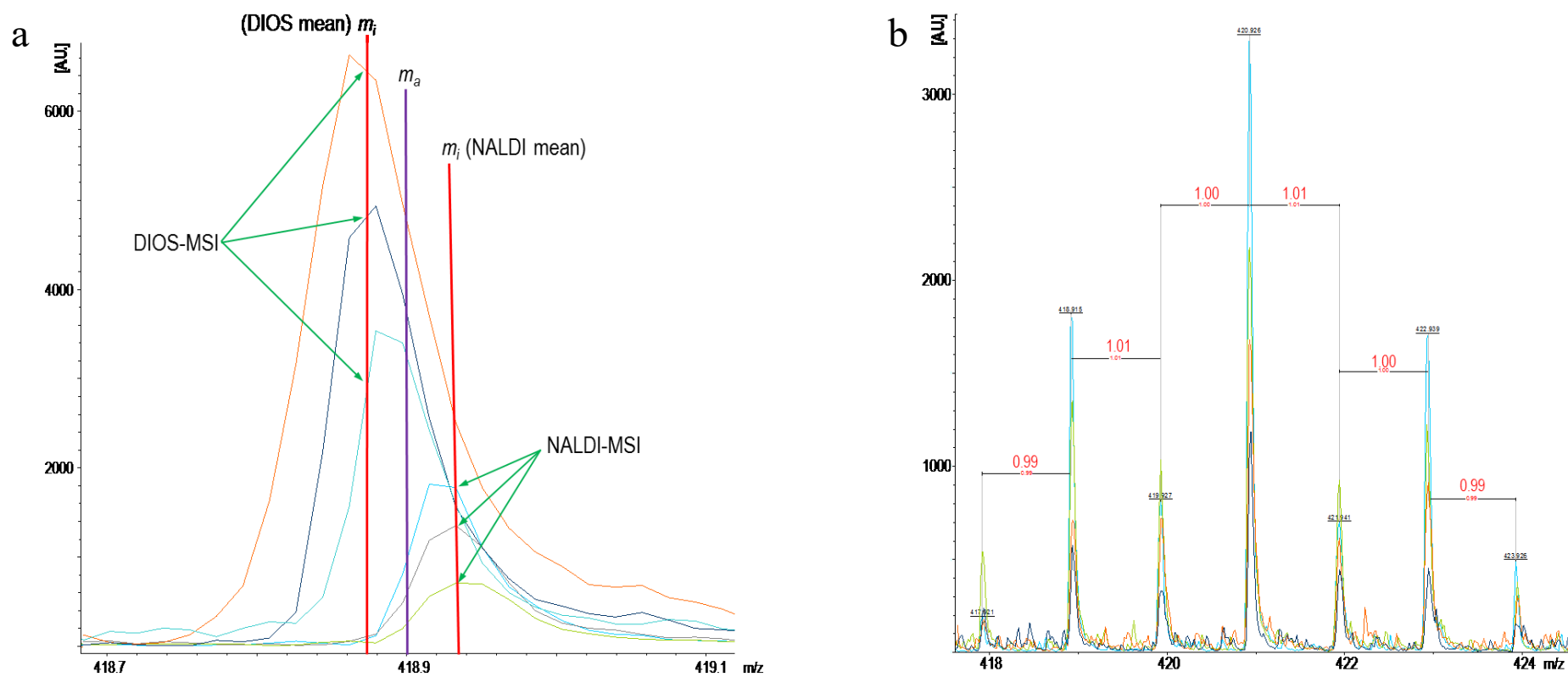


**Figure 2.8** (a) Comparison of 6,6'-dibromoindigo  $[M+H]^+$  monoisotopic peak of three replicate spots from both DIOS and NALDI-MSI data sets with; ( $m_i$ ) mean peak measurements and ( $m_a$ ) exact calculated measurement. (b) Measurement of the  $m/z$  difference in the di-brominated spectral pattern of six spots from both DIOS and NALDI data-sets for 6,6'-dibromoindigo.

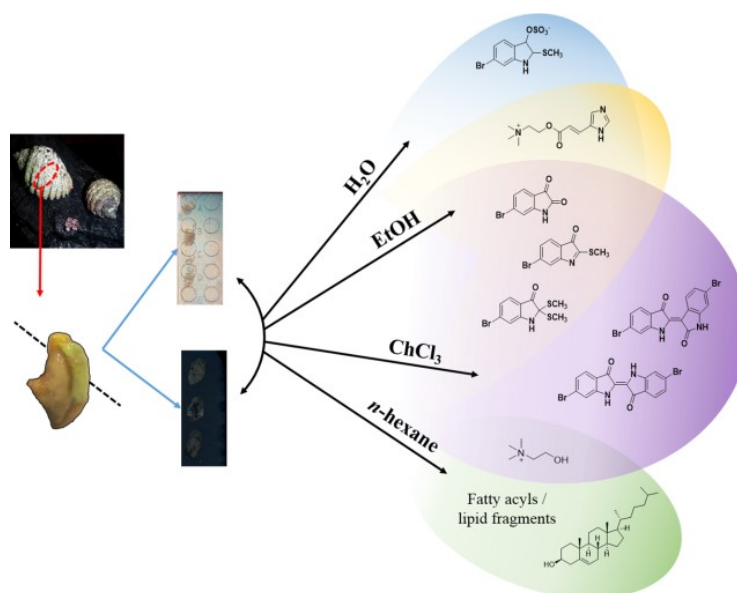
## **2.5 Conclusion**

In conclusion, we reported about the application of surface engineered pSi as support for mass spectrometry imaging in the small molecules domain, using the tissue contact printing approach. The method is simple and reliable, and it has several advantages over conventional MALDI-MSI in the low mass range, such as potentially high lateral resolution, limited background noise, possibility of using thick tissue sections (tens of micrometers), shorter acquisition times, and longer MALDI source-cleaning intervals. The protocol has been used to analyse the distribution of bioactive compounds synthesized in the hypobranchial gland of the marine sea snail, *D. orbita*, showing strong correlation between histological regions and the localization of both known and unknown metabolites. Our approach could become a valuable imaging tool to study the distribution of drugs and metabolites in biological tissues.

## **2.6 Acknowledgements**

This project was supported in part by a Flinders University, Faculty of Science and Engineering research grant to K.B. D.R. was supported by an Australian Postgraduate Award scholarship with additional funding from an anonymous philanthropic foundation awarded to K.B. Thanks are extended to Marc Cirera for his help in the realization of the abstract graphic.

### 3 Chapter Three - Solvent Separating Secondary Metabolites Directly from Biosynthetic Tissue for Surface-Assisted Laser Desorption Ionisation Mass Spectrometry



#### 3.1 Abstract

Marine bioactive metabolites are often heterogeneously expressed in tissues both spatially and over time. Therefore, traditional solvent extraction methods benefit from an understanding of the *in situ* sites of biosynthesis and storage to deal with heterogeneity and maximize yield. Recently, surface-assisted mass spectrometry (MS) methods namely nanostructure-assisted laser desorption ionisation (NALDI) and desorption ionisation on porous silicon (DIOS) surfaces, have been developed to enable the direct detection of low molecular weight metabolites. Since direct tissue NALDI-MS or DIOS-MS produce complex spectra due to the wide variety of other metabolites and fragments present in the low mass range, we report here the use of “on surface” solvent separation directly from mollusc tissue onto nanostructured surfaces for MS analysis as a mechanism for simplifying data annotation and detecting possible artefacts from compound delocalization during the preparative steps. Water, ethanol, chloroform and hexane selectively extracted a range of choline esters, brominated indoles and lipids from *Dicathais orbita* hypobranchial tissue imprints. These

compounds could be quantified on the nanostructured surfaces by comparison to standard curves generated from the pure compounds. Surface-assisted MS could have broad utility for detecting a broad range of secondary metabolites in complex marine tissue samples.

### **3.2 Introduction**

Secondary metabolites play an important role in the ecological interactions of marine organisms (Hay, 2009), and are fast become a promising source of bioactive compounds with therapeutic potential (Gerwick and Moore, 2012). Secondary metabolites are produced by species to serve specific functions (Hay, 2009), for example reproduction, predation or defence, and can therefore have heterogeneous expression in tissues both spatially and over time (Garson, 1993, Yarnold et al., 2012, Westley and Benkendorff, 2008, Capon, 2010). Traditional solvent separation methodologies are not well adapted for capturing heterogeneously expressed secondary metabolites, requiring either more biological material for recovery (Mendola, 2003) or optimized targeted extraction (Gerwick and Moore, 2012), repeated across an ecologically relevant temporal framework.

Yield is a major consideration for both the structural and biological characterisation of secondary metabolites. As metabolites are heterogeneously expressed, determining the optimal tissues and time for extraction can be difficult without some prior knowledge of the biological processes that initiate biosynthesis and storage. Therefore, there is a major benefit in direct analysis of biosynthetic tissue responsible for secondary metabolite production, which can help overcome some of the problems associated with obtaining sufficient bioactive material for isolation and characterisation (Mendola, 2003).

Although not involved in primary metabolism, secondary metabolites lie within a complex and abundant mixture of primary metabolites, and their precursors are often

synthesized from dietary origins (Garson, 1993). Therefore, discerning secondary from primary metabolites in tissue can be challenging. Recent bioactive discoveries are showing a trend towards low molecular weight compounds (Dias et al., 2012, Camp et al., 2011), placing many secondary metabolites in the same molecular weight range as primary metabolites including adenylates, nucleotides, fatty acids and monosaccharides (Fujimura and Miura, 2014). Secondary metabolites can also be in very low abundance compared to primary metabolites (Gerwick and Moore, 2012), thus requiring extraction enrichment for detection. Structural features can also help discern secondary from primary metabolites and there are many examples of unique structures in recent discoveries that demarcate them from primary metabolites (Gerwick and Moore, 2012). Marine secondary metabolites in part have a higher probability of halogenation than terrestrial natural products (Pauletti et al., 2010b). Methods that can accurately map molecular species in the low molecular mass range, and are tolerant of heterogeneous marine tissue, will enhance spatial analysis and contribute to our understanding of biosynthesis and function. Spatial analysis and biosynthesis can act as a guide for extraction and subsequent studies on bioactivity. Although there are many strategies for the qualitative, quantitative and spatial analysis of secondary metabolites, the chosen methods must be amenable to the particular tissue being analyzed and be suitable for the accurate detection of the metabolite size range and structural features of interest.

Mass spectrometry imaging (MSI) has emerged as a sophisticated platform for the spatial analysis of proteins, peptides, lipids and small mass metabolites *in situ*. Depending on sample preparation, MSI has the ability to detect thousands of molecular signals simultaneously, reflecting the complexity of biological samples. Across all the mass imaging techniques, matrix-assisted laser desorption ionisation (MALDI)-MSI is the most frequently utilised (Bouslimani et al., 2014) of the laser desorption ionisation

(LDI) methods. Unfortunately, MALDI-MSI has limitations in the low mass range, due to interference from spectra generated by the applied matrix (Bergman et al., 2014). The use of matrix in the analysis of low molecular weight metabolites complicates data and further challenges the identification of secondary metabolites. MSI also generates considerable spectral data requiring molecular identification, which is a major hurdle in MSI workflows (Bouslimani et al., 2014), often complicated by matrix ion signals.

New technologies using surface-assisted LDI methodologies (Calavia et al., 2012) have been developed as an alternative to the use of matrices. Nanostructured surfaces have emerged that enhance the detection of small molecules, with an emphasis on increased sensitivity, minimal background signal and simplified sample preparation (Greving et al., 2010). Ionization techniques from nanostructured surfaces, such as nanostructure-assisted laser desorption ionization (NALDI) (Calavia et al., 2012) and desorption ionization on silicon (DIOS) (Lewis et al., 2003, Liu et al., 2007, Guinan et al., 2014, Wei et al., 1999), offer improved mass analysis in the low molecular weight range. Nanostructured surfaces eliminate the need for a matrix as the physical properties of the surface allow effective absorption of the UV laser light, thereby transferring energy to the analyte of interest (Lewis et al., 2003, Liu et al., 2007). The properties of the nanostructured surfaces also have considerable advantages for some tissue types, specifically mucus rich biosynthetic tissues (Ronci et al., 2012). Functionalization of the DIOS surface attracts small molecule metabolites through hydrophobic effects or specific molecular recognition (Trauger et al., 2004, Lowe et al., 2010), which allows other contaminants, such as salts and mucus aggregate clumps, to wash away from the area of LDI-MS analysis (Ronci et al., 2012). NALDI bears some of the same attractive properties as DIOS surfaces, but requires less laser energy for ionization, greatly limiting fragmentation (Alhmoud et al., 2014). Nanostructured surfaces provide a

matrix-free strategy within the LDI suite of methods when generating spectra, as an alternative to using other direct methods for non-matrix analysis, e.g., ambient methods like direct electrospray ionization mass spectrometry (ESI-MS) in the form of liquid surface extraction analysis (LESA<sup>®</sup>), desorption electrospray ionization (DESI) and nano-desorption electrospray ionization (nanoDESI) (Ellis et al., 2013).

Recently, we applied NALDI-MSI and DIOS-MSI to detect the spatial distribution of mollusc secondary metabolites *via* a tissue imprinting approach (Ronci et al., 2012). This approach allowed us to map the distribution of Tyrian purple and its precursors, but the elucidation of some spatially interesting spectra became challenging due to the complexity of spectral signals from the imprinted heterogeneous tissue samples. Spectral data from fragments of larger more labile molecules can be found within the low mass region, making identification of known secondary metabolites difficult and the interpretation of unknown or unexpected secondary metabolites complex. In order to improve secondary metabolite detection and elucidation, a simple chromatographic separation scheme was devised to selectively extract metabolites directly from the tissue on to the nanostructured surface for analysis. Direct separation onto the nanostructured surfaces can be done from frozen sections and under nitrogen gas (Figure 3.1), reducing enzymatic changes and atmospheric oxidative degradation, while maintaining the benefits of the nanostructured surfaces. Since LDI-MS analysis is also conducted in a high vacuum environment without light, oxidative and photo catalytic degradation affecting less stable secondary metabolites is reduced. The solvent wash area adjacent to the tissue (Figure 3.2) can subsequently be used to concentrate particular subsets of compounds according to their solubility, thus facilitating identification based on simpler spectra and structural features, e.g. polarity, halogenation.

An advantage of this technique is the quantification of natural products from tissue imprints by generating standard concentration curves from the purified compounds on

the adjacent nanostructured surfaces for comparison of the LDI-MS signal intensity. Serial separation of secondary metabolites helps in annotating known peaks and quantifying them, but also allows for the discovery of new brominated secondary metabolites based on mono- and di-brominated spectral patterns.



b

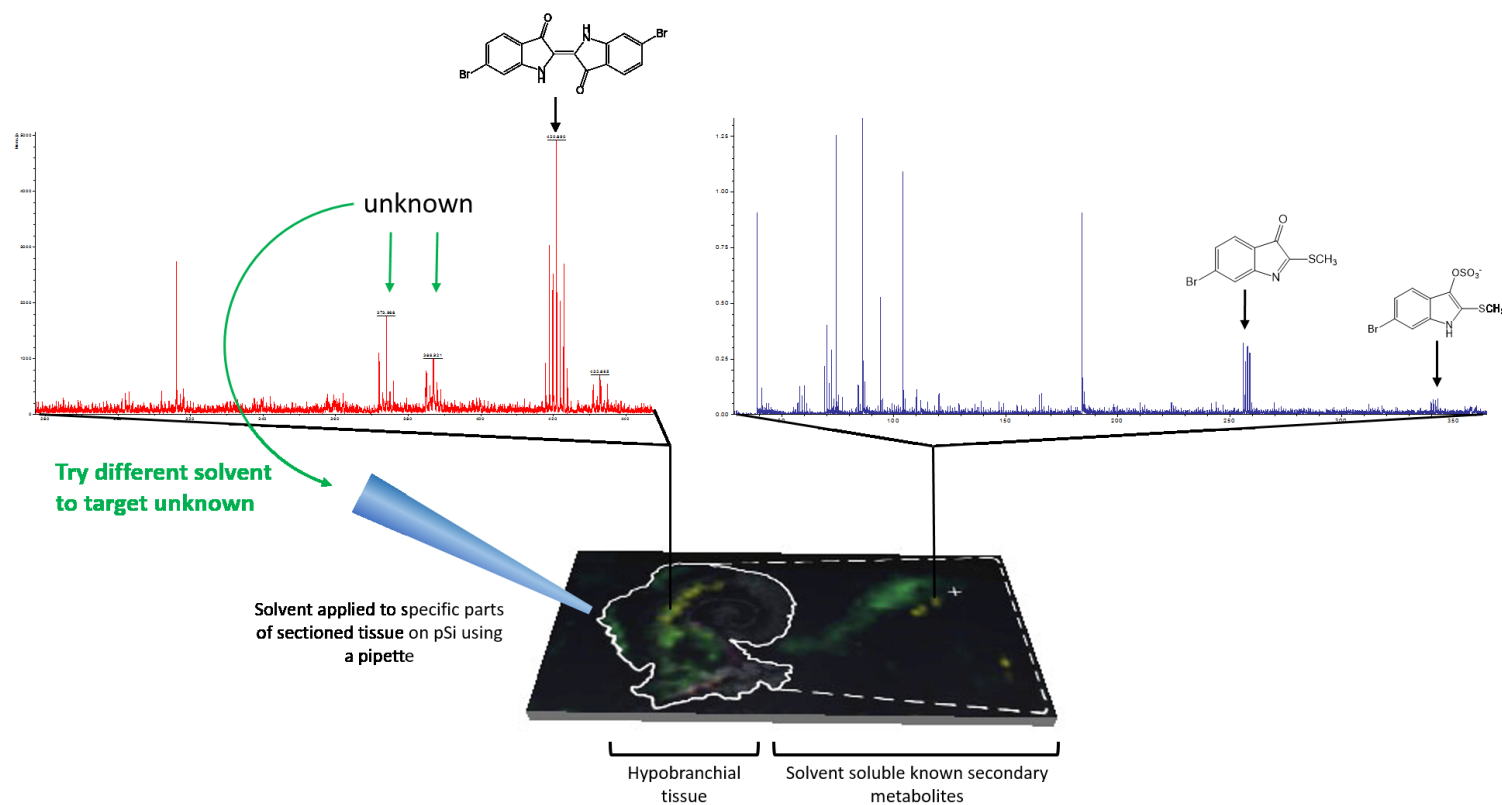


**Figure 3.1** a) Concept of “on-surface” solvent separation to concentrate secondary metabolites of various polarities from tissue imprints of the biosynthetic regions of *D. orbita*, onto nanostructure-assisted laser desorption ionisation (NALDI) and desorption ionisation on porous silicon (DIOS) surfaces for mass spectrometry imaging (MSI). b) Example of using solvent separation to annotate peaks and discover new brominated compounds and their likely solubility for future purification.

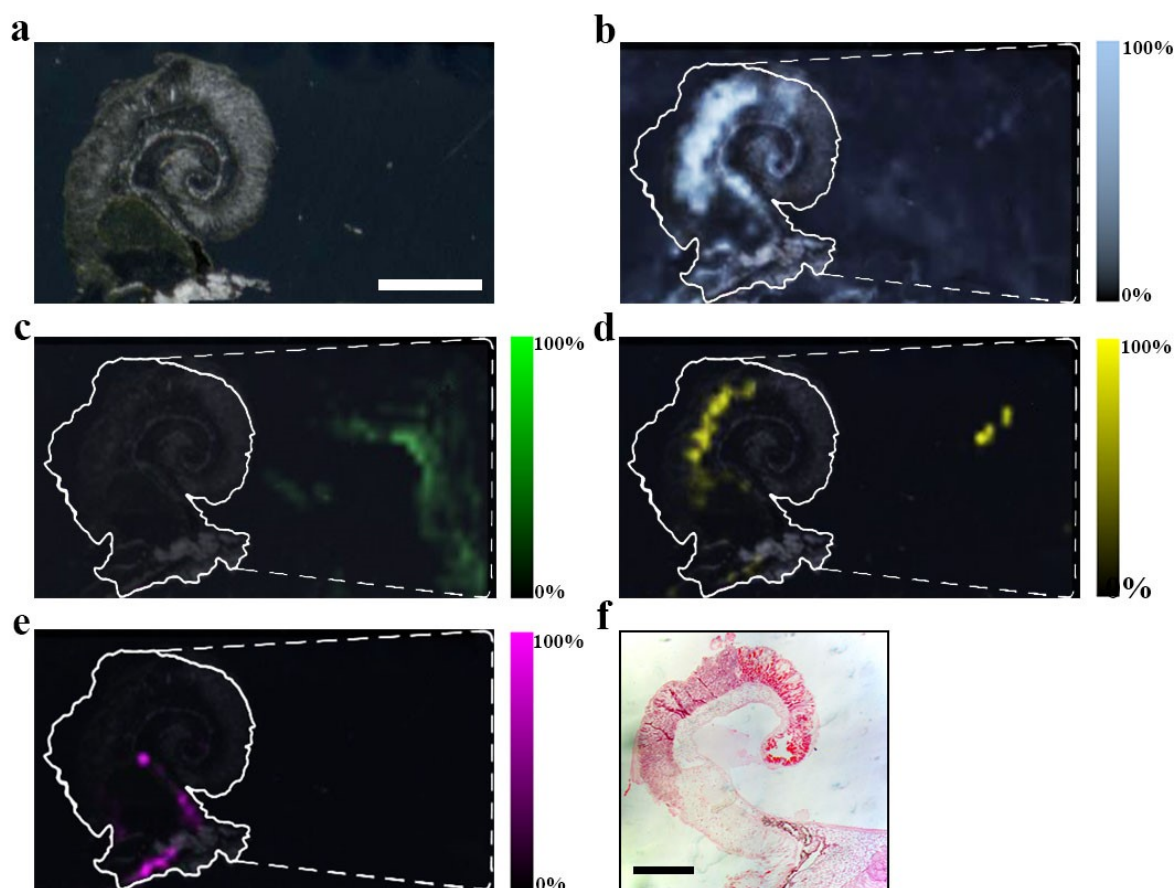


**Figure 3.2** MSI detection region after EtOH separation of secondary metabolites on a DIOS surface. 15  $\mu\text{m}$  thick tissue sections were imprinted onto the nanostructured surface then washed by gently pipetting solvent over the imprint area, onto a clean section of the surface (-----), where the solvent was then allowed to evaporate before LDI-MS: (a) scan of tissue on DIOS; (b) MSI of murexine  $m/z$  224; (c) MSI of tyrindoxyl sulfate  $m/z$  340; (d) MSI of tyrindoleninone  $m/z$  256; (e) MSI of Tyrian purple  $m/z$  420 and (f) example of a histological tissue section of the hypobranchial region stained with haematoxylin and eosin.

Tyrian purple, brominated indole precursors and choline esters have previously been detected in the hypobranchial gland, reproductive structures and egg capsules (Westley and Benkendorff, 2008, Benkendorff et al., 2000) of muricid molluscs. The choline esters have potent neuromuscular blocking activity (Erspamer and Glasser, 1957, Roseghini et al., 1996) and have been implied to aid predation, whilst the brominated indoles are suggested to provide antimicrobial defence in the egg capsules (Roseghini et al., 1996, Westley et al., 2006). In addition to their ecological value, the choline esters have undergone human clinical trials for pain management (Erspamer and Glasser, 1957), whereas the brominated indoles, tyrindoleninone and 6-bromoisatin, have shown promise as anti-cancer compounds, inducing an apoptotic response in a range of cell lines and *in vivo* models (Westley et al., 2010c, Edwards et al., 2012, Esmaeelian et al., 2013b, Esmaeelian et al., 2014). Understanding the distribution of these two classes of secondary metabolites, and the optimization of rapid detection methods, will not only contribute to the ongoing ecological research into their functional ecology, but could also facilitate biodistributional studies in future *in vivo* animal models for development of muricid hypobranchial gland extracts as natural medicines (Benkendorff, 2013).

Here we describe the use of “on-surface” solvent separation of secondary metabolites from tissue imprints of the biosynthetic regions of a marine mollusc (Figure 3.1). This process allowed solvent extraction of subsets of secondary metabolites, according to polarity, directly from hypobranchial tissue onto nanostructured surfaces for immediate LDI-MS to gain qualitative and relative quantitative data that is compatible with LDI-imaging data (Ronci et al., 2012). Water (H<sub>2</sub>O), ethanol (EtOH), chloroform (CHCl<sub>3</sub>) and *n*-hexane were independently applied to tissue, to cover a typical solvent profile able to capture hydrophilic to lipophilic low molecular weight secondary metabolites (Figure 3.1). The identification of particular secondary metabolites that were either retained in

the tissue imprints, or washed onto the nanostructured surfaces after solvent separation (Figure 3.2), was confirmed by standard extraction methods and solvation characteristics, e.g., Log P. Relative quantification of secondary metabolites on the nanostructured surfaces was determined against available standards for 6-bromoisatin, tyrindoleninone and Tyrian purple. Nanostructured surfaces provide an excellent platform for spatial analysis of secondary metabolites (Esquenazi et al., 2009) using LDI and simple chromatographic manipulations can greatly simplify annotation and de-replication efforts (Škrášková and Heeren, 2013). Direct solvent extraction onto nanostructured surfaces from biosynthetic hypobranchial tissue regions allows rapid and simplified quantitative and qualitative analysis of both brominated indoles and choline esters in the absence of spectra that would otherwise suppress detection.

### **3.3 Experimental**

#### **3.3.1 Tissue preparation for extraction and solvent separation on**

##### **MSI substrates**

Adult *D. orbita* samples were collected off rocky intertidal coastlines on southern metropolitan rocky reefs in South Australia using an Exemption Permit to the South Australian Fisheries Management Act 2007 section 70 (Permit No. 9902638). The selected adult specimens were prepared by cracking open the shell with a vice at the junction between the primary body whorl and spire and the soft body was removed by cutting the columnar muscle. The soft tissue was then rinsed in MilliQ water to reduce residual salt. Males were identified by the presence of a penis above the tentacles (Noble et al., 2009) and the absence of egg capsule glands and ovaries. The male hypobranchial glands were removed by incision along the connective mantle tissue between the ctenidium and the branchial hypobranchial and the posterior prostate and digestive gland. The hypobranchial gland and prostate gland were left connected

(Westley and Benkendorff, 2008) and placed in 5 mL polypropylene sample tubes (Sarstedt, Nümbrecht, Germany) and snap frozen in liquid nitrogen. Frozen tissue samples were protected from light and stored at  $-80\text{ }^{\circ}\text{C}$  until required.

### **3.3.2 Extraction of secondary metabolites for LC-MS**

#### **3.3.2.1 Extraction and chemical analysis of brominated indoles**

Solvents were purchased from Sigma-Aldrich (CHROMASOLV<sup>®</sup>, HPLC grade). Eight fresh hypobranchial glands (6.58 g) were solvent extracted as previously described (Rudd and Benkendorff, 2014) to obtain brominated indoles. Briefly, secondary metabolites were extracted from glandular tissue in an equal portion of chloroform and methanol (1:1 v/v, Sigma) and continuously stirred overnight. After vacuum filtering (Whatman filter paper 1), the polar and lipophilic fractions were separated using 20 mL MilliQ water. The chloroform fraction contained the intermediate precursor brominated indoles and Tyrian purple, whilst the methanol fraction contained the hydrophilic, tyrindoxyl sulfate. Each fraction was evaporated to dryness on a Rotavapor<sup>®</sup> R-114 (BÜCHI Labortechnik AG, Flawil, Switzerland), weighed and re-dissolved in 1 mL of acetonitrile within amber vials for LC-MS analysis.

Brominated indoles in hypobranchial extracts were analyzed by high performance liquid chromatography (HPLC; Waters 2695, Waters Alliance<sup>®</sup>) coupled to a mass spectrometer (MS; Micromass Quatro micro<sup>™</sup> tandem quadrupole MS System, Waters, Milford, MA, USA). HPLC separation was performed on a reverse-phase hydrophobic column (Synergi<sup>™</sup>, Hydro-RP, 4  $\mu\text{m}$  C18 phase, 80 Å, 250 mm  $\times$  4.6 mm i.d., Phenomenex, Lane Cove, NSW, Australia) using a gradient of acetonitrile (ACN) in water with 0.1% formic acid detecting extract components with parallel UV/Vis diode-array at 300 and 600 nm (Esmaelian et al., 2013b). The gradient was applied at a 1 mL/min flow rate starting with 30% ACN for 1 min, 60% for 3 min, and 100% for

15 min before returning to 30% for 15 min. ESI-MS detected brominated indoles at a flow rate of 300  $\mu\text{L}/\text{min}$ , in full scan mode, and recorded using the MassLynx 4.1 data system (Waters Alliance). Retention times were standardized using 4  $\mu\text{M}$  synthetic 5-bromoisatin (Sigma-Aldrich, technical grade) in ACN. The identification of brominated indoles was based on peak retention time, expected calculated mass and isotopic clusters for the mono- and di-brominated compounds within mass spectra (Esmaelian et al., 2013b).

### 3.3.2.2 Extraction and chemical analysis of choline ester murexine

Murexine was extracted from 1.3 g of hypobranchial tissue in three times 30 mL volumes of acetone and pooled. The extract was vacuum filtered through a PTFE membrane filter (pore size 0.2  $\mu\text{m}$ ), evaporated to dryness, and washed three times with 10 mL of diethyl ether to remove fats. Total extract was then taken up in 5 mL of ACN for LC-MS.

Murexine was detected by ultra-performance liquid chromatography (UPLC)-MS. Separation was provided by an Acquity UPLC<sup>®</sup> system (Waters Alliance), using a 10  $\mu\text{L}$  injection volume, on a reverse-phase column (Atlantis T3, 3  $\mu\text{m}$  C18, 3  $\times$  100 mm i.d., Waters Alliance) with a mobile phase of 0.5% formic acid (A) and acetonitrile (B) at a flow rate of 0.5 mL/min (gradient of solvent: 0-10 min, 98% A and 2% B), with parallel UV/Vis PDA detection. ESI-MS detected the murexine structure on the Micromass Quatro micro<sup>™</sup> tandem quadrupole mass spectrometer and data was acquired using MassLynx 4.1 data system (Waters Alliance). To see the structural features of murexine in ESI, a scan at 20 V was compared to a collision induced dissociation (CID) scan at 35 V cone voltage (positive ion electrospray, 80 to 500 Da mass range) for comparison to post source fragmentation that occurs in both NALDI and DIOS-MS.

### 3.3.3 NALDI and DIOS surface fabrication, oxidation and functionalization

NALDI substrates were obtained from Bruker Daltronics. DIOS surfaces were fabricated according to (Ronci et al., 2012). Briefly, monocrystalline (0.008–0.02  $\Omega\text{cm}$ ) antimony doped *n*-type Si (100) wafers (Silicon Quest International, CA, USA) were cut, methanol sonicated for cleaning and dried prior to substrate fabrication by light-assisted anodic etching (Ronci et al., 2012, Guinan et al., 2012). Silicon substrates were secured using a custom built Teflon cell in contact with a gold foil anode (Space Products International, CA, USA) and a platinum wire cathode (0.5 mm, 99.9%; Aldrich, WA, USA), shaped into a ring. Etching was achieved through the addition of an electrolyte solution 1:1 hydrofluoric acid (HF):EtOH. The submerged pSi surfaces were illuminated using a fiber optic light source passing through a set of two aspheric lenses,  $f = 80$  mm (OptoSigma, CA, USA) for collimation. A 20 mA constant current was applied across the Teflon cell for 2 min via a 2425 current source meter (Keithley, Cleveland, Ohio USA), operated via a meter program constructed in LabView 6.1. Fabricated pSi were washed with methanol prior to being dried under nitrogen gas.

Freshly etched pSi were oxidized using ozone at a flow rate of 3.25 g/h (Ozone-Generator 500, Fischer, Germany). After oxidation, pSi were subjected to a second pore broadening etch with 5% HF/H<sub>2</sub>O for 30 s and re-ozone oxidised. The hydroxyl-terminated pSi surfaces were then silanized using 80  $\mu\text{L}$  of neat silane (F<sub>5</sub>PhPr) for 15 min at 90 °C. Silanized pSi were washed with methanol, dried under nitrogen gas and stored in a desiccator until required.

### **3.3.4 Tissue sectioning, deposition and solvent separation on NALDI and DIOS surfaces**

Tissue selection was based on the imaging results generated for NALDI and DIOS-MSI of 15  $\mu\text{m}$  sections of the medial hypobranchial gland from adult male *D. orbita* (Ronci et al., 2012), Figure 1. Fresh frozen glands were mounted and prepared for sectioning according to Ronci *et al.* (2012). Glands were transversely cryo-sectioned until the medial region was exposed. The mounted frozen gland was then rotated to section only the medial tissue region of the hypobranchial gland, allowing only that single region to be collected for depositing onto NALDI and DIOS-MS substrates. Thin 15  $\mu\text{m}$  thick sections were placed on either a NALDI or DIOS surface. Three replicate tissues sections ( $n = 3$ ) were cut for each solvent separation for both NALDI and DIOS surfaces (total  $n = 24$ ). Secondary metabolites were separated out of each tissue section by washing across the tissue onto a clean section of the nanostructured surface adjacent to the tissue, Figure 3.2, using either 200  $\mu\text{L}$  of  $\text{H}_2\text{O}$ , EtOH,  $\text{CHCl}_3$  or *n*-hexane for both NALDI and DIOS surfaces. Solvent was applied by gentle pipetting. The solvent was then allowed to evaporate from the surface in a fumehood under a stream of  $\text{N}_2$  gas at room temperature before MS.

### **3.3.5 NALDI and DIOS-MS acquisition**

NALDI surfaces, post solvent separation, were mounted into a specialized steel adapter target, whilst DIOS surfaces were mounted onto a customized MTP 384 ground steel target plate (Bruker-Daltronics GmbH, Bremen, Germany), secured with conductive carbon tape, and loaded into an Autoflex III TOF/TOF mass spectrometer (Bruker-Daltronics) equipped with a SmartBeam 200 Hz laser. Quadratic external calibration of the TOF tube was performed before each new surface acquisition using  $\alpha$ -cyano-4-hydroxycinnamic acid (CHCA) adducts together with bradykinin (1–7) and

angiotensin II, spotted on a free area of the surface. Monoisotopic peaks for the calibration range included:  $K^+$  38.9637, CHCA  $[M + H - H_2O]^+$  172.0399, CHCA  $[M + H]^+$  190.0504, CHCA  $[M + Na]^+$  212.0324, CHCA  $[2M + H - CO_2]^+$  335.1032, CHCA  $[2M + H]^+$  379.0930, bradykinin Fragment 1–7  $[M + H]^+$  757.3991 and angiotensin II  $[M + H]^+$  1046.5418. Surface calibration was determined based on the brominated indole standards used to generate standard curves.

Samples were run in reflectron positive mode in the 20–1000 Da range, with a medium laser focus, corresponding to a 50  $\mu\text{m}$  diameter. Electronic gain was set to regular. Laser intensity was maintained at 42%, with a 20 ns pulse delay to allow plume formation for low mass molecules. Ion and detector settings were: ion source 1 – 19.00 kV, ion source 2 – 16.80 kV, lens – 8.25 kV, reflector 1 – 21.00 kV, reflector 2 – 9.40 kV. Data sets were further processed by baseline subtraction (1) and normalized noise threshold settings (0.5).

Spectra were acquired up to 20 mm from the margin of the tissue section to evaluate any effect on concentration distribution. At each sampling point a summed spectra was acquired by five 200 pulsed laser shots (1000 shots). Each different surface had a standard reference for purified 6-bromoisatin at 600, 300, 150, 75 and 37.5 mg/L; purified tyrindoleninone at 600, 300, 150, 75 and 37.5 mg/L; and purified Tyrian purple, 6,6'-dibromoindigo at 600, 300, 150, 75 and 37.5 mg/L, all using serial dilution in triplicate.

### **3.3.6 Mass spectrometry imaging**

Imprinted pSi chips were mounted onto a customised MTP 384 ground steel target plate (Bruker-Daltronics GmbH, Bremen, Germany), secured with conductive carbon tape, and loaded into an Autoflex III TOF/TOF mass spectrometer (Bruker-Daltronics) equipped with a SmartBeam 200 Hz laser. NALDI plates were mounted onto the

NALDI adaptor target and loaded into the Autoflex III. Scanned tissue images, on pSi or NALDI substrates prior to solvent separation, were loaded into FlexImaging 2.1 (build 25) and aligned with the steel target plate containing the pSi or NALDI sample based on three teach points. The imaging area was selected based on the tissue area plus the 20 mm solvent wash area adjacent to the tissue. FlexImaging 2.1 distribution maps were used to control FlexControl 3.3 (build 85) during image acquisition. Samples were run in reflectron positive mode in the 20–1000 Da range, with a spatial resolution of 150  $\mu\text{m}$  and medium laser focus, corresponding to a 50  $\mu\text{m}$  diameter. Colour maps for secondary metabolites were based on the corresponding  $m/z$  which was evaluated using spot spectra analysed in FlexAnalysis 3.3 (build 65).

### 3.3.7 Statistical analyses

Statistical analyses were undertaken using Primer V6 + PERMANOVA add-on. For all analyses, Euclidean distance similarity matrices were generated from the normalised relative intensity values and 9999 permutations were run. A two factor multivariate analysis was used to compare the overall composition of compounds detected on DIOS and NALDI, as well as between the different solvent separations. Two factor univariate PERMANOVs were also used for each individual compound. In cases where a significant interaction was detected between factors, pairwise tests on were run grouped according to the nanostructure, as well as the solvent. Monte Carlo tests were used to establish significance in the cases where  $\leq 10$  unique permutations were possible. The multivariate data was also graphically represented using a principle coordinate ordination with vector overlay based on Pearson correlation  $r > 0.3$ .

## 3.4 Results and discussion

On surface solvent extraction from biosynthetic regions of marine mollusc tissue (Figure 3.1) was effective in detecting spectral signals associated with secondary

metabolites on both NALDI and DIOS substrates (Table 3.1). This approach not only simplified identification (Figure 3.3) and but also allowed specific metabolite fragments to be co-detected in the absence of complicated spectral patterns associated with primary metabolites and lipid fragments (e.g., murexine, Figure 3.3). Known metabolites had comparable masses for both NALDI-MS and DIOS-MS, but varied in +H additions compared to LC-MS (Figure 3.3). Using matrix free LDI-MS, the metabolites were all detected using positive ionization in reflectron mode. High resolution for detected compounds could effectively discern isotopic patterns for identification of bromine. Only two known precursor brominated indoles were not detected using nanostructured surfaces; tyrindoxyl and tyriverdin remained elusive, most likely due to rapid oxidation (Benkendorff, 2013, Cooksey, 2001).

**Table 3.1** NALDI-MS and DIOS-MS detected secondary metabolites from the nanostructured surfaces adjacent to the hypobranchial gland after solvent separation. + Indicates detection within combined spectra. The heading “calc. exact mass” refers to the  $M_{\text{monoisotopic}}$  mass whilst major ions refers to the nominal mass to account for slight mass shifts between surfaces.

Compound Class/ Compound	Formula	calc. [M] exact mass	Detected in Solvent Wash				LDI-MS	Major Ions m/z		Major Ions m/z	
			Water	Ethanol	Chloroform	Hexane	[M]	NALDI	DIOS	RT (min)	LC-MS
Brominated indoles											
Tyrindoxyl sulfate	$C_9H_7BrNO_4S_2^-$	335.9011	+	+			$[M + 2H]^+$	337, 339	337, 339	6.52	336, 338
Tyrindoxyl sulfonic acid	$C_9H_8BrNO_4S_2$	336.9078					$[M+3H]^+$	339, 341	339, 341		
Tyrindoxyl	$C_9H_8BrNOS$	256.9510									
Tyrindoleninone	$C_9H_6BrNOS$	254.9353		+	+		$[M+2H]^+$	256, 258	256, 258	10.96	256, 258
Tyrindolinone	$C_{10}H_{10}BrNOS_2$	302.9387		+	+		$[M+2H]^+$	304, 306	-		
6-Bromoisatin	$C_8H_4BrNO_2$	224.9425		+	+		$[M-H]^+$	224, 226	223, 225	6.35	224, 226
Tyriverdin	$C_{18}H_{14}Br_2N_2O_2S_2$	511.8863								11.67	511, 513, 515
Tyrian purple (6,6'-Dibromoindigo)	$C_{16}H_8Br_2N_2O_2$	417.8953			+		$[M + H]^+$	418, 420, 421	418, 420, 421	14.34	417, 419, 421
6,6'-Dibromoindirubin	$C_{16}H_8Br_2N_2O_2$	417.8953			+		$[M + H]^+$	418, 420, 421	418, 420, 421		
Choline esters											
Choline	$C_5H_{14}NO^+$	104.1075	+	+		+	$[M]^+$	104	104		
Murexine	$C_{11}H_{18}N_3O_2^+$	224.1394	+	+			$[M]^+$	224	224	1.83	224

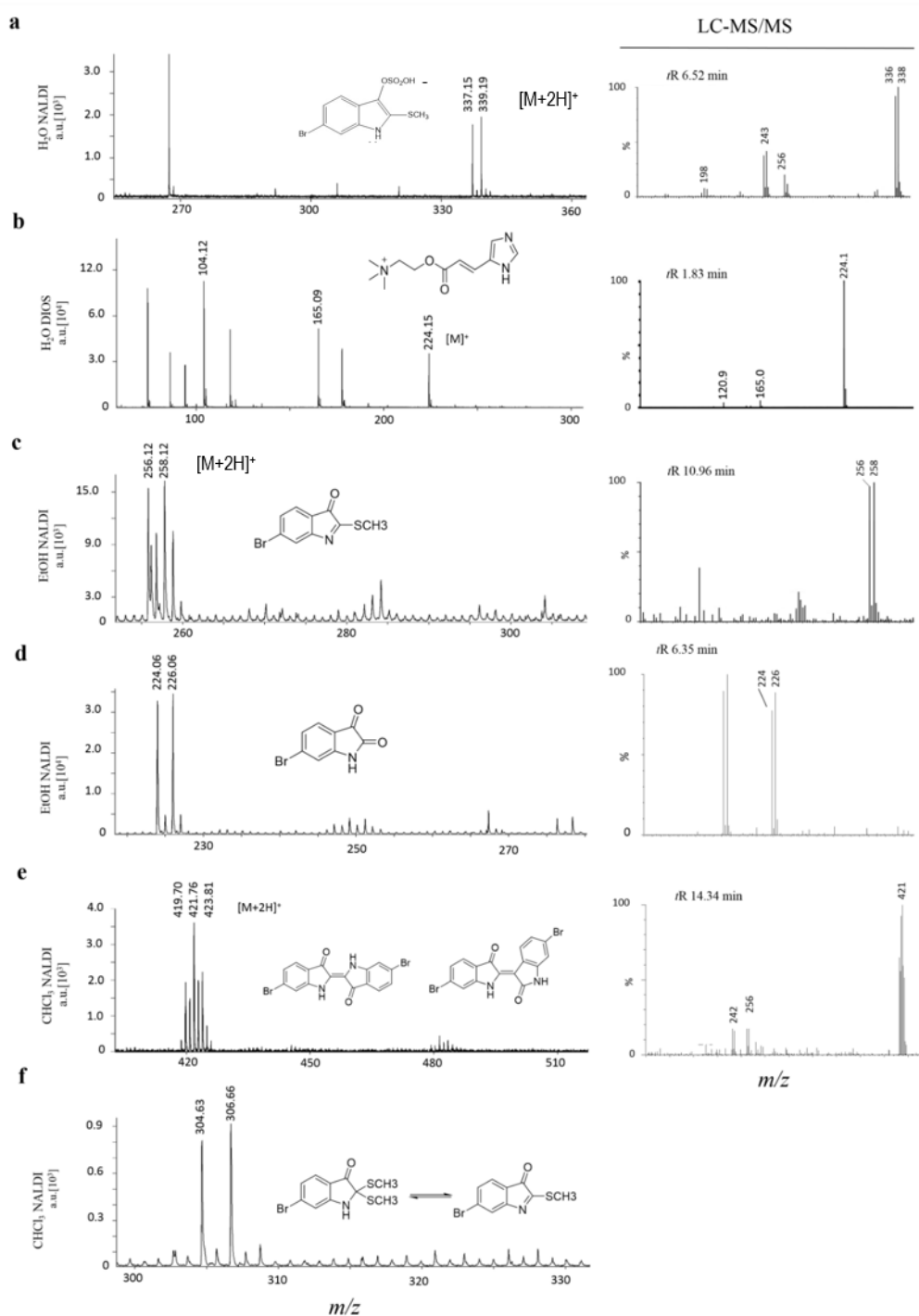


**Figure 3.3** Mass spectra from solvent wash area directly adjacent to hypobranchial tissue. Secondary metabolites on either NALDI or DIOS substrates with adjacent LC-MS/MS of medial hypobranchial extract. Metabolites include: (a) tyrindoxyl sulfate; (b) murexine; (c) tyrindoleninone; (d) 6-bromoisatin; (e) Tyrian purple 6,6'-dibromoindigo (may include isomer 6,6'-dibromoindirubin); and (f) tyrindolinone (not detected in LC-MS but known to generate from tyrindoleninone and methane thiol).

Permutational multivariate analysis (PERMANOVA) revealed that the overall composition of secondary metabolites (Figure 3.4) varied according to both the type of nanosurface (Pseudo F = 5.5,  $p = 0.004$ ) and the solvent used for on-surface separation (Pseudo F = 23.5,  $p = 0.001$ ) and there was a significant interaction between these factors (Pseudo F = 4.7,  $p = 0.001$ ). Pair-wise tests revealed that there was no significant difference in the secondary metabolite composition detected by DIOS and NALDI after separation in water ( $p = 0.97$ ) or chloroform ( $p = 0.27$ ), however, the type of nanosurface did influence the compound composition after separation in ethanol ( $p = 0.006$ ) and hexane ( $p = 0.0008$ ) (Figure 3.4). Irrespective of whether DIOS or NADLI was used, the composition of compounds detected was significantly different between every pair of solvents ( $p < 0.05$ ). Principal coordinate ordination with trajectory overlay based on Pearson correlation (Figure 3.4) confirms that differences between solvents are driven by polarity, with a strong correspondence between the polarity of the solvent and the hydrophobicity of the compounds (Log P, Table 3.2). These results imply that the type of nanosurface used for MSI and any solvent used for washing the surface after tissue imprinting should be optimised according to the polarity of the secondary metabolites of interest.

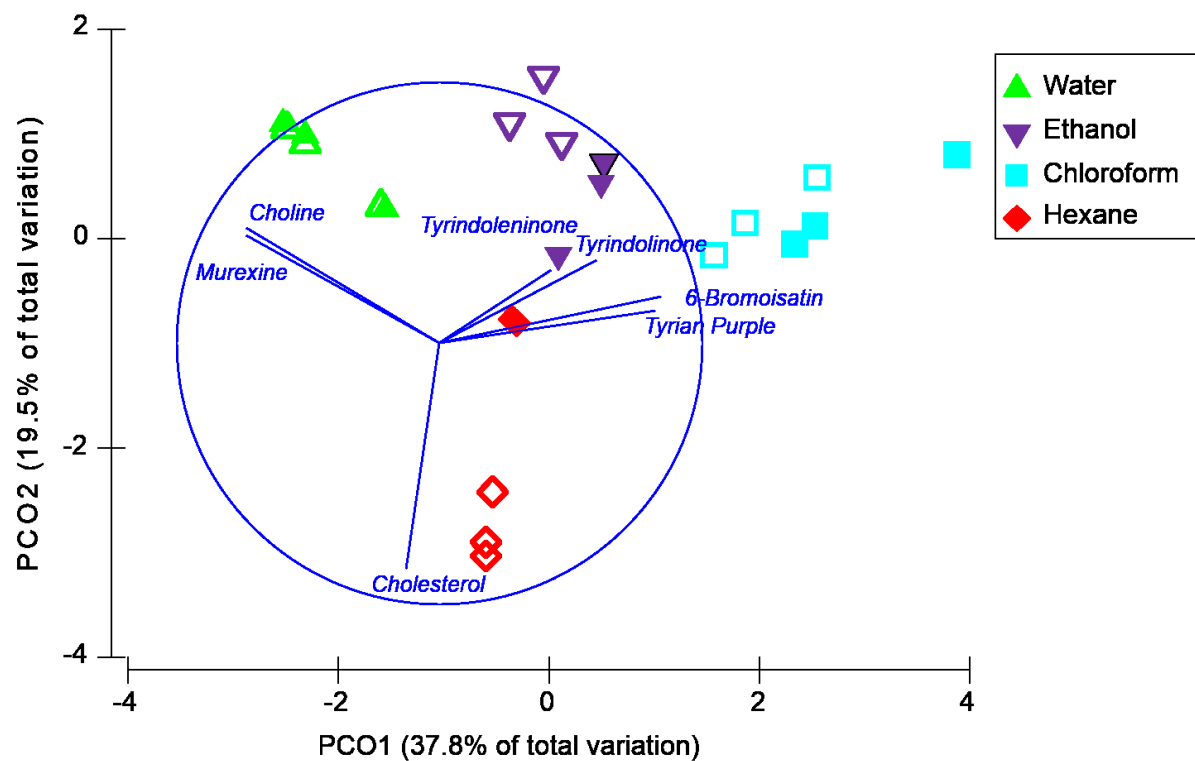


**Figure 3.4** Principal coordinate analysis based on the normalised relative intensities of secondary metabolites detected after solvent separation on NALDI (open symbols) and DIOS (filled symbols) surfaces, grouped according to the type of solvent used ( $n = 3$ ). Trajectory overlay is based on Pearson correlations ( $r > 0.3$ ).

**Table 3.2** Mean ion intensity ( $n = 3$ )  $\pm$  standard deviation for secondary metabolites in the solvent wash area after separation from the hypobranchial gland tissue imprints on NALDI and DIOS nanostructured surfaces with corresponding LogP values (calculated using chemoinformatics software ChemBioDrawUltra 13.0). Significant differences in the ion intensity for each compound were tested using univariate two factor PERMANOVA, followed by pairwise-tests.

Compound	LogP	NALDI				DIOS			
		Water	Ethanol	Chloroform	Hexane	Water	Ethanol	Chloroform	Hexane
Choline	-4.236	78,500 ( $\pm 49,374$ ) <sup>a</sup>	25,067 ( $\pm 1,6050$ ) <sup>b</sup>	N.D.	19,500 ( $\pm 7378$ )	79,000 ( $\pm 46,776$ ) <sup>a</sup>	19,500 ( $\pm 7378$ ) <sup>b</sup>	N.D.	6264 ( $\pm 2139$ ) <sup>c</sup>
Murexine	-3.373	33,000 ( $\pm 3812$ ) <sup>a</sup>	5320 ( $\pm 1959$ ) <sup>b</sup>	N.D.	N.D.	33,067 ( $\pm 3782$ ) <sup>a</sup>	1450 ( $\pm 704$ ) <sup>b</sup>	N.D.	N.D.
Tyrindoxyl sulfate **	-0.346	2625 ( $\pm 711$ ) <sup>a</sup>	22,133 ( $\pm 2108$ ) <sup>b</sup>	N.D.	N.D.	1809 ( $\pm 135$ ) <sup>a,c</sup>	5651 ( $\pm 3922$ ) <sup>c</sup>	N.D.	N.D.
6-Bromoisatin *	1.615	N.D.	360 ( $\pm 213$ ) <sup>a</sup>	1775 ( $\pm 725$ ) <sup>b</sup>	N.D.	N.D.	656 ( $\pm 646$ ) <sup>a</sup>	3678 ( $\pm 485$ ) <sup>c</sup>	N.D.
Tyrindoleninone *	2.889	N.D.	2506 ( $\pm 1736$ ) <sup>a</sup>	2945 ( $\pm 1277$ ) <sup>a</sup>	N.D.	N.D.	7957 ( $\pm 2704$ ) <sup>b</sup>	2581 ( $\pm 1311$ ) <sup>a,b</sup>	N.D.
Tyrindolinone	2.999	N.D.	424 ( $\pm 107$ )	958 ( $\pm 233$ )	N.D.	N.D.	N.D.	373 ( $\pm 647$ )	N.D.
Tyrian purple (6,6'-Dibromoindigo 6,6'-Dibromoindirubin)	4.47	N.D.	N.D.	6447 ( $\pm 2093$ )	N.D.	N.D.	N.D.	10848 ( $\pm 4118$ )	N.D.
Cholesterol	7.11	4722 ( $\pm 755$ )	N.D.	N.D.	N.D.	N.D.	N.D.	N.D.	N.D.

Different letters <sup>a, b & c</sup> indicate significant differences between each nanosurface and solvent combination ( $p < 0.05$ ); Overall differences between the ion intensity on NALDI and DIOS are also indicated for each compound as  $p \leq 0.05$  (\*) and  $p \leq 0.01$  (\*\*); N.D. = not detected.

### 3.4.1 Hydrophilic compounds

H<sub>2</sub>O extraction from the medial hypobranchial gland was effective in concentrating the hydrophilic compounds tyrindoxyl sulfate, choline and choline ester murexine directly onto the mass spectrometry surfaces (Figure 3.3, Table 3.1). Both NALDI-MS and DIOS-MS detected ions at  $m/z$  337, 339, corresponding to the  $[M + H]^+$  ion for tyrindoxyl sulfate (Figure 3.3). Interestingly, tyrindoxyl hydrogen sulfate,  $[M + 4H]^+$ , was detected in the tissue and immediately adjacent to the tissue for DIOS-MS only. The  $[M + H]^+$  for tyrindoxyl hydrogen sulfate was detected on both substrates, but further out from the tissue margin, 10 to 20 mm away (e.g., Figure 3.2c).

NALDI-MS and DIOS-MS consistently detected peaks at  $m/z$  224.1, the  $[M]^+$  ion for murexine, up to 20 mm away from the tissue margin. The assignment for murexine is further supported by the fragment ion at  $m/z$  165, seen co-located with the parent ion (Figure 3.3). Cleaner spectra afforded by solvent separation for murexine makes the assignment of ions and fragment ions easier due to the consistency in the co-localized peaks, which is comparable to collision induced dissociation (CID) fragment ions from LC-MS/MS (Figure 3.3). Choline was also detected co-localized with murexine using both surfaces.

Choline was the most dominant ion detected from H<sub>2</sub>O separation (Table 3.2), followed by murexine (mean intensity ~33,000 a.u. for both surfaces; Table 3.2). Tyrindoxyl sulfate was also detected by H<sub>2</sub>O separation, but at less than one tenth of the intensity of murexine (Table 3.2). Tyrindoxyl sulfate forms a salt complex with both choline ester murexine and choline in the hypobranchial gland (Baker and Duke, 1976). This is considered to be a mechanism by which these secondary metabolites are stored prior to liberation from the medial region into the external environment (Benkendorff, 2013). The detection of tyrindoxyl hydrogen sulfate  $[M + 4H]^+$  within and immediately adjacent to the tissue may be an indication of the salt of choline ester

complex, whereas the  $[M + H]^+$  of tyrindoxyl sulfate could be the liberated compound, which undergoes enzymatic cleavage by an arylsulfatase enzyme (Laffy et al., 2013). Murexine is a natural tranquiliser secreted by predatory species of the Muricidae, and has been suggested to be a predatory specialization due to its absence in herbivorous or scavenging molluscs (Roseghini et al., 1996).

Washing is often a part of MSI workflows as a means of removing residual salt during sample preparation. As demonstrated with the H<sub>2</sub>O solvent separation here, excessive washing could lead to delocalisation of hydrophilic secondary metabolites and a complete loss of detection (Figure 3.2). Previous MSI of the hypobranchial region show tyrindoxyl sulfate is still detected and largely remains localised to the medial hypobranchial gland (Ronci et al., 2012), an expected location, but can be completely washed out of tissue if using enough solvent (Figure 3.2).

### 3.4.2 Ethanol solvent separation

Signals for tyrindoxyl sulfate  $[M + H]^+$ , choline and murexine were detected on both substrates after EtOH separation from the tissue (Table 3.1). EtOH also removed tyrindoleninone  $m/z$  256, 258  $[M]^+$ ; tyrindolinone  $m/z$  304, 306  $[M]^+$ ; and 6-bromoisatin  $m/z$  224, 226  $[M]^+$ , detected across the entire solvent area 20 mm from the tissue margin (Figure 3.3, Table 3.1). Tyrindoxyl sulfate, was detected only as the  $[M + H]^+$  ion and showed a significantly higher mean intensity on NALDI than DIOS surfaces ( $p = 0.0026$ ). In comparison to H<sub>2</sub>O separation, the mean intensity of tyrindoxyl sulfate had an almost tenfold increase in intensity in the EtOH residue on NALDI-MS ( $p = 0.001$ , Table 3.2). Conversely, on-surface detection of murexine after EtOH separation resulted in a significant six times reduction in mean intensity, compared to H<sub>2</sub>O separation from both NALDI and DIOS surfaces ( $p = 0.007$ , Table 3.2). Choline intensity was also significantly reduced after EtOH separation ( $p = 0.04$ ,

Table 3.2). Of the solvents tested, H<sub>2</sub>O is ideal for the extraction of the cationic murexine and choline, whilst EtOH extraction maximizes recovery of the counter ion tyrindoxyl sulfate.

Tyrindoleninone was detected at a significantly higher intensity on DIOS-MS compared to NALDI-MS and DIOS after EtOH separation ( $p = 0.045$ , Table 3.2), whereas tyrindolinone was only detected on NALDI-MS at a low intensity (Table 3.2). Tyrindoleninone, tyrindolinone and 6-bromoisatin are intermediate indoles which form after the enzymatic cleavage of tyrindoxyl sulfate (Cooksey, 2001) by an arylsulfatase enzyme (Laffy et al., 2013). Intermediate brominated indoles are formed by oxidative and photolytic degradation, which leads to variability in their relative quantities in tissue samples. This variability can be minimized across samples by careful handling, particularly by minimizing exposure to light and oxygen. The major point at which samples are most exposed to light and oxygen during on-surface solvent separation is during the placement of sections onto the nanostructured surface. Degradation was further reduced using a gentle stream of nitrogen gas when handling. Outside of sample placement, degradation can be minimized as tissue can be sectioned frozen (held at  $-80$  °C and brought up to  $-20$  °C in the cryostat during cutting), and LDI-MS is done in a high vacuum with no light. Therefore, LDI-MS detection should be done immediately after solvent separation to prevent on-surface degradation of precursors that have separated from the tissue.

The differences in measured intensity of some secondary metabolites between the two surfaces could be attributed to the differences in the surface chemistry. NALDI plates are surface coated with a layer of inorganic nanostructures to absorb laser energy (Bruker Daltronics), whilst the pSi are functionalized with silanes (F<sub>5</sub>PhPr) and the etched porosity provides laser energy absorption preventing excessive fragmentation from the laser shot (Trauger et al., 2004). In this case, the use of ethanol solvent

separation shows NALDI to desorb and ionise hydrophilic compounds better than DIOS. This indicates that DIOS may be more hydrophobic than NALDI surfaces. The advantage of DIOS, over NALDI, is that DIOS can be treated with different silanes (Trauger et al., 2004), which can change the hydrophobicity of the surface to target specific classes of secondary metabolites.

### 3.4.3 CHCl<sub>3</sub> solvent separation

Both NALDI-MS and DIOS-MS failed to detect the more hydrophilic compounds after CHCl<sub>3</sub> separation, as anticipated (Table 3.2). Tyrindoleninone, tyrindolinone and 6-bromoisatin were detected on both substrates across the solvent area. CHCl<sub>3</sub> also effectively extracted Tyrian purple with detected spectra showing a triplet cluster centred at  $m/z$  421  $[M + 2H]^+$  (Figure 3.4e) on both NALDI and DIOS substrates. CHCl<sub>3</sub> has been the solvent of choice when extracting brominated indoles from fresh macerated hypobranchial glands (Westley et al., 2010c, Edwards et al., 2012, Esmaeelian et al., 2013b) and NALDI-MS and DIOS-MS detected all expected metabolites except tyrindoxyl and tyriverdin (Cooksey, 2001). Tyrindoxyl is an unstable intermediate created by enzymatic cleavage of tyrindoxyl sulfate with an arylsulfatase enzyme (Cooksey, 2001), which is also expressed in the medial hypobranchial gland (Laffy et al., 2013). The absence of tyrindoxyl from LDI analysis could be due to the unstable nature of the compound. The absence of tyriverdin from both substrates, indicated by the lack of the parent ion calculated as a triplet ion cluster centred on  $m/z$  514, may be due to the high instability of this compound, as previously reported from mass spectrometry analyses (Westley and Benkendorff, 2008). Triplet ion clusters, characteristic of di-brominated compounds, were detected with centre peaks at  $m/z$  483 and 438, which may be fragment ions of tyriverdin.

6-Bromoisatin was detected at significantly higher intensities on DIOS-MS compared to NALDI-MS ( $p = 0.0157$ ) and showed a significant five-fold increase after  $\text{CHCl}_3$  separation in comparison to EtOH ( $p = 0.0005$ , Table 3.2). Tyrian purple was only detected in  $\text{CHCl}_3$  separations and the mean LDI-MS detection was not significantly different on DIOS compared to NALDI surfaces ( $p = 0.17$ , Table 3.2). Therefore, despite the fact that a greater diversity of compounds were detected after EtOH separation,  $\text{CHCl}_3$  increases the detection of some brominated indoles. This could be a result of higher LogP and solvation characteristics that are more suited to  $\text{CHCl}_3$  extraction. Alternatively, as 6-bromisatin and 6,6-dibromoindigo are both end-products in a series of oxidative and photolytic reactions, solubility of intermediate precursors in  $\text{CHCl}_3$  may facilitate increased degradation.

### 3.4.4 Lipophilic separation using *n*-hexane

After hexane solvent separation, LDI-MS detected a consistent signal at  $m/z$  104, which is the  $[\text{M}]^+$  ion for choline (Tables 3.1 and 3.3). Choline has been detected in *D. orbita* from the medial hypobranchial gland (Roseghini et al., 1996) co-localized with choline esters, the natural tranquilizers found in many members of the Muricidae (Roseghini et al., 1996). Choline is also known to be associated with tyrindoxyl sulfate, acting as a counter ion prior to secretion from the tissue (Roseghini et al., 1996, Baker and Duke, 1976). The mean intensity of choline was significantly lower after hexane separation in comparison to water ( $p = 0.0172$ ) and ethanol ( $p = 0.0121$ ), as would be expected from its high polarity (Table 3.2). However, other consistent peaks detected in hexane samples include  $m/z$  184, corresponding to phosphocholine headgroup (Table 3.3), which is a characteristic fragment ion of phosphatidylcholine lipid groups (Passarelli et al., 2013). The  $m/z$  184 ion has been detected during secondary ion mass spectrometry imaging of *Aplysia californica* neurons (Passarelli et al., 2013), where it is a fragment from the lipid component of the neural cell membrane.

**Table 3.3** Primary metabolites and associated lipophilic ions detected after hexane separation originating from either free fatty acids or phospholipid origin. References indicate previous detection in molluscan tissues.

m/z	Formula	[M]	Tentative match	Reference
86.119				
104.136	C <sub>5</sub> H <sub>14</sub> NO	[M] <sup>+</sup>	Choline	(Baker and Duke, 1976)
184.101	C <sub>5</sub> H <sub>15</sub> NPO <sub>4</sub>	[M + H] <sup>+</sup>	Phosphocholine headgroup	(Passarelli et al., 2013)
198.114				
228.277				
256.309				(Benkendorff et al., 2005, Idler and Wiseman, 1971, Jarzębski et al., 1986)
368.448	C <sub>27</sub> H <sub>46</sub> O	[M – H <sub>2</sub> O] <sup>+</sup>	Cholesterol	

Consistent ions at  $m/z$  256 and 228 (Table 3.3) could be attributed to fatty acids washed out during hexane separation. Many gastropod species (Bergmann, 1949) and the benthic encapsulated embryos of gastropods molluscs, including *D. orbita* (Benkendorff et al., 2005) are rich in fatty acids. Fatty acids and choline may also originate from phospholipid fragments, such as the  $m/z$  184 ion, which can be generated from post source decay (Kruse et al., 2001). The other remaining consistent peak in the hexane separation on NALDI is possibly cholesterol, detected as the  $[M - H_2O]^+$  at  $m/z$  368.4 (Tables 3.2 and 3.3). Cholesterol is known to be a major sterol found in molluscan tissue (Idler and Wiseman, 1971) and the dominant sterol in benthic spawn (Benkendorff et al., 2005). Cholesterol can often be found largely intact using mass spectrometry analysis, usually in the  $[M + H - OH]^+$  form, and has been detected in *Aplysia* neurons (Passarelli et al., 2013).

Cholesterol, fatty acids, and lipids more generally, provide a considerable proportion of the fuel reserves within the muscles and organs of adult molluscs (Benkendorff et al., 2005, Jarzębski et al., 1986). Cholesterol is also known to be a major component of the cell membrane, where it interacts with sphingolipids to order the membrane structure, influencing membrane permeability and fluidity (Munro, 2003). As lipids contribute to fuel reserves in molluscs, lipid-rich tissues or organs adjacent to secretory or storage regions may be an indication of biosynthetic sites where secondary metabolites are constructed prior to storage and deployment. Alternatively, lipid-rich regions in adult females may be sites where fatty acids, cholesterol or specialised lipid structures are incorporated into egg capsules or spawning material. The lipid content of mollusc egg masses have shown antimicrobial activity, which would aid in the viability of benthic egg masses during development (Benkendorff et al., 2005). Simplified spatial analysis of maternally derived lipid classes would be an excellent tool for assessing resource partitioning within the field of chemical ecology.

### 3.4.5 Quantification of secondary metabolites using SALDI-MS

Quantification using mass spectrometry intensity data requires the adjacent use of known standards or purified compound to establish the level of comparative ion intensity. Available standards applied adjacent to the solvent area allowed the quantification of the highest intensity detected for tyrindoleninone, 6-bromoisatin and Tyrian purple (Table 3.2) compared to linear concentration curves (Figure 3.5). Not all metabolites behave in the same fashion during mass spectrometry ionisation/vaporisation or subsequent time-of-flight analysis (TOF) (Hortin, 2006). When using reflectron mode for LDI-MS, which has suitable resolving power in the low molecular mass range, the pulsed laser extraction delay is optimised to allow plume formation and equivalent ion velocities entering into the TOF tube (Brown and Lennon, 1995). Lower delayed extraction times create a window for ion selection which produces a bias towards the low molecular mass range (Hortin, 2006), reducing resolution and peak intensity for larger compounds. Therefore LDI mass window settings must remain constant during acquisition and intensity values cannot be extrapolated outside of the parameters for each acquisition.

Purified fractions of 6-bromoisatin, tyrindoleninone and Tyrian purple were used effectively to generate standard curves (Figure 3.5). This facilitated approximation of metabolite *ex situ* relative quantification, as the increases in intensity follow linear trends (Figure 3.5). The *ex situ* distribution changes across the solvent wash area (Figure 3.2), so the highest intensity detected for each compound from the summed spectra was selected for comparison to standard curves. Purified 6-bromoisatin dissolved in DMSO at 600, 300, 150, 75 and 37.5 mg/L applied to both NALDI and DIOS surfaces adjacent to solvent separation wash, produced a linear concentration gradient ( $R^2 = 0.9941$ , Figure 3.5a). Tyrindoleninone also produced a linear

concentration gradient ( $R^2 = 0.959$ , Figure 3.5b) when dissolved in DMSO at the same five concentrations. Finally, a purified fraction of Tyrian purple (600, 300, 150, 75 and 37.5 mg/L) gave a linear concentration gradient for LCI-MS signal intensity ( $R^2 = 0.989$ , Figure 3.5c). There are some limitations in this approach, in that the matrix effect from other constituents in the washed tissue sample is not present for the spotted standards. In light of this limitation a stable isotopic standard or deuterated standard included into the sample would replicate the matrix effects seen for endogenous secondary metabolites, if labelled standard are available.

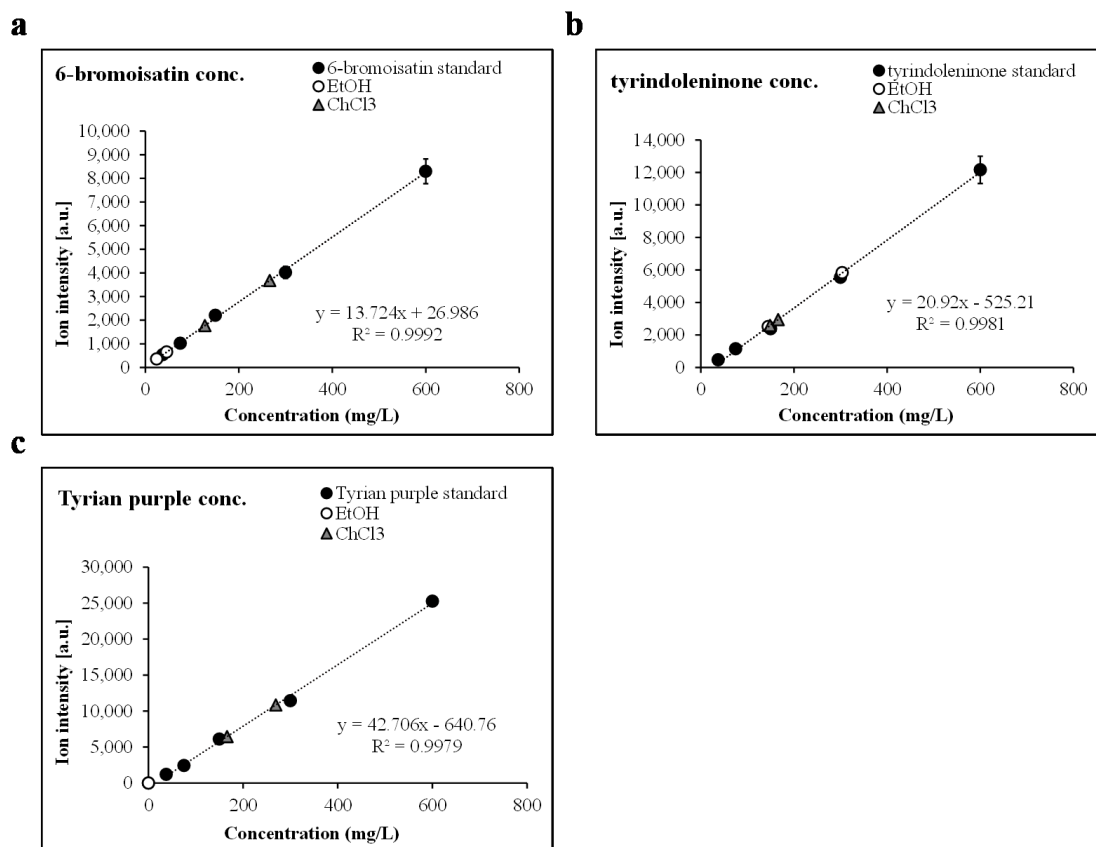


**Figure 3.5** Relative quantity of *ex situ* secondary metabolites from the hypobranchial gland compared to standard curves for (a) 6-bromoisatin; (b) tyrindoleninone and (c) Tyrian purple from triplicate samples at five concentrations. Error bars for each standard relate to one standard deviation above and below the mean.

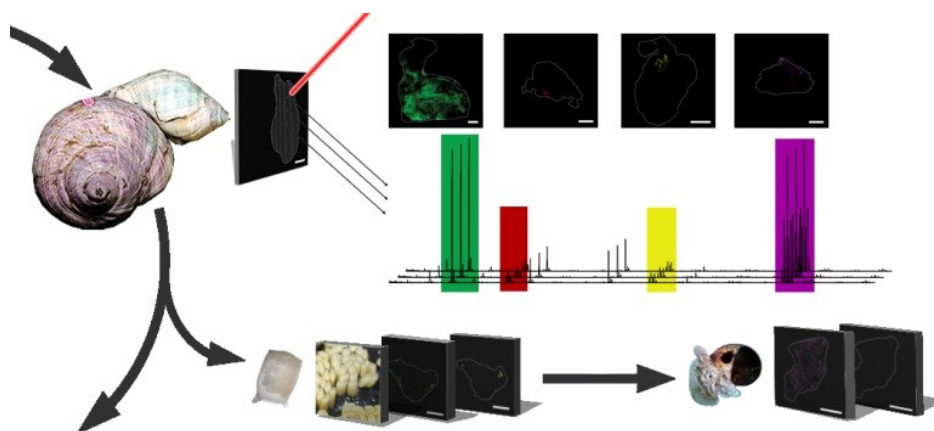
### **3.5 Conclusions**

Nanostructured surfaces for use in LDI-MS analysis broaden the qualitative, quantitative and spatial MS analysis of low molecular weight compounds. They are ideal for small molecular weight primary and secondary metabolites because they are not masked or impeded by matrix ions. Surface-assisted LDI-MS provides an effective platform for the spatial analysis of heterogeneous tissue, requiring minimal samples sizes (effective for 4  $\mu\text{m}$  thick samples) and detecting metabolites across multiple structural classes over a wide polarity range. Simple chromatographic separations on NALDI and DIOS surfaces after tissue imprinting can effectively simplify the efforts for annotating LDI spectra. The NALDI and DIOS surfaces also show promise for quantifying known metabolites in tissue samples. The simplified analytical technique combined with the broad utility of the surfaces are a good reason for their adoption in chemical ecology, marine natural products, metabolomics and any field concerned with characterizing metabolites.

### **3.6 Acknowledgments**

We would like to thank the Flinders Analytical department, especially Daniel Jardine and Jason Young, for assistance with the Bruker AutoFlex III operation and maintenance. Special thanks are extended to Taryn Guinan for the supply of DIOS chips. This paper was financially supported by an Australian Postgraduate Award and Philanthropic funding awarded to Kirsten Benkendorff.

## 4 Chapter Four - Mass spectrometry imaging reveals new biological roles for choline esters and Tyrian purple precursors in muricid molluscs



### 4.1 Abstract

Despite significant advances in chemical ecology, the biodistribution, temporal changes and ecological function of most marine secondary metabolites remain unknown. One such example is the association between choline esters and Tyrian purple precursors in muricid molluscs. Mass spectrometry imaging (MSI) on nanostructured surfaces has emerged as a sophisticated platform for spatial analysis of low molecular mass metabolites in heterogeneous tissues. Here we applied desorption-ionisation on functionalised porous silicon (DIOS) to examine *in situ* changes in biodistribution over the reproductive cycle. The muscle-relaxing choline ester murexine was found to co-localize with tyrindoxyl sulfate in the biosynthetic hypobranchial glands, but during egg-laying both compounds were transferred to the capsule gland, followed by the egg capsules, where chemical ripening resulted in Tyrian purple formation. Murexine was found to tranquilise the larvae and may relax the reproductive tract. This study shows that DIOS-MSI is a powerful tool providing new insights into marine chemo-ecology.

## 4.2 Introduction

Secondary metabolites are known to chemically mediate intra- and interspecies interactions between organisms (Hay, 1996). In molluscs, secondary metabolites have been detected and identified during mate attraction (Cummins et al., 2004), defence (Cimino et al., 1991, Kelley et al., 2003), predatory behaviour (Olivera et al., 1990), anti-fouling (Benkendorff et al., 2001b, Benkendorff, 2010) and reproduction (Zatylny et al., 2002). The importance of understanding the mechanisms behind these chemical interactions within a species cannot be underestimated, particularly when specific secondary metabolites impart a competitive advantage. Advantageous secondary metabolites have been known to have community wide effects across multiple trophic levels, termed “keystone” molecules (Derby and Zimmer, 2014, Benkendorff, 2014). The initial step in understanding the function, and therefore relevance of secondary metabolites to the producing organism, is to understand the *in situ* synthesis, storage and deployment (Kroiss et al., 2010, Garson, 1993). To place secondary metabolites in an ecological context, their biodistribution and abundance should be examined on a temporal scale relevant to the biological phenomena which they mediate. Reproducible methods that can spatially and temporally detect secondary metabolites *in situ* will significantly advance the field of chemical ecology (Esquenazi et al., 2009).

Current advances in mass spectrometry imaging (MSI) provide a sophisticated platform to spatially map the distribution of biologically-relevant molecules or mixtures by detection of their molecular mass and characteristic fragment ions in tissues (Kroiss et al., 2010, Bouslimani et al., 2014). MSI is often based on matrix-assisted laser desorption ionisation (MALDI) (Caprioli et al., 1997, Cornett et al., 2007), a soft ionisation technique that relies on aromatic molecules (the matrix) for

energy transfer from a UV laser to the analyte. MSI has been gaining traction in the analysis of ecologically relevant chemical exchanges, demonstrating bacterial metabolic communication (Watrous and Dorrestein, 2011, Yang et al., 2009, Watrous et al., 2013, Watrous et al., 2010), symbiotic interactions (Kroiss et al., 2010, Simmons et al., 2008) and chemical defence (Lane et al., 2009). However, the standard matrix used in MALDI can suppress signals from small molecules, particularly when present in low abundance (Alhmoud et al., 2014). Consequently, matrix-free MSI approaches, such as desorption-ionisation on silicon mass spectrometry (DIOS-MS), which uses a thin porous silicon (pSi) film (Wei et al., 1999), have been developed to enhance detection of small molecular weight organic compounds (typically <1000 Da), without the need for a matrix (Lowe et al., 2009, Guinan et al., 2012). Recently, we reported a new method to detect brominated indoles from mollusc tissue using DIOS-MSI (Ronci et al., 2012). This approach uses tissue stamping onto a pSi film to extract low molecular weight molecules by affinity into the porous surface, whilst retaining the spatial distribution of secondary metabolites that occurs *in situ*. Imprinting from frozen cryo-sections also allows the spatial organisation of the tissue to be maintained, an advantage for the analysis of exceptionally soft marine secretory tissue. Exploiting DIOS-MSI to detect secondary metabolites comes with a major benefit, namely the possibility of chemically functionalising the pSi to target specific compounds or classes of compounds that would otherwise be difficult to detect (Ronci et al., 2012). Functionalised pSi therefore provides an optimal substrate for monitoring micro-changes in complex heterogeneous marine tissue, in space and time.

Muricidae molluscs have been of significant interest as biological and chemical resources since antiquity (Cooksey, 2001, Cooksey, 2013). They are a source of biologically active brominated indoles (Figure 4.1) that are precursors to the historically significant dye Tyrian purple (Benkendorff, 2013). Tyrian purple (6,6'

dibromoindigo) was the first marine natural product to be structurally elucidated (Friedlander et al., 1912) and is still commonly used as a tool for teaching organic chemistry (Schatz, 2001). Nevertheless, the biological function of Tyrian purple remains unknown and is suggested to simply be an artefact formed from the degradation of indoxyl sulfate precursors, which are stored as salts of choline ester derivatives (e.g. murexine, Figure 4.1) in the hypobranchial gland of these molluscs (Baker and Duke, 1976). Tyrian purple production is initiated by reaction of the indoxyl sulfate precursors with an aryl sulfatase enzyme (Figure 4.1), which is also produced and stored in the mollusc (Laffy et al., 2013), thus suggesting a regulated ecological function for the precursors. Muricidae choline esters show marked neuromuscular blocking activity (Roseghini et al., 1996) and have been implicated in the paralysis of prey by these predatory molluscs (Roseghini et al., 1996), whereas the brominated indole intermediates have antibacterial activity and have been implicated in the defense of the egg capsules (Benkendorff et al., 2000). The brominated indoles have also been found in extracts of the reproductive organs (Westley and Benkendorff, 2008), suggesting a maternal source for the egg capsules. However, it is unclear if the choline esters are also transferred into the egg capsules or why the molluscs constitutively produce and store these two distinct classes of compounds as an indoxyl sulfate-choline ester salt in the hypobranchial glands for controlled release on reaction with aryl sulfatase.

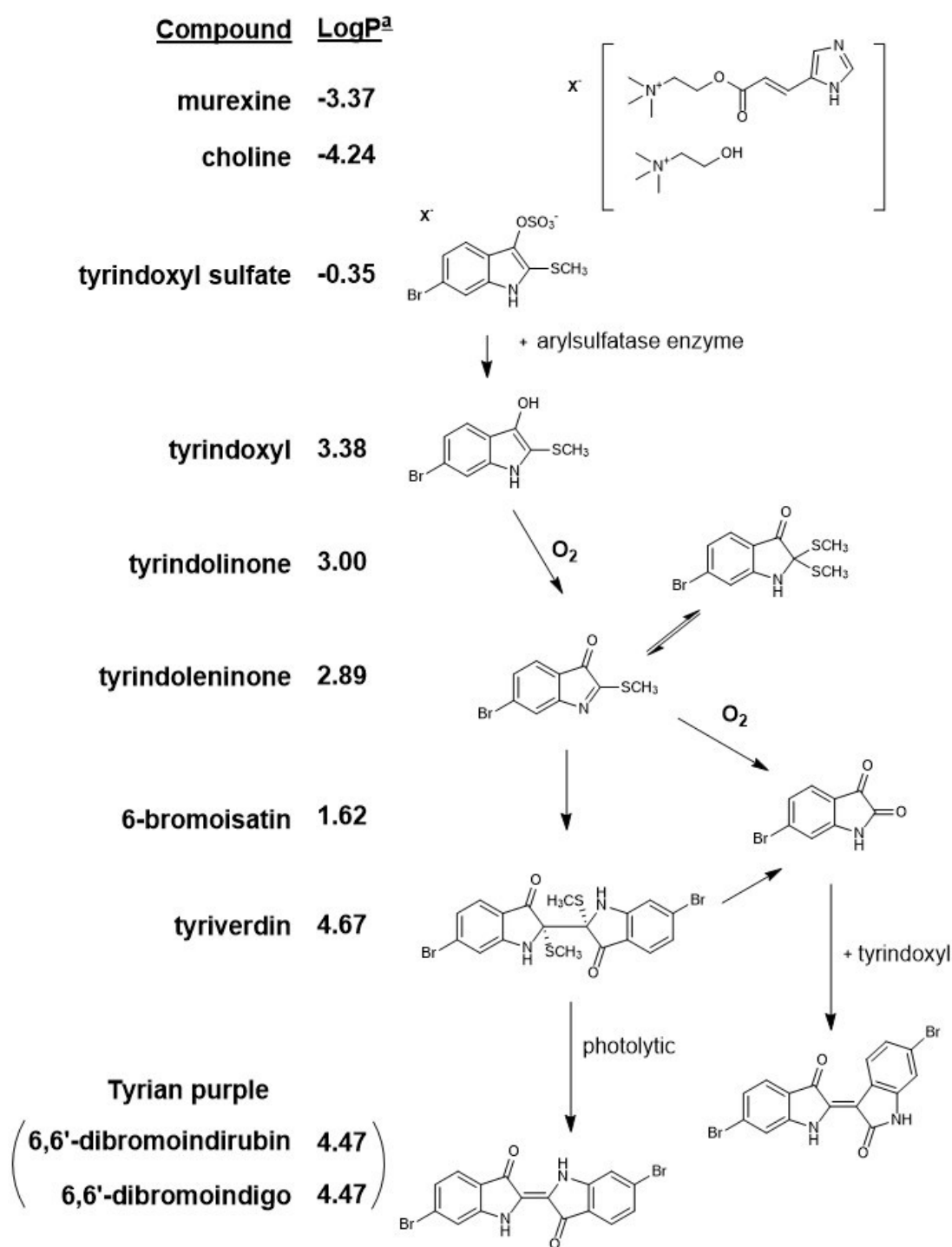


**Figure 4.1** The enzymatic, oxidative and photolytic reaction of bioactive compounds found in *Dicathais orbita* hypobranchial glands (Muricidae, Mollusca) with corresponding solubility indicator. <sup>a</sup>Log P was calculated using the chemoinformatics software Molinspiration

Here, we report the *in situ* spatial identification of brominated indoles and choline esters and examine temporal changes in their distributions within adult *Dicathais orbita* (Muricidae, Neogastropoda, Mollusca). MSI analysis was applied at different stages of the reproductive cycle of mature female *D. orbita*, along with early and late stages of encapsulated larval development, to investigate the role of these two classes of secondary metabolites in reproduction. Based on these results we hypothesised new biological roles for murexine in the reproduction and larval development of Muricidae. The tranquilising effect of murexine on the encapsulated larvae was then confirmed in biological assays. Overall, this approach allows spatial and temporal changes of secondary metabolites to be defined within the context of biological processes, such as reproductive activities.

### **4.3 Experimental methods**

#### **4.3.1 Collection and maintenance of whelk breeding population**

Pursuant to section 115, *D. orbita* samples were collected using an Exemption Permit to the South Australian Fisheries Management Act 2007 section 70 under the exemption number 9902638. Prior to the start of the breeding season, adult *D. orbita* were collected from rocky intertidal shores on southern metropolitan coast in South Australia and housed in recirculating aquarium systems at Flinders University. The breeding population was maintained at temperate marine conditions (18 °C and 35 psu seawater) and fed *ad libitum* on a diet of bivalves. Conditioned boulders were provided for egg capsule deposition. Pre-reproductive adult females ( $n = 3$ ) were selected for mass spectrometry imaging (MSI) to analyze secondary metabolite distribution 30 days prior to the standard breeding time (early September). During the breeding period, a female ( $n = 1$ ), observed in the process of egg capsule deposition was selected for MSI. Post-reproductive females ( $n = 3$ ), two weeks after egg capsule deposition, were

selected to image the post-reproductive tissue. Duplicate ( $n = 2$ ) egg capsules deposited from reproductive females were selected immediately after deposition to assess early stage embryos and maternal capsule contents by MSI. The remaining capsules were maintained for full intra-capsular development of 35 days, after which two ( $n = 2$ ) capsules with actively swimming larvae were selected to assess the veliger larvae and late stage capsule contents by MSI.

#### **4.3.2 Tissue preparation for mass spectrometry imaging (MSI)**

Selected adult specimens were prepared by cracking open the shell with a vice at the junction between the primary body whorl and spire. The soft body was then removed by cutting the columnar muscle. Soft tissue was rinsed in MilliQ water to reduce residual salt. Female hypobranchial glands and pallial gonoduct, including the egg capsule glands, were removed by incision along the connective mantle tissue between the ctenidium and the branchial hypobranchial gland, along the posterior gonoduct and digestive gland. The hypobranchial gland and pallial gonoduct were left connected and were placed in 5 mL polypropylene cryo-vials (Sarstedt, Nümbrecht, Germany) and snap frozen in liquid nitrogen. Frozen tissue samples were protected from light and stored at  $-80\text{ }^{\circ}\text{C}$  until required.

Egg capsules were retrieved from the substrate by an incision underneath the basal membrane of the capsule wall, to maintain capsule integrity, rinsed in MilliQ filtered water and snap frozen in liquid nitrogen within 5 mL cryo-vials for storage at  $-80\text{ }^{\circ}\text{C}$  until required.

#### **4.3.3 MSI pSi substrate fabrication, oxidation and functionalisation**

Monocrystalline ( $0.008\text{-}0.02\ \Omega\text{cm}$ ) antimony doped n-type Si (100) wafers (Silicon Quest International, CA, USA) were cut, methanol sonicated for cleaning and dried prior to substrate fabrication by light-assisted anodic etching (Lowe et al., 2009).

Photopatterned pSi arrays were secured in a custom built Teflon cell in contact with a gold foil anode (Space Products International, CA, USA), with platinum wire (0.5 mm, 99.9%; Aldrich, WA, USA) shaped into a ring acting as a cathode. The teflon cell was then filled with an electrolyte solution of 1:1 hydrofluoric acid (HF):ethanol. The submerged Si surfaces were illuminated using a fiber optic light source passing through a set of two aspheric lenses,  $f = 80$  mm (OptoSigma, CA, USA) for collimation. A 20 mA constant current was then applied across the cell for 2 min via a source meter program, constructed in LabView 6.1 to operate a 2425 current source meter (Keithley, Ohio, USA). Fabricated pSi were washed several times with methanol prior to being dried under nitrogen gas.

Freshly etched pSi were ozone-oxidized with a flow rate of 3.25 g/h using an Ozone-Generator 500 (Fischer, Germany). After oxidation, pSi were subjected to a second pore broadening etch with 5% HF/H<sub>2</sub>O for 30 s. The double etched pSi surfaces were ozone oxidised as above. Etched hydroxy-terminated pSi surfaces were then silanized using 80  $\mu$ l of neat silane (F<sub>5</sub>PhPr) for 15 min at 90 °C. Silanized pSi arrays were washed with methanol, dried under nitrogen gas and stored in a dessicator until required

#### **4.3.4 Tissue sectioning and imprinting for DIOS-MS**

Hypobranchial glands (with connected pallial gonoduct) were mounted on cryo-section specimen holders and fixed into place with a minimal amount of embedding medium (Optimum Cutting Temperature Compound (OCT); Tissue-Tek), on the base away from the target tissue. The hypobranchial gland with connected pallial gonoduct was serially transverse cryo-sectioned (Leica 1800 Cryostat, Leica Microsystems) until the mid-region of the medial hypobranchial gland was exposed. Sections to be imaged contained both medial hypobranchial tissue and attached capsule gland tissue. A 15  $\mu$ m thick cryo-section was placed on a glass slide for optical imaging using light

microscopy (Zeiss Axio Imager Compound Microscope and Axio Imaging software). The serial 15  $\mu\text{m}$  thick cryo-section was placed on a functionalised pSi chip for tissue imprinting and kept for 30 min at room temperature in a desiccator to promote tissue analyte-surface interaction and extract small molecules by affinity. Imprinted pSi chips were digitally scanned using a conventional desktop scanner (Epson V700 Photo Scanner). Prior to MSI the residual tissue on the pSi surface was removed by immersion in MilliQ at 70 °C for 10 min. Tissue removal was aided with a gentle stream of hot water from a pipette, dried and rinsed twice in fresh MilliQ water.

Egg capsules were mounted on cryo-section specimen holders on an anterior-posterior axis and fixed in place with a minimal amount of OCT. Capsules were serially sectioned down to half width, removed from the specimen holder and stamped onto pSi chips for 30 min in a desiccator for capsule analyte-surface interaction at room temperature. Imprinted pSi chips were digitally scanned (Epson V700 Photoscanner) and remaining tissue was removed as above.

#### **4.3.5 DIOS-MS and MSI**

Imprinted pSi chips were mounted onto a customised MTP 384 ground steel target plate (Bruker-Daltronics GmbH, Bremen, Germany), secured with conductive carbon tape, and loaded into an Autoflex III TOF/TOF mass spectrometer (Bruker-Daltronics) equipped with a SmartBeam 200 Hz laser. Scanned tissue images, on pSi substrate prior to tissue removal, were loaded into FlexImaging 2.1 (build 25) and aligned with the steel target plate containing the pSi sample based on three teach points. A small margin around each tissue area was allowed for capillary movement of fluids out of the tissue. FlexImaging 2.1 distribution maps were used to control FlexControl 3.3 (build 85) during image acquisition.

Quadratic external calibration of the TOF tube was performed prior to each acquisition using  $\alpha$ -cyano-4-hydroxycinnamic acid (CHCA) adducts together with

bradykinin (1-7) and angiotensin II, spotted on a free area of the pSi substrate. Specifically, monoisotopic peaks for the calibration range included:  $K^+$  38.9637, CHCA  $[M+H-H_2O]^+$  172.0399, CHCA  $[M+H]^+$  190.0504, CHCA  $[M+Na]^+$  212.0324, CHCA  $[2M+H-CO_2]^+$  335.1032, CHCA  $[2M+H]^+$  379.0930, Bradykinin Fragment 1-7  $[M+H]^+$  757.3991 and Angiotensin II  $[M+H]^+$  1046.5418.

Samples were run in reflectron positive mode in the 20-1000 Da range, with a spatial resolution of 100  $\mu m$  and medium laser focus, corresponding to a 50  $\mu m$  diameter. Mass spectrometer settings: Ion source 1 – 19.00 kV, ion source 2 – 16.80 kV, lens – 8.25 kV, reflector 1 - 21.00 kV, reflector 2 – 9.40 kV. Data sets were further processed by baseline subtraction (1) and normalised noise threshold settings (0.5).

Ion peak distribution maps were generated in FlexImaging 2.1 and mass spectra were analysed in FlexAnalysis 3.3. Resulting masses associated with known compounds were assigned colours for visual localisation with reference to histological sections. Selected masses were not based on the monoisotopic mass of the secondary metabolite but chosen based on the peak that had the least overlap from unidentified peaks, validated manually by checking selected spots within the summed data-set.

To calculate co-localisation of mass spectra across all tissue samples from DIOS-MS imaging, data files were imported into SCiLS Lab (Bremen, Germany) and run through an unsupervised cluster analysis of spatially similar  $m/z$  distribution patterns providing a summed spectrum of peaks that co-localise within tissue regions. Correlation analysis identified where brominated indole distribution patterns overlapped with murexine based on the reproductive cycle. The peak distribution correlation of representative samples was plotted with corresponding peak intensity for each  $m/z$  value.

### 4.3.6 Extraction and elucidation of brominated indoles

Fresh hypobranchial glands (6.58 g) were solvent extracted (Benkendorff et al., 2000). Glandular tissue was dissolved in an equal portion of chloroform and methanol (1:1 v/v, Sigma, CHROMASOLV®, HPLC grade) and continuously stirred overnight. After vacuum filtering (Whatman filter paper 1), the polar and lipophilic fractions were separated using 20 mL milliQ water. The chloroform fraction contained the intermediate precursor brominated indoles, whilst the methanol/water fraction contained the ultimate precursor to Tyrian purple, tyrindoxyl sulfate and tyrindoleninone. Each extract fraction was evaporated to dryness under reduced pressure of 470 mbar at 40 °C on a Rotavapor® R-114 (BÜCHI Labortechnik AG, Flawil, Switzerland), weighed (214.7 mg) and then re-dissolved in 1 mL of acetonitrile (Sigma, CHROMASOLV®, HPLC grade) within amber vials for LC-MS analysis.

Brominated indoles were separated with a Waters 2695 high performance liquid chromatographer (HPLC; Waters Alliance®) coupled to a mass spectrometer (MS; Micromass Quatro micro™ tandem quadrupole MS System, Waters, Milford, MA, USA) for identification. HPLC separation was performed on a reverse-phase hydrophobic column (Synergi™, Hydro-RP, 4 µm C18 phase, 80 Å, 250 x 4.6 mm i.d., Phenomenex, Lane Cove, NSW, Australia) according to the previously reported elution gradient (Westley and Benkendorff, 2008) of acetonitrile in water with 1% formic acid at a flow rate of 300 µL/min with parallel UV/Vis photo-diode array (PDA) detection at 300 and 600 nm. Electrospray ionisation (ESI-MS) facilitated the identification of brominated indole structures and data were analyzed using the Masslynx 4.1 data system (Waters). Retention times were standardised using 40 µM synthetic 5-bromoisatin (Sigma-Aldrich, technical grade) in acetonitrile, a structural isomer of the Tyrian purple precursor 6-bromoisatin. The identification of brominated indoles was based on peak retention time, expected mass and isotopic clusters for the

mono- and dibrominated compounds within mass spectra, with reference to previously published structures for this species (Baker and Duke, 1976, Benkendorff et al., 2000, Baker and Duke, 1973, Cooksey, 2001), listed in Appendix 4.1.

#### **4.3.7 Extraction and elucidation of murexine structure**

The remaining frozen tissue (1.3 g) from the reproductive female, after MSI tissue collection, was used for extraction of reproductive female-derived murexine to ensure specificity of detection in DIOS-MSI. Murexine was extracted three times in 30 mL volumes of acetone and pooled. The extract was vacuum filtered through a PTFE membrane filter (pore size 0.2  $\mu\text{m}$ ), evaporated to dryness, and washed three times with 10 mL of diethyl ether (Ajax Finechem, AR grade) to remove fats (Roseghini et al., 1996). Total extract was then taken up in 5 mL of acetonitrile (ACN) for TLC detection (Roseghini et al., 1996), LC-MS and NMR analysis.

Thin layer chromatography (TLC) was used for the initial detection of murexine, based on previous reports of choline ester compounds in members of the Muricidae (Roseghini et al., 1996). Approximately 5  $\mu\text{L}$  of extract was collected into glass capillary tubes (32 mm, 0.6 mm i.d., BLU-TIP®), spotted on aluminum-backed silica TLC plates (F60, Merck) and separated using a n-butanol-ethanol-acetic acid-water (8:2:1:3) gradient for the mobile phase. Visualisation of the choline ester spots was achieved using Dragondorff reagent (Fluka, Sigma-Aldrich Chemie GmbH) according to the retention times previously reported (Roseghini et al., 1996).

Three replicate 10  $\mu\text{L}$  subsamples of the capsule gland extract were subjected to ultra-performance liquid chromatography (UPLC)-MS, based on a modified LC-MS protocol for detection of acetylcholine (Keski-Rahkonen et al., 2007). Separation was provided by an Acquity UPLC system (Waters), 10  $\mu\text{L}$  injection volume, on a reverse-phase column (Atlantis T3, 3  $\mu\text{m}$  C18, 3 x 100 mm i.d., Waters) using 0.5% formic acid (A) and acetonitrile (B) at a flow rate of 0.5 mL/min (gradient of solvent: 0-10

min, 98% A and 2% B), with UV PDA. ESI-MS detected the murexine structure on the Micromass Quatro micro™ tandem quadrupole mass spectrometer and MS and UV data was acquired using Masslynx 4.1 data system (Waters). To see the structural features of murexine, in ESI, a scan at 20 V was compared to a collision induced dissociation (CID) scan at 35 V cone voltage (positive ion electrospray, 80 to 500 m/z mass range).

The remaining reproductive female tissue extract was used for <sup>1</sup>H-NMR and <sup>13</sup>C-NMR fingerprinting for identification of reproductive female capsule gland extract components. The bulk of contaminants were removed by solid phase extraction column (Prevail™C18 reversed-phase, 4 mL 500 mg packed bed, Grace, Deerfield, IL, USA), resuspended in methanol-d<sub>4</sub> followed by acetonitrile-d<sub>3</sub> in 5mm (600 MHz) NMR tubes (Bruker-Daltronics). Chemical shifts were recorded on a 600 MHz NMR spectrometer (Bruker Avance, Karlsruhe, Germany) using an inverse multinuclear probe (5 mm) and a triple resonance HCN probe and referenced to residual solvent peaks. Structural confirmation of individual compounds was elucidated using <sup>1</sup>H-NMR and <sup>13</sup>C-NMR chemical shifts and correlation analysis. Chemical shift assignment of murexine was based on similarity to previously reported <sup>1</sup>H-NMR from murexine (in a mixture of 90 % acetonitrile-d<sub>3</sub>) (Bender et al., 1974) and <sup>1</sup>H-NMR for tyrindoxyl sulfate and the complex in methanol-d (Baker and Duke, 1976). Reproductive derived murexine was validated against a semi-purified acetone extract from adult hypobranchial gland extractions (106 mg).

#### **4.3.8 Bioassay of murexine in hatching stage *D. orbita* larvae**

To assess the effect of murexine on larval motility, fresh hypobranchial glands were extracted (127 g) using acetone. Fresh glands were extracted overnight, with continuous stirring, in 200 mL of acetone and remaining tissue further extracted in 200 mL overnight. The supernatant was collected, pooled, and then vacuum filtered

through a PTFE membrane filter (0.2  $\mu\text{m}$ ) and evaporated to dryness. The extract was resuspended in 30 mL of MilliQ filtered water. Fats were removed by three washes with an equal portion of diethyl ether. Murexine was separated from the bulk of contaminants using a solid phase extraction column (Prevail<sup>TM</sup>C18 reversed-phase, 4 mL 500 mg packed bed, Grace, Deerfield, IL, USA) and a purified fraction of the choline ester was collected by concentration on a normal-phase SPE column (Alltech<sup>®</sup> normal-phase silica column, 4 mL 500 mg packed bed) eluted with successive additions of 10, 30, 40, 50, 60, 70, 80, 95, and 99% ethanol. Fractions of 10 – 30 mL were collected and run on TLC for purity. The fractions containing murexine were evaporated to dryness and resuspended in artificial seawater to collect murexine for bioassays.

Late stage intracapsular *D. orbita* larvae were subjected to semi-purified murexine at a concentration of 50 ppm and motility was recorded over a 60 min motility assay. Replicate ( $n = 12$ ) assays were run in 24 well cell culture plates using 4 mL of artificial seawater. Seawater was pipetted onto larvae just prior to the addition of murexine to ensure larvae were actively swimming. Murexine in artificial seawater (0.25 mg in 1 mL) was added slowly to larvae (in two amounts) and swimming activity was assessed by short 30 s video recordings at timed intervals 0, 5, 10, 20, 30 and 60 minutes. Movement by beating cilia across still shots during short videos were scored as swimming.

## **4.4 Results and discussion**

### **4.4.1 Detection and identification of secondary metabolite patterns on functionalised pSi**

To explore the biological roles of muricid cholines esters and brominated indoles using DIOS-MSI in the context of egg laying and maternal investment, established

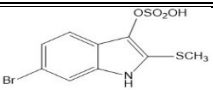
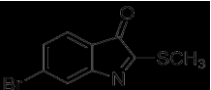
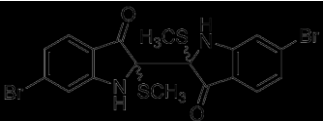
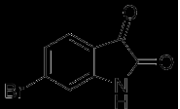
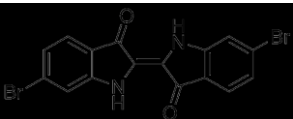
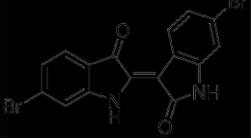
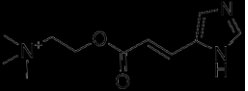
spatial patterns based on previous histochemical staining (Westley et al., 2010b) were used as a basis to track altering temporal changes. The reliable performance of pSi in detecting the range of secondary metabolites was validated using organic extracts prepared from the same population of breeding individuals. Extracts were analysed by liquid chromatography mass spectrometry (LC-MS/MS) according to established procedures in our laboratory (Benkendorff et al., 2000, Rudd and Benkendorff, 2014, Westley and Benkendorff, 2008), and used as a comparison for those detected in DIOS-MS and MSI (Figure 4.2 and 4.3). The capacity for pSi to desorb and ionise brominated indoles was confirmed using crude extracts and purified fractions for the compounds detected during tissue analysis (Table 4.1). DIOS-MS takes advantage of the van der Waals interaction and hydrogen bonding between the analyte containing the secondary metabolites and the silanised pSi surface. Attractive properties combined with high porosity ( $\sim 600 \text{ m}^2 \text{ cm}^{-3}$ ) allow pSi to selectively extract small molecules in a sponge-like manner (Stewart and Buriak, 2000). Consistent with our previous study (Ronci et al., 2012), brominated indoles across a broad range of polarities (Cooksey, 2001) in the low mass region from  $m/z$  256 – 421 (Figure 4.2 and Appendix II), showed affinity to the pSi surface.

Stamping allowed low mass metabolite transfer from cryostat sections of the tissue to the pSi (Figure 4.2), whilst the hydrophobic pSi surface facilitated the subsequent removal of residual tissue with minimal delocalisation. The removal of larger biological material reduces spectral complication by eliminating fragments from highly abundant larger compounds like membrane lipids, which can suppress low abundant target spectra. The isotopic clusters for mono- and dibrominated indole structures allow for the assignment of brominated secondary metabolites detected in DIOS-MS, including the hydrophilic dye precursor tyrindoxyl sulfate (tentatively assigned as tyrindoxyl sulfonic acid; duplet ion cluster at  $m/z$  339, 341  $[\text{M}+3\text{H}]^+$ ), the

intermediate tyrindoleninone (duplet ion cluster at  $m/z$  256, 258  $[M+2H]^+$ ), and the least soluble end product Tyrian purple (triplet ion cluster centered at  $m/z$  421  $[M+2H]^+$ ) (Figures 4.2 and 4.3).

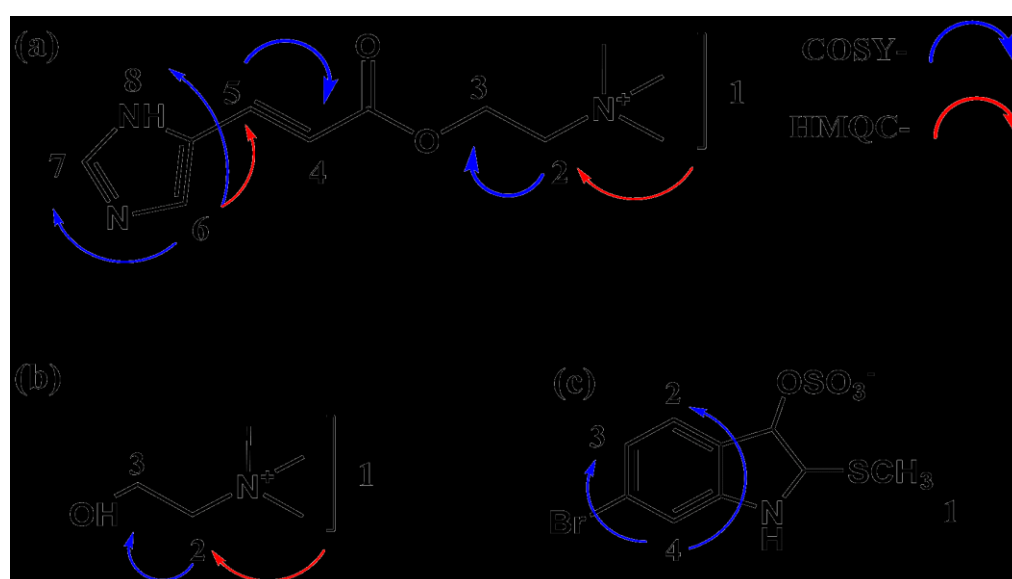
DIOS-MS was also effective in detecting the choline ester murexine (urocanylcholine; major ion  $m/z$  224  $[M]^+$ , Figures 4.2 and 4.3), in the first spatial analysis of this well-studied (Roseghini et al., 1996) secondary metabolite. The presence of murexine was confirmed by extraction from the remaining tissue of a reproductively active female and was structurally elucidated using LC-MS-MS (Appendix II),  $^1H$ -NMR and  $^{13}C$ -NMR fingerprinting (Table 4.2), and confirmed by comparison to choline and choline ester salts of tyrindoxyl sulfate previously reported from *D. orbita* and other muricidae molluscs (Baker and Duke, 1976, Duke et al., 1978). Apart from major ion  $m/z$  224, murexine showed major fragment ions in LC-MS-MS at  $m/z$  165 and 121 (Appendix II). These same fragment ions were detectable in DIOS-MS spectra co-localized with the major ion  $m/z$  224 (165 and 121  $m/z$ ; Appendix II), confirming the detection of murexine using post source decay, and more broadly demonstrating the accuracy of DIOS-MS in the low mass range, whilst eliminating matrix suppression and non-target spectral “noise” in analysis.

**Table 4.1** Summary of brominated indoles and choline esters detected in *Dicathais orbita* hypobranchial tissue from LC-MS, DIOS-MS and <sup>1</sup>H-NMR (tyrindoxyl sulfate and murexine from this study, intermediate brominated indoles from Benkendorff et al. 2000). Tyrindoxyl sulfonic acid is a tentative assignment.

Structure	Compound	Formula	[M]	RT [min]	Major ions m/z		<sup>1</sup> H NMR
					LC-MS	DIOS-MS	
	tyrindoxyl sulfate (reduced to sulfonic acid on DIOS)	C <sub>9</sub> H <sub>7</sub> BrNO <sub>4</sub> S <sub>2</sub> <sup>-</sup> (C <sub>9</sub> H <sub>8</sub> BrNO <sub>4</sub> S <sub>2</sub> )	335.901 (336.907)	6.59	336, 338	(sulfonic acid) 339.98, 340.99, 341.98, 342.98	δH 9.76s (1H), 7.14m (3H), 2.42s (3H)
	tyrindoleninone	C <sub>9</sub> H <sub>6</sub> BrNOS	254.935	10.96	256, 258	255.95, 256.94, 257.94, 258.95	(CD <sub>3</sub> CN), δH 7.46 (1H, dd, <i>J</i> =0.5, 1.4 Hz), 7.42 (1H, dd, <i>J</i> =0.5, 7.6 Hz), 7.39 (1H, dd, <i>J</i> =7.6, 1.4 Hz), 2.63 (3H, s)
	tyriverdin	C <sub>18</sub> H <sub>14</sub> Br <sub>2</sub> N <sub>2</sub> O <sub>2</sub>	511.886	11.67	417, 419, 421, 463, 465, 467, 511, 513, 515	n.d.	(DMSO- <i>d</i> <sub>6</sub> ), δH 7.46d (8.4), 7.27d (1.5), 6.96dd (8.4, 1.5), 1.90s
	6-bromoisatin	C <sub>8</sub> H <sub>4</sub> BrNO <sub>2</sub>	224.943	6.35	224, 226	n.d.	(CD <sub>3</sub> CN), δH 8.96 (1H, s), 7.44 (1H, d, <i>J</i> =8.08 Hz), 7.30 (1H, dd, <i>J</i> =1.64, 8Hz), 7.19 (1H, d, <i>J</i> =1.6 Hz)
	6,6'-dibromoindigo	C <sub>16</sub> H <sub>8</sub> Br <sub>2</sub> N <sub>2</sub> O <sub>2</sub>	417.895	14.34	417, 419, 421	418.88, 419.88, 420.88, 421.88, 422.88, 423.88, 424.88	(N,N'-bistrifluoroacetyl derivative, CDCl <sub>3</sub> ), δH 8.3d (1.2), 8.06d (8.4), 7.95d (7.7), 7.79td (7.4, 1.3), 7.75d (8.1), 7.56dd (8.1, 1.4), 7.42t (7.4)
	6,6'-dibromoindirubin	C <sub>16</sub> H <sub>8</sub> Br <sub>2</sub> N <sub>2</sub> O <sub>2</sub>	417.895	n.d.	417, 419, 421	418.88, 419.88, 420.88, 421.88, 422.88, 423.88, 424.88	(DMSO- <i>d</i> <sub>6</sub> ), δH 11.2brs, 11.1brs, 8.67d (8.5), 7.68d (1.6), 7.62d (8.1), 7.22dd (8.5, 1.7), 7.20dd (7.9, 1.6), 7.05d (1.8)
	murexine	C <sub>11</sub> H <sub>18</sub> N <sub>3</sub> O <sub>2</sub> <sup>+</sup>	224.139	1.83	224.1	224.17, 225.17	(D <sub>2</sub> O, CD <sub>3</sub> COOD), δH 7.05 (1H, d, <i>J</i> =16), 8.08 (1H, d, <i>J</i> =16), 8.28 (1H, s), 9.28 (1H, s), 5.10 (2H, m), 4.23 (2H, m), 3.77 (9H, s)

**Table 4.2**  $^1\text{H-NMR}$  assignment for purified ethanolic extract containing (a) murexine, (b) choline and counterion (c) tyrindoxyl sulfate. <sup>a</sup>Relative area is influenced by compound integration for counter ion tyrindoxyl sulfate, where in  $\text{CD}_3\text{CN}$  the charges balance.

compound	$\delta$ (p.p.m.)	mutiplicity		relative area	Assignment
<b>a - Murexine</b>	3.11	s		9	1
	3.60 - 3.61	m		2	2
	4.50 - 4.52	m		2	3
	6.49	d	$J = 15.7 \text{ Hz}$	1	4
	7.61	d	$J = 15.7 \text{ Hz}$	1	5
	7.39	s		1	6
	7.75	s		1	7
	9.42	bs		2 <sup>a</sup>	8
<b>b - Choline</b>	3.06	s		9	1
	3.32 - 3.34	m		2	2
	3.88 - 3.90	m		2	3
<b>c - Tyrindoxyl sulfate</b>	2.46	s		3	1
	7.13	dd	$J = 15.7 \text{ Hz}, 1.7 \text{ Hz}$	1	2
	7.45	d	$J = 1.7 \text{ Hz}$	1	3
	7.66	d	$J = 15.7 \text{ Hz}$	1	4



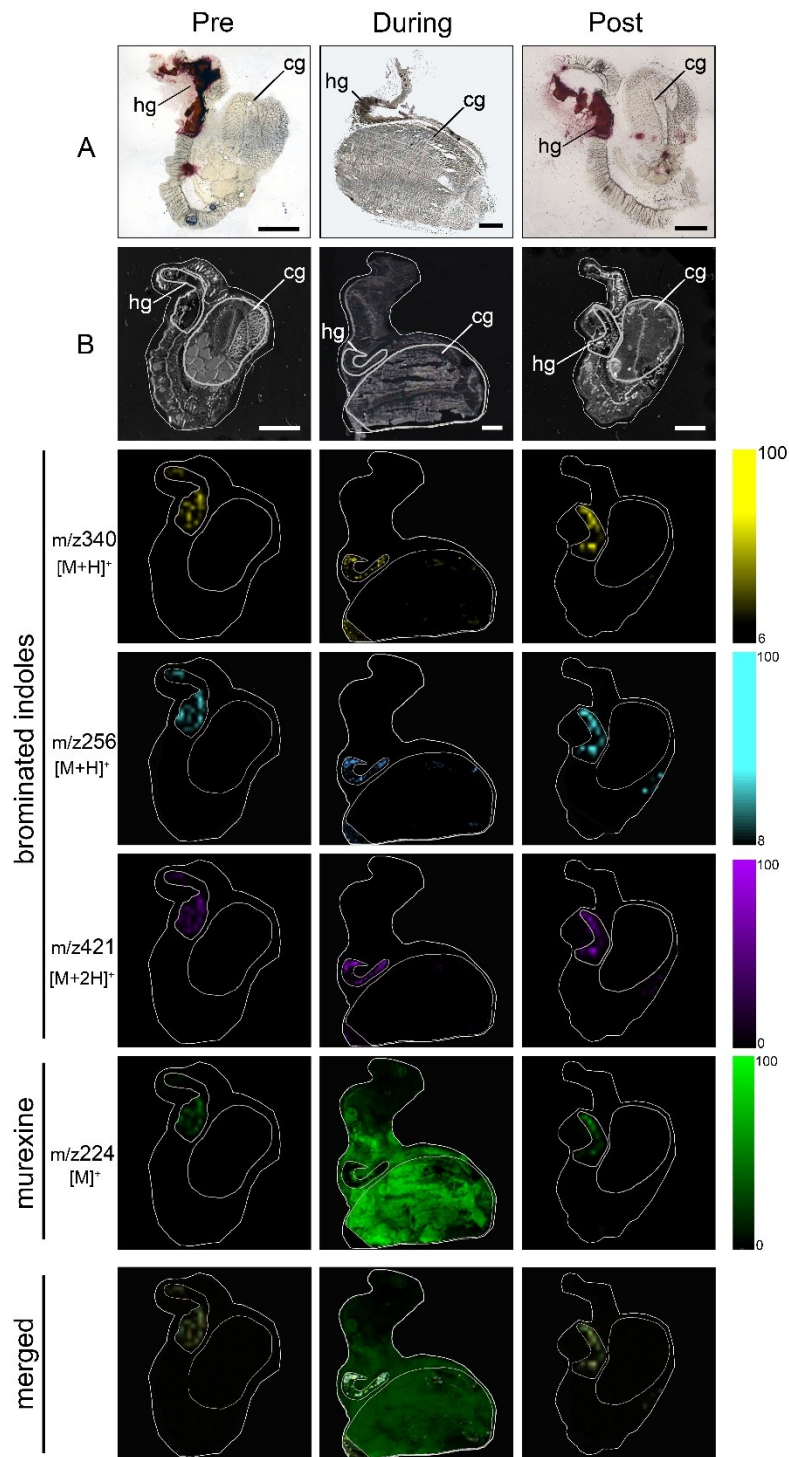


**Figure 4.2** DIOS-MSI maps of secondary metabolites imprinted onto pSi from female *Dicathais orbita* across the reproductive cycle. (Pre) representative female section sampled 30 days prior to the start of the breeding season. (During) a female during encapsulation. (Post) representative female section sampled 14 days post encapsulation. Maps are compared to (A) histological sections and (B) scanned tissue sections on pSi prior to removal. Tissue regions include (hg) medial hypobranchial gland and (cg) capsule gland. Scale bar set to 2 mm.

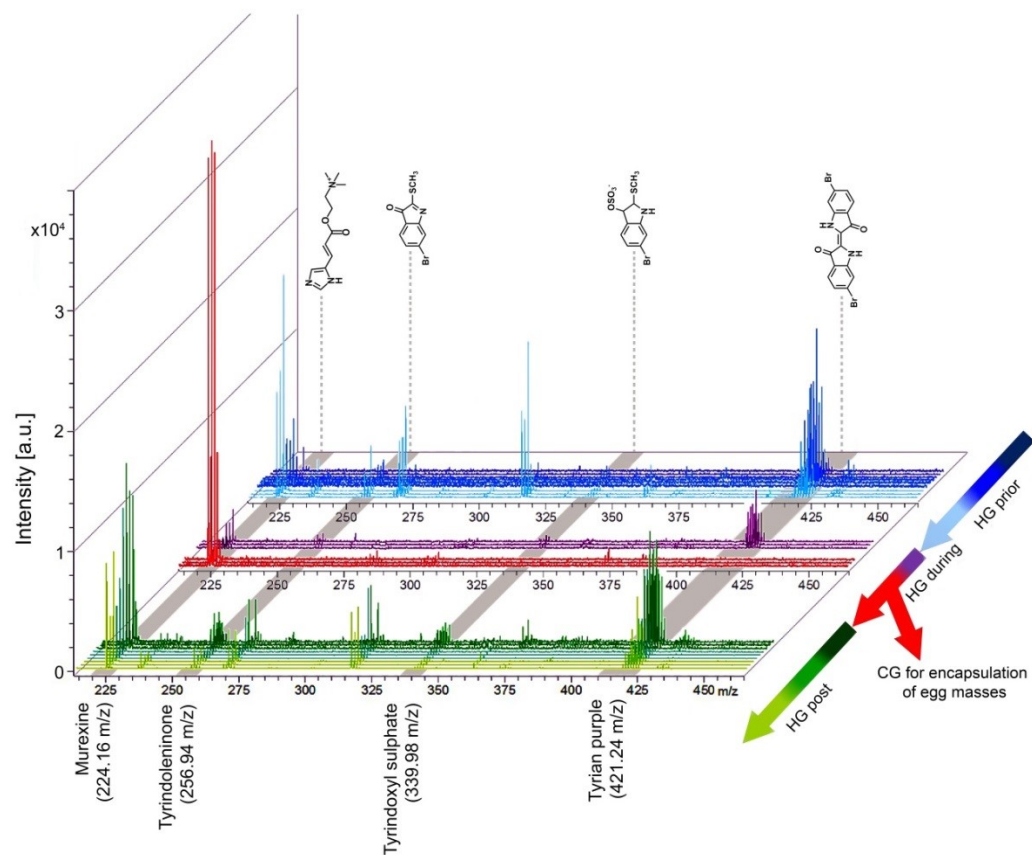


**Figure 4.3** *Dicathais orbita* secondary metabolite mass spectra from across the reproductive cycle. Spectra show mono- and dibrominated ion clusters for the brominated indoles and murexine detected using DIOS-MSI in the medial hypobranchial gland and capsule gland from reproductively active females. (HG) hypobranchial gland; (CG) capsule gland

#### 4.4.2 Biodistribution of secondary metabolites across the reproductive cycle

A major change in the biodistribution of Muricidae secondary metabolites is clearly apparent across the reproductive cycle of female *D. orbita*, with both the brominated indole and murexine moving from the hypobranchial glands to the capsule glands during the breeding season (Figure 4.2 and 4.3). Furthermore, there is a substantial increase in the intensity of murexine detected in egg laying females, in comparison to the pre- and post- breeding stages (Figure 4.2 and 4.3). This suggests that the choline ester murexine may play a fundamental role in the reproduction of Muricidae molluscs. A role in reproduction has been previously suggested for the brominated indole precursors of Tyrian purple (Westley and Benkendorff, 2008, Westley et al., 2006), whereas the choline esters have been suggested to play a role in the feeding activities of these predatory snails (Roseghini et al., 1996, Westley et al., 2006) and/or simply assumed to stabilise the indoxyl sulfate precursors as salts for storage within the hypobranchial gland tissue (Benkendorff, 2013, Baker and Duke, 1976). Here DIOS-MSI has provided novel information suggesting an up-regulation of choline esters for reproduction that may in fact be far more important for neogastropods than previously anticipated.

The co-localisation of murexine with the brominated indoles, tyrindoxyl sulfate and Tyrian purple in the medial region of hypobranchial glands (Figure 4.3) was confirmed by correlation analysis of DIOS-MSI for the pre-reproductive females ( $R^2 = 0.883 \pm 0.1$ ; Figure 4.4a) and post-reproductive females ( $R^2 = 0.713 \pm 0.27$ ; Figure 4.4c). However, during the spawning (egg deposition) stage of the reproductive cycle, there was a substantial increase in the intensity (Figure 4.3) and spatial detection of murexine in the capsule gland (Figure 4.2), but not in the brominated indoles.

Consequently, there was no longer a correlation between these secondary metabolites in egg laying females ( $R^2 = 0.009$ ; Figure 4.4b). The increase in murexine in the capsule gland during egg deposition appears to be at the expense of the medial hypobranchial gland (Figure 4.2 and Appendix 4.5). This implies that availability of murexine for feeding activities (Roseghini et al., 1996, Westley et al., 2006) is reduced during spawning. Few studies have investigated the energetic cost of maternal provisioning for non-primary metabolites (Hay, 1996), and MSI may provide an attractive method for tracking mother to offspring transfer.

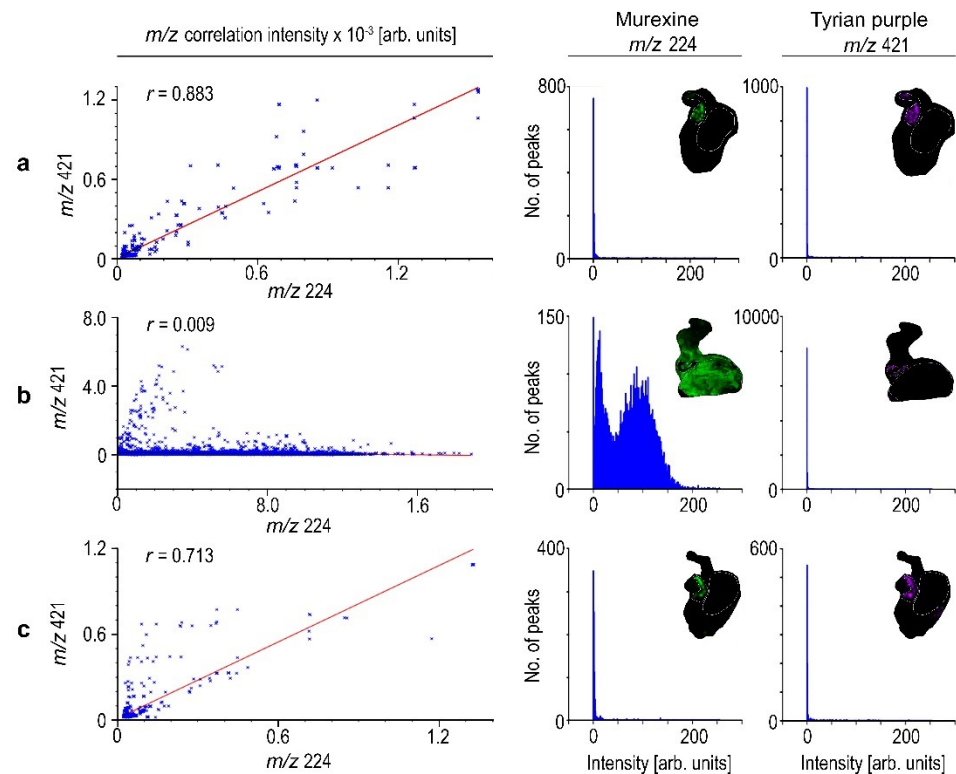


**Figure 4.4** Representative correlation plots (left hand panels) for co-localised m/z patterns for murexine against Tyrian purple with corresponding intensity histograms of murexine (middle panels) and Tyrian purple (right hand panels) spot spectra generated in SCLiS Lab imaging software (Bremen, Germany). Where Tyrian purple and murexine co-localise within; (a) pre-reproductive female tissue section; (b) reproductive female tissue section; and (c) post-reproductive female tissue section, with intensities for murexine and Tyrian purple.

### **4.4.3 Maternal provisioning and chemical changes during encapsulated larval development**

DIOS-MSI on the egg capsules (Figure 4.5) confirmed that murexine is transferred from the female capsule gland into the capsular fluid. To the best of our knowledge, this is the first report of murexine in Neogastropod egg capsules. DIOS-MSI detected murexine only in the egg capsules containing early stage embryos, where it is co-localised with tyrindoxyl sulfate and some minor intermediate brominated indoles and end products (Figure 4.5b). In the capsules with late stage veliger larvae, water soluble murexine was no longer detectable. Tyrindoxyl sulfate also decreased in intensity and distribution during encapsulated larval development (Figure 4.5, Appendix 4.7). Conversely, insoluble Tyrian purple increased in the late stage capsules but was barely present at the early stage. This provides evidence for a unique form of chemical ripening in the egg capsules involving two distinct classes of secondary metabolites specific to the Muricidae family of marine molluscs. The apparent high abundance of murexine relative to tyrindoxyl sulfate in breeding snails implies a naturally selected role for this compound during reproduction and early stage development, whereas tyrindoxyl sulfate could be acting as a controlled release counter ion to murexine within the egg capsules and hypobranchial gland. In this case, the formation of antimicrobial brominated indole intermediates during intracapsular development (Benkendorff et al., 2000) could be a secondary function fortuitously acquired over the course of Muricidae evolution.

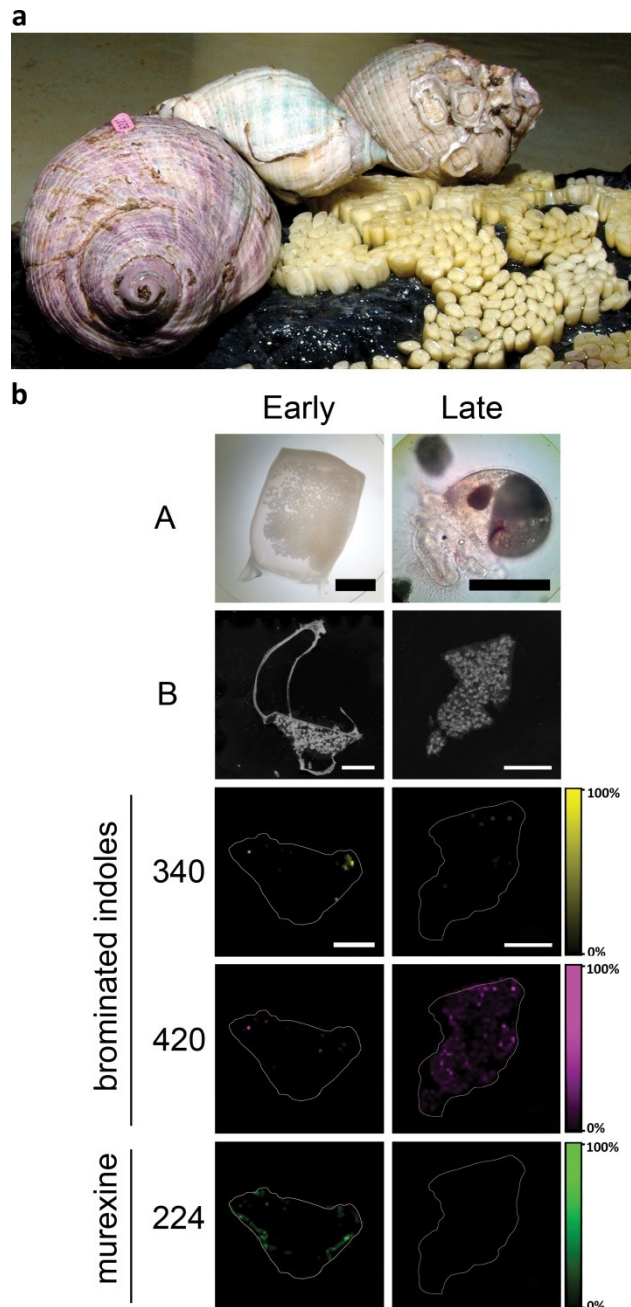


**Figure 4.5** *Dicathais orbita* during egg deposition and DIOS-MSI maps of egg capsules across the developmental period. (a) Reproductive adults during the encapsulation of larvae and early stage capsules adhered to substrate. (b) DIOS-MSI of an early stage capsule sampled immediately post deposition and late stage capsule after 35 days post deposition. Maps are compared to (A) serial histological sections and (B) scanned tissue sections on pSi prior to removal. Scale bar set to 1 mm.

#### 4.4.4 Biological role for murexine

The purpose of murexine within the female capsule gland is open to interpretation. However, since this compound is a potent muscle relaxant (Roseghini et al., 1996), it may help relax the reproductive tract during egg deposition. Murexine has been suggested as a ligand for the muscle type nicotinic-acetylcholine receptor (Roseghini et al., 1996) (nAChR) based on the pharmacological actions of murexine *in vivo* within vertebrates (Roseghini et al., 1996, Erspamer and Glasser, 1957, Keyl and Whittaker, 1958). The *in vivo* paralytic effect of murexine has the greatest similarity to suxamethonium, a muscle type nAChR agonist (Roseghini et al., 1996). The choline esters are expected to become biologically active only when not complexed with tyridoxyl sulfate (Duke et al., 1978), as generally the quaternary ammonium of choline esters contribute to receptor binding and are required for the tranquilising activity for a range of other choline ester structures and acetylcholine (Hey, 1952, Williamson et al., 2007). The detection of murexine in the absence of brominated indoles indicates active muscle relaxing effects in the capsule gland environment.

The role of murexine within the egg capsules as a natural tranquiliser during larval development is also a plausible hypothesis. To test this, we purified murexine at 0.22 mM (50 mg/L) and confirmed that it has a temporary tranquilising effect on late stage intracapsular larvae lasting over 60 minutes (Figure 4.6a; <https://youtu.be/rICvyyhnXAE>). Larvae post immersion in murexine are actively swimming after 60 mins suggesting recovery.

Whilst fully purified murexine would have been optimal for an unequivocal evaluation of murexine bioactivity, chromatographic separation has continuously produced a fraction that contains small amounts of choline (Appendix II Figure A2.5a), a product of murexine degradation (Roseghini et al., 1970, Roseghini et al., 1996). The  $[M]^+$  that is likely to correspond to choline can be detected in both the hypobranchial

gland and the capsule gland of egg laying females, Table 4.2 and Appendix II Figure A2.6, but muricid derived choline has never been shown to have an anaesthetic effect either *in vitro* or *in vivo* (Roseghini et al., 1996). Further bioassays with purified murexine or concomitant assays with choline would provide greater support for temporary larval relaxation, but a better chromatographic method for separation is required, possibly preparative HPLC.

Developing larvae shells are delicate and oxygen is limited during muricid intracapsular development (Cumplido et al., 2011), despite this period being a metabolically active period. *D. orbita* reproductive females could be provisioning offspring with intracapsular tranquilisers to ensure they develop ready for life in the open sea. Indeed nearly 100 % hatching success rate has been reported for the thousands of delicate larvae contained within each egg capsule of *D. orbita* (Phillips, 1969). Natural tranquilisers have been previously reported in molluscan egg masses, specifically in the common squid *Loligo vulgaris*, which incorporates an unidentified natural tranquiliser in perivitelline fluid within egg cases (Marthy et al., 1976), preventing premature hatching. Although the bioactive compound in squid perivitelline fluid does not appear to have been identified to date, cephalopods do not possess a hypobranchial gland and there are no reports of murexine in the venom glands, ink or chemical messengers involved in the reproduction of cephalopods, despite extensive studies (Roseghini et al., 1996, Dias et al., 2012, Camp et al., 2011). Therefore, the new biological role proposed here for murexine appears to be an interesting example of functional convergent evolution between the gastropods and cephalopods. These two classes of marine molluscs have independently evolved the deposition of benthic masses, as well as chemical sedatives to protect the encapsulated larvae.

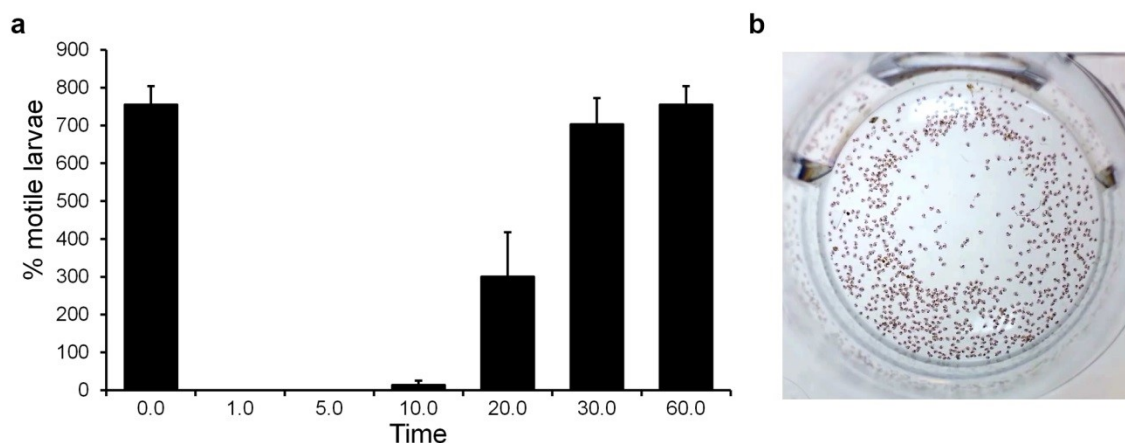


**Figure 4.6** The proposed biological role of murexine in the *Dicathais orbita* egg capsules using alarval motility assay in the presence of 50 ppm murexine extract: (a) percentage of motile larvae counted using short 30 s videos over 60 min and (b) a video still photograph of larvae at time 0 prior to the addition of murexine extract.

## 4.5 Conclusion

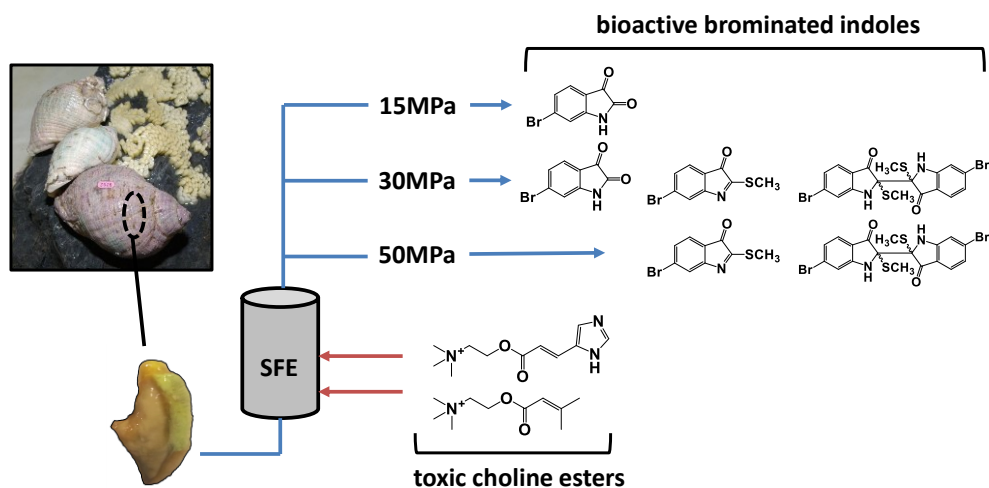
Overall, this study has confirmed the usefulness of MSI for providing new insights into marine chemical ecology. DIOS –MSI has been used to map the distribution of two distinct classes of compounds over the adult reproductive and encapsulated larval stage in a muricid mollusc, revealing a significant upregulation of muscle relaxing choline esters in the capsule gland of females during egg deposition, and proposing a role for this compound in the egg masses during the earlier stages of intracapsular development. The co-localisation of murexine with tyrindoxyl sulfate in both the hypobranchial glands of adults and in the early stage egg capsules confirms the intrinsic link between these secondary metabolites and provides evidence for a novel chemical ripening system that is likely to play a fundamental role in the encapsulated development of Muricidae larvae.

## 4.6 Acknowledgements

Thanks are extended to Flinders Microscopy and Flinders Analytical staff. This project was supported in part by a Flinders University, Faculty of Science and

Engineering research grant to K.B. D.R. was supported by an Australian postgraduate Award Scholarship with additional funding from an anonymous philanthropic foundation awarded to K.B.

## 5 Chapter Five - Supercritical CO<sub>2</sub> extraction of bioactive Tyrian purple precursors from the hypobranchial gland of a marine gastropod



### 5.1 Abstract

Supercritical CO<sub>2</sub> provides considerable advantages over traditional solvents for the extraction of bioactive compounds from organic matter. Here we demonstrate the use of supercritical CO<sub>2</sub> as an efficient and safe alternative to traditional solvent extraction for the recovery of bioactive Tyrian purple precursors tyrindoleninone, 6-bromoisatin and tyriverdin, from the marine mollusc *Dicathais orbita*. The effect of pressure on the selective extraction of brominated indoles was tested at 15, 30 and 50 MPa CO<sub>2</sub>, and was compared to traditional chloroform extract composition and yields. Extracts obtained from 15 MPa selectively concentrated 6-bromoisatin, at 78% of the extract composition, whereas increased pressures of 30 and 50 MPa increased the solvating power of supercritical CO<sub>2</sub> to include the more lipophilic tyrindoleninone at 35 and 29% respectively, and tyriverdin at 23 and 40% respectively. This extraction method was also effective in separating the brominated indoles from toxic choline esters in the mollusc extracts. Extract yields from supercritical CO<sub>2</sub> were comparable

to solvent extraction relative to whole whelk weight. This provides a viable alternative for nutraceutical development that does not rely on the use of toxic solvents.

## 5.2 Introduction

The development of new nutraceuticals and pharmaceuticals from natural sources requires optimized extraction and purification techniques to maximize the yield and quality of the bioactive component. Traditional liquid solvent extraction systems cause a number of concerns for downstream applications. Draw-backs include inherent toxicity from organic volatile impurities in pharmaceutical preparations (Witschi and Doelker, 1997), variability in yield (Reverchon and De Marco, 2006), stabilization of the active compound (Wakimoto et al., 2011), and the relative expense of analytical grade solvents (Herrero et al., 2010). The use of supercritical fluid extraction (SFE) with CO<sub>2</sub> (herein termed SFE) provides a viable alternative to liquid solvent extraction for natural product chemistry and nutraceutical development. Supercritical CO<sub>2</sub> is environmentally benign at small quantities, dramatically cheaper than analytical grade solvents, and has a high diffusivity for extraction from dense and complex samples (Herrero et al., 2010). The solvating power of supercritical CO<sub>2</sub> can also be manipulated to target specific compounds or classes of compounds, usually via pressure and temperature, due to the polar attributes of CO<sub>2</sub> (Herrero et al., 2010, Raveendran et al., 2005). SFE can be run at low temperatures and provides a non-oxidant medium, which is ideal for thermally labile compounds and compounds that are susceptible to oxidation (Herrero et al., 2010).

The use of SFE in the extraction of anti-inflammatory fatty acids from green-lipped mussels (Lyprinol®) is an example of the benefits of SFE for nutraceutical development and production from a marine source. Lyprinol has been shown to be effective in clinical trials for arthritis (Gibson, 2000) and asthma (Emelyanov et al., 2002). Highly unstable furan fatty acids in Lyprinol show potent radical scavenging

ability *in vivo* (Wakimoto et al., 2011). SFE allows stabilization of the furan fatty acids and the low temperature extraction prevents activation of enzymes and oxidative degradation in the Lyprinol fraction (Whitehouse et al., 1997). This provides evidence for the benefit of SFE in extracting unstable compounds from mollusc tissue for nutraceutical production (Wakimoto et al., 2011, Wolyniak et al., 2005).

More broadly, marine molluscs are used in a range of complementary and alternative medicines and have provided a number of interesting leads for research into bioactive compounds with potential pharmaceutical value (Mayer et al., 2011). Mollusc-derived secondary metabolites have yielded a number of novel approved therapeutic drugs, as well as compounds still in clinical trials (Molinski et al., 2009). Stand out examples of molluscan derived compounds in clinical use or final stage clinical trials include the analgesic Zinconotide (Prialt®); a synthetic  $\omega$ -conotoxin peptide from the cone snail *Conus magus* (Alonso et al., 2003), and the anti-lymphoma Brentuximab vedotin (Senter and Sievers, 2012), designed from the sea hare, *Dollabella auricularia*, compound Dolstatin-10 (Pettit et al., 1987) later ascribed to cyanobacteria. Other novel mollusc compounds in the clinical trial pipeline include anti-tumor depsipeptide Kahalalide F (Suarez et al., 2003), isolated from the sea slug *Elysia rufescens* (Hamann et al., 1996), and anti-tumor agent ES-285, obtained from the clam *Mactromeris polynima* (Salcedo et al., 2007). With over one thousand research articles produced in the last three decades on mollusc secondary metabolites (Benkendorff, 2010), there has been an increase in bioactivity testing to explore potential biomedical benefit, and molluscs could be considered a largely untapped resource (Molinski et al., 2009, Blunt et al., 2013, Benkendorff, 2010).

The Muricidae family of gastropod molluscs has been investigated for two classes of bioactive compounds, brominated indoles and choline esters (Benkendorff et al., 2001a, Cooksey, 2001, Roseghini et al., 1996), which combine to form the ultimate

precursor to Tyrian purple (6,6'-dibromoindigo, Figure 5.1). Tyrian purple is considered one of the oldest dyes known in chemical industries (Cooksey, 2013) with archaeological evidence for a Phoenician dye industry dating back to the 13th Century B.C. (McGovern and Michel, 1985). Tyrian purple is highly insoluble in most solvents and, therefore, traditional dyeing methods require extraction of the precursors from the mollusc tissue. These are then used to impregnate the cloth, prior to the development of the final colour in sunlight (Cooksey, 2001, Cooksey, 2013, Sterman and Sterman, 2012). Precursor indole compounds from the dye were collected exclusively from the hypobranchial glands of muricids for oxidation once absorbed into cloth (Cooksey, 2001). The brominated dye pigments originate from a single precursor, tyrindoxyl sulfate (Baker and Duke, 1976). Tyrindoxyl sulfate salt undergoes enzymatic cleavage by aryl sulfatase (Laffy et al., 2013) once secreted from the tissue. The liberated tyrindoxyl is highly unstable and rapidly undergoes a series of oxidative and photolytic reactions to produce a number of bioactive intermediates before the formation of the final pigment, Tyrian purple (Figure 5.1). Traditional methods of extracting the dye precursors were manually labour intensive and unpleasant, mostly due to the intense smell of rotting flesh and the production of sulfurous mercaptans. The snails were fermented for weeks under controlled temperature and pH in large vats in what has been described as one of the worst jobs in history (Sterman and Sterman, 2012). Although a range of alternative purple pigments, that are cheaper to synthesize and easier to use, has now mostly superseded Tyrian purple in the dye industry (Baker, 1974), there is still some interest in the natural product, including traditional artisan use in South America (Naegel and Cooksey, 2002), and the rediscovery of biblical blue tekhelet from Mediterranean Muricidae (Sterman and Sterman, 2012).

Interestingly, supercritical CO<sub>2</sub> has also been utilized as an alternative to conventional aqueous dyeing processes, sharing some of the same advantages of SFE

bioactive recovery, such as reduction in the use of toxic solvents and the relatively low cost of CO<sub>2</sub> (Banchero, 2013). Supercritical CO<sub>2</sub> could therefore act as a natural dye extraction medium for precursor compounds prior to Tyrian purple dye development. The reaction of precursors leading to Tyrian purple formation is an interesting example of a novel reactive dye, where the precursor characteristics are more suitable to both the dyeing process and the impregnation in natural fibres, whilst the resulting dye is insoluble in the dyeing medium and is colorfast (Cooksey, 2001). Super-critical dyeing has not been previously tested using Tyrian purple or Muricidae mollusc extracts.

15, 30, 50 MPa

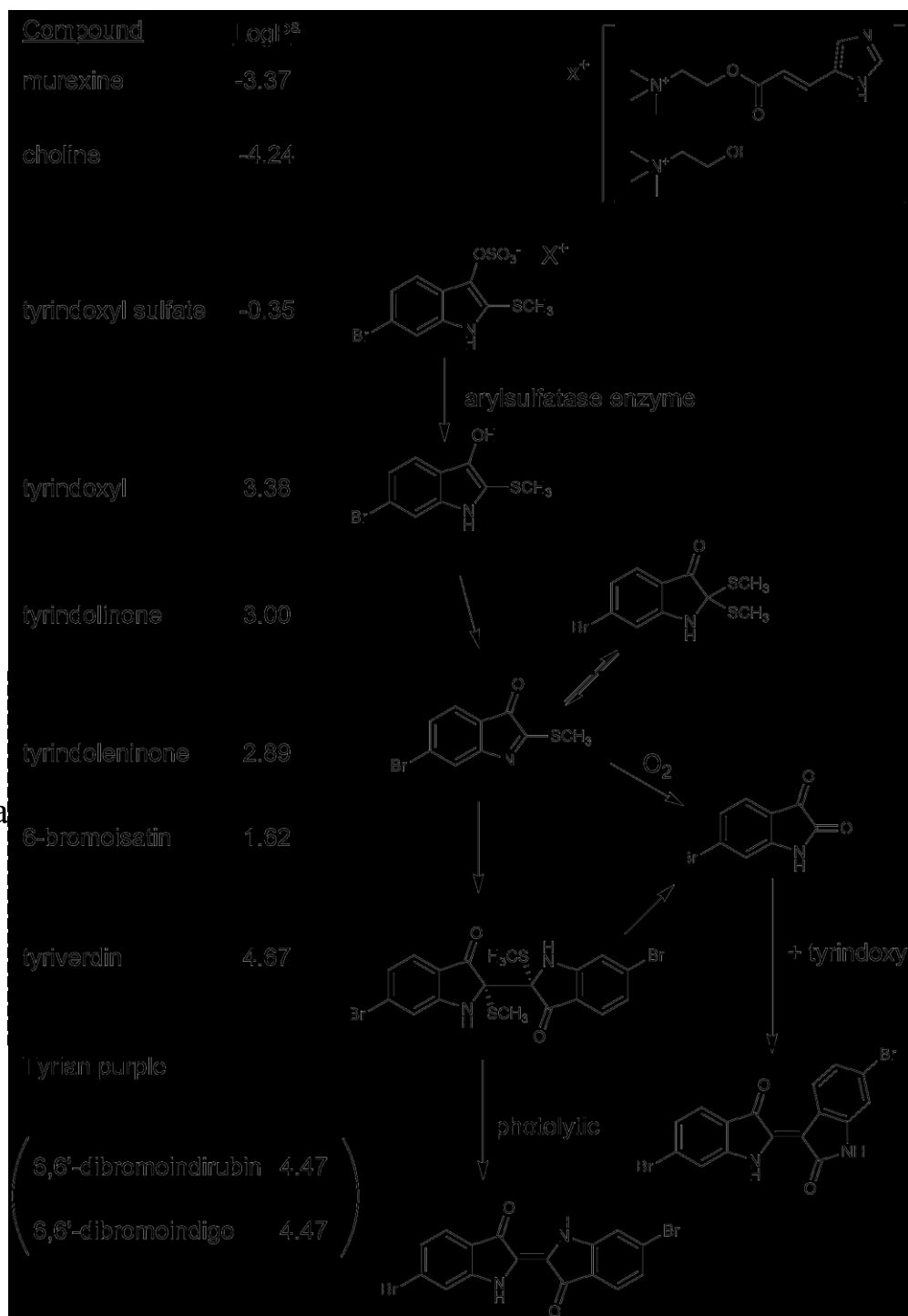


**Figure 5.1** Bioactive compounds found in *Dicathais orbita* (Muricidae, Mollusca) hypobranchial glands with corresponding solubility indicator. LogP is based on octanol-water partition coefficient calculated using the chemo-informatics software Molinspiration. The bioactive indole intermediate precursors of Tyrian purple that are soluble in supercritical CO<sub>2</sub> are shown in the box. Murexine and seneciylcholine are choline esters; the structure of seneciylcholine could also be the isomeric tigloylcholine found in other muricids (Shiomi et al., 1998).

More recently, the brominated indole precursors of Tyrian purple have attracted interest for their biologically active properties and nutraceutical potential (Benkendorff, 2013). The brominated indoles tyrindoleninone, tyrindolinone and 6-bromoisatin (Fig 5.1) have shown positive *in vitro* anticancer activity (Edwards et al., 2012, Vine et al., 2007, Benkendorff et al., 2011). These compounds also show bacteriolytic activity, whilst tyriverdin (Figure 5.1) has apparent bacteriostatic activity (Benkendorff et al., 2001b). An extract containing the concentrated cytotoxic brominated indoles, including 6-bromoisatin and tyrindoleninone, has also displayed *in vivo* chemo-preventative potential in rodent models for colon cancer (Westley et al., 2010c, Esmaeelian et al., 2014), with minimal toxic side effects (Westley et al., 2013). 6-Bromoisatin has been identified as the main anti-cancer compound (Esmaeelian et al., 2013b). The hypobranchial gland also contains various choline esters including murexine, seneciroylcholine (Roseghini et al., 1996), the structural isomer tigloylcholine (Shiomi et al., 1998) and dihydromurexine (Roseghini et al., 1996), depending on the species, which have shown to be associated with the brominated indoles (Baker and Sutherland, 1968). These compounds have muscle relaxing activity and have been clinically tested for pain relief (Roseghini et al., 1996). The choline esters are relatively potent compounds, displaying sedative effects in clinical trials with as little as 1–1.2 mg/kg (Erspamer and Glasser, 1957), yet can induce toxicity at higher concentrations (Shiomi et al., 1998). The cancer preventative and pain relieving compounds in Muricidae extracts make them a good candidate for nutraceutical development, but separation of the choline esters from the brominated indole fraction is essential due to the toxicity of the choline esters at higher concentrations. To date, the bioactive indole compounds have only been extracted with chlorinated solvents (Benkendorff et al., 2011, Vine et al., 2007), which are inappropriate for human use.

In this paper we present the extraction of brominated bioactive Tyrian purple precursors using SFE from muricid hypobranchial tissue. Previous extraction methods from marine mollusc tissue for bioactive recovery have mostly focused on the retrieval of primary metabolites and lipid fractions (Grienke et al., 2014); here we describe the first example of a targeted SFE extraction of bioactive secondary metabolites. Extracts from the model species, *Dicathais orbita*, were qualitatively analyzed for composition of brominated indoles and different pressure extractions were assessed to maximize the yield. Partial fractionation of the brominated indoles from the choline esters was also examined and the yield of the SFE was compared to chloroformic solvent extraction.

## **5.3 Methods**

### **5.3.1 Raw materials and sample preparation**

*D. orbita* samples were collected from sea-cage abalone farms situated on the Eyre Peninsula in South Australia. The whelk hypobranchial gland was accessed by cracking the shell at the join between the main whorl and spire. Glands were separated for extraction by cutting away the columnar muscle and dissecting away from the surrounding tissue. Sufficient glands to make 10–15 g were then macerated and rapidly frozen in liquid nitrogen for each replicate batch ( $n = 3$ ), which equates to approximately 3–5 g dry weight post freeze-drying. Rapid freezing and handling time for wet glands reduces oxidation/enzymatic degradation of the compounds, which will have an effect on yield; thus, all sample preparation was kept within a 5 min timeframe. Once frozen, samples were protected from light by covering them with aluminium foil and were then placed in a freeze-dryer for two days (BenchTopTMK Freezedryer, VirTis). The dry hypobranchial gland was crushed to a fine powder using a mortar and pestle under a stream of nitrogen gas. A pre-CO<sub>2</sub> extraction subsample was collected

for LC–MS analysis and was directly dissolved in acetonitrile (LiChrosolv®, Merck). A chloroform extraction of the fresh macerated glands was used as a control to assess extraction composition and yield, and any effect of freeze-drying on extract composition.

### **5.3.2 Liquid solvent extraction**

Three replicate batch samples of fresh and freeze-dried hypobranchial glands were solvent extracted, according to previously published methods (Westley and Benkendorff, 2008), for comparison with supercritical CO<sub>2</sub> extracts. The glands were dissolved in an equal portion of AR grade chloroform and methanol (1:1, v/v, CHROMASOLV®, Sigma®), and were continuously stirred overnight. After gravity filtering, the solvent extract was fractioned into a chloroform and methanol layer using 20 mL of distilled water (Milli-Q). The collected chloroform fraction was retained for the brominated indoles (Benkendorff et al., 2000), whilst the methanol fraction was collected for the choline esters (Roseghini et al., 1996). Solvents were then evaporated from each fraction using rotary evaporation (Büchi Rotovapor®R-114, Flawil, Switzerland). Each fraction was weighed and then redissolved in 1 mL of 100% dichloromethane (CHROMASOLV®, Sigma®) within amber vials for analysis.

### **5.3.3 Supercritical CO<sub>2</sub> extraction**

The supercritical extraction was carried out in a laboratory grade CO<sub>2</sub> Spe-ed™ supercritical fluid extractor (Applied Separations). The extraction unit was coupled to a temperature-controlled, stirred cooling bath (Grant Instruments) to maintain optimal temperature in the column chamber. CO<sub>2</sub> (99% pure) pressure was maintained using an air compressor (GAST – Rocking Piston 71R) and supplied by two 30 kg cylinders (Air Liquide). The Spe-ed extractor column was packed with glass wool, then a known quantity (between 3 and 5 g) of freeze-dried hypobranchial gland tissue, followed by

more glass wool, with the remaining column space filled with sterile silica. Samples were run in static mode for 1 h, then run dynamically at a solvent rate of 1.5 L/min for the remaining 2 h, collected directly in foil covered vials. Three replicate batches were run at three different pressures to assess optimal extraction at 15, 30 and 50 MPa pressure. Extractor column temperature was kept at 50°C and the micro-metering valve temperature was maintained at 70°C to ensure clear removal of the extract. The extractor column temperature was maintained at 50°C; lower temperatures were tested but these resulted in the extract collecting onto the collection valve end, even at high flow rates (data not shown). Higher temperatures could cause degradation of the main bioactive compounds, whereas 50°C had little influence on the reactive cascade of precursors to Tyrian purple, allowing for a predictable mixture of precursors whilst still allowing the free flow of compounds from the collection valve. Extracts were then weighed on an analytical balance (0.0001 g precision, Mettler Toledo).

### **5.3.4 Brominated indole analysis by liquid chromatography–mass spectrometry**

Extract constituents were analysed using high performance liquid chromatography (HPLC; Waters Alliance®) and coupled to an electron spray ionisation-mass spectrometer (ESI-MS, Micro-mass, Quatro micro™ tandem quadrupole MS system, Waters Alliance®, Milford, MA, USA) according to the methods of Westley and Benkendorff 2008. HPLC separation was performed on a reverse-phase hydrophobic column (Synergi™, Hydro-RP, 4 µm C18 phase, 80°A, 250 × 4.6 mm i.d., Phenomenex, Lane Cove, NSW, Australia). Brominated indoles in the extracts were identified based on peak retention times compared to previously reported retention times (Westley and Benkendorff, 2008) and characteristic mass spectral isotope patterns for Br<sup>79</sup> and Br<sup>81</sup>. Retention times across samples were standardised using 40

$\mu$ M synthetic 5-bromoisatin (Sigma–Aldrich, technical grade) in acetonitrile (CHROMASOLV®, Sigma® HPLC grade). Relative concentrations of brominated indoles from the extracts were calculated from the integrated peak area in diode array at 600 nm in positive ion mode using Mass Lynx 4.0 software and were expressed as the mean percentage ( $\pm$ SD) of the total brominated compound composition and total extract composition. Brominated indoles from the three different CO<sub>2</sub> column pressures were analysed and compared to chloroform extracts from fresh and freeze dried hypobranchial glands.

### **5.3.5 Choline ester analyses by thin layer chromatography**

Thin layer chromatography (TLC) was used to test for the presence of choline esters in SFE and post extracted tissue. A combined subsample was taken from each of the replicate extractions at 15, 30 and 50 MPa, as well as the corresponding post extracted tissue. Approximately 5 mg of extract was dissolved in 5 mL of acetone for detection of choline esters, whereas 15 g of post extracted tissue was placed in 20 mL of acetone, covered, allowed to dissolve overnight, gravity filtered and was allowed to evaporate to 5 mL. TLC of acetone extracts were run on aluminium-backed silica (Merck F60) using an n-butanol–ethanol–acetic acid–water (8:2:1:3) gradient for the mobile phase. Visualisation of the choline esters spots was achieved using Dragendorff reagent (Fluka™, Sigma–Aldrich®) according to the methods of Roseghini et al. (1996).

## **5.4 Results and discussion**

### **5.4.1 SFE extraction yield**

Supercritical CO<sub>2</sub> was successful in obtaining a crude extract, comparable to chloroform solvent extraction (Table 5.1), and in recovering the main bioactive brominated indole precursors of Tyrian purple previously used for bioactivity testing

(Benkendorff et al., 2011, Vine et al., 2007, Edwards et al., 2012) from the hypobranchial glands of *D. orbita* (Table 5.2 and Figure 5.1). The yields shown in Table 5.1 are expressed as a percent recovery from hypobranchial gland wet weight, raw material (dry weight) and whole whelk weight, which allows for comparison to other studies on extraction of bioactive compounds from raw biological material (Herrero et al., 2010) and from marine fisheries data (Leiva and Castilla, 2001). The mean extraction efficiency of SFE ranged from 2.12 to 2.66% of the original wet weight (freeze dried hypobranchial gland), showing no significant difference (ANOVA  $P = 0.3937$ ) to mean extraction of the fresh hypobranchial gland tissue using organic solvents at 2.88% (Table 5.1). Extraction efficiency based on whole whelk weight (including shell) provides an equivalent efficiency of 0.05% at 30 MPa (Table 5.1). Some of the lower values seen for SFE compared to solvent extraction could be due to channelling or compaction of the dry powdered tissue in the SFE column (Halim et al., 2012). The hypobranchial gland is comprised of different tissue types including secretory, connective and muscular tissue (Westley et al., 2010b), and also includes sticky mucus into which the bioactives are expelled (Noble et al., 2009). This represents a complex biological matrix with wide variation in molecular composition which could influence porosity and bulk density in the extraction chamber. This type of variation is known to cause differences in mass resistance creating channelling effects from the pressurized solute (King, 2000). Pre-treatment of glandular tissue to increase homogeneity prior to freeze drying may aid in more even particle size and improved mass transfer dynamics.

**Table 5.1** Chloroform extraction yields for fresh and freeze-dried *Dicathais orbita* hypobranchial glands in comparison with supercritical CO<sub>2</sub> extraction at increasing pressures of 15, 30 and 50 MPa. *N* = the total number of adult individuals for each starting weight.

<b>Extraction method / CO<sub>2</sub> pressure MPa</b>	<b><i>N</i></b>	<b>Total whelk weight g (including shell)</b>	<b>Total hypobranchial wet weight g (mean ± SD)</b>	<b>Total dry weight g (mean ± SD)</b>	<b>Total extract weight mg (mean ± SD)</b>	<b>Mean extraction efficiency % wet hypobranchial weight</b>	<b>Mean extraction efficiency % total whelk weight</b>
Solvent extraction	23	1106	18.94 (1.52 ± 0.27)		547 (23 ± 8)	2.88	0.05
Freeze dry solvent extraction	20	857	15.34 (0.73 ± 0.26)	6.09 (0.29 ± 0.10)	484 (23 ± 8)	3.16	0.06
SFE 15	27	1273	24.08 (0.89 ± 0.33)	9.40 (0.67 ± 1.72)	510 (36 ± 93)	2.12	0.04
SFE 30	35	1124	19.63 (0.56 ± 0.22)	7.67 (0.22 ± 0.08)	516 (15 ± 6)	2.63	0.05
SFE 50	26	1753	29.52 (1.14 ± 0.42)	11.41 (0.44 ± 0.16)	786 (30 ± 11)	2.66	0.04

## **5.4.2 Extraction composition**

### **5.4.2.1 Pre extraction composition**

The percent composition of the freeze-dried hypobranchial gland dissolved directly in acetonitrile (Table 5.2) shows the relative proportion of components in the starting material that have shown bioactivity. LC–MS spectra of the freeze dried hypobranchial gland shows a high proportion of tyrindoxyl sulfate, 78.56% (Table 5.2), which is reduced in the chloroform extract of fresh tissue, and is lost altogether in the chloroform and supercritical CO<sub>2</sub> extraction process of the freeze-dried tissue (Table 5.2, Figure 5.2). This is presumably due to the hydrophilic structure of tyrindoxyl sulfate which shows a negative LogP value of  $-0.346$  (Figure 5.1). Removal of the hypobranchial gland from the surrounding tissue also allows tyrindoxyl sulfate and the enzyme arylsulfatase to mix, mimicking the way these compounds are secreted into the environment (Baker and Duke, 1976), which starts the oxidative, photocatalytic cascade of precursors to Tyrian purple (Figure 5.1). The timing between enzymatic removal of the sulfate group from tyrindoxyl sulfate and freezing, prior to freeze drying, will partially determine the starting relative proportion of each compound.

**Table 5.2** Mean percent brominated indole composition of chloroform extracts from fresh, freeze-dried hypobranchial glands, and 15, 30 and 50 MPa SFE extracts of *Dicathais orbita* hypobranchial glands ( $\pm$ standard deviation;  $n = 3$ ). Percent composition was based on integrated peak area from HPLC chromatograms at 600 nm, relative to all peaks assigned using MassLynx 4.0 software.

Compound	Rt	Freeze-dry <sup>a</sup> %	Chloroform extract		Freeze-dry extract		15MPa SFE		30MPa SFE		50MPa SFE	
			%	( $\pm$ SD)	%	( $\pm$ SD)	%	( $\pm$ SD)	%	( $\pm$ SD)	%	( $\pm$ SD)
<b>Tyrindoxyl sulfate</b>	6.52	78.56	31.41	(0.9)	n.d.		n.d.		n.d.		n.d.	
<b>Tyrindolinone</b>	9.57	n.d.	n.d.		n.d.		n.d.		n.d.		n.d.	
<b>Tyrindoleninone</b>	10.2	7.57	24.76	(0.8)	32.37	(1.4)	10.18	(0.9)	35.12	(1.0)	29.99	(4.2)
<b>6-Bromoisatin</b>	6.27	13.93	21.28	(0.7)	26.76	(2.7)	78.84	(2.5)	22.24	(0.7)	12.92	(6.2)
<b>Tyriverdin</b>	10.85	1.49	9.52	(0.9)	19.64	(1.7)	n.d.		23.54	(1.4)	40.88	(12.7)
<b>6,6'-Dibromoindigo / 6,6'-Dibromoindirubin</b>	14.6	n.d.	n.d.		n.d.		n.d.		n.d.		n.d.	

<sup>a</sup>Freeze-dried percent yield is the composition of the subsample of freeze-dried hypobranchial gland dissolved directly in acetonitrile immediately prior to injection into the LC–MS, whereas the freeze-dry extract is from an overnight chloroform extract dried and then redissolved in acetonitrile. Not detected (n.d.).

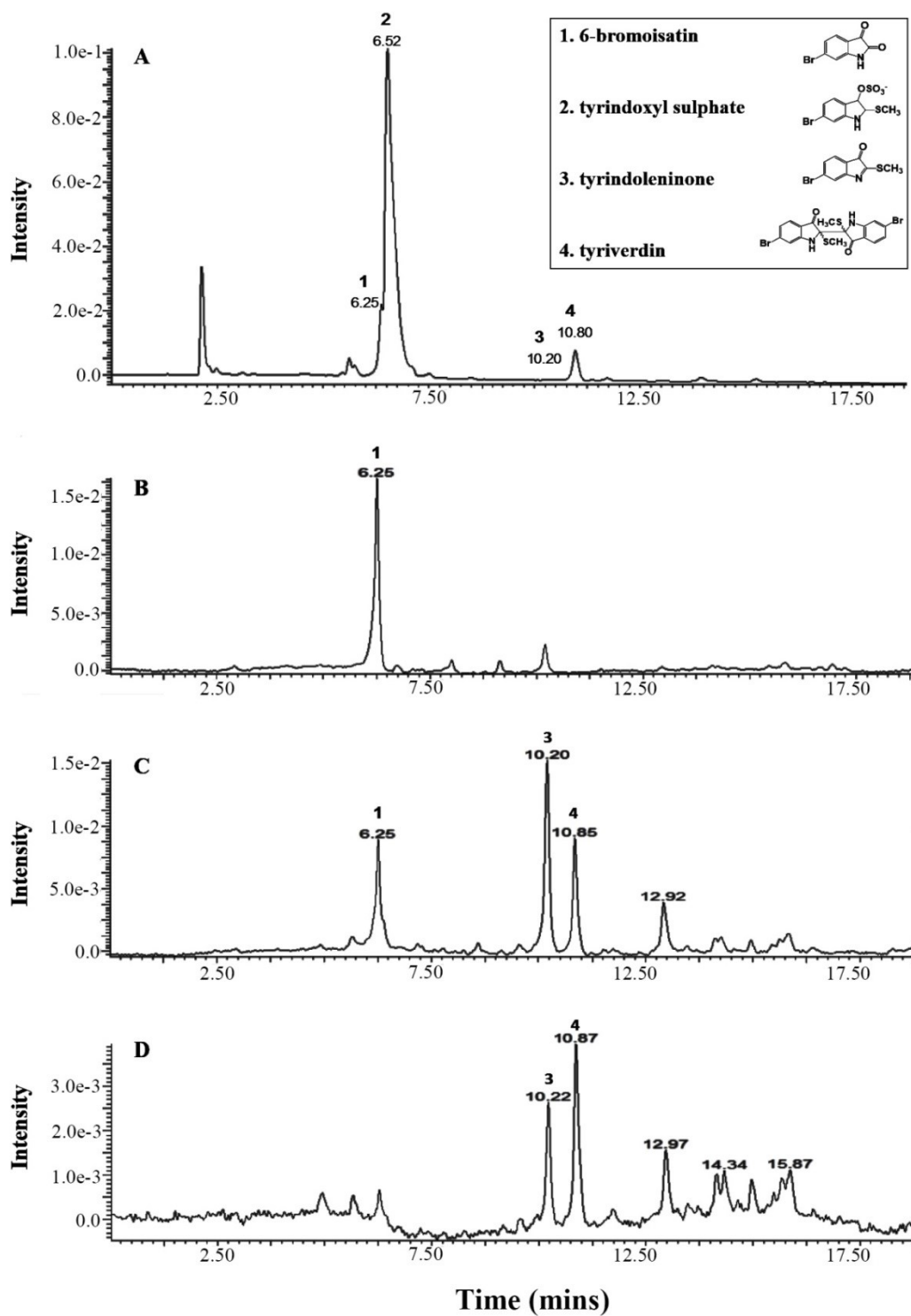


**Figure 5.2** Chromatograph of *Dicathais orbita* hypobranchial gland extracts (A) pre extraction starting material dissolved directly in HPLC grade acetonitrile (Merck); (B) 15 MPa SFE extract; (C) 30 MPa SFE extract; and (D) 50 MPa SFE extract. Peak designation was given based on the molecular ion  $[MH^+]$  and fragmentation patterns by comparison to known standards (Esmaelian et al., 2013b).

The other main constituents of the starting material include the brominated indoles tyrindoleninone, tyriverdin and 6-bromoisatin (Figure 5.2A). Tyrindoxyl was undetectable in starting material and extracts (Table 5.2, Figure 5.2) which is unsurprising as it is known to readily oxidize into tyrindoleninone (Cooksey, 2001). The absence of tyrindoleninone in our samples may be a result of the low pressure environment in the freeze-drying unit. Tyrindoleninone is produced when tyrindoleninone reacts with methane thiol by adding a thioether (Cooksey, 2001) which is easily evaporated in the 100 Millitorr vacuum environment of the freeze dryer. Methane thiol and the thioether functional group of tyrindoleninone can also be lost during chromatographic separation (Cooksey, 2001) although they have been detected in LC–MS spectra in previous studies of chloroform extracts (Westley and Benkendorff, 2008).

The end products Tyrian purple, 6,6'-dibromoindigo and 6,6'-dibromoindirubin, were not detectable either visually or by LC–MS analysis before or after extraction (Figure 5.2). The absence of the Tyrian purple components in the pre-extract material could be due to the short handling time from dissection to freezing in liquid nitrogen prior to freeze drying and to the exclusion of light, thus preventing the photolytic cleavage of tyriverdin (Figure 5.1). Tyrian purple, 6,6'-dibromoindigo and 6,6'-dibromoindirubin, are highly non-polar with a LogP value of 4.47 (Figure 5.1), and have previously only been detected in hypobranchial gland extracts after being dissolved in hot dimethylformamide and dimethyl sulfoxide (Benkendorff, 2013). Supercritical CO<sub>2</sub> without the aid of a co-solvent may not have the ability to solubilize Tyrian purple. Although SFE has been employed in the extraction of indigo compounds from *Isatis tinctoria* (Danz et al., 2001), the indigo structure does not contain bromine and is therefore more soluble in supercritical CO<sub>2</sub>.

#### 5.4.2.2 Solvent versus SFE composition

The main brominated indole components of SFE extract includes tyrindoleninone, 6-bromoisatin and tyriverdin. Supercritical CO<sub>2</sub> was able to match the solvating power of chloroform at higher pressure, with both the 30 and 50 MPa extracts containing all three compounds (Figure 5.2). However, pressure did have an effect on percent composition, with predominately 6-bromoisatin and no tyriverdin being detected in the 15 MPa SFE extract (Table 5.2, Figure 5.2A). While it had little effect on yield (Table 5.1), increasing the pressure to 30 MPa, augmented the relative proportion of tyrindoleninone by more than three times (Table 5.2, Figure 5.2C), although this compound was at a lower concentration again at 50 MPa (Figure 5.2D). Higher SFE pressure also changed the relative proportion of tyriverdin, undetectable at 15 MPa to 40.88% ( $\pm 12.7$ ) at 50 MPa (Figure 5.2D). The change in the relative proportion of tyriverdin, as a function of increasing pressure, may result in denser CO<sub>2</sub>, thereby increasing the solute solubility in SFE, as demonstrated previously with naphthalene in supercritical CO<sub>2</sub> (Hourri et al., 1998). Higher pressure supercritical CO<sub>2</sub> also increases the dielectric constant (Reynolds et al., 1996), which may bring tyriverdin, or the conditions for its formation, into the solvating range of supercritical CO<sub>2</sub>. The main benefit of changing the solvating power of CO<sub>2</sub>, where brominated indoles are concerned, is the capacity to target particular compounds based on their solubility at varying pressure. 6-Bromoisatin shows considerable promise for development as a nutraceutical compound either in isolation or as a mixture (Edwards et al., 2012, Vine et al., 2007, Esmaelien et al., 2014), and low pressure SFE extract targets this compound above tyrindoleninone and tyriverdin. SFE therefore provides a semi-fractionation method at low pressure for 6-bromoisatin. Supercritical fluid chromatography would be a suitable methodology for the purification of the

brominated indoles (Chester et al., 1996), particularly 6-bromoisatin at lower pressures.

Supercritical CO<sub>2</sub> extracts showed no recovery of choline ester compounds in any of the extracts, irrespective of pressure. This was confirmed by the absence of choline ester visualization spots on TLC (Figure 5.3). Three choline ester compounds remained in the post-extracted tissue (Figure 5.3) recovered from the Spe-ed extractor column after SFE of the brominated indoles. As muricid choline esters show potent neuromuscular blocking activity (Roseghini et al., 1996), they should be selectively extracted away from the anti-cancer brominated indoles for nutraceutical development due to the differences in *in vivo* activity associated with these two classes of compounds. Lethal dose concentrations for the choline ester tigloylcholine, from muricid *Thais clavigera* occurred at 0.92 mg/kg in mice (Shiomi et al., 1998), whilst *D. orbita* extracts with only brominated indole compounds showed no general health effects *in vivo* at 1 mg/kg in mice (Westley et al., 2013). Residual choline esters in the brominated indole fraction would be a concern for future Food and Drugs Administration approvals, due to the relative potency of the choline ester compounds. The negative LogP of the choline esters and the ultimate precursor, tyrindoxyl sulfate (Figure 5.1), indicate their highly hydrophilic structures. In previous organic solvent extractions these compounds were typically separated out in the methanol fraction; however this method would be less reliable than SFE which produces no residual choline esters (e.g. Figure 5.3). Nevertheless, the choline esters can still be selectively recovered from the post SFE tissue using different percentages of methanol, ethanol or acetone depending on the choline ester present in the species (Roseghini et al., 1996, Shiomi et al., 1998).

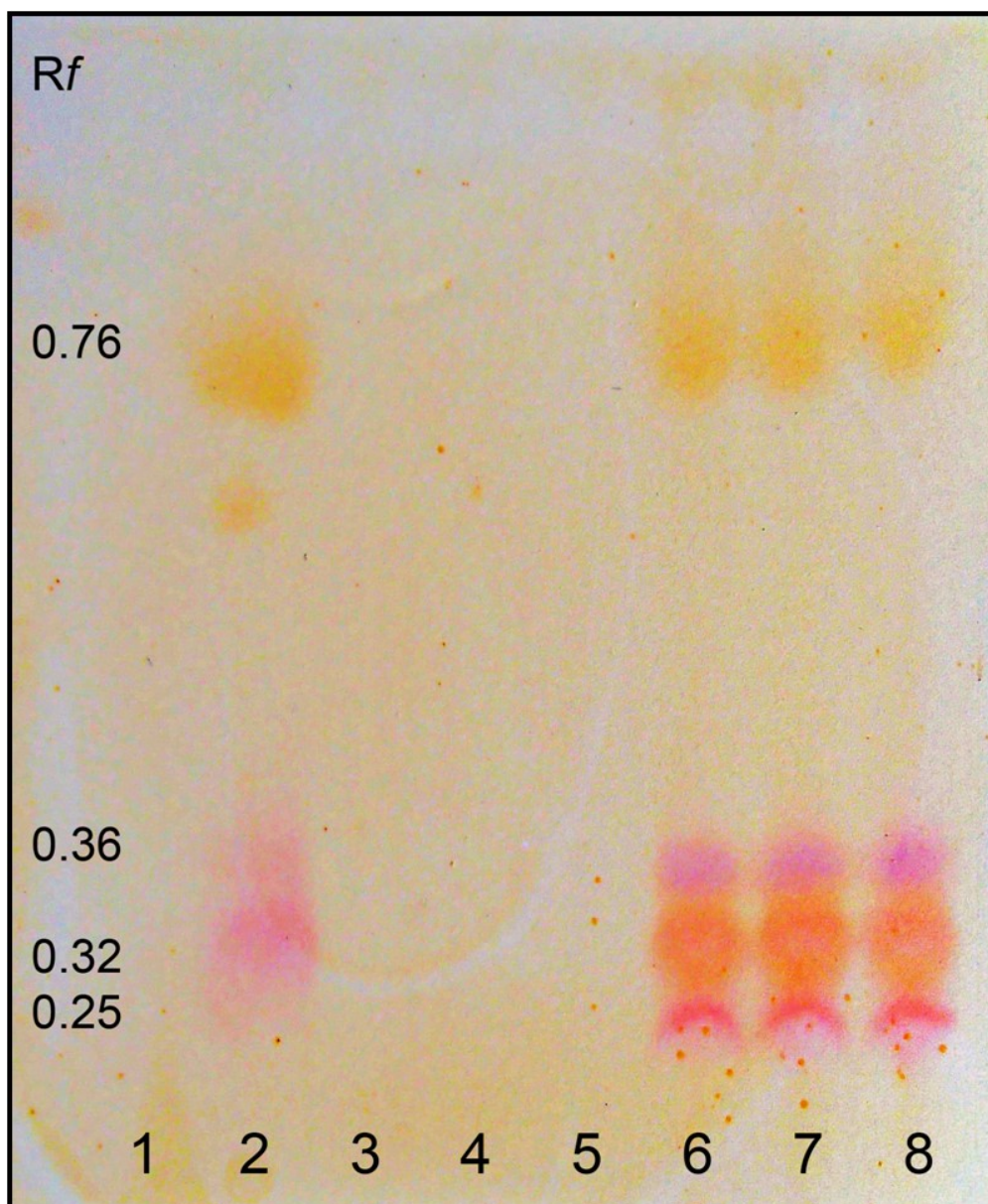


**Figure 5.3** Thin layer chromatography of choline ester compounds from *Dicathais orbita* hypobranchial glands on aluminum-backed silica plates visualized using Dragendorff reagent. Mobile phase: butanol–ethanol–acetic acid–water (8:2:1:3). 1) negative control using distilled water; 2) positive control using fresh hypobranchial extracted with acetone; 3) 15 MPa SFE; 4) 30 MPa SFE; 5) 50 MPa SFE; 6) post extracted tissue from 15 MPa SFE; 7) post extracted tissue from 30 MPa SFE; 8) post extracted tissue from 50 MPa SFE. Rf values for 0.25 corresponds to dihydromurexine; 0.32 corresponds to murexine; 0.36 corresponds to choline, and 0.76 corresponds to senecioylcholine or the isomer tigloylcholine (Shiomi et al., 1998, Roseghini et al., 1996).

## 5.5 Conclusion

The extraction and semi-purification of brominated Tyrian purple precursors using increasing SFE CO<sub>2</sub> pressure demonstrates an effective method to selectively extract variably soluble compounds from *D. orbita* hypobranchial tissue. SFE extraction, in comparison to liquid solvent extraction, had little effect on yield and has the additional benefit of targeting the partial fractionation of precursors based on their solubility. The selective extraction of 6-bromoisatin at low pressure provides an environmentally benign and safe method for development of this compound as a nutraceutical. The absence of choline esters in the 15 MPa SFE extract is another advantage of the SFE method, as the toxicity of choline esters has been eliminated, compared to solvent extraction where small amounts of choline esters may contaminate fractions if not handled correctly. SFE also shows considerable promise as an alternative to traditional dyeing methods for Tyrian purple, namely the ability to target colour precursors prior to the full colour reaction.

## 5.6 Acknowledgements

Live *Dicathais orbita* were supplied by Australian Bight Abalone collected under Fisheries Exemption Permit 9902638. We would like to thank Peng Su and Prof. Wei Zhang from the Flinders Centre for Marine Bioproducts Development for assistance with the SFE equipment and Daniel Jardine from Flinders Analytical for assistance with LC–MS analysis. D. Rudd is thankful to Dr. James Harris for PhD supervision and Flinders University for an Australian Post-graduate Award scholarship.

## 6 Chapter Six – General Discussion

### 6.1 Secondary metabolites *in situ*

“The molecular characterization of our natural world with mass spectrometry is at a pivotal and exciting stage”, Pieter Dorrestein (Dorrestein, 2014).

Mass spectrometry imaging provides a truly exciting tool for the molecular characterisation of the natural world, giving a precise molecular snapshot of chemical entities from biological tissues *in situ*. The work presented in this thesis demonstrates a novel approach to the spatial analysis of muricid secondary metabolites using SALDI-MSI based techniques and preparative tools for the natural product development of muricid brominated indoles. The MSI methods developed in Chapters 2 and 3, were effective in the detection and identification of choline esters and brominated indoles across a range of polarities from marine mollusc tissue, providing accurate spatial maps of secondary metabolite distributions. In Chapter 3, secondary metabolite annotation and relative *ex situ* quantification were used to build on the SALDI-MSI results. In Chapter 4 DIOS-MSI was able to describe the movement of murexine from the hypobranchial gland to the capsule gland in *D. orbita* females across the reproductive cycle and finally into the egg capsules. Coupled with larval motility assays, this highlighted a new putative role for murexine in the reproductive biology of *D. orbita*. SALDI-MSI is considered a relatively new tool for natural product analysis and the information afforded by spatial mapping could be more routinely adopted in natural product and chemo-ecological research. Chapter 5 also involved method development, however, in this case using supercritical fluid extraction (SFE) to facilitate the natural product development of the brominated indoles.

The method development for SALDI-MSI in Chapters 1 and 2, and SFE in Chapter 5, could not have been possible without the extensive chemical characterisation of the already known brominated indoles. Bromination in this case provided a spectral ‘reference point’ in MSI data, by mono- and di-brominated spectral patterns, which could be combined with the structural characteristics, Log P and solvent solubility for compound separation and identification. In Chapter 4, <sup>1</sup>H-NMR and <sup>13</sup>C-NMR was used to confirm the identification of murexine in the combined choline ester indoxyl salt, from the capsule gland of a reproductive female and egg capsules. The detection of murexine in Chapter 4 is the first time this compound has been identified in the capsule gland tissue and as an early stage compound in egg capsule fluid. Among the tools used for compound elucidation, DIOS-MSI in particular shows considerable promise in the analysis of halogenated secondary metabolites and could provide an effective tool for identifying sites of biosynthesis, storage and deployment in the context of biological processes.

## 6.2 Tools for biorational drug discovery

“The secret of finding something is knowing where to look”

Annon (quoted in Beattie, 1994)

There is a growing interest in applying a biorational approach to natural product discovery, where the natural history and evolutionary biology of a species will guide bioactive resource discovery (Beattie et al., 2011, Benkendorff, 1999, Beattie, 1994, Leal et al., 2012). The approach developed in this study, specifically SALDI-MSI of secondary metabolites, is compatible with the biorational principle by allowing NP discovery to occur in a biological context, *in situ*. The results of DIOS-MSI in particular have shown a number of unexpected secondary metabolite signals (Chapter 2 and 4), as well as some interesting spectral patterns worth further investigation. Data

from Chapters 2 and 4 show un-annotated, but distributionally interesting peaks (Chapter 2; Figure 2.5: 98.11, 118.16  $m/z$ ), when considered in the context of the hypobranchial gland anatomy. The unexpected choline ester distributions detected in Chapter 4 also support a biologically guided top-down analytical approach to secondary metabolites. Low mass SALDI-MSI may be an exciting complimentary tool in biorational NP discovery, which shows its full potential when combined with knowledge of the biological properties of a sample or structure, for example, the tranquilising effects of choline esters. Chemical ecology gives us clues for “where to look”, such as the hypobranchial tissue, and novel analytical imaging tools provide us with knowing ‘how to look’, detecting the low molecular weight chemo-diversity of tissues.

### **6.2.1 DIOS-MSI as a top-down approach to biodiscovery**

Although some of the limitations from the use of a matrix during LDI-MS can be overcome through careful sample preparation, matrix choice and post processing, these methods require some prior knowledge of the expected  $m/z$  and or structure to obtain reliable spectra (Bergman et al., 2014, Svatos, 2010). Consequently, in many cases low molecular weight NP imaging could be in part considered a targeted form of analysis when using MALDI-MSI because the expected mass must not overlap with matrix signals or fall within a mass region where suppression obscures peak detection. Targeted analysis assumes some knowledge of the compound and optimization that has occurred prior to imaging. However, not all studies are targeted. One of the advantages of LDI-MS and MSI is their ability to handle a wide variety of chemical entities, including ‘contaminants’ and keep molecular structures intact during analysis. The major innovation of DIOS-MSI is the absorption of low molecular weight compounds from a broad range of polarities into the functionalized silicon matrix for retention, allowing larger molecular weight contaminants to be removed, eliminating

interfering matrix signals and preventing signal suppression. This makes DIOS-MSI an excellent platform for top-down analytical descriptions of tissue, but focused on the low molecular weight region. The detection of murexine in the capsule gland in Chapter 3 was entirely unexpected, providing an example of the merits in examining all detectable low mass metabolites simultaneously.

Top-down analysis, where there is an active intention to remove bias, has the ability to detect both ‘known unknowns’ and more excitingly the ‘unknown unknowns’, for example, un-annotated distributional maps detected in Chapter 2 and 4. Marine tissues are also far less characterised by MS/MSI compared to other tissue types including plant tissue (Ernst et al., 2014), non-marine bacteria (Watrous and Dorrestein, 2011), and *in vivo* model species tissue (Goodwin and Pitt, 2010). As fewer marine species have been characterised by MS/MSI, SALDI-MSI could be a promising tool for de-replication studies. Scanning the hypobranchial glands of different molluscs may show how widely distributed the known choline esters and brominated indoles are within the Muricidae, find structural analogues or detect novel choline esters and novel non-/brominated indole precursors. SALDI-MSI was effective in detecting secondary metabolites with little sample material, for example, 15µm thick sections (Chapter 2, 3, and 4), also supporting its use as an effective de-replication tool.

### **6.3 The ecological significance of choline esters in muricid reproduction and egg capsule development**

The distribution of murexine within the female capsule gland during the egg laying process provides evidence for a functional role in egg capsule formation or deposition in *D. orbita* (Chapter 4). The muscle relaxing properties of murexine may be employed in the relaxation of the oviduct for the passage of fertilized eggs and albumen towards the capsule gland for subsequent capsule membrane formation. Interestingly, previous

histochemical analysis of the capsule lamina indicates the passage of eggs and albumen into the capsule environment occurs prior to the secretion of the capsule wall lamina (Westley and Benkendorff, 2009b), a process that would require space be created in the oviduct. Murexine may also be involved in regulating the secretion of egg capsule lamina, which is a complex process of building multiple proteinaceous and carbohydrate rich layers around eggs, prior to capsule sculpting and hardening, resulting in the typical leathery quality seen in muricid capsules (Westley and Benkendorff, 2009b, D'Asaro, 1988, D'Asaro, 1992). Alternatively, murexine could be relaxing the capsule/pedal gland prior to capsule sculpting, allowing the species specific capsule shape to be formed (Westley and Benkendorff, 2009b, D'Asaro, 1992). In any of the above cases, capsule gland relaxation is a significant deviation away from the original proposed functional role of the choline esters, predominantly seen to aid in the predatory lifestyle of the carnivorous Muricidae (Roseghini et al., 1996).

The detection of murexine in the egg capsules during the early stages of capsular development suggests an additional functional role that could be integral to larval development in *D. orbita* (Chapter 4). A role for murexine in capsular fluid has previously been suggested (Westley, 2008), but as an anti-predatory secondary metabolite acting via predator learned aversion. The abundance of murexine detected in the capsular fluid in Chapter 4, Figure 4.5, is substantially less than that detected in the medial hypobranchial gland of all the adults (Chapters 2, 3 and 4), with capsule concentrations unlikely to match those required for predator aversion. Therefore, a role in the relaxation of intracapsular larvae is more fitting, especially when coupled with the slow regulated release of the counter ion tyrindoxyl sulfate (Chapter 4) to generate intermediate brominated indoles (Westley and Benkendorff, 2009b, Benkendorff et al., 2004b). Murexine in the capsular environment would also need to be at

concentrations that do not permanently intoxicate larvae, allowing larvae to recover for capsule release at the end of the intracapsular period. The alternative hypothesis for the role of choline esters is that they prevent predation but larvae have a mechanism to prevent intoxication. A closer investigation of the controlled release of choline esters in the capsular fluid sampled directly from environmental samples and across more stages of larval development (egg, multi-cell cleavage stage, early and late trochophores, early to late veligers and pre-hatchling larvae (Noble et al., 2013)) would further elucidate the period of relaxation afforded by murexine. Murexine and the other choline esters have been detected in many neogastropods (Roseghini et al., 1996). DIOS-MS and MSI of other muricid capsules and female reproductive tracts during egg laying may expand on the potential larval tranquilising properties of the choline esters. If it were to act in relaxing larvae for the intracapsular developmental period, the choline esters could be considered to be providing an ecological advantage to the Muricidae. Certainly, studies of *D. orbita* larval development have reported an almost 100% hatching success rate (Phillips and Campbell, 1974). The ecological function of choline esters may be as multifunctional molecules, acting in predation and as a tranquiliser for larval deposition and development, and are therefore likely to be of “keystone significance” (Chapter 1, section 1.3.4) by allowing muricids to thrive in intertidal reef communities.

#### **6.4 Analysing the ecological significance of the brominated indoles**

DIOS-MSI has been a highly successful approach for the analysis of the brominated indoles (Chapters 2, 3 and 4). The properties of the functionalized surfaces allow the detection of the brominated precursor, intermediates and Tyrian purple simultaneously and within *in situ* spatial distribution; this manner of spatial analysis of muricid tissue has not been achieved before with other analytical approaches. The removal of tissue prior to imaging could be seen as a form of selective enrichment, to

enhance the detection of the low abundant secondary metabolites. The brominated indoles predominantly maintained a spatial distribution in the medial hypobranchial gland of all adult samples, irrespective of sex. Some delocalisation occurred with tyrindoxyl sulfate during the sample preparation for DIOS-MSI, with its highly hydrophilic structure (Chapter 2 and purposely in 3). This was gradually refined with more careful sample preparation after the preliminary DIOS-MSI data acquisition in Chapter 2, through more gentle washing procedures. Subsequent samples maintained the expected distribution of tyrindoxyl sulfate in the medial hypobranchial gland and within intracapsular fluid. Future MSI analysis could explore the use of nanostructure initiated mass spectrometry (NIMS) imaging, more suited to the capture of hydrophilic low mass metabolites (Calavia et al., 2012) in spatially analysing tyrindoxyl sulfate. The remaining brominated indoles are well suited to the analyte capture properties of functionalised porous silicon (Chapter 3).

There are some limitations encountered with using functionalised and nano-fabricated surfaces for MSI. Unlike conventional MALDI, the majority of the tissue has to be removed for adequate desorption / ionisation of the low molecular weight metabolites. The removal of the tissue also means the removal for the subsequent histological processing that allows co-registration of ions to tissue regions / sections. DIOS and NALDI-MSI must then rely on a scan of the original tissue, which is unstained and on a dark background, and a serial H and E section that can differ slightly from the original imaged tissue. Minor variations occur 15  $\mu\text{m}$  along the tissue section that could include small cellular structures, e.g. ducts, nervous tissue, specific cell clusters or connective tissues, which might be missed or misinterpreted. To compensate for this, spectral component analysis can aid in using spectral patterns to define tissue regions, see Appendix III pLSA analysis, allowing spatial interpretation to be done on the same section. Another limitation of both DIOS and NALDI-MSI is

quantitation of the absolute concentration of secondary metabolites in tissue sections. This comes from the imprinting approach, where the amount of transfer of secondary metabolites into the porous surface may be variable. The transfer rate could be calculated if the removed tissue could be extracted and quantitatively analysed, say in GC-MS or LC-MS or even single shot LDI-MS, and then compared to the quantitative spatial method used in Chapter 3.

Assigning functional ecology to the brominated indoles still requires further investigation. The putative role of anti-microbial intermediate brominated indoles in capsular development (Westley et al., 2006, Benkendorff et al., 2000) would support a multifunctional role of the combined choline ester indoxyl salt in providing relaxation and antimicrobial activity in the developing capsule (Chapter 4). The function of tyrindoxyl sulfate could also be in the prevention of uncontrolled binding of murexine to nicotinic acetylcholine receptors during storage in hypobranchial or capsule gland tissue. The computational binding of murexine into an acetylcholine-binding protein (Appendix 1), shows little available space in the binding pocket for the combined salt. In particular, if the methyl ammonium plays a significant part in binding affinity, the release of murexine from tyrindoxyl sulfate is required for active binding. Structural modelling of acetylcholine binding to the nicotinic acetylcholine receptor (Schapira et al., 2002) combined with *ab initio* quantum mechanics predictions of binding affinity show a strong cation- $\pi$  interaction between the quaternary ammonium of acetylcholine and a tryptophan residue on the sub-unit (Zhong et al., 1998). Availability of the quaternary ammonium may also be required for the choline esters to have an effect, which can be seen in one of the binding positions of murexine (Appendix 1, Figure 3). The presence of an aryl sulfatase enzyme in *D. orbita* provides a mechanism for controlled release of murexine, where it liberates tyrindoxyl sulfate through the hydrolysis of the sulfate group to form

unstable tyrindoxyl (Cooksey, 2001, Baker and Sutherland, 1968). The slow releases of both classes of secondary metabolites fill the dual needs of developing larvae. Capsules need adequate defence and physiological conditions to suit cellular development and respiration, for example, the limitation of oxygen usage in capsular environments where larvae can be seen actively swimming (Cumplido et al., 2011).

The biodistributional data gained in Chapters 2 and 4 could also be combined with other MSI techniques to investigate the biosynthesis of the precursor tyrindoxyl sulfate. The role of bacterial symbionts in the biosynthesis of the brominated indoles is yet to be excluded. Single cell SIMS imaging combined with laser capture microdissection would be ideal for isolating the secretory cells types found in the medial hypobranchial gland (Westley et al., 2010b), to investigate the presence of biosynthetic enzymes associated with production (e.g. bromoperoxidase or brominase enzymes (Jannun and Coe, 1987)). SIMS imaging has been successfully used at the single cell level on *Aplysia* neurons (Passarelli et al., 2013). SIMS imaging could also be used to identify precursor metabolites prior to the final synthesis of tyrindoxyl sulfate (Benkendorff, 2013).

If bacterial symbionts are present in the medial hypobranchial gland, combination imaging could also be used for detecting the presence of bromoperoxidase, specifically vanadium bromoperoxidase. Laser ablation-inductively coupled plasma-mass spectrometry (LA-ICP-MS) has been successfully used in the analysis of low concentration vanadium levels in crude oil samples (Chirinos et al., 2013). LA-ICP-MS has also been used in the analysis of mollusc tissue, mainly in imaging metal contamination in the neogastropod whelk *Nassarius reticulatus* (Santos et al., 2009). LA-ICP-MS of vanadium distributions in the hypobranchial gland may provide evidence of the site of synthesis, the type of bromoperoxidase activity (if involving vanadium) and allow more detailed studies such as SIMS to be directed to cells

associated with synthesis. LA-ICP-MS distributions may correlate with DIOS-MSI distributions of tyrindoxyl sulfate.

## **6.5 The biomedical potential of the brominated indoles**

The use of chlorinated solvents in the extraction the brominated indoles for *in vivo* testing is a partial impediment to the development of muricid extracts as potential nutraceuticals. The development of a novel supercritical CO<sub>2</sub> method for the selective extraction and collection of the bioactive intermediates 6-bromoisatin and tyrindoleninone (Chapter 5) draws on the lipophilic properties of the intermediate compounds, as well as the exclusory hydrophilic properties of the choline esters (Chapter 3). Future *in vivo* assessment of the SFE product would determine if this is the preferred extraction process for the bioactive properties, and potentially other bioactive lipophilic components worth investigating. The lipid fraction of green-lipped mussel extract, Lyprinol, has multiple anti-inflammatory activities (Grienke et al., 2014). Muricid lipid fraction extracts processed using a method like SFE may in fact have many more bioactive properties above the chemo-preventative qualities currently being examined (Benkendorff, 2013).

The biomedical potential of the intermediate brominated indoles, particularly 6-bromoisatin, as chemo-preventative compounds could also benefit from the use of the SALDI-MSI methods developed in Chapter 2. The success of short term *in vivo* models has led to a 14 week *in vivo* colorectal cancer model to test the chemo-preventative efficacy of crude extract and 6-bromisatin, using AOM induced tumour formation in wild type C57BL/6J black mice (Esmaelian, 2014, Chahal, 2014). Treatment included oral administration of crude extract, 0.5 and 0.05 mg/g, and 6-bromoisatin, 0.05, 0.025 and 0.01 mg/g, delivered in sunflower oil with 0.02% vitamin E and was compared to an oil control group. Assessment of early tumour formation indicator,

aberrant crypt foci (ACFs), showed 6-bromoisatin, 0.025 and 0.01 mg/g, to be effective in reducing ACF counts in the colon. Crude extract, 0.05 mg/g, and 6-bromoisatin, 0.05 and 0.025 mg/g, were also effective in reducing colon tumour counts after 14 weeks (Chahal, 2014). All treatment groups increased the apoptotic index, in agreement with previous *in vivo* studies of the brominated indoles (Chahal, 2014, Esmacelian et al., 2014, Westley et al., 2010c). These studies suggest that 6-bromoisatin in particular holds good potential for development as a natural chemopreventative agent.

DIOS-MSI can be used to investigate the *in situ* absorption and metabolism of the brominated indoles within the gastrointestinal tract, faeces, blood serum, liver, and kidneys. The value of DIOS-MSI in this approach is the ability to capture a range of low mass metabolites with varying polarity and solubility, within the gastrointestinal tract. Xenobiotic metabolism aims to alter the structure of xenobiotics/drugs via various mechanisms including oxidation, reduction, hydrolysis and/or hydration (Lewis, 2000). Therefore lipophilic compounds such as the brominated indoles may become more hydrophilic or conjugated after gastrointestinal or hepatic metabolism. Appendix 6 shows preliminary DIOS- and NALDI-MSI analysis of collected tissues from the gastrointestinal tract, faeces and serum of mice treated with crude extract (0.5 mg/g), 6-bromoisatin (0.05 mg/g) and control groups. Multiple brominated metabolites can be detected in the digesta and faeces using SALDI-MSI techniques and tissue metabolite differences can be effectively isolated using probabilistic latent semantic analysis (PLSA). This demonstrates the possibility of transferring MSI methods developed to detect marine invertebrate natural products *in situ* to the analysis of the same bioactive molecules in animal models for drug development (Appendix 6).

## 6.6 Conclusion

New analytical and preparative tools are increasingly becoming an integral component of successful research in the field of chemical ecology and natural product research. Both fields of study strive to gain greater insights into secondary metabolites and their function with ever decreasing sample sizes, a challenge that can be met with mass spectrometry methods. The most promising results from this study of muricid secondary metabolites originating in the hypobranchial gland have come from an analysis of the *in situ* distribution, to examine ecological roles, as well as guide supercritical fluid preparative methods for future nutraceutical research. The significance of the choline esters to *D. orbita*, putatively suggested to aid in predation, embryo encapsulation and promote larval development, could certainly be seen to influence the success of this widely distributed species. The intrinsic link between the choline esters and the brominated indoles provides evidence for a chemical ripening process that ensures larval success in *D. orbita*, and may extend to other members of the Muricidae. Future studies of this unique secondary metabolite combination could confirm choline esters and brominated indoles as molecules of ‘keystone significance’.

## 7 Appendix I

### 7.1 Computational binding model of murexine to the ligand-binding domain of acetylcholine-binding protein (AChBP): A model for the nicotinic acetylcholine receptor (nAChR).

The pharmacological actions of murexine *in vivo* provides support for murexine binding to the muscle type nAChR, having a similar pharmacological action to suxamethonium (Erspamer and Glasser, 1957; Roseghini et al., 1996), a known partial agonist of the  $\alpha$ -subunit nAChR. A structure and function homology model of the binding site of the  $\alpha$ -subunit nAChR was used to determine murexine binding potential, using the molluscan AChBP from pond snail *Lymnaea stagnalis* (PDB: 1I9B; Brejc et al., 2001).

#### 7.1.1 *In silico* docking methods of murexine in AChBP

The AChBP crystal structure was downloaded from the Protein Data Bank (<http://www.rcsb.org/pdb/>) through the Chimera Interface (PDB: 1I9B), Figure A1.1. Flexible structures of the murexine ligand were docked into the AChBP using AutoDock 4.2, using grid based sphere generation of the receptor pocket space from the co-crystallized HEPES buffer with the AChBP. Up to 500 conforming poses were run and the top 50 poses for each of the five binding sites were scored based on grid score, a combination of van der Waals interactions and electrostatic components. Ligand orientation was assessed based on visual inspection of the top 50 scoring orientations and compared to HEPES bound AChBP and a

computational binding of acetylcholine into the AChBP. Molecular graphics and visualizing docked models was achieved with the UCSF Chimera package.

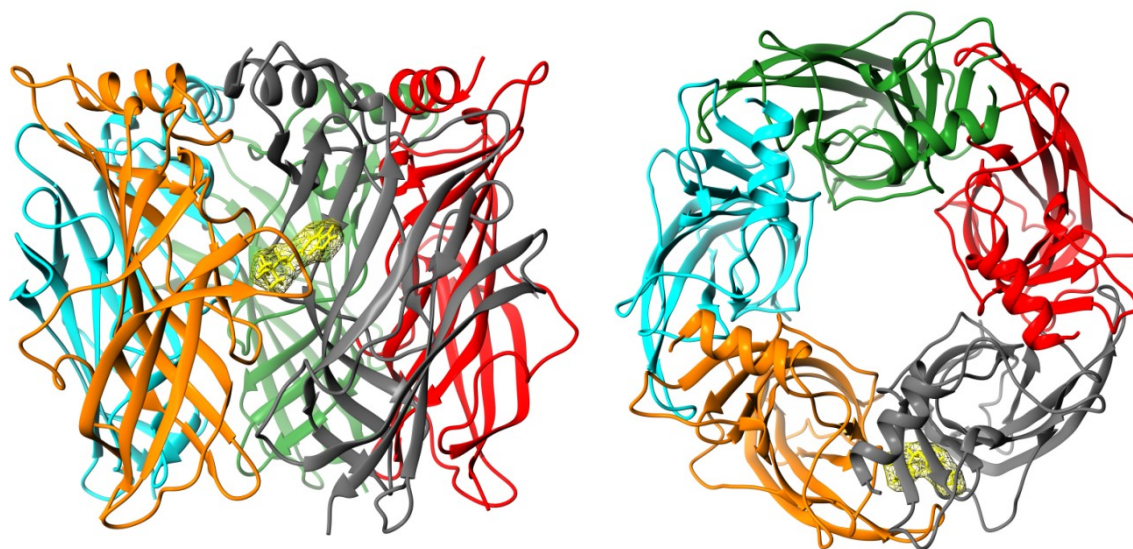


**Figure A1.1** The pentameric AChBP from *Lymnaea stagnalis* (Brejc et al., 2001; PDB: 1I9B). Left - lateral view of the structure representation with each subunit a different colour and murexine positioned in the receptor binding site between the interfaces of two subunits. Right – top view of the structure representation demonstrating the receptor pore.

### 7.1.2 *In silico* results of flexible murexine docking

Docked murexine showed no clashes with the receptor pocket space created by the co-crystallisation of HEPES buffer (Brejc et al., 2001) (Figure A1.2). The cysteine loop on the nAChR is believed to be flexible in regard to ligand binding (Brejc et al., 2001), allowing larger ligands to bind to nAChR, e.g. conotoxins. Multiple residues around the binding pocket contribute to binding affinity (Figures A1.3 and A1.4). The two main orientations of docked murexine based on the top 50 scoring conformations are shown in Figure A1.5, with hydrophobicity surface

rendering. The conformational scoring for grid based docking when compared to the native ligand, acetylcholine, shows better scoring values compared to acetylcholine. Typically scores less than -32 are considered good candidates for binding free energy calculations and murexine meets this prerequisite, Table A1.1. As the AChBP was co-crystalised with HEPES buffer, the highest scoring redocking conformation, the cysteine loop is in a relatively compact state. The cysteine loop has the ability to flex away from the binding site to allow larger peptides to activate the nAChR, e.g. conotoxins (Teichert et al., 2005), allowing the binding pocket space to change. Unusually, acetylcholine scored lower than the choline esters, this may be a consequence of the influence of water molecules on binding affinity or the use of a simplistic grid based model that doesn't fully account for all non-covalent interactions. The usefulness of this model is not necessarily to compare and calculate free binding energy or activation of the receptor, which requires co-crystalisation of purified murexine into an *in vitro* model, but gives an indication of whether the choline esters fit the size requirements of the receptor binding pocket space and supports the biological evidence (Roseghini et al., 1996) that these small choline esters could be targeting the nAChR.

**Table A1.1** Conformational and binding scores for the grid based

<b>Ligand (conformation pose ranking)</b>	<b>Conformational grid scoring</b>			<b>Internal energy</b>
	<b>Grid score</b>	<b>Grid van der Waals</b>	<b>grid electrostatic</b>	
HEPES buffer				
1	-41.00	-29.18	-11.82	0.16
2	-36.88	-25.37	-11.51	0.16
Acetylcholine				
1	-18.74	-12.87	-5.87	2.77
2	-17.99	-12.37	-5.62	2.57
Tigloylcholine				
1	-26.47	-20.68	-5.8	4.85
2	-26.33	-19.59	-6.74	4.9
Dihydromurexine				
1	-28.47	-23.04	-5.43	1.99
2	-24.34	-17.96	-6.38	1.79
Murexine				
1	-32.3	-24.97	-7.33	5.52
2	-30.23	-22.52	-7.71	2.88

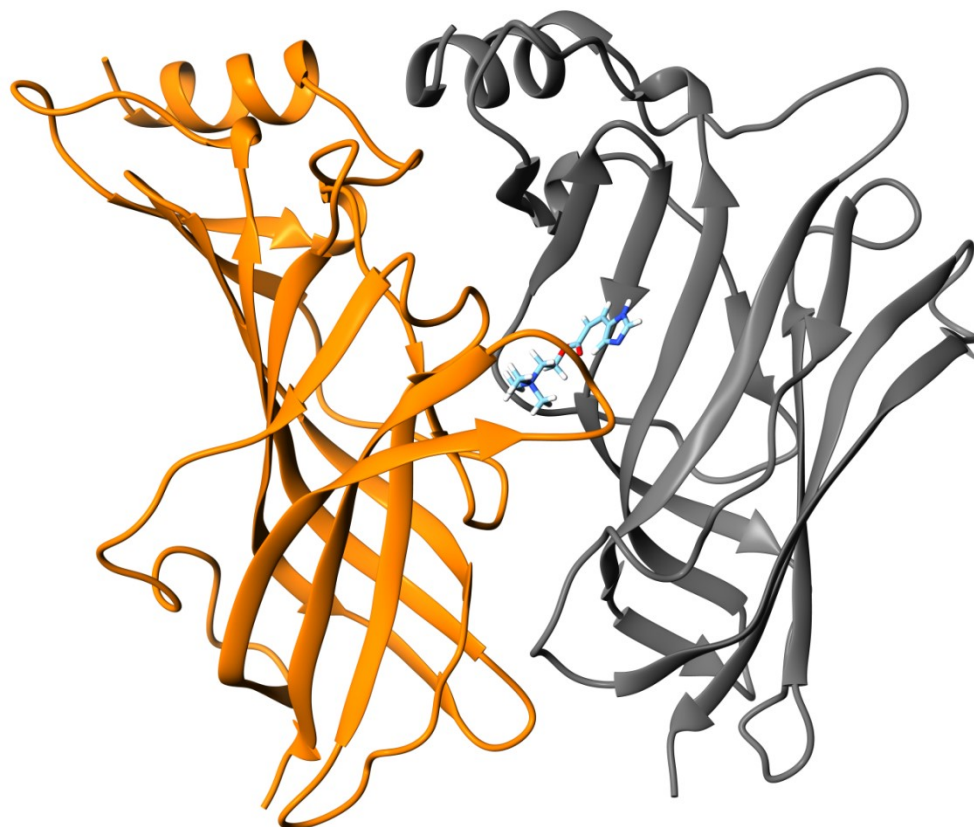


**Figure A1.2** The highest scoring docking conformation for murexine in the receptor binding site between two subunits.

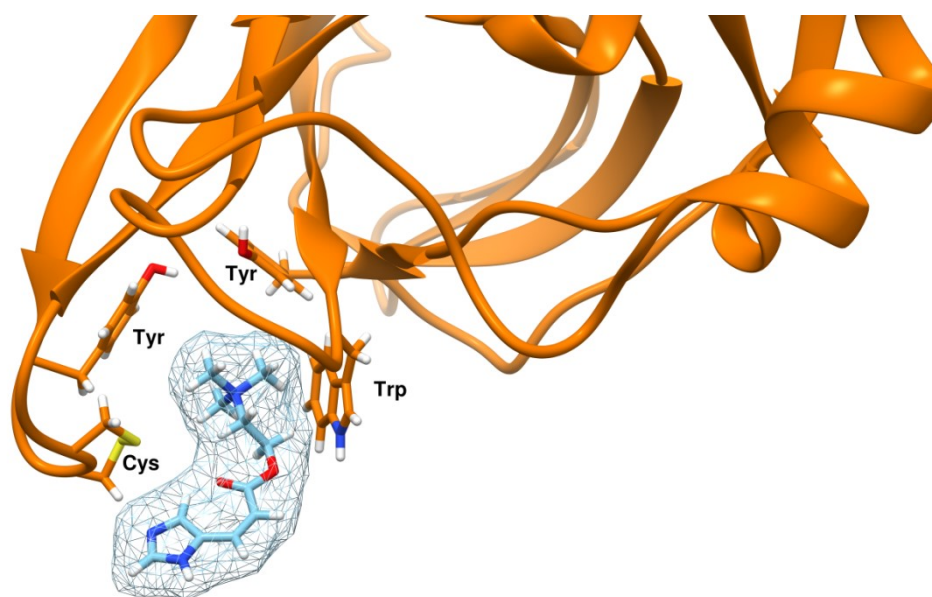


**Figure A1.3** Bound murexine with surface mesh rendering showing residues likely to be contributing to ligand binding on the cysteine loop interface of the subunit. Amino acids are indicated.

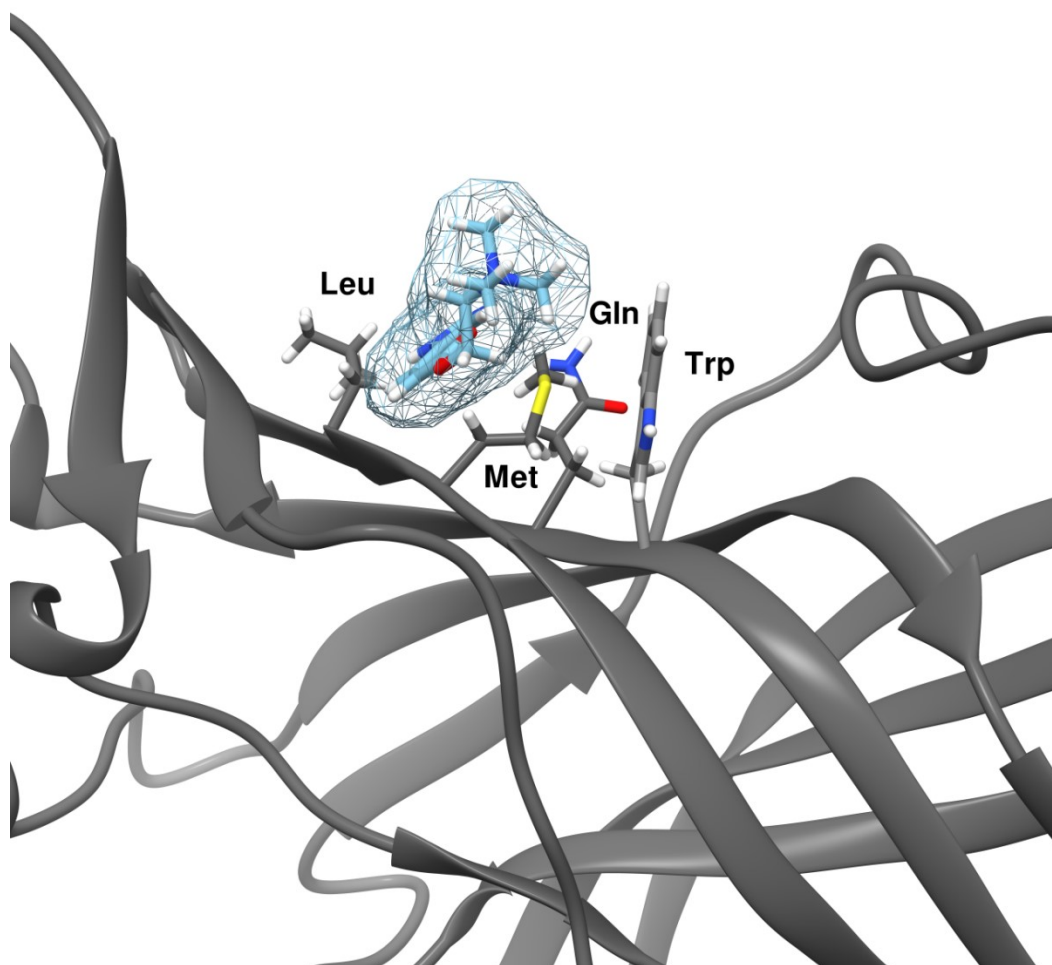


**Figure A1.4** Bound murexine with surface mesh rendering showing residues likely to be contributing to ligand binding on the opposing interface to Figure A3. Amino acids are indicated.

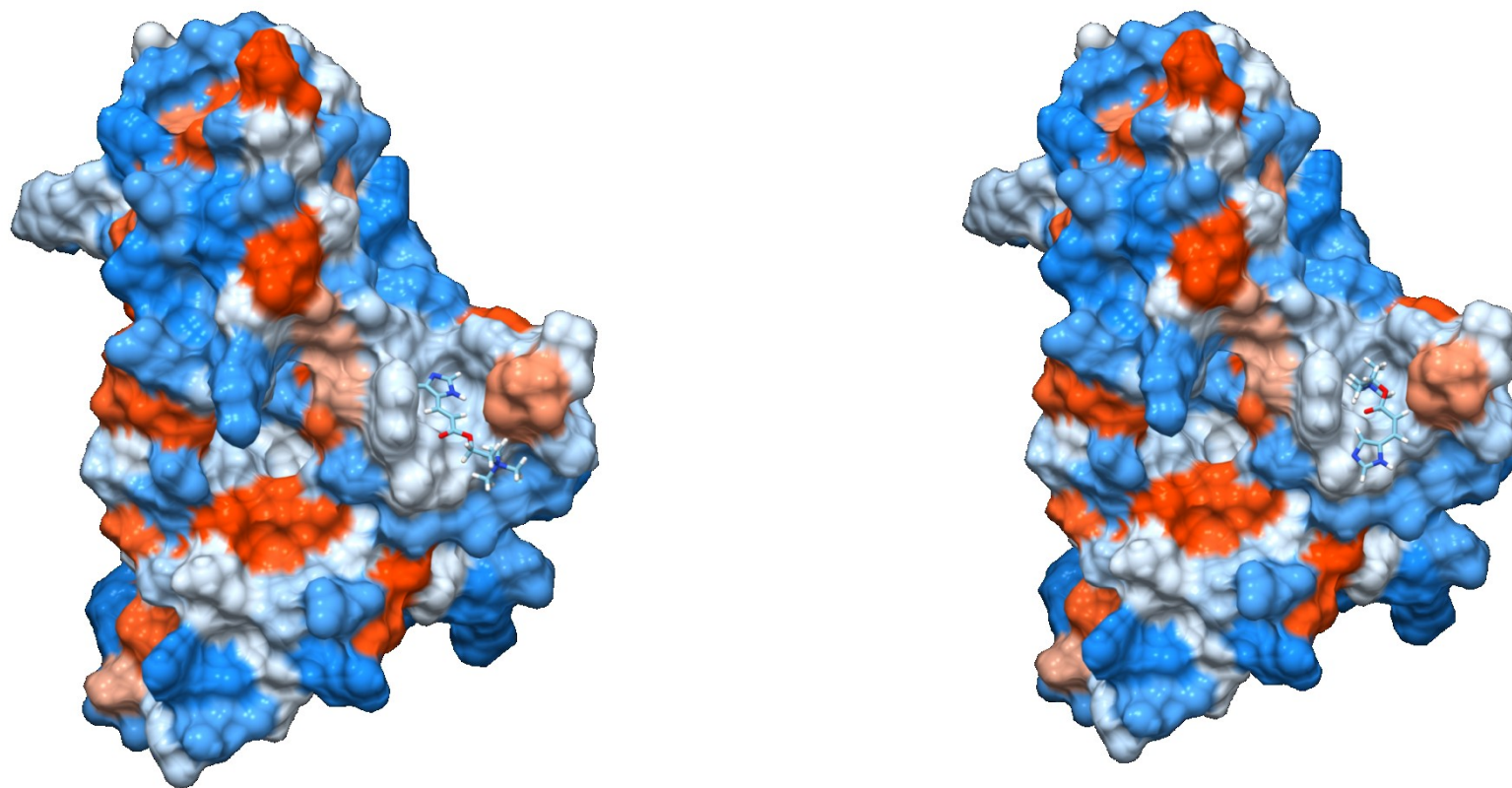


**Figure A1.5** The two main docking orientations of murexine in the hydrophobicity surface rendered AChBP subunits based on visual inspection from the top 50 scoring conformational poses.

## 8 Appendix II

### 8.1 Supplementary results for Chapter 4

As ion peak intensity changes across the tissue region over time, heatmaps for hypobranchial tissue sections are provided as reference for colour intensity maps shown in the results section of Chapter 4. Supplementary results also include structural validation of the ions detected using DIOS-MS, as this is a novel method for detecting brominated indoles and choline esters over time in hypobranchial tissue, capsule gland and egg capsules.

#### 8.1.1 Detection of brominated indoles

##### 8.1.1.1 LC-MS of brominated indoles

The main brominated indole extracted in the methanol fraction from the hypobranchial gland was the ultimate precursor compound tyrindoxyl sulfate eluting at 6.59 min (major ions duplet peak  $m/z$  336, 338; Figure A2.1 and A2.2) and tyrindoleninone eluting at 10.96 min (major ion duplet peak  $m/z$  256, 258; Figure A2.1 and A2.2). The remaining intermediate brominated indoles were extracted in the chloroform fraction from the hypobranchial gland including: tyriverdin eluting at 11.67 min (major ion triplet peak centered  $m/z$  419 and 465; Figure A2.1 and A2.2) and 6-bromoisatin eluting at 6.35 min (major ion duplet peak  $m/z$  224, 226; Figure A2.1 and A2.2). Tyrian purple 6'6-dibromoindigo, the final brominated indole product, was detected in the chloroform fraction from the hypobranchial gland eluting at 14.34 min (major ion triplet peak  $m/z$  419; Figure A2.1 and A2.2). Spectra for ESI-MS were run in negative mode causing a slight mass shift compared to DIOS-MS.

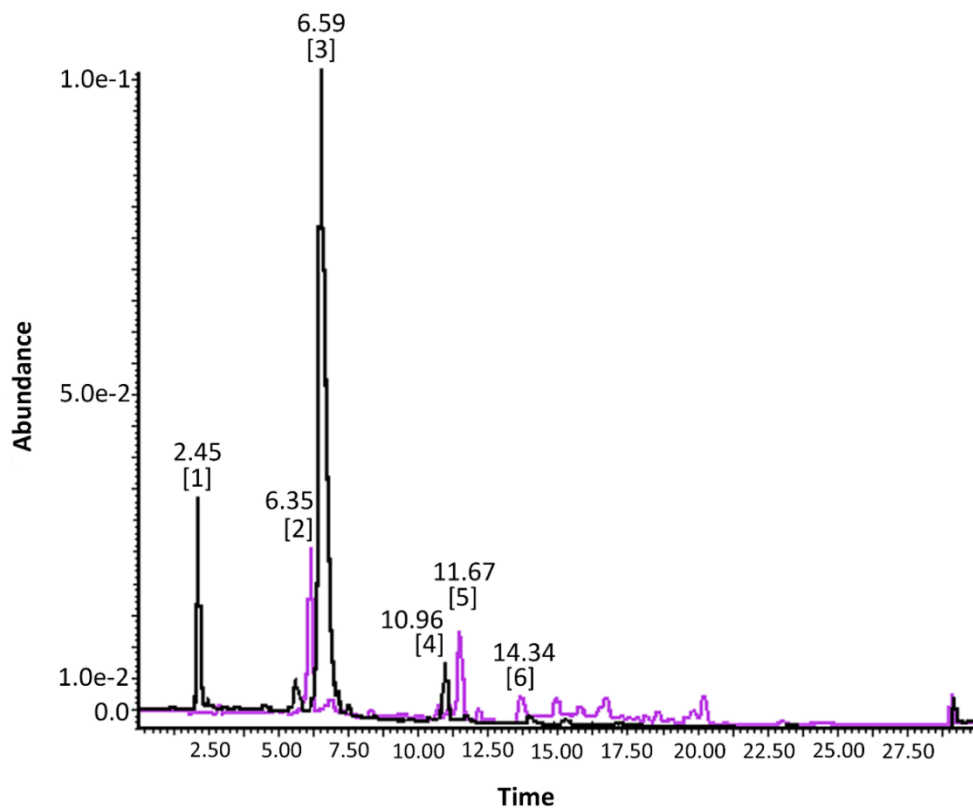


**Figure A2.1.** LC-MS trace of brominated indoles from *Dicathais orbita*. (Black line) methanol fraction containing: [1] murexine eluting at 2.45 min, [2] tyrindoxyl sulfate eluting at 6.59 min and [4] tyrindoleninone eluting at 10.96 min. (Purple line) chloroform fraction containing [2] 6-bromoisatin eluting at 6.35 min, [5] tyriverdin eluting at 11.67 min and [6] 6'6-dibromoindigo (Tyrian purple) eluting at 14.34 mins.

### 8.1.1.2 DIOS-MS and imaging of brominated indoles

Tyrindoxyl sulfate, tyrindoleninone and 6'6-dibromoindigo (or the isomer 6'6-dibromoindirubin) were all detected in DIOS-MS based on the ion clusters for the mono and di-brominated structures from both semi-purified fractions (Figure A2.2) and from tissue sections (Figure A2.3). Tyrian purple 6'6-dibromoindigo showed the most consistent pattern for localisation in the hypobranchial gland and comparison of spectra showed a consistent triplet peak structure at  $m/z$  419.88, 421.88 and 423.88 for  $\text{Br}^{79} \text{Br}^{79}$ ,  $\text{Br}^{79} \text{Br}^{81}$  and  $\text{Br}^{81} \text{Br}^{81}$  (Figure A2.2). Tyrindoxyl hydrogen sulfate was detected consistently within the hypobranchial gland of the encapsulating female and post-reproductive female and two of the three pre-reproductive females (Figure A2.3). Tyrindoleninone was detected in the pre-reproductive females localised in the medial hypobranchial gland of the encapsulating and post-reproductive females (Figure A2.3). Peak intensity heatmaps are provided as a supplementary concentration reference for Chapter 4 results (Figure A2.3)

Egg capsule contents showed a slow chemical ripening process consistent with the enzymatic, oxidative and photolytic reaction seen in the medial hypobranchial gland (Fig. 5 and S7), but extended over the 35 day intracapsular period, rather than the few hours required after liberation from the adult hypobranchial secretory tissue. Peak intensity heatmaps for capsule contents are provided as a supplementary concentration reference for Chapter 4 results (Figure A2.4).

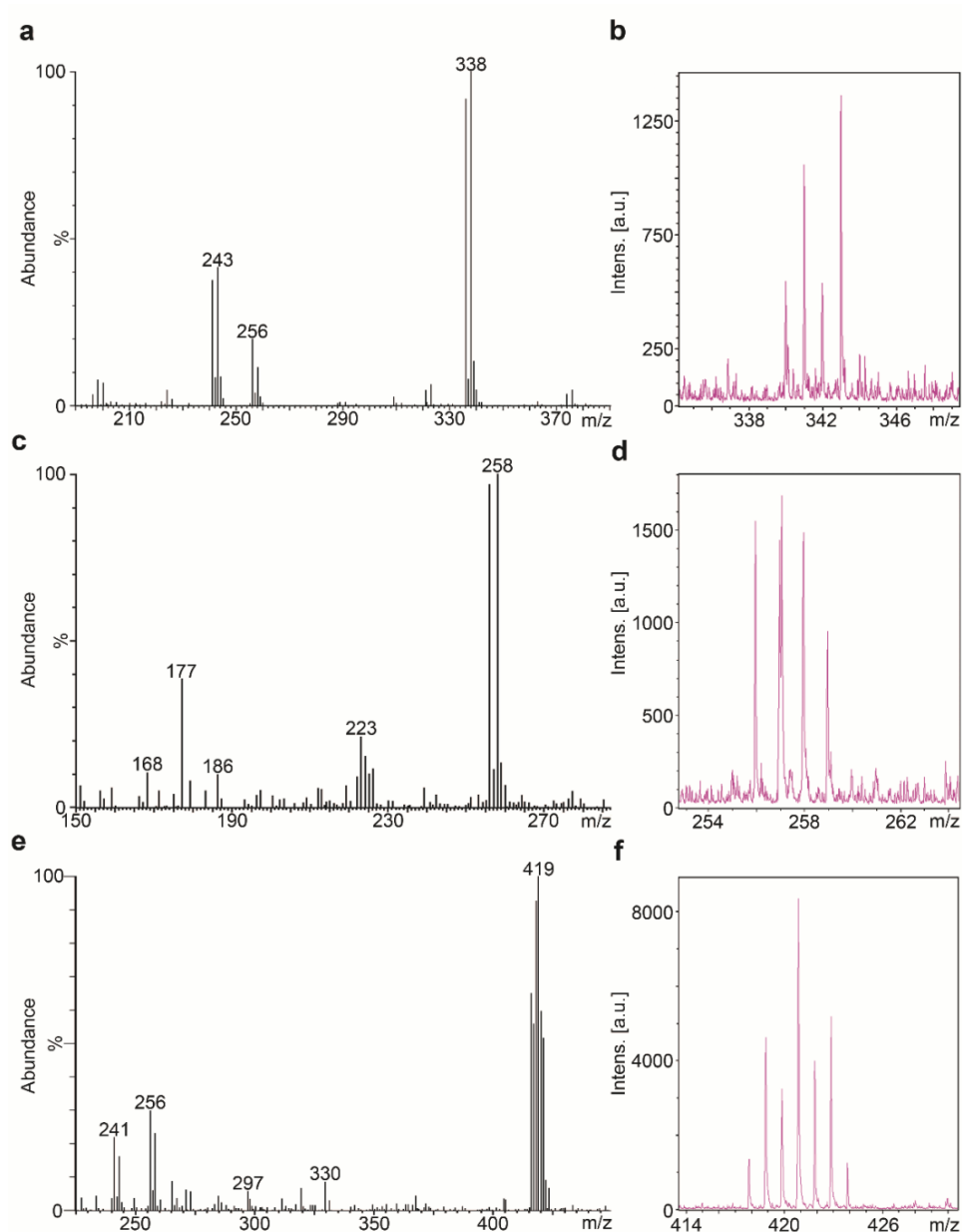


**Figure A2.2.** MS-MS spectra for brominated indoles detected from hypobranchial gland extracts of *Dicathais orbita* by LC-MS (in negative mode) and representative DIOS-MS (see Chapter 4, Figure 4.3 and Table 4.1; in positive mode); (a) MS-MS spectrum for precursor compound tyrindoxyl sulfate, (b) corresponding DIOS mass spectrum of tyrindoxyl hydrogen sulfate [ $m/z$  339.98, 340.99, 341.98, 342.98  $\pm$  0.05  $[M+H]^+$ ], (c) MS-MS spectrum for intermediate tyrindoleninone, (d) corresponding DIOS mass spectrum of tyrindoleninone [ $m/z$  255.95, 256.94, 257.94, 258.95  $\pm$  0.05  $[M]^+$ ], (e) MS-MS spectrum for Tyrian purple 6,6'-dibromoindigo, (f) corresponding spectrum in DIOS-MS of 6,6'-dibromoindigo [ $m/z$  419.88, 421.88, 423.88,  $\pm$  0.05  $[M+2H]^+$ ]

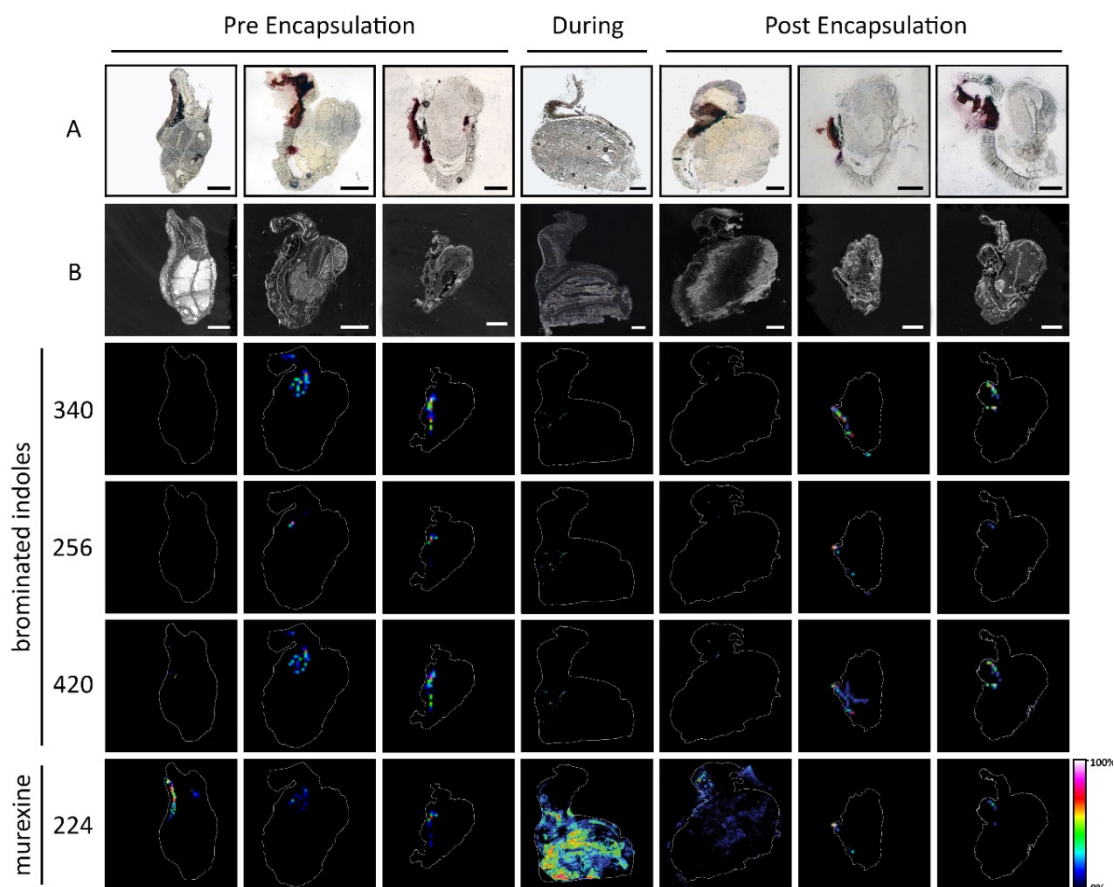


**Figure A2.3** DIOS-MSI of reproductively active female *Dicathais orbita*. 15 $\mu$ m thick cryo-sections of the central hypobranchial gland with attached capsule gland were imaged. Pre Encapsulation) female sections sampled 30 days prior to the start of the standard breeding season. During) a female section sampled during egg encapsulation. Post Encapsulation) female sections sampled 14 days post egg encapsulation. A) serial histological sections, where (hg) indicates the medial hypobranchial gland and (cg) indicates the capsule gland. B) scanned images of gland tissue cryo-section on pSi chip.  $m/z$  340 is tyrindoxyl hydrogen sulfate  $[M+H]^+$ .  $m/z$  256 is tyrindoleninone  $[M+H]^+$ .  $m/z$  420 is Tyrian purple (6'6-dibromoindigo)  $[M+H]^+$ .  $m/z$  224 is murexine  $[M]^+$ . Scale bar set to 2 mm. Intensities of ions in the imaged sections are color coded using a heat map.

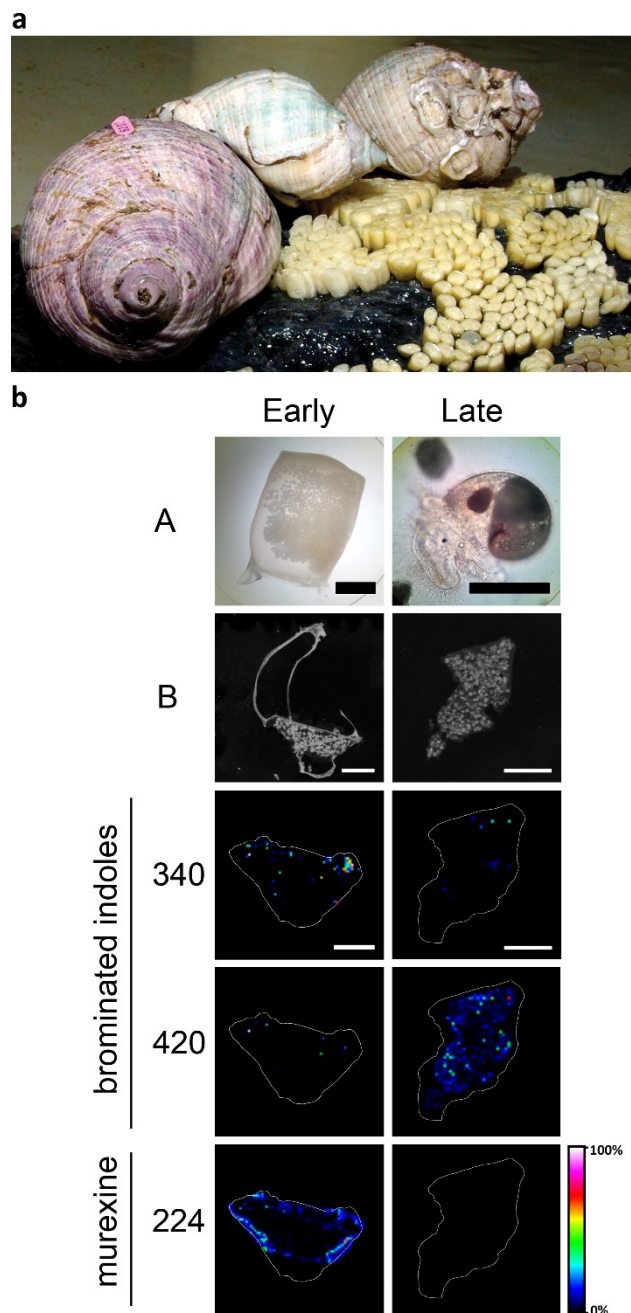


**Figure A2.4** *Dicathais orbita* reproductive adults and early stage egg capsules with DIOS-MS of capsule contents. (a) Reproductive adults during the encapsulation of larvae and early stage capsules adhered to substrate. (b) DIOS-MSI of an early stage capsule sampled immediately post deposition and late stage capsule, 35 days post deposition. A is a microphotograph of the entire capsule and late stage larvae. B is a scanned image of the cryo-section capsules imprinted onto pSi chip.  $m/z$  340 is tyrindoxyl hydrogen sulfate  $[M+H]^+$ .  $m/z$  420 is Tyrian purple (6'6-dibromoindigo)  $[M+H]^+$ .  $m/z$  224 is murexine  $[M]^+$ . Scale bar set to 1mm. Intensity of ions detected in egg capsule contents are colour coded using a heat map.

## **8.1.2 Detection and structural elucidation of murexine**

### **8.1.2.1 LC-MS**

The major compound eluting at 1.83 min provided a molecular ion [M]<sup>+</sup> peak in positive mode at 224.1 m/z (Figure A2.5), consistent with the presence of murexine (C<sub>11</sub>H<sub>18</sub>N<sub>3</sub>O<sub>2</sub><sup>+</sup>; 224.284 MW). When subjected to a higher cone voltage to induce fragmentation, in ESI (35V), the eluting compound showed a fragment at 165 m/z which is the same loss of 59 that is observed in acetylcholine (see Chapter 4 results and Figure A2.5, A2.6). Early intracapsular fluid contained murexine (Figure A2.4), which was absent in the late stage capsules.

### **8.1.2.2 DIOS-MSI for murexine in the capsule gland of a reproductively active female**

Murexine was distributed predominantly in the capsule gland of the reproductive female which had a much higher comparative intensity to the hypobranchial distribution (Figure A2.7).

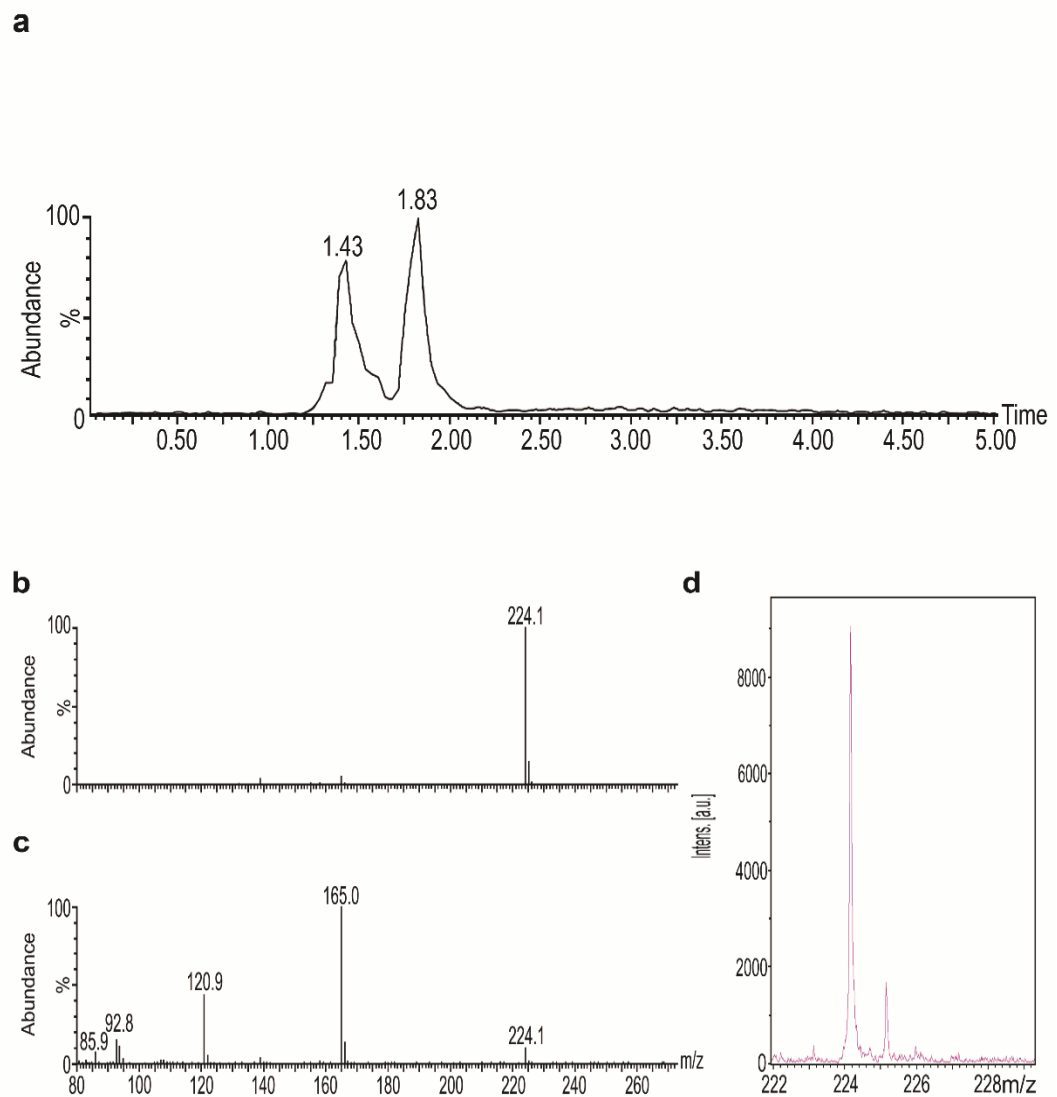


**Figure A2.5** LC-MS of the capsule gland extract from a reproductively active female *Dicathais orbita*, containing (a) murexine eluting at 1.83 min in the liquid chromatograph; (b) MS-MS spectra of murexine; (c) collision induced dissociation of murexine with  $m/z$  165 representing  $N^+(CH_3)_3$  loss of 59 and (d) representative DIOS mass spectra of murexine [ $m/z$   $224.17 \pm 0.02$   $[M]^+$ ].

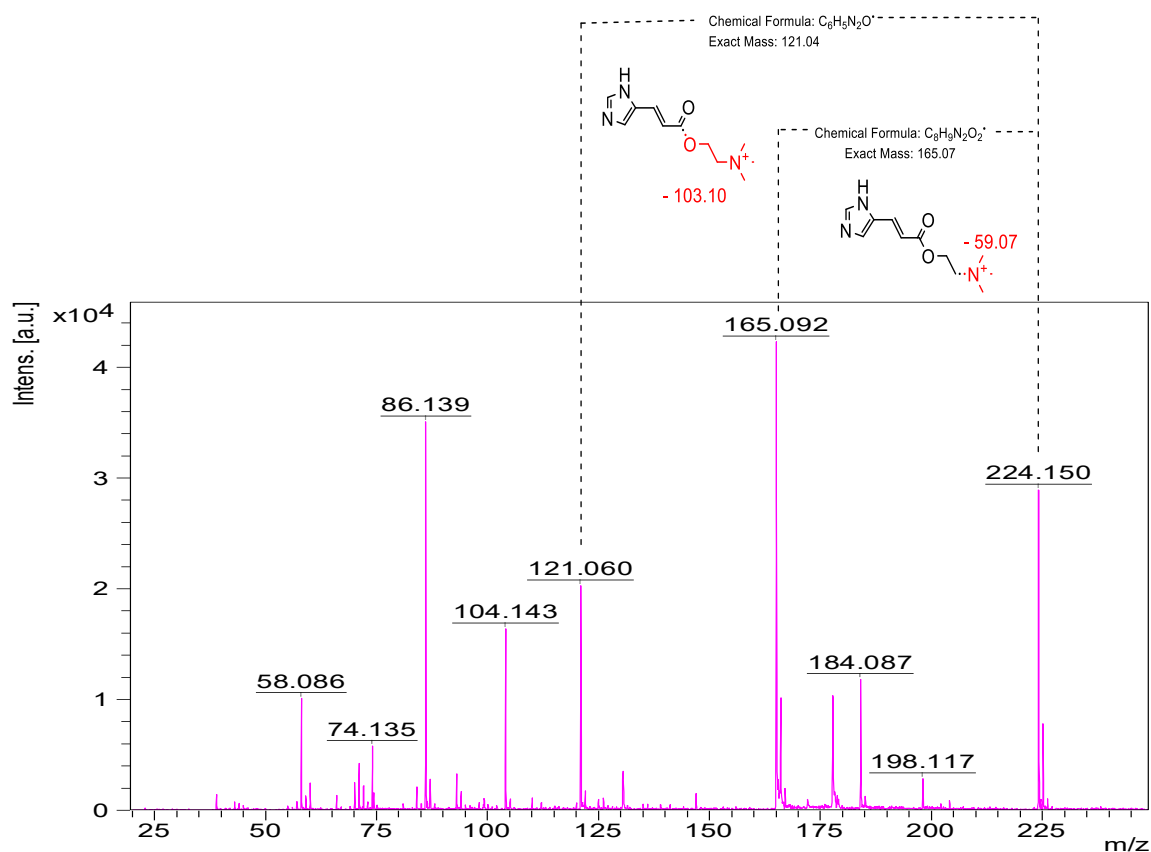


**Figure A2.6.** Murexine structural fragmentation seen in DIOS-MS mass spectrum from reproductively active *Dicathais orbita* female capsule gland. The same extract was used for  $^1\text{H-NMR}$  (see Chapter 4, Table 4.2)

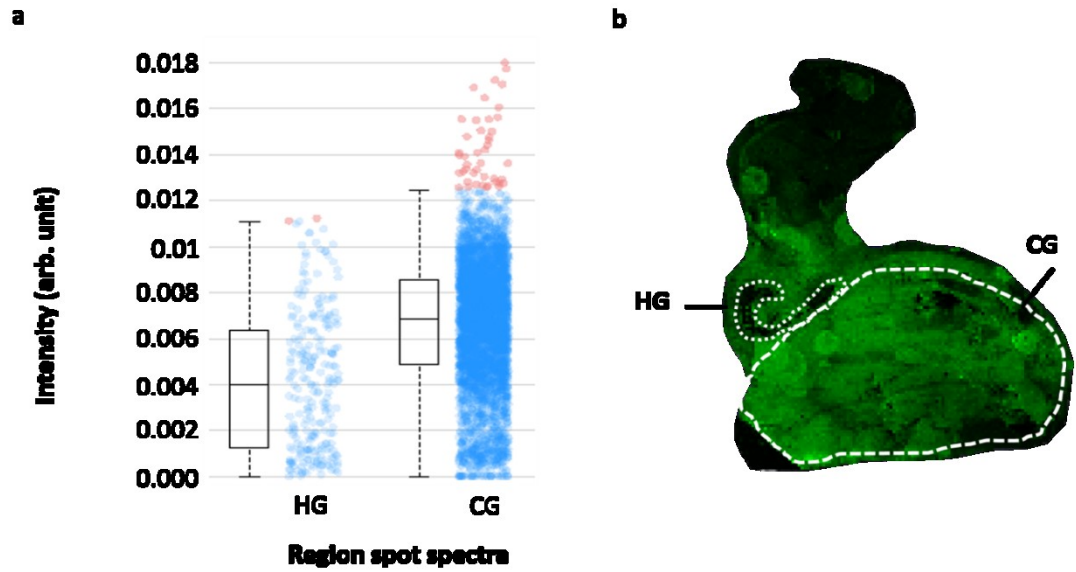
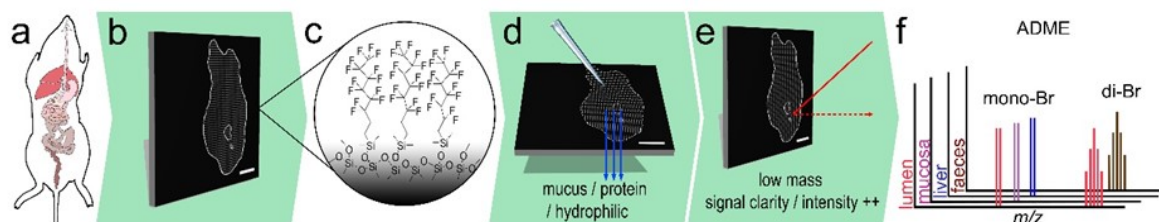


**Figure A2.7** Region specific ion intensities for murexine  $m/z$  224.16, where: a) each dot represents a spot in the tissue section plotted against intensity value for the hypobranchial gland (HG) and the capsule gland (CG) with quartile distribution shown with associated box plots. Blue dots represent intensity spots that lie within the normal distribution and red spots represent outlier intensity spots. The corresponding female  $m/z$  224.16 distribution detected in DIOS-MSI is shown in b) with specific regions indicated.

## 9 Appendix III

### Mass spectrometry imaging the absorption, distribution, metabolism and excretion of a halogenated marine natural indole



Chapter 6 highlights the potential advantages of DIOS-MSI as an imaging platform for tracking the gastrointestinal absorption of muricid extract and synthetic 6-bromoisatin from a 14 week early stage colorectal cancer (CRC) model. The acute apoptotic response to genotoxic carcinogens (AARGC) is effective at determining chemo-preventative qualities of administered compounds. Preliminary analysis of the highest concentration groups of crude extract (0.5 mg/g) and synthetic 6-bromoisatin (0.05 mg/g) compared to controls from the 14 week model tissue show effective detection of brominated indoles from the crude extract group and possible metabolites from the 6-bromoisatin group.

### 9.1 Introduction

The ability of mass spectrometry imaging to spatially discriminate a drug from its metabolites against the background of endogenous compounds has seen it emerge as a revolutionary technology in pharmaceutical research (Schwamborn and Caprioli, 2010, Caprioli et al., 1997, Patti et al., 2010). Limitations of detecting the low mass range in the traditional approach (Svatos, 2010), matrix assisted laser desorption ionization-MSI (MALDI-MSI) (Svatos, 2010, Ronci et al., 2012), has

seen the emergence of nanostructure imaging mass spectrometry (NIMS), a matrix free alternative (Greving et al., 2010). NIMS eliminates chemical noise in the low mass range (>500 Da) where matrix ions often obscure drugs and metabolites. NIM-MSI is able to be applied in a selective manner to reduce the complex chemical background of mammalian tissue (Yanes et al., 2009), imaging imprints of metabolites as opposed to direct tissue imaging (Ronci et al., 2012, Greving et al., 2010). Fast effective determination of drug metabolites, under reduced spectral noise, is especially valuable in early screenings of drug leads, where both financial and animal costs are influencing factors in advancing interesting compounds. NIMS can be easily integrated into *in vivo* efficacy models to extract the maximum pharmacokinetic profile, providing a ‘road-map’ for further progression of lead candidates. Electrochemically etched, perfluorinated porous silicon substrates (pSi) are the nanostructured surfaces utilised in the highly effective NIMS platform, desorption/ionization on pSi (DIOS), and when combined with imaging termed, DIOS-MSI. Selective choice of surface functionalities allow a “tunable” surface to be created. This tuneable platform allows retainment of particular classes of compounds and when combined with the high surface area (>600 m<sup>2</sup>/g) and UV absorptivity of pSi, DIOS-MSI can be a highly effective approach for finding drug metabolites, even for structural classes that lack background or *in silico* supporting data.

One such structural group where drug absorption, distribution, metabolism and excretion (ADME) is not easily predicted is the indole derivatives. Indole as a structural nucleus is widely distributed throughout many mammalian biochemical systems (Yong-Jin Wu, 2010), being a precursor of tryptophan, from which protein and the cascade of substituted tryptamines are biosynthesized (Frazer and Hensler, 1999). The effect of indole based endogenous metabolites is substantial, serotonin

for instance is implicated in practically every type of behaviour including appetitive, emotional, motor, cognitive and autonomic (Frazer and Hensler, 1999, Richard et al., 2009). The ubiquitous presence of indole based metabolites is one of the reasons that indole alkaloids feature heavily in emerging drug reviews (Yong-Jin Wu, 2010), many targeting the 5-HT receptor (Yong-Jin Wu, 2010, Kochanowska-Karamyan and Hamann, 2010). Apart from neuroendocrine functions, many naturally derived indole alkaloid drugs or secondary metabolites are used or recommended in the treatment and prevention of cancer. The application of small indole alkaloids range from treating advanced cancers, for example the use of sunitinib to treat gastrointestinal stromal tumours (Demetri et al.), to chemo-preventative metabolites found in cruciferous vegetable, including indole-3-carbinol (Higdon et al., 2007). Predicating the bioactivity of indole based structures is difficult, dimerization and cyclization of monomeric indole bases creates complexity when administered in *in vivo* animal models. Indole-3-carbinol undergoes acid condensation to generate over 17 different metabolites, not all sharing the same bioactive function (Aggarwal and Ichikawa, 2005). Indole dimeric structures, including bisindole alkaloids, also include a suite of highly bioactive compounds, including the antineoplastic vinca alkaloids (Levêque and Jehl, 2007) and low bioavailable monomeric structures when administered can act as prodrugs after first pass metabolism (Rodrigues et al., 2008). Considering the varied targets and biological effects of small indole based metabolites and structures, and resulting cyclization in the gastrointestinal environment, predicting the pharmacokinetic fate of administered indole based drugs is far from straight forward.

The elaboration of indole features heavily in the marine environment, where predominantly invertebrates biosynthesize small indole and bisindole alkaloids,

terpenes and a range of structures with indole functional moieties that possess potent biological activity (Pauletti et al., 2010b, Franca et al., 2014, Kochanowska-Karamyan and Hamann, 2010, Gul and Hamann, 2005). Marine secondary metabolites of this nature are considered promising drug discovery leads (Faulkner, Gerwick and Moore, 2012), with numerous compounds under assessment for efficacy in clinical trials (Mayer et al., 2015, Kaushik et al., 2013). In addition to the elaboration of indole structures during biosynthesis, another modification typically encountered from the marine environment is halogenation, most commonly bromination (Pauletti et al., 2010a). Halogenation is also a common tactic used in medicinal chemistry, generally added to lead compounds, to improve steric effects and enhance stability and binding affinity (Marcelo Zaldini et al., 2010). Halogenation has been used to increase lipid solubility, an advantage when there is a desired for better absorption or for the drug to cross the blood brain barrier (Gentry et al., 1999).

Recent work on a group of brominated indoles originating in Muricidae molluscs (Benkendorff et al., 2015) has resulted in a promising chemo-preventative compound, 6-bromoisatin (Esmacelian et al., 2014). No work has been undertaken on the ADME properties of 6-bromoisatin or the crude hypobranchial extract from which it originates. Here we combine the attributes of DIOS-MSI and the characteristic spectral patterns obtained when analysing mono- and di-brominated structures in MS. The combination of the two properties can track the ADME of 6-bromoisatin and its crude extract origin, which can be integrated into an established colorectal chemo-preventative murine model, the acute apoptotic response to genotoxic carcinogen (AARGC).

## 9.2 Methods

### 9.2.1 Materials

All solvents used were chromatography grade. Methanol, hydrofluoric acid (HF, 48%; see (Ronci et al., 2012) for safe handling protocols), and chloroform were obtained from Merck (VIC, Australia). Ethanol was purchased from Chem Supply (SA, Australia). (Pentafluorophenyl)-dimethylchlorosilane (F5PhPr) was purchased from Gelest Inc. (Morrisville, PA, USA). 6-bromoisatin was synthesized by Tokyo Chemical Industry (Tokyo, Japan), the structure and purity having been previously validated (Esmaelian et al., 2014).

### 9.2.2 *In vivo* murine model

Male C57BL/6 mice at 10 weeks of age were purchased from the Animal Research Centre (Perth, Australia). During experimental conditions mice were kept in groups of four per cage, given food (rodent chow) and water *ad libitum*, and maintained at  $22 \pm 2^\circ\text{C}$  on a 12 hour light / dark cycle. To assess the effects of 6-bromoisatin on general health parameters mice were weighed weekly, or daily if showing signs of weight loss, and monitored daily for signs of ill health. Based on the apoptotic index values from a previous short term *in vivo* colorectal cancer model (Esmaelian et al., 2014) a minimum sample size of  $n=8$  would be required to achieved a power value of 0.99 (*post hoc* analysis where the s.d. was 25% of the group mean and an  $\alpha$  error probability of 0.05). As AOM has a significant impact on the liver (Matkowskyj et al., 1999), mice showing a continual weight loss of more than (10%), continual signs of ill health or significant deviations from expected ethics parameters (3 continuous days), were eliminated from the study. All animal work was conducted according to the Australian Code of Practice for

the Care and Use of Animals for Scientific Purposes under the Flinders University Animal Ethic Committee approval notice 751-10.

The experimental design was based on an established AARGC model for the early stage prevention of colorectal cancer (CRC) (Hu et al., 2005), which has previously been used in short term rodent studies with purified and synthetic 6-bromoisatin (Westley et al., 2010c, Esmaelian et al., 2014). As crude extract and 6-bromoisatin are made up of lipophilic compounds, mice were administered the desired concentration dissolved in 100  $\mu$ L of sunflower oil with 0.02% vitamin E via oral gavage, described in Figure A6.1. Mice were randomly assigned to an oil control group ( $n=11$ ), crude hypobranchial extract at 0.5 mg/g ( $n=11$ ), and 0.05 mg/g ( $n=11$ ), or synthetic 6-bromoisatin at 0.05 mg/g ( $n=8$ ), 0.025 mg/g ( $n=11$ ) and 0.01 mg/g bodyweight (BW;  $n=12$ ). Oral gavage of treatments or oil control was administered daily for 14 weeks and 4 hours prior to the mice being killed, Figure A6.1. Genotoxic damage was induced after an initial 2 weeks by six weekly intraperitoneal injections of azoxymethane (AOM) at a dosage of 10 mg/kg BW, followed by no injections 6 weeks prior to killing. Mice were killed using a single injection of ketamine (75 mg/kg BW) and xylazine (5 mg/kg BW), followed by cardiac bleed immediately prior to cervical dislocation. Blood was collected into sodium heparinised-EDTA vials (BD Microtainer®), sample coded and sent to a pathology clinic (Gribbles Pathology) to test blood biochemistry and haematology including . Mice were dissected immediately post kill, after which colons were collected to evaluate signs of early stage CRC formation (Esmaelian et al., 2014), whilst livers, stomachs and small intestines were frozen in liquid nitrogen for DIOS-MSI. Pooled urine was collected directly from the bladder for urinalysis and faeces were collected directly from the colon lumen for excretion data. Frozen tissue was stored at  $-80^{\circ}\text{C}$  till required for analysis.

### **9.2.3 AARGC evaluation**

The chemo-preventative model and evaluating the effects of crude hypobranchial and synthetic 6-bromoisatin was conducted as part of another PhD and Master project (Chahal, 2014, Esmacelian, 2014). The content of this chapter focuses on the tissue collection, sample preparation and development of the mass spectrometry imaging method and how the results align with the efficacy of both crude extracts and synthetic 6-bromoisatin *in vivo*.

#### **9.2.3.1 Tumour and aberrant crypt foci (ACF) count**

Colons were laid out on hybond C membrane (NL1011; GE Healthcare) by longitudinal incision and fixed in 10% formalin for 24 hours prior to being transferred to 70% ethanol. ACF and tumours were counted (double blind) after 0.2% methylene blue staining as described (Esmacelian, 2014).

#### **9.2.3.2 Apoptotic index and colon histological characteristics**

Distal colon segments were paraffin embedded, sectioned to 4-5  $\mu\text{m}$  thick and fixed on glass slides (3-4 sections). The sections were stained with haematoxylin to identify apoptotic cells in distal colon epithelia as described (Esmacelian et al., 2013a). The stained slides were mounted using DPX mounting solution, covered with a cover slip and viewed with a light microscope (Motic BA300). The apoptotic cells were identified based on a distinct dark blue stained large nucleus surrounded by unstained halo, condensed chromatin and cell shrinkage (Le Leu et al., 2003b). 10 random crypts per slide were counted in two halves each. The apoptotic index was calculated as the mean number of apoptotic cells per crypt divided by the total number of cells in the crypt and multiplied by 100 to give a percentage.

Paraffin embedded distal colon segments were sectioned at 4-5  $\mu\text{m}$  thin (3-4 sections) and fixed on Superfrost<sup>R</sup> Plus slides (Lomb Objekttrager 021913-9). Proliferative activity of the epithelial cells was determined by staining with an antibody specific for nuclear proliferating antigen Ki67 (Abcam) (Esmaeelian et al., 2013a). The staining protocol was tested with variable antigen retrieval methods and optimised at using 100 degree water bath for 40 minutes.

#### **9.2.4 Surface fabrication of pSi**

DIOS surfaces were fabricated using light assisted anodic etching of silicon wafers as described (Rudd et al., 2015a, Ronci et al., 2012) to create a hydroxyl-terminated surface. Etched pSi surfaces were subsequently functionalized using neat silane ( $\text{F}_5\text{PhPr}$ ) for 15 min at 90°C according to (Ronci et al., 2012).

#### **9.2.5 Tissue preparation and DIOS-MSI**

Stomach, duodenum, jejunum, ileum or liver were mounted onto frozen stubs using optimum cutting temperature compound (OCT; Tissue-Tek<sup>®</sup>) ensuring none contaminated the tissue section to be imaged. Gastrointestinal tissue was cryo-sectioned to 15  $\mu\text{m}$  thick at -20°C, whilst liver tissue was cryo-sectioned at -14°C (Leica 1800 Cryostat, Leica Microsystems). The fundus portion of stomachs were sectioned down until the frozen gut content was exposed to evaluate metabolism within the stomach as well as absorption into the mucosa. Small intestinal segments and livers were cryo-sectioned till a clean surface was created for effective serial sectioning. For each tissue sectioned used for DIOS-MSI a serial section was cut for haematoxylin and eosin staining (H and E). Sections for DIOS-MSI were thaw mounted onto the fabricated surface and place in a desiccator for 30 mins to allow surface imprinting followed by digital scanning (Epson V700). The residual tissue

was then removed from the pSi surface with a gentle stream of 25°C milli-Q water from a pipette prior to MSI. Sections for H and E were mounted onto polyethyleneimine (PEI) polymer coated slides (Vancha et al., 2004), allowed to air dry in a desiccator and stained using a standard protocol. To separate acid condensation products of 6-bromoisatin from xenobiotic metabolites, 0.1 mg/g, 0.05 mg/g and 0.01 mg/g (6-bromoisatin per mg control mice weight) was homogenised with control mouse stomach tissue, and heated at 37°C with 1mL of lysis buffer for 1 hour in microfuge tubes. The homogenised tissue was then frozen in liquid nitrogen, cryo-sectioned as previously described and imprinted on pSi.

### 9.2.6 DIOS-MSI analysis

DIOS-MSI analysis was performed on an ultrafleXtreme™ MALDI-TOF/TOF mass spectrometer (Bruker-Daltronics) equipped with a smartbeam-II™ 2kHz pulsed laser operating at 2000Hz repetition rate in reflectron positive and reflectron negative mode. Spectra were collected in the 20-1500 Da range at a spatial resolution of 60 µm, with laser attenuator set at 38 %. Laser diameter was set to medium, corresponding to 50 µm. An average of 500 laser shots were used at each sampling point. The imaging area was designated using Fleximaging 2.1 (build 25, Bruker-Daltronics) and mapped using Flexcontrol 3.3 (build 85, Bruker-Daltronic). External quadratic calibration was achieved using caesium iodide (CsI) mixed with 2-[(2E)-3-(4-tert-Butylphenyl)-2-methylprop-2-enylidene]malononitrile (DCTB) in a 1:1 ratio of 5 µl (10 mg/ml CsI) to 5 µl (10 mg/ml DCTB) (Guinan et al., 2015). Calibration was based on CsI adducts including: Cs 132.90490, CsI 392.71483, (Cs)<sub>2</sub> 652.52475, (Cs)<sub>3</sub> 912.33468, (Cs)<sub>4</sub> 1172.14460, and (Cs)<sub>5</sub> 1431.95453 *m/z*. Imaging was run in both positive and negative ionisation modes. Maps were generated using SCiLS Lab (version 2.02.5366, SCiLS GmbH, Bremen, Germany)

after baseline subtraction (TopHat), data reduction (resampled TIC preserving) and peak selection.

### **9.2.7 Statistical analysis**

Summed processed spectra, with reference to the serial H and E section, were run through probabilistic latent semantic analysis to establish likeness to tissue regions and define the ‘spectral environment mono and di-brominated signatures were detected in. Peak clusters that fit the typical mono and di-brominated spectral pattern were run through spatial correlation analysis to find co-localised brominated signatures. Spectral patterns of interest were referenced back to the homogenised control spiked with 0.1, 0.05, and 0.01 mg/g 6-bromoisatin.

### In vivo colorectal model

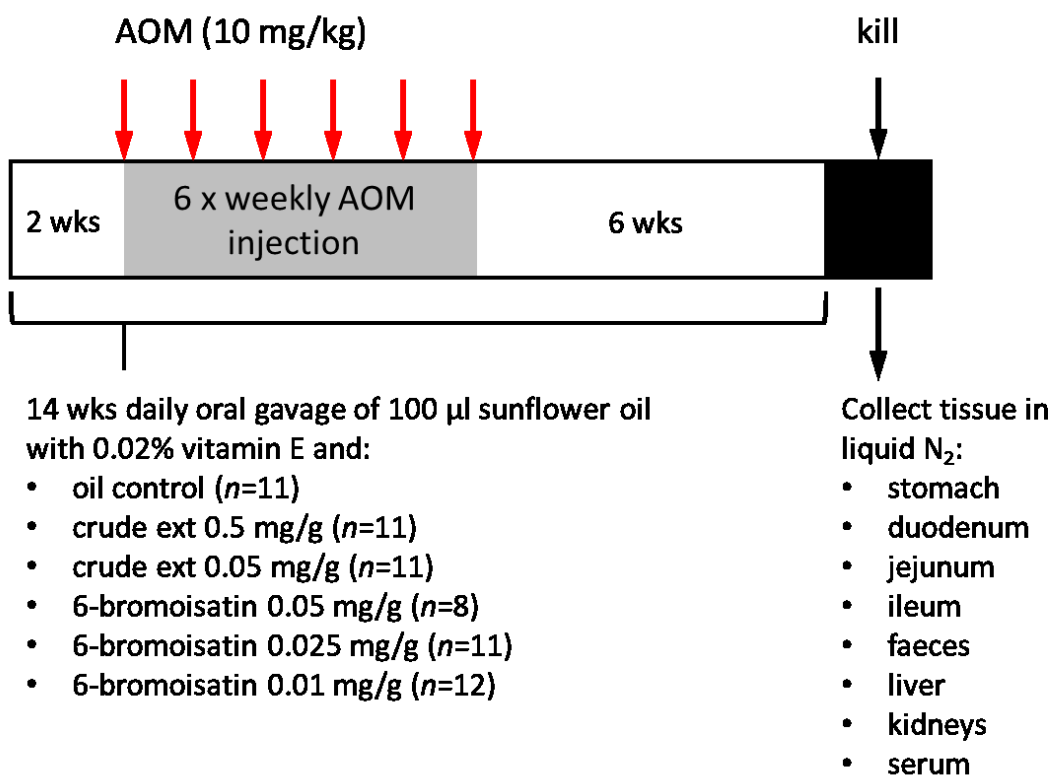


**Figure A9.1** Experimental design for AOM colorectal cancer model and tissue collection used for DIOS-MSI

## 9.3 Results

### 9.3.1 Brominated metabolite discovery in tissue sections

The advantages of DIOS-MSI, Figure A9.2a-g, above standard MALDI and traditional pharmacokinetic profiling (HPLC or some form of solvent extraction) is the clear characteristic spectral patterns associated with mono- and di-brominated structures in the low mass range (Ronci et al., 2012, Rudd et al., 2015b). These spectra provide a starting point to manually search for metabolites in the entire gastrointestinal tract, and enable the subsequent use of correlation analysis of selected  $m/z$  patterns for major peaks in the summed spectra to co-localise known or postulated metabolites. Using a threshold cut-off relevant to the expected

distribution (i.e. gut content only, 0.7 or mucosa, 0.85) we were able to find co-localized spectra originating from brominated acid condensation products (Figure A9.2h,i), metabolites (Figure A9.3a,b) and mass fragmentation (Figure A9.3c). The brominated signatures in this case identify drug metabolites effectively from endogenous spectra, which is very relevant to indole structures during oral administration because they would typically be difficult to differentiate from endogenous compounds or food related metabolites (Benkendorff et al., 2015, Herraiz and Galisteo, 2004).

A major advantage of combining DIOS-MSI (Figure A9.1 a-f) as a precursor to a dispositional study, within the efficacy model and prior to an escalating dose pharmacokinetic model, is attention can be redirected towards detected metabolites in the vicinity of the site of action, in this case developing adenomas in the lower small intestine and excreta from the colon. 6-bromoisatin is no longer detected after oral administration and acid condensation, demonstrating that 6-bromoisatin as a structure is now less relevant than its metabolites. Signatures of metabolites in the duodenum, jejunum and ileum predominate the discoverable brominated compounds in the GI tract, Figure A9.3.

Additionally the presence of bromine can indicate condensation products in the acidic stomach environment, where di-bromination can be a clue for dimerization or polymeric structures forming, Figure A9.2h,i. Some of these cyclisation products can become too large in molecular weight for effective absorption, losing their 'drug-likeness' (Biswas et al., 2006), where they move through the gastrointestinal tract and exit the body in faeces. Concentrations of 0.1 ( $n=3$ ), 0.05 ( $n=3$ ) and 0.01mg/g control BW ( $n=3$ ) 6-bromoisatin homogenised in control stomach tissue produce high intensity poly- brominated spectral patterns not present in homogenised controls ( $n=3$ ), Figure A9.2h,i. These spectral patterns also show a

concentration dependent intensity level across the samples, Figure A9.2h, providing further evidence that the signals originate from the introduction of 6-bromoisatin into the acidic environment. When compared to the gastrointestinal DIOS-MSI dataset some of the poly-brominated patterns can be detected in the jejunum and ileum tissue sections, Figure A9.2, which shows polymerisation products that formed in the stomach, plus the added advantage of demonstrating gut retention times for these compounds.

Surprisingly, the main predicted metabolite, 6,6'-dibromoindirubin, was not detected in the homogenised stomach samples with 6-bromoisatin. A characteristic di-brominated spectral pattern, typical of 6,6'-dibromoindirubin, was detected in the ileum at very low intensity during negative mode imaging,  $m/z$  417.062, 418.076, 419.064, 420.070, 421.075, 422.071, 423.082, Figure 9.3b. For stomach samples of mice administered 6-bromoisatin, not dimer was detected A9.4, but stomach contents could be spatially defined using the spectra generated from gut contents. This unlike the effect of crude extract administered to mice, where it can be detected within the stomach contents even after 4 hours post administration.

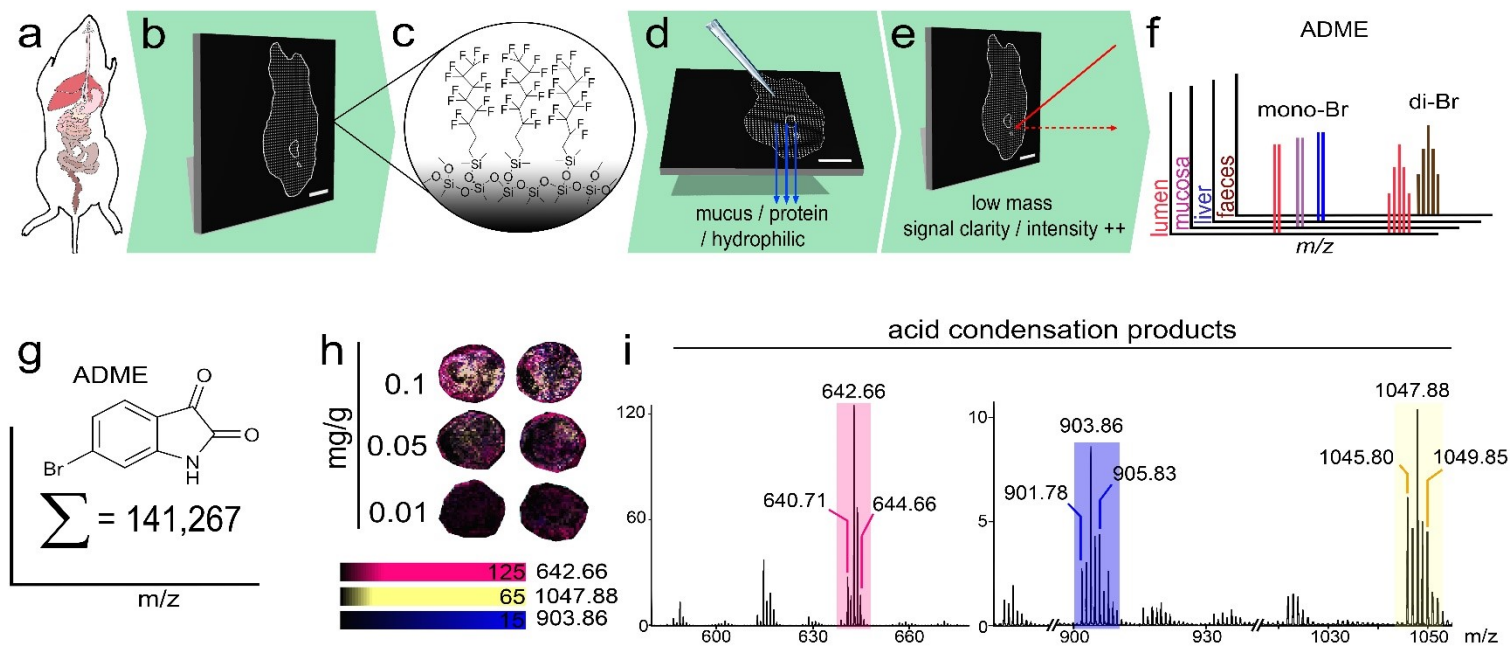


**Figure A9.2** Schematic of DIOS-MSI analysis platform; a) absorption, distribution, metabolism and excretion can be described via MSI from the gastrointestinal tract, liver and faeces whilst retaining the colon and residual tissue for *in vivo* drug efficacy, b) tissue sections are imprinted on pSi, c) surfaces functionalised with perfluorinated silanes, d) washed to remove tissue leaving a metabolite imprint, which results in, e) cleaner spectra that enhances the discovery of, f) mono-, di-, and poly-brominated spectral patterns. For data analysis, g) the sum of all the spectra from tissue sections can be compared to, h) acid condensation of 6-bromoisatin or Tyrian purple homogenised in control stomachs showing, i) polybrominated structures.

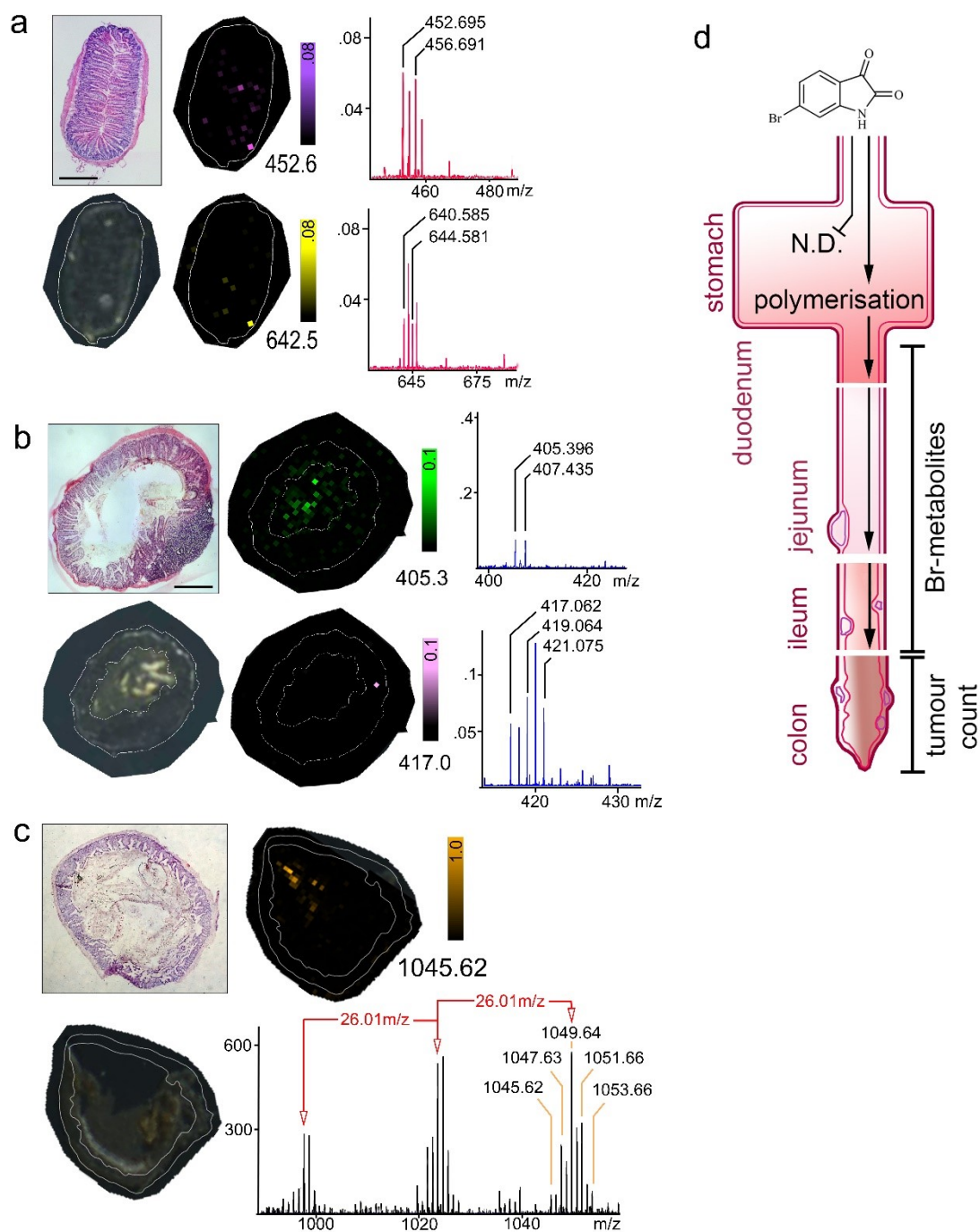


**Figure A9.3** Brominated spectral patterns detected in the, a) duodenum, b) lower jejunum, and c) ileum. Mass fragmentation of the brominated pattern in the ileum shows high correlation suggestive of fragmentation with a mass loss of  $m/z$  26.01, corresponding to HCCH, typically from aromatic compounds. The distribution of metabolites and polymerisation products that match the acid induced condensation of 6-bromoisatin in stomach tissue is shown in d).

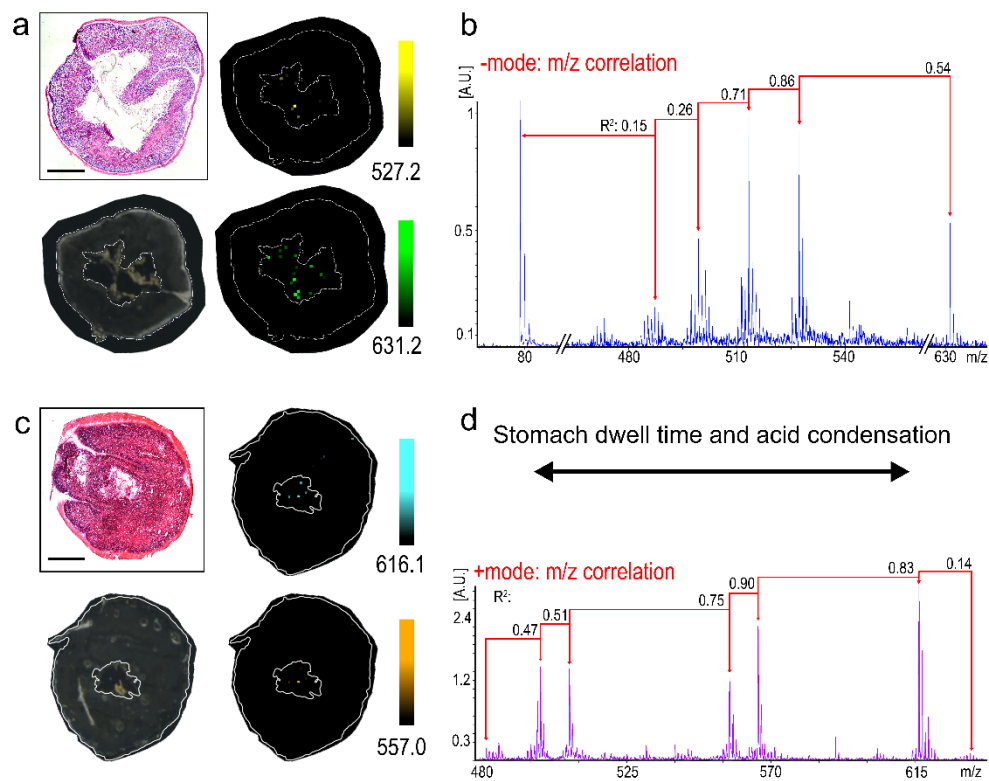


**Figure A9.4** Stomach sections where the lumen content is clearly differentiated from the mucosa. A stomach, a), after negative mode imaging showing the method used to find metabolites in the acidic environment in the stomach based on, b) correlation analysis. A similar spectral pattern can be detected in, c) positive mode imaging with, b) a comparable spectra used for correlation analysis.

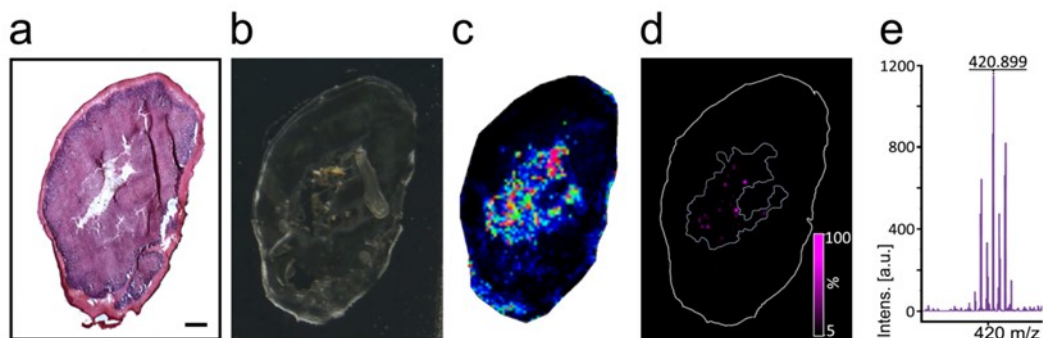


**Figure A9.5** DIOS-MSI Tyrian purple *in situ* within stomach tissue from a colorectal murine model administered 0.5 mg/g crude *D. orbita* extract. Where a) histological serial section stained with haematoxylin and eosin, b) scan of tissue imprinted on pSi, c) pLSA component with strong correlation to the disgesta, d) DIOS-MSI map of Tyrian purple  $m/z$  420.899  $[M+H]^+$ , and e) spectra from highest intensity spot in DIOS-MSI map.

### 9.3.2 DIOS-MSI effectively defines tissue distribution

The attributes that make DIOS-MSI effective in analyte capture prevent the use of the imprinted tissue section being subsequently stained for H and E, which normally provide an unequivocal co-registered image of the tissue. Probabilistic latent semantic analysis provides a spatial spectral clustering approach to define tissue by spectral patterns. When we interrogated resulting principal coordination groups we found that pLSA analysis could effectively differentiate the intestinal lumen from the mucosa for stomach tissue, Figure A9.6.

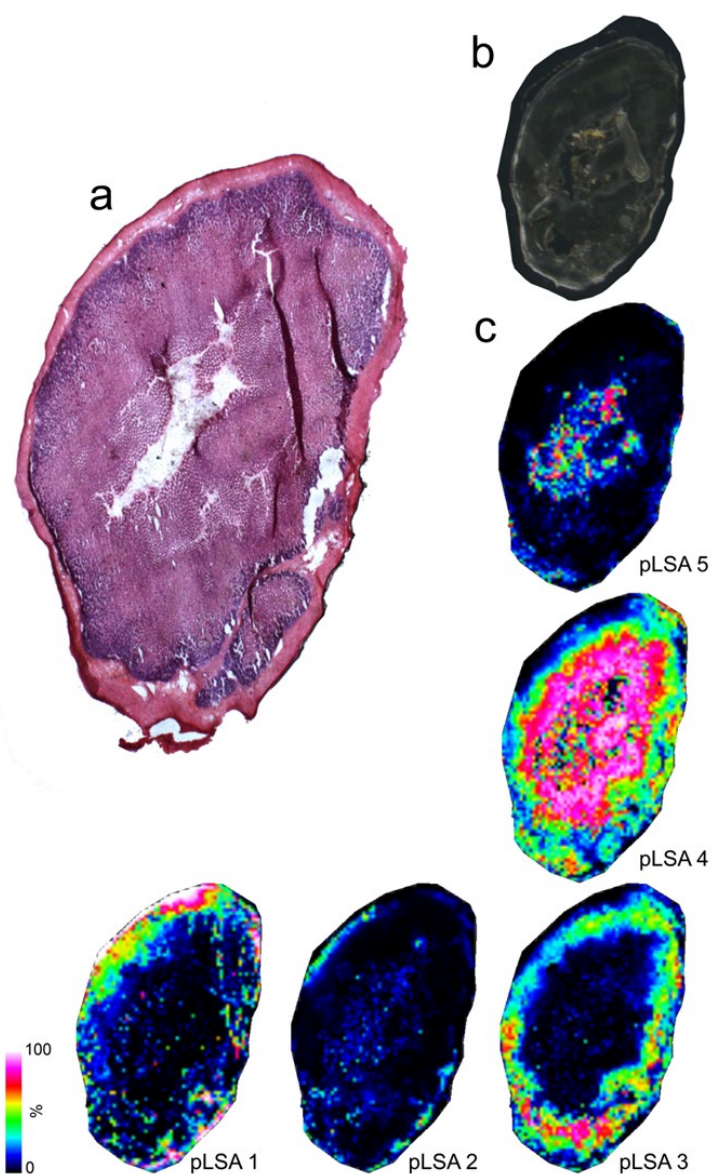


**Figure A9.6** Random initialization probabilistic latent semantic analysis (pLSA) of DIOS-MSI distribution from a 15  $\mu\text{m}$  thick stomach sections of the 0.5 mg/g crude extract treatment where, a) histological serial section stained with haematoxylin and eosin, b) scan of tissue imprinted on pSi, and c) principle components 1 – 5 showing strong similarity to the muscularis, sub-mucosa, mucosa and digesta.

### 9.3.3 Pro-apoptotic effect of 6-bromoisatin

6-bromoisatin at 0.05 and 0.025 mg/g significantly reduced the number of tumours in mouse colons (Figure A9.7a, c), while weight increased in all groups across the 14 week model (Figure A9.7e). There was also a significant reduction in ACF in the 0.025 mg/g group (Figure A9.7b, d), concomitant with a significant reduction in tumours, yet a slight increase in ACF in the 0.05 mg/g group (Figure A9.7b) converse to tumour reduction.

A critical step in the prevention of colorectal cancer is the removal of alkylated DNA adducts, typically O<sup>6</sup>-methylguanine (O<sup>6</sup>-mG) post induction by AOM (Nyskohus et al., 2013). O<sup>6</sup>-mG and other oxidative DNA base adducts can be introduced into the colon through exposure to genotoxic carcinogens of either dietary or chemically induced origin (Povey et al., 2002), or via persistent inflammation (Wiseman and Halliwell, 1996). DNA adducts may be eliminated through intrinsic repair mechanisms, whilst other extensively damaged cells are removed by activation of the apoptotic cascade in a targeted manner.

There is increasing evidence to suggest apoptotic activation requires a threshold mechanism, which is trans-versed when the tumor suppressor, p53 transcription factor, responds to genotoxic, oncogenic and other stresses (Kracikova et al., 2013). An orally administered dose of 0.05 mg/g 6-bromoisatin significantly increased the apoptotic index, Figure 1, but not at 0.025 and 0.01 mg/g. The higher dose of 6-bromoisatin could be acting via a direct effect on the p53 activation pathway crossing the threshold required, or a subsidiary system that targets apoptosis but not necrosis. Dietary constituents have been known to activate the cellular AARGC (Le Leu et al., 2003a), including constituents that escape digestion, i.e. resistant starch (Le Leu et al., 2003a). 6-bromoisatin may in fact generate cyclization products that evade digestion but could have a therapeutic effect. These products would not typically be targeted in a

traditional pharmacological approach to ADME studies, or in some cases detected at all with traditional extraction methods. The natural degradation product of 6-bromoisatin in molluscs, 6,6'-dirbomoindirubin, is only soluble in a few solvents including dimethyl sulfoxide (DMSO) and hot dimethyl formamide (DMF), and would typically precipitate in liquid chromatography solvent systems. DIOS-MSI in this case can detect the suite of compounds that would arrive in the colon environment within the digesta and differentiate it from metabolites in the tissue.

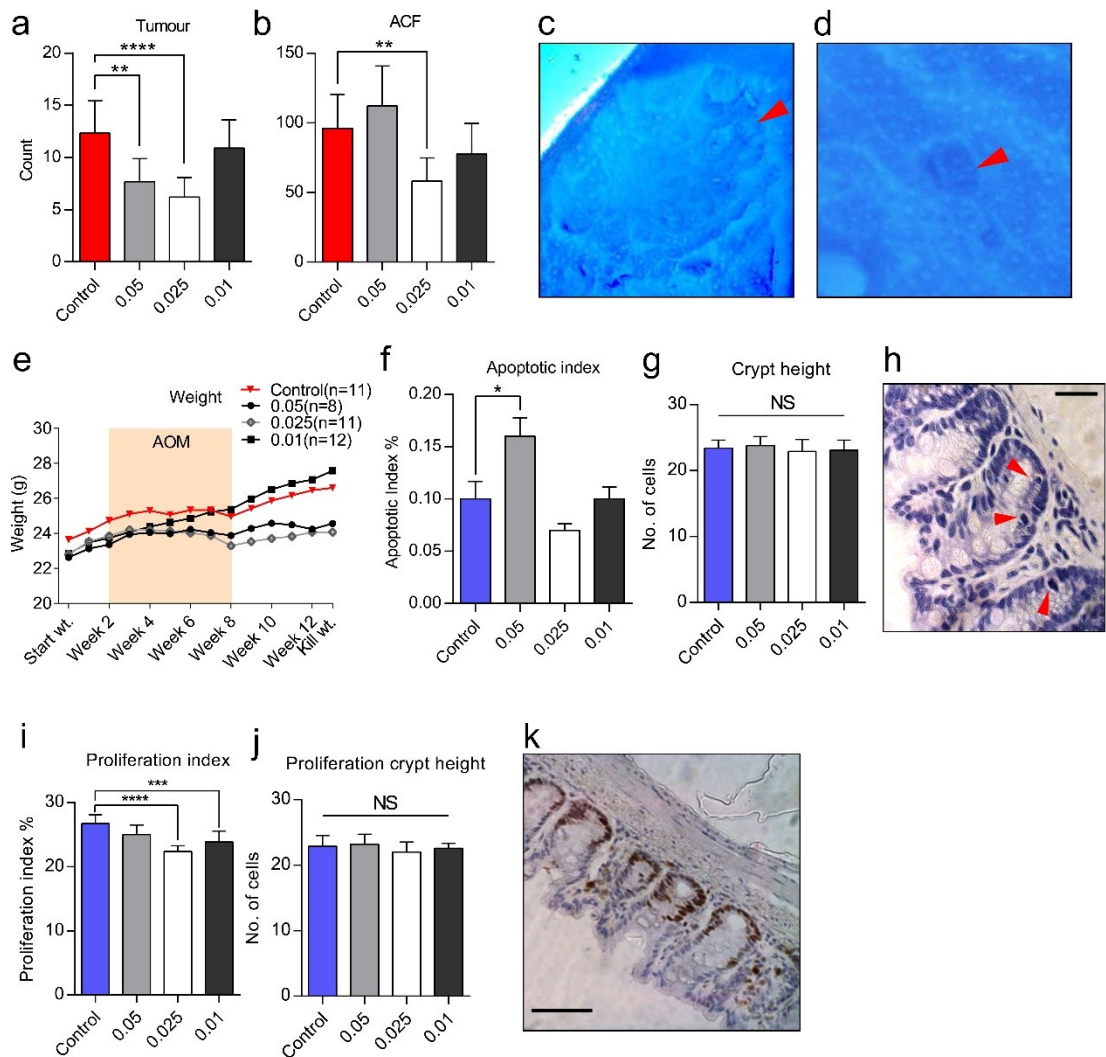


**Figure A9.7** The chemo-preventative effect of 6-bromoisatin *in vivo* within a murine model. The data has been analysed and modified from (Esmaelian, 2014, Chahal, 2014). Orally administered 6-bromoisatin affects, a) tumour counts, b) aberrant crypt foci (ACF) counts, visualised with methelene blue staining in c), d) respectively. Orally administered 6-bromoisatin had little effect on weight, e). The apoptotic index, f), was significantly increased in 0.05 mg/g group, without increasing crypt height, g), visualised using, h) hematoxylin staining (scale bar 50 μm). The proliferation index, i), was also significantly reduced in the lower 6-bromoisatin groups without changing crypt height, j), visulaised using Ki-67 staining, k).

## 9.4 Discussion

DIOS-MSI effectively detected a number of brominated indoles throughout the gastrointestinal tract of mice using tissue amounts that would otherwise not provide adequate detection by conventional methods. The type of compounds detected, particularly di-brominated structures, are highly unsuitable for LC-MS, which would lack spatial data. DIOS-MSI also effectively tracked the timecourse of brominated compounds through the digestive system giving an effective ADME profile for future targeted analysis of the *in vivo* effect of brominated metabolites. The ADME profile of 6-bromoisatin shares many similarities to another dietary chemo-preventative compound, indole-3-carbinol, found in cruciferous vegetables. It too undergoes acid condensation catalysed by acid in the stomach (Aggarwal and Ichikawa, 2005, Wang et al., 2016), and the spontaneous dimer, diindolylmethane, has been implicated as the bioactive metabolite (Wang et al., 2016). Whether the 6-bromoisatin metabolites or polymeric structures act from within the intestinal lumen introduced via digesta or via a metabolite re-introduced into the colon remains unknown and worth further investigation of the xenobiotic metabolism of 6-bromoisatin metabolites.

## 10 REFERENCES

- ABEL, E. L. 1995. Behavioral effects of isatin on open field activity and immobility in the forced swim test in rats. *Physiology & Behavior*, 57, 611-3.
- ADMINISTRATION, T. G. 2009. Impurities: Guideline for Residual Solvents. *In*: AGENCY, T. G. A. E. M. (ed.) *ICH Topic Q3C (R4)*. London, UK: European Union.
- AGGARWAL, B. B. & ICHIKAWA, H. 2005. Molecular targets and anticancer potential of indole-3-carbinol and its derivatives. *Cell Cycle*, 4, 1201-15.
- AGUILAR-CRUZ, C. A. 2006. The hypobranchial gland from the purple snail *Plicopurpura pansa* (Gould, 1853) (Prosobranchia: Muricidae). *Journal of Shellfish Research*, 25, 391-394.
- ALHMOUD, H. Z., GUINAN, T. M., ELNATHAN, R., KOBUS, H. & VOELCKER, N. H. 2014. Surface-assisted laser desorption/ionization mass spectrometry using ordered silicon nanopillar arrays. *Analyst*, 139, 5999-6009.
- ALONSO, D., KHALIL, Z., SATKUNANTHAN, N. & LIVETT, B. G. 2003. Drugs from the sea: conotoxins as drug leads for neuropathic pain and other neurological conditions. *Mini-Reviews in Medicinal Chemistry*, 3, 785-7.
- AMSLER, C. D., MCCLINTOCK, J. B. & BAKER, B. J. 2001. Secondary metabolites as mediators of trophic interactions among Antarctic marine organisms. *American Zoologist*, 41, 17-26.
- ANAND, P., GRIGORYAN, A., BHUIYAN, M. H., UEBERHEIDE, B., RUSSELL, V., QUINOÑEZ, J., MOY, P., CHAIT, B. T., POGET, S. F. & HOLFORD, M. 2014. Sample limited characterization of a novel disulfide-rich venom

peptide toxin from terebrid marine snail *Terebra variegata*. *PLoS ONE*, 9, e94122.

ANDERSEN, R. J., DESJARDINE, K. & WOODS, K. 2006. Skin chemistry of nudibranchs from the west coast of North America. *Progress in Molecular and Subcellular Biology*, 43, 277-301.

ANDREWS, E. B. 1991. The fine structure and function of the salivary glands of *Nucella lapillus* (Gastropoda: Muricidae). *Journal of Molluscan Studies*, 57, 111-126.

APPELTANS, W., AHYONG, S. T., ANDERSON, G., ANGEL, M. V., ARTOIS, T., BAILLY, N., BAMBER, R., BARBER, A., BARTSCH, I., BERTA, A., BLAZEWICZ-PASZKOWYCZ, M., BOCK, P., BOXSHALL, G., BOYKO, C. B., BRANDAO, S. N., BRAY, R. A., BRUCE, N. L., CAIRNS, S. D., CHAN, T. Y., CHENG, L. N., COLLINS, A. G., CRIBB, T., CURINI-GALLETTI, M., DAHDOUH-GUEBAS, F., DAVIE, P. J. F., DAWSON, M. N., DE CLERCK, O., DECOCK, W., DE GRAVE, S., DE VOOGD, N. J., DOMNING, D. P., EMIG, C. C., ERSEUS, C., ESCHMEYER, W., FAUCHALD, K., FAUTIN, D. G., FEIST, S. W., FRANSEN, C. H. J. M., FURUYA, H., GARCIA-ALVAREZ, O., GERKEN, S., GIBSON, D., GITTENBERGER, A., GOFAS, S., GOMEZ-DAGLIO, L., GORDON, D. P., GUIRY, M. D., HERNANDEZ, F., HOEKSEMA, B. W., HOPCROFT, R. R., JAUME, D., KIRK, P., KOEDAM, N., KOENEMANN, S., KOLB, J. B., KRISTENSEN, R. M., KROH, A., LAMBERT, G., LAZARUS, D. B., LEMAITRE, R., LONGSHAW, M., LOWRY, J., MACPHERSON, E., MADIN, L. P., MAH, C., MAPSTONE, G., MCLAUGHLIN, P. A., MEES, J., MELAND, K., MESSING, C. G., MILLS, C. E., MOLODTSOVA, T. N., MOOI, R., NEUHAUS, B., NG, P. K. L., NIELSEN, C., NORENBURG, J.,

OPRESKO, D. M., OSAWA, M., PAULAY, G., PERRIN, W., PILGER, J. F., POORE, G. C. B., PUGH, P., READ, G. B., REIMER, J. D., RIUS, M., ROCHA, R. M., SAIZ-SALINAS, J. I., SCARABINO, V., SCHIERWATER, B., SCHMIDT-RHAESA, A., SCHNABEL, K. E., SCHOTTE, M., SCHUCHERT, P., SCHWABE, E., SEGERS, H., SELF-SULLIVAN, C., SHENKAR, N., SIEGEL, V., et al. 2012. The magnitude of global marine species diversity. *Current Biology*, 22, 2189-2202.

AVILA, C. 2006. Molluscan natural products as biological models: chemical ecology, histology, and laboratory culture. *Progress in Molecular and Subcellular Biology*, 43, 1-23.

BAKER, J. T. 1974. Tyrian purple - Ancient dye, a modern problem. *Endeavour*, 32, 11-17.

BAKER, J. T. & DUKE, C. C. 1973. Chemistry of the indoleninones. II. Isolation from the hypobranchial glands of marine molluscs of 6-bromo-2,2-dimethylthioindolin-3-one and 6-bromo-2-methylthioindoleninone as alternative precursors to Tyrian purple. *Australian Journal of Chemistry*, 26, 2153-2157.

BAKER, J. T. & DUKE, C. C. 1974. Precursors of Tyrian purple. *Food-Drugs from the Sea Proceedings*.

BAKER, J. T. & DUKE, C. C. 1976. Isolation of choline and choline ester salts of tyrindoxyl sulfate from marine mollusks *Dicathais orbita* and *Mancinella keineri*. *Tetrahedron Letters*, 15, 1233-1234.

BAKER, J. T. & SUTHERLAND, M. D. 1968. Pigments of marine animals VIII. Precursors of 6,6'-dibromoindigotin (Tyrian purple) from the mollusc *Dicathais orbita* Gmelin. *Tetrahedron letters*, 1, 43 - 46.

- BANCHERO, M. 2013. Supercritical fluid dyeing of synthetic and natural textiles - a review. *Coloration Technology*, 129, 2-17.
- BANDARANAYAKE, W. N. 1998. Mycosporines: are they nature's sunscreens? *Natural Product Reports*, 15, 159-172.
- BARCO, A., CLAREMONT, M., REID, D. G., HOUART, R., BOUCHET, P., WILLIAMS, S. T., CRUAUD, C., COULOUX, A. & OLIVERIO, M. 2010. A molecular phylogenetic framework for the Muricidae, a diverse family of carnivorous gastropods. *Molecular Phylogenetics and Evolution*, 56, 1025-1039.
- BEATTIE, A. J. 1994. Conservation, evolutionary biology and the discovery of future biological resources. *In*: MORITZ, C. & KIKKAWA, J. (eds.) *Conservation Biology in Australia and Oceania*. Sydney: Surrey Beatty and Sons.
- BEATTIE, A. J., HAY, M., MAGNUSSON, B., DE NYS, R., SMEATHERS, J. & VINCENT, J. F. V. 2011. Ecology and bioprospecting. *Austral Ecology*, 36, 341-356.
- BENDER, J. A., DERIEMER, K., ROBERTS, T. E., RUSHTON, R., BOOTHE, P., MOSHER, H. S. & FUHRMAN, F. A. 1974. Choline esters in marine gastropods *Nucella emarginata* and *Acanthina spirata* - new choline ester, tentatively identified as n-methylmurexine. *General Pharmacology*, 5, 191-198.
- BENKENDORFF, K. 1999. *Bioactive molluscan resources and their conservation: biological and chemical studies on the egg masses of marine molluscs*. Doctor of Philosophy doctoral, University of Wollongong.
- BENKENDORFF, K. 2009. Aquaculture and the production of pharmaceuticals and nutraceuticals. *In*: BURNELL, G. & ALLEN, G. (eds.) *New technologies in*

*aquaculture: improving production efficiency, quality and environmental management*. Cambridge: Woodhead Publishing.

BENKENDORFF, K. 2010. Molluscan biological and chemical diversity: secondary metabolites and medicinal resources produced by marine molluscs. *Biological Reviews*, 85, 757-775.

BENKENDORFF, K. 2013. Natural product research in the Australian marine invertebrate *Dicathais orbita*. *Marine Drugs*, 11, 1370-1398.

BENKENDORFF, K. 2014. Chemical diversity in molluscan communities: from natural products to chemical ecology. In: COSMO, A. D. & WINLOW, W. (eds.) *Neuroecology and neuroethology in molluscs: the interface between behaviour and environment*. New York: Nova Science Publishers.

BENKENDORFF, K., BREMNER, J. B. & DAVIS, A. R. 2000. Tyrian purple precursors in the egg masses of the Australian muricid, *Dicathais orbita*: A possible defensive role. *Journal of Chemical Ecology*, 26, 1037-1050.

BENKENDORFF, K., BREMNER, J. B. & DAVIS, A. R. 2001a. Indole derivatives from the egg masses of muricid molluscs. *Molecules*, 6, 70-78.

BENKENDORFF, K. & DAVIS, A. R. 2004. Gastropod egg mass deposition on a temperate, wave-exposed coastline in New South Wales, Australia: implications for intertidal conservation. *Aquatic Conservation: Marine and Freshwater Ecosystems*, 14, 263-280.

BENKENDORFF, K., DAVIS, A. R. & BREMNER, J. 2001b. Chemical defense in the egg masses of benthic invertebrates: An assessment of antibacterial activity in 39 mollusks and 4 polychaetes. *Journal of Invertebrate Pathology*, 78, 109-118.

BENKENDORFF, K., DAVIS, A. R., ROGERS, C. N. & BREMNER, J. B. 2005. Free fatty acids and sterols in the benthic spawn of aquatic molluscs, and

- their associated antimicrobial properties. *Journal of Experimental Marine Biology and Ecology*, 316, 29-44.
- BENKENDORFF, K., MCIVER, C. M. & ABBOTT, C. A. 2011. Bioactivity of the murex homeopathic remedy and of extracts from an Australian muricid mollusc against human cancer cells. *Evidence-Based Complementary and Alternative Medicine*, nep042.
- BENKENDORFF, K., PILLAI, R. & BREMNER, J. B. 2004a. 2,4,5-Tribromo-1H-imidazole in the egg masses of three muricid molluscs. *Natural Product Research*, 18, 427-431.
- BENKENDORFF, K., RUDD, D., NONGMAITHEM, B. D., LIU, L., YOUNG, F., EDWARDS, V., AVILA, C. & ABBOTT, C. A. 2015. Are the traditional medical uses of Muricidae molluscs substantiated by their pharmacological properties and bioactive compounds? *Marine Drugs*, 13, 5237-75.
- BENKENDORFF, K., WESTLEY, C. B. & GALLARDO, C. S. 2004b. Observations on the production of purple pigments in the egg capsules, hypobranchial and reproductive glands from seven species of Muricidae (Gastropoda: Mollusca). *Invertebrate Reproduction & Development*, 46, 93-102.
- BERGMAN, N., SHEVCHENKO, D. & BERGQUIST, J. 2014. Approaches for the analysis of low molecular weight compounds with laser desorption/ionization techniques and mass spectrometry. *Analytical and Bioanalytical Chemistry*, 406, 49-61.
- BERGMANN, W. 1949. Comparative biochemical studies on the lipids of marine invertebrates, with special reference to the sterols. *Journal of Marine Research*, 8, 137-176.

- BERKENKAMP, S., KIRPEKAR, F. & HILLENKAMP, F. 1998. Infrared MALDI mass spectrometry of large nucleic acids. *Science*, 281, 260-262.
- BHATTACHARYA, S. K. & CHAKRABARTI, A. 1998. Dose-related proconvulsant and anticonvulsant activity of isatin, a putative biological factor, in rats. *Indian Journal of Experimental Biology*, 36, 118-21.
- BHATTACHARYA, S. K., MITRA, S. K. & ACHARYA, S. B. 1991. Anxiogenic activity of isatin, a putative biological factor, in rodents. *Journal of Psychopharmacology*, 5, 202-6.
- BISWAS, D., ROY, S. & SEN, S. 2006. A Simple Approach for Indexing the Oral Druglikeness of a Compound: Discriminating Druglike Compounds from Nondruglike Ones. *Journal of Chemical Information and Modeling*, 46, 1394-1401.
- BLUNT, J. W., COPP, B. R., KEYZERS, R. A., MUNRO, M. H. & PRINSEP, M. R. 2013. Marine natural products. *Natural Product Reports*, 30, 237-323.
- BOUSLIMANI, A., SANCHEZ, L. M., GARG, N. & DORRESTEIN, P. C. 2014. Mass spectrometry of natural products: current, emerging and future technologies. *Natural Product Reports*, 31, 718-29.
- BREJC, K., VAN DIJK, W. J., KLAASSEN, R. V., SCHUURMANS, M., VAN DER OOST, J., SMIT, A. B. & SIXMA, T. K. 2001. Crystal structure of an ACh-binding protein reveals the ligand-binding domain of nicotinic receptors. *Nature*, 411, 269-276.
- BROWN, R. S. & LENNON, J. J. 1995. Mass resolution improvement by incorporation of pulsed ion extraction in a matrix-assisted laser desorption/ionization linear time-of-flight mass spectrometer. *Analytical Chemistry*, 67, 1998-2003.

- CALAVIA, R., ANNANOUCHE, F. E., CORREIG, X. & YANES, O. 2012. Nanostructure initiator mass spectrometry for tissue imaging in metabolomics: future prospects and perspectives. *Journal of Proteomics*, 75, 5061-5068.
- CAMP, D., DAVIS, R. A., CAMPITELLI, M., EBDON, J. & QUINN, R. J. 2011. Drug-like properties: guiding principles for the design of natural product libraries. *Journal of Natural Products*, 75, 72-81.
- CAPON, R. J. 2010. Marine natural products chemistry: past, present, and future. *Australian Journal of Chemistry*, 63, 851-854.
- CAPRIOLI, R. M., FARMER, T. B. & GILE, J. 1997. Molecular imaging of biological samples: localization of peptides and proteins using MALDI-TOF MS. *Analytical chemistry*, 69, 4751-60.
- CARBONE, E. & LUX, H. D. 1988. Omega-conotoxin blockade distinguishes Ca from Na permeable states in neuronal calcium channels. *Pflugers Archiv : European journal of physiology*, 413, 14-22.
- CARBONE, M., GAVAGNIN, M., HABER, M., GUO, Y. W., FONTANA, A., MANZO, E., GENTA-JOUVE, G., TSOUKATOU, M., RUDMAN, W. B., CIMINO, G., GHISELIN, M. T. & MOLLO, E. 2013. Packaging and delivery of chemical weapons: a defensive trojan horse stratagem in chromodorid nudibranchs. *PLoS One*, 8, e62075.
- CASTELLINO, S., GROSECLOSE, M. R. & WAGNER, D. 2011. MALDI imaging mass spectrometry: bridging biology and chemistry in drug development. *Bioanalysis*, 3, 2427-41.
- CHAHAL, C. S. 2014. *A study of the anticancer properties of crude extract and synthetic 6-bromoisatin from Dicathais orbita: an in vivo colorectal cancer model*. Masters of Biotechnology Masters, Flinders University.

- CHESTER, T. L., PINKSTON, J. D. & RAYNIE, D. E. 1996. Supercritical fluid chromatography and extraction. *Analytical Chemistry*, 68, R487-R514.
- CHIRINOS, J., OROPEZA, D., GONZÁLEZ, J., RANAUDO, M. & RUSSO, R. E. 2013. Determination of vanadium/nickel proportionality in the asphaltene fraction of crude oil using thin-layer chromatography with femtosecond laser ablation–inductively coupled plasma–mass spectrometry. *Energy & Fuels*, 27, 2431-2436.
- CHRISTOPHERSEN, C., WÄTJEN, F., BUCHARDT, O. & ANTHONI, U. 1978. A revised structure of tyriverdin: The precursor of tyrian purple. *Tetrahedron*, 34, 2779-2781.
- CIMINO, G., FONTANA, A., CUTIGNANO, A. & GAVAGNIN, M. 2004. Biosynthesis in opisthobranch molluscs: General outline in the light of recent use of stable isotopes. *Phytochemistry Reviews*, 3, 285-307.
- CIMINO, G., FONTANA, A., GIMÉNEZ, F., MARIN, A., MOLLO, E., TRIVELLONE, E. & ZUBÍA, E. 1993. Biotransformation of a dietary sesterterpenoid in the Mediterranean nudibranch *Hypselodoris orsini*. *Experientia*, 49, 582-586.
- CIMINO, G. & GHISELIN, M. T. 1998. Chemical defense and evolution in the Sacoglossa (Mollusca: Gastropoda: Opisthobranchia). *Chemoecology*, 8, 51-60.
- CIMINO, G., PASSEGGIO, A., SODANO, G., SPINELLA, A. & VILLANI, G. 1991. Alarm pheromones from the Mediterranean opisthobranch *Haminoea navicula*. *Experientia*, 47, 61-63.
- CIMINO, G., ROSA, S., STEFANO, S., SODANO, G. & VILLANI, G. 1983. Dorid nudibranch elaborates its own chemical defense. *Science*, 219, 1237-8.

- COOKSEY, C. 2013. Tyrian purple: the first four thousand years. *Science Progress*, 96, 171-86.
- COOKSEY, C. J. 2001. Tyrian purple: 6,6'-dibromoindigo and related compounds. *Molecules*, 6, 736-769.
- CORNETT, D. S., REYZER, M. L., CHAURAND, P. & CAPRIOLI, R. M. 2007. MALDI imaging mass spectrometry: molecular snapshots of biochemical systems. *Nature Methods*, 4, 828-33.
- CUMMINS, S. F., NICHOLS, A. E., AMARE, A., HUMMON, A. B., SWEEDLER, J. V. & NAGLE, G. T. 2004. Characterization of *Aplysia* enticin and temptin, two novel water-borne protein pheromones that act in concert with attractin to stimulate mate attraction. *Journal of Biological Chemistry*, 279, 25614-25622.
- CUMMINS, S. F., SCHEIN, C. H., XU, Y., BRAUN, W. & NAGLE, G. T. 2005. Molluscan attractins, a family of water-borne protein pheromones with interspecific attractiveness. *Peptides*, 26, 121 - 129.
- CUMPLIDO, M., PAPPALARDO, P., FERNANDEZ, M., AVERBUJ, A. & BIGATTI, G. 2011. Embryonic development, feeding and intracapsular oxygen availability in *Trochophora geversianus* (Gastropoda: Muricidae). *Journal of Molluscan Studies*, 77, 429-436.
- CUTIGNANO, A., AVILA, C., ROSICA, A., ROMANO, G., LARATTA, B., DOMENECH-COLL, A., CIMINO, G., MOLLO, E. & FONTANA, A. 2012a. Biosynthesis and cellular localization of functional polyketides in the gastropod mollusc *Scaphander lignarius*. *ChemBioChem*, 13, 1759-66, 1701.
- CUTIGNANO, A., CIMINO, G., VILLANI, G. & FONTANA, A. 2009. Shaping the polypropionate biosynthesis in the solar-powered mollusc *Elysia viridis*. *ChemBioChem*, 10, 315-322.

- CUTIGNANO, A., VILLANI, G. & FONTANA, A. 2012b. One metabolite, two pathways: convergence of polypropionate biosynthesis in fungi and marine molluscs. *Organic Letters*, 14, 992-5.
- D'ASARO, C. N. 1988. Micromorphology of neogastropod egg capsules. *Nautilus*, 102, 134-148.
- D'ASARO, C. N. 1992. Gunnar Thorson's world-wide collection of prosobranch egg capsules: Muricidae. *Ophelia*, 35, 1-101.
- DANG, V. T., SPECK, P., DOROUDI, M., SMITH, B. & BENKENDORFF, K. 2011. Variation in the antiviral and antibacterial activity of abalone *Haliotis laevigata*, *H. rubra* and their hybrid in South Australia. *Aquaculture*, 315, 242-249.
- DANZ, H., STOYANOVA, S., WIPPICH, P., BRATTSTROM, A. & HAMBURGER, M. 2001. Identification and isolation of the cyclooxygenase-2 inhibitory principle in *Isatis tinctoria*. *Planta Medica*, 67, 411-6.
- DAVIS, J., FRICKE, W. F., HAMANN, M. T., ESQUENAZI, E., DORRESTEIN, P. C. & HILL, R. T. 2013. Characterization of the bacterial community of the chemically defended Hawaiian sacoglossan *Elysia rufescens*. *Applied and Environmental Microbiology*, 79, 7073-81.
- DE CASTRO, B. M., DE JAEGER, X., MARTINS-SILVA, C., LIMA, R. D. F., AMARAL, E., MENEZES, C., LIMA, P., NEVES, C. M. L., PIRES, R. G., GOULD, T. W., WELCH, I., KUSHMERICK, C., GUATIMOSIM, C., IZQUIERDO, I., CAMMAROTA, M., RYLETT, R. J., GOMEZ, M. V., CARON, M. G., OPPENHEIM, R. W., PRADO, M. A. M. & PRADO, V. F. 2009. The vesicular acetylcholine transporter is required for neuromuscular development and function. *Molecular and Cellular Biology*, 29, 5238-5250.

- DEBAT, J. 1972. *Promotion of analgesic and sedative action with 5-bromoisatin*.  
France patent application.
- DEBOIS, D., HAMZE, K., GUERINEAU, V., LE CAER, J. P., HOLLAND, I. B.,  
LOPES, P., OUAZZANI, J., SEROR, S. J., BRUNELLE, A. &  
LAPREVOTE, O. 2008. *In situ* localisation and quantification of surfactins in  
a *Bacillus subtilis* swarming community by imaging mass spectrometry.  
*Proteomics*, 8, 3682-91.
- DECHO, A. W. 2000. Microbial biofilms in intertidal systems: an overview.  
*Continental Shelf Research*, 20, 1257-1273.
- DEMETRI, G. D., VAN OOSTEROM, A. T., GARRETT, C. R., BLACKSTEIN, M.  
E., SHAH, M. H., VERWEIJ, J., MCARTHUR, G., JUDSON, I. R.,  
HEINRICH, M. C., MORGAN, J. A., DESAI, J., FLETCHER, C. D.,  
GEORGE, S., BELLO, C. L., HUANG, X., BAUM, C. M. & CASALI, P. G.  
Efficacy and safety of sunitinib in patients with advanced gastrointestinal  
stromal tumour after failure of imatinib: a randomised controlled trial. *The  
Lancet*, 368, 1329-1338.
- DERBY, C. 2014. Cephalopod ink: production, chemistry, functions and  
applications. *Marine Drugs*, 12, 2700-2730.
- DERBY, C. D. & ZIMMER, R. K. 2014. Neuroecology and the molluscan  
connection. In: COSMO, A. D. & WINLOW, W. (eds.) *Neuroecology and  
neuroethology in molluscs: the interface between behaviour and  
environmental* New York: Nova Science Publishers.
- DIAS, D. A., URBAN, S. & ROESSNER, U. 2012. A historical overview of natural  
products in drug discovery. *Metabolites*, 2, 303-336.

- DIXSON, D. L., ABREGO, D. & HAY, M. E. 2014. Chemically mediated behavior of recruiting corals and fishes: A tipping point that may limit reef recovery. *Science*, 345, 892-897.
- DORRESTEIN, P. C. 2014. Editorial: Mass spectrometry of small molecules and natural products. *Natural Product Reports*, 31, 704-705.
- DUDA, T. F. & PALUMBI, S. R. 2004. Gene expression and feeding ecology: evolution of piscivory in the venomous gastropod genus *Conus*. *Proceedings of the Royal Society B: Biological Sciences*, 271, 1165-1174.
- DUKE, C. C., EICHHOLZER, J. V. & MACLEOD, J. K. 1978. N-Methylmurexine - naturally occurring marine compound. *Tetrahedron Letters*, 5047-5048.
- EDWARDS, V. 2012. *The effects of bioactive compounds from the marine mollusc *Dicathais orbita* on human reproductive cells and human reproductive cancer cells*. Ph.D. Doctoral, Flinders University.
- EDWARDS, V., BENKENDORFF, K. & YOUNG, F. 2012. Marine compounds selectively induce apoptosis in female reproductive cancer cells but not in primary-derived human reproductive granulosa cells. *Marine Drugs*, 10, 64-83.
- EIKEL, D., VAVREK, M., SMITH, S., BASON, C., YEH, S., KORFMACHER, W. A. & HENION, J. D. 2011. Liquid extraction surface analysis mass spectrometry (LESA-MS) as a novel profiling tool for drug distribution and metabolism analysis: the terfenadine example. *Rapid Communications in Mass Spectrometry*, 25, 3587-3596.
- ELLIS, S. R., BROWN, S. H., IN HET PANHUIS, M., BLANKSBY, S. J. & MITCHELL, T. W. 2013. Surface analysis of lipids by mass spectrometry: more than just imaging. *Progress in Lipid Research*, 52, 329-53.

- EMELYANOV, A., FEDOSEEV, G., KRASNOSCHEKOVA, O., ABULIMITY, A.,  
TRENDELEVA, T. & BARNES, P. J. 2002. Treatment of asthma with lipid  
extract of New Zealand green-lipped mussel: a randomised clinical trial.  
*European Respiratory Journal*, 20, 596-600.
- ERNST, M., SILVA, D. B., SILVA, R. R., VENCIO, R. Z. N. & LOPES, N. P.  
2014. Mass spectrometry in plant metabolomics strategies: from analytical  
platforms to data acquisition and processing. *Natural Product Reports*, 31,  
784-806.
- ERSPAMER, V. & BENATI, O. 1953. Identification of murexine as beta-  
(imidazolyl-(4))-acrylcholine. *Science*, 117, 161-2.
- ERSPAMER, V. & GLASSER, A. 1957. The pharmacological actions of murexine  
(urocanylcholine). *British Journal of Pharmacology and Chemotherapy*, 12,  
176-84.
- ESMAEELIAN, B. 2014. *Preclinical in vitro and in vivo effects of purified and  
synthetic bioactive compounds from marine mollusc Dicathais orbita on  
colorectal cancer: cancer prevention and toxicity study*. Doctor of  
Philosophy Doctoral, Flinders University.
- ESMAEELIAN, B., ABBOTT, C. A., LE LEU, R. K. & BENKENDORFF, K.  
2013a. 6-Bromoisatin Found in Muricid Mollusc Extracts Inhibits Colon  
Cancer Cell Proliferation and Induces Apoptosis, Preventing Early Stage  
Tumor Formation in a Colorectal Cancer Rodent Model. *Marine drugs*, 12,  
17-35.
- ESMAEELIAN, B., ABBOTT, C. A., LE LEU, R. K. & BENKENDORFF, K. 2014.  
6-Bromoisatin found in muricid mollusc extracts inhibits colon cancer cell  
proliferation and induces apoptosis, preventing early stage tumor formation in  
a colorectal cancer rodent model. *Marine Drugs*, 12, 17-35.

- ESMAEELIAN, B., BENKENDORFF, K., JOHNSTON, M. R. & ABBOTT, C. A. 2013b. Purified brominated indole derivatives from *Dicathais orbita* induce apoptosis and cell cycle arrest in colorectal cancer cell lines. *Marine Drugs*, 11, 3802-22.
- ESPIRITU, D. J. D., WATKINS, M., DIA-MONJE, V., CARTIER, G. E., CRUZ, L. J. & OLIVERA, B. M. 2001. Venomous cone snails: molecular phylogeny and the generation of toxin diversity. *Toxicon*, 39, 1899-1916.
- ESQUENAZI, E., JONES, A. C., BYRUM, T., DORRESTEIN, P. C. & GERWICK, W. H. 2011. Temporal dynamics of natural product biosynthesis in marine cyanobacteria. *Proceedings of the National Academy of Sciences of the United States of America*, 108, 5226-31.
- ESQUENAZI, E., YANG, Y. L., WATROUS, J., GERWICK, W. H. & DORRESTEIN, P. C. 2009. Imaging mass spectrometry of natural products. *Natural Product Reports*, 26, 1521-1534.
- FAIRWEATHER, P. G. 1985. *Interactions between predators and prey, and the structure of rocky intertidal communities*. Doctor of Philosophy Doctoral, University of Sydney.
- FAIRWEATHER, P. G. 1988a. Movements of intertidal whelks (*Morula marginalba* and *Thais orbita*) in relation to availability of prey and shelter. *Marine Biology*, 100, 63-68.
- FAIRWEATHER, P. G. 1988b. Predation creates haloes of bare space among prey on rocky seashores in New South Wales. *Australian Journal of Ecology*, 13, 401-409.
- FAULKNER, D. J. Marine pharmacology. *Antonie van Leeuwenhoek*, 77, 135-145.

- FEHER, M. & SCHMIDT, J. M. 2002. Property distributions: differences between drugs, natural products, and molecules from combinatorial chemistry. *Journal of Chemical Information and Computer Sciences*, 43, 218-227.
- FOUQUET, H. & BIELIG, H. J. 1971. Biological precursors and genesis of Tyrian Purple. *Angewandte Chemie International Edition*, 10, 816-817.
- FRANCA, P. H. B., BARBOSA, D. P., DA SILVA, D. L., RIBEIRO, E. A. N., SANTANA, A. E. G., SANTOS, B. V. O., BARBOSA-FILHO, J. M., QUINTANS, J. S. S., BARRETO, R. S. S., QUINTANS-JUNIOR, L. J. & DE ARAUJO-JUNIOR, J. X. 2014. Indole alkaloids from marine sources as potential leads against infectious diseases. *BioMed Research International*, 2014, 12.
- FRANCK, J., ARAFAH, K., ELAYED, M., BONNEL, D., VERGARA, D., JACQUET, A., VINATIER, D., WISZTORSKI, M., DAY, R., FOURNIER, I. & SALZET, M. 2009. MALDI imaging mass spectrometry: state of the art technology in clinical proteomics. *Molecular & Cellular Proteomics : MCP*, 8, 2023-2033.
- FRAZER, A. & HENSLER, J. G. 1999. Serotonin involvement in physiological function and behavior. In: SIEGEL, G., J., AGRANOFF, B. W., ALBERS, R. W., FISHER, S. K. & UHLER, M. D. (eds.) *Basic Neurochemistry: Molecular, Cellular, and Medical Aspects*. Philadelphia: Lippincott-Raven.
- FRETTER, V., GRAHAM, A. 1994. *British prosobranch molluscs*, Dorset, The Ray Society.
- FRIEDLANDER, P., BRUCKNER, S. & DEUTSCH, G. 1912. Bromo- and methoxy derivatives of indigo *Annalen*, 388, 23-49.

- FUJIMURA, Y. & MIURA, D. 2014. MALDI mass spectrometry imaging for visualizing *in situ* metabolism of endogenous metabolites and dietary phytochemicals. *Metabolites*, 4, 319-346.
- GARSON, M. J. 1993. The biosynthesis of marine natural products. *Chemical Reviews*, 93, 1699-1733.
- GASALLA, M. A., RODRIGUES, A. R. & POSTUMA, F. A. 2010. The trophic role of the squid *Loligo plei* as a keystone species in the South Brazil Bight ecosystem. *ICES Journal of Marine Science*, 67, 1413-1424.
- GENJI, T., FUKUZAWA, S. & TACHIBANA, K. 2010. Distribution and possible function of the marine alkaloid, norzoanthamine, in the zoanthid *Zoanthus sp.* using MALDI imaging mass spectrometry. *Marine Biotechnology*, 12, 81-7.
- GENTRY, C. L., EGLETON, R. D., GILLESPIE, T., ABBRUSCATO, T. J., BECHOWSKI, H. B., HRUBY, V. J. & DAVIS, T. P. 1999. The effect of halogenation on blood–brain barrier permeability of a novel peptide drug. *Peptides*, 20, 1229-1238.
- GERWICK, W. H. & MOORE, B. S. 2012. Lessons from the past and charting the future of marine natural products drug discovery and chemical biology. *Chemistry & Biology*, 19, 85-98.
- GIBSON, S. L. M. 2000. The effect of a lipid extract of the New Zealand green-lipped mussel in three cases of arthritis. *Journal of Alternative and Complementary Medicine*, 6, 351-354.
- GO, E. P., PRENNI, J. E., WEI, J., JONES, A., HALL, S. C., WITKOWSKA, H. E., SHEN, Z. & SIUZDAK, G. 2003. Desorption/ionization on silicon time-of-flight/time-of-flight mass spectrometry. *Analytical Chemistry*, 75, 2504-2506.
- GO, E. P., URITBOONTHAI, W., APON, J. V., TRAUGER, S. A., NORDSTROM, A., O'MAILLE, G., BRITTAIN, S. M., PETERS, E. C. & SIUZDAK, G.

2007. Selective metabolite and peptide capture/mass detection using fluoruous affinity tags. *Journal of Proteome Research*, 6, 1492-1499.
- GOODWIN, R. J. & PITT, A. R. 2010. Mass spectrometry imaging of pharmacological compounds in tissue sections. *Bioanalysis*, 2, 279-93.
- GOODWIN, R. J. A., PENNINGTON, S. R. & PITT, A. R. 2008. Protein and peptides in pictures: imaging with MALDI mass spectrometry. *Proteomics*, 8, 3785-3800.
- GOWLETT-HOLMES, K. L. 2008. *A field guide to the marine invertebrates of South Australia*, Sandy Bay, Tasmania, Notomares.
- GREVING, M. P., PATTI, G. J. & SIUZDAK, G. 2010. Nanostructure-initiator mass spectrometry metabolite analysis and imaging. *Analytical Chemistry*, 83, 2-7.
- GRIENKE, U., SILKE, J. & TASDEMIR, D. 2014. Bioactive compounds from marine mussels and their effects on human health. *Food Chemistry*, 142, 48-60.
- GUINAN, T., KIRKBRIDE, P., PIGOUE, P. E., RONCI, M., KOBUS, H. & VOELCKER, N. H. 2014. Surface-assisted laser desorption ionisation mass spectrometry techniques for application in forensics. *Mass Spectrometry Reviews*, 1-14.
- GUINAN, T., RONCI, M., KOBUS, H. & VOELCKER, N. H. 2012. Rapid detection of illicit drugs in neat saliva using desorption/ionization on porous silicon. *Talanta*, 99, 791-798.
- GUINAN, T. M., GUSTAFSSON, O. J. R., MCPHEE, G., KOBUS, H. & VOELCKER, N. H. 2015. Silver Coating for High-Mass-Accuracy Imaging Mass Spectrometry of Fingerprints on Nanostructured Silicon. *Analytical Chemistry*, 87, 11195-11202.

- GUL, W. & HAMANN, M. T. 2005. Indole alkaloid marine natural products: An established source of cancer drug leads with considerable promise for the control of parasitic, neurological and other diseases. *Life Sciences*, 78, 442-453.
- HADFIELD, M. G. 2011. Biofilms and marine invertebrate larvae: what bacteria produce that larvae use to choose settlement sites. *Annual Review of Marine Science*, 3, 453-470.
- HALIM, R., DANQUAH, M. K. & WEBLEY, P. A. 2012. Extraction of oil from microalgae for biodiesel production: A review. *Biotechnology Advances*, 30, 709-732.
- HALL-SPENCER, J. M. & MOORE, P. G. 2000. *Limaria hians* (Mollusca: Limacea): a neglected reef-forming keystone species. *Aquatic Conservation : Marine and Freshwater Ecosystems*, 10, 267-277.
- HAMANN, M. T., OTTO, C. S., SCHEUER, P. J. & DUNBAR, D. C. 1996. Kahalalides: bioactive peptide from a marine mollusk *Elysia rufescens* and its algal diet *Bryopsis* sp. *Journal of Organic Chemistry*, 61, 6594-6600.
- HARVEY, A. L., EDRADA-EBEL, R. & QUINN, R. J. 2015. The re-emergence of natural products for drug discovery in the genomics era. *Nature Reviews Drug Discovery*, 14, 111-129.
- HAY, M. E. 1996. Marine chemical ecology: What's known and what's next? *Journal of Experimental Marine Biology and Ecology*, 200, 103-134.
- HAY, M. E. 2009. Marine chemical ecology: chemical signals and cues structure marine populations, communities, and ecosystems. *Annual Review of Marine Science*, 1, 193-212.
- HAY, M. E. & FENICAL, W. 1996. Chemical ecology and marine biodiversity: insights and products from the sea. *Oceanography*, 9, 11.

- HERRAIZ, T. & GALISTEO, J. 2004. Endogenous and dietary indoles: a class of antioxidants and radical scavengers in the ABTS assay. *Free Radical Research*, 38, 323-31.
- HERRERO, M., MENDIOLA, J. A., CIFUENTES, A. & IBANEZ, E. 2010. Supercritical fluid extraction: Recent advances and applications. *Journal of Chromatography A*, 1217, 2495-2511.
- HEY, P. 1952. On relationships between structure and nicotine-like stimulant activity in choline esters and ethers. *British Journal of Pharmacology and Chemotherapy*, 7, 117-29.
- HICKMAN, C. P., ROBERTS, L. S., KEEN, S. L., LARSON, A. & EISENHOUR, D. 2008. *Animal Diversity*, McGraw-Hill Higher Education.
- HIGDON, J. V., DELAGE, B., WILLIAMS, D. E. & DASHWOOD, R. H. 2007. Cruciferous vegetables and human cancer risk: epidemiologic evidence and mechanistic basis. *Pharmacological Research*, 55, 224-236.
- HILLENKAMP, F. & KARAS, M. 2007. The MALDI Process and Method. *MALDI MS*. Wiley-VCH Verlag GmbH & Co. KGaA.
- HÖLSCHER, D., DHAKSHINAMOORTHY, S., ALEXANDROV, T., BECKER, M., BRETSCHNEIDER, T., BUERKERT, A., CRECELIUS, A. C., DE WAELE, D., ELSER, A., HECKEL, D. G., HEKLAU, H., HERTWECK, C., KAI, M., KNOP, K., KRAFFT, C., MADDULA, R. K., MATTHÄUS, C., POPP, J., SCHNEIDER, B., SCHUBERT, U. S., SIKORA, R. A., SVATOŠ, A. & SWENNEN, R. L. 2013. Phenalenone-type phytoalexins mediate resistance of banana plants (*Musa spp.*) to the burrowing nematode *Radopholus similis*. *Proceedings of the National Academy of Sciences of the United States of America*.

- HOOPER, C., DAY, R., SLOCOMBE, R., HANDLINGER, J. & BENKENDORFF, K. 2007. Stress and immune responses in abalone: Limitations in current knowledge and investigative methods based on other models. *Fish & Shellfish Immunology*, 22, 363-379.
- HORTIN, G. L. 2006. The MALDI-TOF mass spectrometric view of the plasma proteome and peptidome. *Clinical Chemistry*, 52, 1223-1237.
- HOURRI, A., ST-ARNAUD, J. M. & BOSE, T. K. 1998. Solubility of solids in supercritical fluids from the measurements of the dielectric constant: Application to CO(2)-naphthalene. *Review of Scientific Instruments*, 69, 2732-2737.
- HSIEH, Y., LI, F. & KORFMACHER, W. A. 2010. Mapping pharmaceuticals in rat brain sections using MALDI imaging mass spectrometry. *Methods Mol Biol*, 656, 147-58.
- HU, H., BANDYOPADHYAY, P., OLIVERA, B. & YANDELL, M. 2011. Characterization of the *Conus bullatus* genome and its venom-duct transcriptome. *BMC Genomics*, 12, 60.
- HU, L., XU, S., PAN, C., ZOU, H. & JIANG, G. 2007. Preparation of a biochip on porous silicon and application for label-free detection of small molecule-protein interactions. *Rapid Communications in Mass Spectrometry*, 21, 1277-1281.
- HU, Y., LE LEU, R. K. & YOUNG, G. P. 2005. Sulindac corrects defective apoptosis and suppresses azoxymethane-induced colonic oncogenesis in p53 knockout mice. *International Journal of Cancer*, 116, 870-5.
- HUANG, C. L. & MIR, G. N. 1972. Pharmacological investigation of salivary gland of *Thais haemastoma* (Clench). *Toxicon*, 10, 111-117.

- HUNT, S. 1973. Fine structure of the secretory epithelium in the hypobranchial gland of the prosobranch gastropod mollusc *Buccinum undatum* L. *Journal of the Marine Biological Association of the United Kingdom*, 53, 59-71.
- IDLER, D. R. & WISEMAN, P. 1971. Sterols of molluscs. *International Journal of Biochemistry*, 2, 516-528.
- IGOSHEVA, N., LORZ, C., O'CONNOR, E., GLOVER, V. & MEHMET, H. 2005. Isatin, an endogenous monoamine oxidase inhibitor, triggers a dose- and time-dependent switch from apoptosis to necrosis in human neuroblastoma cells. *Neurochemistry International*, 47, 216-224.
- IMAI, T., TANABE, K., KATO, T. & FUKUSHIMA, K. 2005. Localization of ferruginol, a diterpene phenol, in *Cryptomeria japonica* heartwood by time-of-flight secondary ion mass spectrometry. *Planta*, 221, 549-556.
- IVANISEVIC, J., THOMAS, O. P., PEDEL, L., PÉNEZ, N., ERESKOVSKY, A. V., CULIOLI, G. & PÉREZ, T. 2011. Biochemical trade-offs: evidence for ecologically linked secondary metabolism of the sponge *Oscarella balibalo*. *PLoS ONE*, 6, e28059.
- JANNUN, R. & COE, E. L. 1987. Bromoperoxidase from the marine snail, *Murex trunculus*. *Comparative Biochemistry and Physiology B: Biochemical Molecular Biology*, 88, 917-922.
- JARZĘBSKI, A., WENNE, R. & HABERMEHL, G. 1986. Anatomical distribution of lipids and sterols in *Macoma balthica* (L.). *Comparative Biochemistry and Physiology B: Biochemistry and Molecular Biology*, 85, 135-137.
- JENSEN, B. S., JORGENSEN, T. D., AHRING, P. K., CHRISTOPHERSEN, P., STROBAEK, D., TEUBER, L. & OLESEN, S. P. 1998. *Use of isatin derivatives as ion channel activating agents*. Denmark patent application PCT/DK99/00679.

- KAMIYA, H., SAKAI, R. & JIMBO, M. 2006. Bioactive molecules from sea hares.  
*In: CIMINO, G. & GAVAGNIN, M. (eds.) Molluscs from chemo-ecological study to biotechnological application.* Berlin Heidelberg, Germany: Springer.
- KARHUNEN, T., AIRAKSINEN, M. S., TUOMISTO, L. & PANULA, P. 1993.  
Neurotransmitters in the nervous system of *Macoma balthica* (Bivalvia). *The Journal of Comparative Neurology*, 334, 477-88.
- KARLIN, A. 2002. Emerging structure of the Nicotinic Acetylcholine receptors.  
*Nature Reviews Neuroscience*, 3, 102-114.
- KAUSHIK, N. K., KAUSHIK, N., ATTRI, P., KUMAR, N., CHUNG HYEOK KIM, VERMA, A. K. & EUN HA CHOI 2013. Biomedical importance of indoles. *Molecules*, 18, 6620-6662.
- KAWASHIMA, Y., NAGASHIMA, Y. & SHIOMI, K. 2004. Determination of tetramine in marine gastropods by liquid chromatography/electrospray ionization-mass spectrometry. *Toxicon*, 44, 185-191.
- KELLEY, W. P., WOLTERS, A. M., SACK, J. T., JOCKUSCH, R. A., JURCHEN, J. C., WILLIAMS, E. R., SWEEDLER, J. V. & GILLY, W. F. 2003.  
Characterization of a novel gastropod toxin (6-Bromo-2-mercaptotryptamine) that inhibits shaker K channel activity. *Journal of Biological Chemistry*, 278, 34934-34942.
- KESKI-RAHKONEN, P., LEHTONEN, M., IHALAINEN, J., SARAJARVI, T. & AURIOLA, S. 2007. Quantitative determination of acetylcholine in microdialysis samples using liquid chromatography/atmospheric pressure spray ionization mass spectrometry. *Rapid Communications in Mass Spectrometry*, 21, 2933-43.

- KEYL, M. J. & WHITTAKER, V. P. 1958. Some pharmacological properties of murexine (urocanoylcholine). *British Journal of Pharmacology and Chemotherapy*, 13, 103-6.
- KING, J. W. 2000. Sub- and supercritical fluid processing of agrimaterials: Extraction, fractionation and reaction modes. *Supercritical Fluids*, 366, 451-488.
- KLITGAARD, A., IVERSEN, A., ANDERSEN, M. R., LARSEN, T. O., FRISVAD, J. C. & NIELSEN, K. F. 2014. Aggressive dereplication using UHPLC-DAD-QTOF: screening extracts for up to 3000 fungal secondary metabolites. *Analytical and Bioanalytical Chemistry*, 406, 1933-43.
- KOCHANOWSKA-KARAMYAN, A. J. & HAMANN, M. T. 2010. Marine indole alkaloids: potential new drug leads for the control of depression and anxiety. *Chemical Reviews*, 110, 4489-4497.
- KRACIKOVA, M., AKIRI, G., GEORGE, A., SACHIDANANDAM, R. & AARONSON, S. A. 2013. A threshold mechanism mediates p53 cell fate decision between growth arrest and apoptosis. *Cell Death and Differentiation*, 20, 576-588.
- KROISS, J., KALTENPOTH, M., SCHNEIDER, B., SCHWINGER, M. G., HERTWECK, C., MADDULA, R. K., STROHM, E. & SVATOS, A. 2010. Symbiotic streptomycetes provide antibiotic combination prophylaxis for wasp offspring. *Nature Chemical Biology*, 6, 261-263.
- KRUSE, R. A., RUBAKHIN, S. S., ROMANOVA, E. V., BOHN, P. W. & SWEEDLER, J. V. 2001. Direct assay of *Aplysia* tissues and cells with laser desorption/ionization mass spectrometry on porous silicon. *Journal of Mass Spectrometry*, 36, 1317-1322.

- LAFFY, P. W., BENKENDORFF, K. & ABBOTT, C. A. 2013. Suppressive subtractive hybridisation transcriptomics provides a novel insight into the functional role of the hypobranchial gland in a marine mollusc. *Comparative Biochemistry and Physiology D-Genomics & Proteomics*, 8, 111-122.
- LAFLEUR, K., HARRISON, J., MANTONE, D., CARROLL, M. & CATAPANE, E. 2014. The presence of histamine in ganglia and tissues of the bivalve mollusc, *Crassostrea virginica*. *The FASEB Journal*, 28.
- LANE, A. L., NYADONG, L., GALHENA, A. S., SHEARER, T. L., STOUT, E. P., PARRY, R. M., KWASNIK, M., WANG, M. D., HAY, M. E., FERNANDEZ, F. M. & KUBANEK, J. 2009. Desorption electrospray ionization mass spectrometry reveals surface-mediated antifungal chemical defense of a tropical seaweed. *Proceedings of the National Academy of Sciences of the United States of America*, 106, 7314-7319.
- LASKIN, J., HEATH, B. S., ROACH, P. J., CAZARES, L. & SEMMES, O. J. 2012. Tissue imaging using nanospray desorption electrospray ionization mass spectrometry. *Analytical chemistry*, 84, 141-8.
- LE LEU, R. K., BROWN, I. L., HU, Y. & YOUNG, G. P. 2003a. Effect of resistant starch on genotoxin-induced apoptosis, colonic epithelium, and luminal contents in rats. *Carcinogenesis*, 24, 1347-52.
- LE LEU, R. K., BROWN, I. L., HU, Y. & YOUNG, G. P. 2003b. Effect of resistant starch on genotoxin-induced apoptosis, colonic epithelium, and luminal contents in rats. *Carcinogenesis*, 24, 1347-1352.
- LEAL, M. C., PUGA, J., SERODIO, J., GOMES, N. C. & CALADO, R. 2012. Trends in the discovery of new marine natural products from invertebrates over the last two decades--where and what are we bioprospecting? *PLoS One*, 7, e30580.

- LEIVA, G. E. & CASTILLA, J. C. 2001. A review of the world marine gastropod fishery: evolution of catches, management and the Chilean experience. *Reviews in Fish Biology and Fisheries*, 11, 283-300.
- LEVÊQUE, D. & JEHL, F. 2007. Molecular pharmacokinetics of catharanthus (vinca) alkaloids. *The Journal of Clinical Pharmacology*, 47, 579-588.
- LEWIS, D. F. V. 2000. Structural characteristics of human P450s involved in drug metabolism: QSARs and lipophilicity profiles. *Toxicology*, 144, 197-203.
- LEWIS, R. J., DUTERTRE, S., VETTER, I. & CHRISTIE, M. J. 2012. *Conus* venom peptide pharmacology. *Pharmacological Reviews*, 64, 259-98.
- LEWIS, W. G., SHEN, Z., FINN, M. G. & SIUZDAK, G. 2003. Desorption/ionization on silicon (DIOS) mass spectrometry: background and applications. *International Journal of Mass Spectrometry*, 226, 107-116.
- LIM, N. S. H., EVERUSS, K. J., GOODMAN, A. E. & BENKENDORFF, K. 2007. Comparison of surface microfouling and bacterial attachment on the egg capsules of two molluscan species representing Cephalopoda and Neogastropoda. *Aquatic Microbial Ecology*, 47, 275-287.
- LINDQUIST, N. & HAY, M. E. 1996. Palatability and chemical defense of marine invertebrate larvae. *Ecological Monographs*, 66, 431-450.
- LIU, Q., GUO, Z. & HE, L. 2007. Mass spectrometry imaging of small molecules using desorption/ionization on silicon. *Analytical Chemistry*, 79, 3535-41.
- LLEWELLYN, L. E. & BURNELL, J. N. 2000. Marine organisms as sources of C4-weed-specific herbicides. *Pesticide Outlook*, 11, 64-67.
- LOH, T. L. & PAWLIK, J. R. 2014. Chemical defenses and resource trade-offs structure sponge communities on Caribbean coral reefs. *Proceedings of the National Academy of Sciences of the United States of America*, 111, 4151-6.

- LOWE, R. D., GUILD, G. E., HARPAS, P., KIRKBRIDE, P., HOFFMANN, P.,  
VOELCKER, N. H. & KOBUS, H. 2009. Rapid drug detection in oral  
samples by porous silicon assisted laser desorption/ionization mass  
spectrometry. *Rapid Communications in Mass Spectrometry*, 23, 3543-8.
- LOWE, R. D., SZILI, E. J., KIRKBRIDE, P., THISSEN, H., SIUZDAK, G. &  
VOELCKER, N. H. 2010. Combined immunocapture and laser  
desorption/ionization mass spectrometry on porous silicon. *Analytical  
Chemistry*, 82, 4201–4208.
- LUESCH, H., MOORE, R. E., PAUL, V. J., MOOBERRY, S. L. & CORBETT, T.  
H. 2001. Isolation of Dolastatin 10 from the Marine Cyanobacterium  
Symploca Species VP642 and Total Stereochemistry and Biological  
Evaluation of Its Analogue Symplostatin 1. *Journal of Natural Products*, 64,  
907-910.
- MARCELO ZALDINI, H., SUELLEN MELO, T. C., DIOGO RODRIGO, M. M.,  
WALTER FILGUEIRA DE AZEVEDO, J. & ANA CRISTINA LIMA, L.  
2010. Halogen atoms in the modern medicinal chemistry: hints for the drug  
design. *Current Drug Targets*, 11, 303-314.
- MARIN, A. & ROS, J. 2004. Chemical defenses in sacoglossan opisthobranchs:  
taxonomic trends and evolutionary implications. *Scientia Marina*, 68, 227-  
241.
- MARSHALL, J., KELLEY, W. P., RUBAKHIN, S. S., BINGHAM, J. P.,  
SWEEDLER, J. V. & GILLY, W. F. 2002. Anatomical correlates of venom  
production in *Conus californicus*. *The Biological Bulletin*, 203, 27-41.
- MARTHY, H. J., HAUSER, R. & SCHOLL, A. 1976. Natural tranquilizer in  
cephalopod eggs. *Nature*, 261, 496-497.

- MARTINS, A., VIEIRA, H., GASPAR, H. & SANTOS, S. 2014. Marketed marine natural products in the pharmaceutical and cosmeceutical industries: tips for success. *Marine Drugs*, 12, 1066-101.
- MATKOWSKYJ, K. A., MARRERO, J. A., CARROLL, R. E., DANILKOVICH, A. V., GREEN, R. M. & BENYA, R. V. 1999. Azoxymethane-induced fulminant hepatic failure in C57BL/6J mice: characterization of a new animal model. *The American Journal of Physiology*, 277, G455-62.
- MAYER, A., NGUYEN, D. & GLASER, K. 2015. The marine pharmacology and pharmaceuticals pipeline in 2014. *The FASEB Journal*, 29.
- MAYER, A. M. 2014. *Marine Pharmacology* [Online]. Marine pharmaceuticals: the preclinical pipeline. Available: [marinepharmacology.midwestern.edu/preclinPipeline.htm](http://marinepharmacology.midwestern.edu/preclinPipeline.htm) [Accessed 05/05/2014 2014].
- MAYER, A. M., RODRIGUEZ, A. D., BERLINCK, R. G. & FUSETANI, N. 2011. Marine pharmacology in 2007-8: Marine compounds with antibacterial, anticoagulant, antifungal, anti-inflammatory, antimalarial, antiprotozoal, antituberculosis, and antiviral activities; affecting the immune and nervous system, and other miscellaneous mechanisms of action. *Comparative Biochemistry and Physiology Part C: Toxicology & Pharmacology*, 153, 191-222.
- MCGOVERN, P. E. & MICHEL, R. H. 1985. Royal purple-dye - Tracing chemical origins of the industry. *Analytical Chemistry*, 57, 1514-&.
- MEDVEDEV, A. E., BUNEEVA, O. & GLOVER, V. 2007. Biological targets for isatin and its analogues: implications for therapy. *Biologics*, 1, 151-62.

- MEDVEDEV, A. E., SANDLER, M. & GLOVER, V. 1998. Interaction of isatin with type-A natriuretic peptide receptor: possible mechanism. *Life Sciences*, 62, 2391-8.
- MENDOLA, D. 2003. Aquaculture of three phyla of marine invertebrates to yield bioactive metabolites: process developments and economics. *Biomolecular Engineering*, 20, 441-58.
- MODICA, M. & HOLFORD, M. 2010. The Neogastropoda: evolutionary innovations of predatory marine snails with remarkable pharmacological potential. In: PONTAROTTI, P. (ed.) *Evolutionary Biology – Concepts, Molecular and Morphological Evolution*. Springer Berlin Heidelberg.
- MOLINSKI, T. F. 2010. NMR of natural products at the 'nanomole-scale'. *Natural Product Reports*, 27, 321-329.
- MOLINSKI, T. F., DALISAY, D. S., LIEVENS, S. L. & SALUDES, J. P. 2009. Drug development from marine natural products. *Nature Reviews Drug Discovery*, 8, 69-85.
- MUNRO, S. 2003. Lipid rafts: elusive or illusive? *Cell*, 115, 377-88.
- NAEGEL, L. C. A. & COOKSEY, C. J. 2002. Tyrian purple from marine muricids, especially from *Plicopurpura pansa* (Gould, 1853). *Journal of Shellfish Research*, 21, 193-200.
- NIU, S., ZHANG, W. & CHAIT, B. T. 1998. Direct comparison of infrared and ultraviolet wavelength matrix-assisted laser desorption/ionization mass spectrometry of proteins. *Journal of the American Society for Mass Spectrometry*, 9, 1-7.
- NOBLE, W. J., BENKENDORFF, K. & HARRIS, J. O. 2013. Growth, settlement and survival of *Dicathais orbita* (Neogastropoda, Mollusca) larvae in

- response to temperature, diet and settlement cues. *Aquaculture Research*, 46, 1455-1468.
- NOBLE, W. J., COCKS, R. R., HARRIS, J. O. & BENKENDORFF, K. 2009. Application of anaesthetics for sex identification and bioactive compound recovery from wild *Dicathais orbita*. *Journal of Experimental Marine Biology and Ecology*, 380, 53-60.
- NYSKOHUS, L. S., WATSON, A. J., MARGISON, G. P., LE LEU, R. K., KIM, S. W., LOCKETT, T. J., HEAD, R. J., YOUNG, G. P. & HU, Y. 2013. Repair and removal of azoxymethane-induced O6-methylguanine in rat colon by O6-methylguanine DNA methyltransferase and apoptosis. *Mutation Research*, 758, 80-6.
- OKINO, T., YOSHIMURA, E., HIROTA, H. & FUSETANI, N. 1996. New antifouling sesquiterpenes from four nudibranchs of the family Phyllidiidae. *Tetrahedron*, 52, 9447-9454.
- OLIVERA, B. M. 2006. Conus peptides: biodiversity-based discovery and exogenomics. *Journal of Biological Chemistry*, 281, 31173-31177.
- OLIVERA, B. M., RIVIER, J., CLARK, C., RAMILO, C. A., CORPUZ, G. P., ABOGADIE, F. C., MENA, E. E., WOODWARD, S. R., HILLYARD, D. R. & CRUZ, L. J. 1990. Diversity of *Conus* neuropeptides. *Science*, 249, 257-63.
- OLIVERIO, M., BARCO, A., MODICA, M. V., RICHTER, A. & MARIOTTINI, P. 2009. Ecological barcoding of corallivory by second internal transcribed spacer sequences: hosts of coralliophiline gastropods detected by the cnidarian DNA in their stomach. *Molecular Ecology Resources*, 9, 94-103.
- OLIVERIO, M. & MODICA, M. V. 2010. Relationships of the haematophagous marine snail *Colubraria* (Rachiglossa: Colubrariidae), within the

- neogastropod phylogenetic framework. *Zoological Journal of the Linnean Society*, 158, 779-800.
- OSTROWSKI, S. G., VAN BELL, C. T., WINOGRAD, N. & EWING, A. G. 2004. Mass spectrometric imaging of highly curved membranes during *Tetrahymena* mating. *Science*, 305, 71.
- PACHOLSKI, M. L. & WINOGRAD, N. 1999. Imaging with mass spectrometry. *Chemical Reviews*, 99, 2977-3006.
- PALMA, H., PAREDES, J. & CRISTI, E. 1999. 6,6'-dibromoindigotin en capsulas de embriones di *Concholepas concholepas* (Bruguiere, 1789). *Medio Ambiente*, 11, 93-95.
- PASSARELLI, M. K., EWING, A. G. & WINOGRAD, N. 2013. Single-cell lipidomics: characterizing and imaging lipids on the surface of individual *Aplysia californica* neurons with cluster secondary ion mass spectrometry. *Analytical Chemistry*, 85, 2231-2238.
- PASTORINO, G. & SCARABINO, F. 2008. Two new deep-sea muricids (Gastropoda) from Argentina. *The Nautilus*, 122, 107-114.
- PATTI, G. J., WOO, H. K., YANES, O., SHRIVER, L., THOMAS, D., URITBOONTHAI, W., APON, J. V., STEENWYK, R., MANCHESTER, M. & SIUZDAK, G. 2010. Detection of carbohydrates and steroids by cation-enhanced nanostructure-initiator mass spectrometry (NIMS) for biofluid analysis and tissue imaging. *Analytical Chemistry*, 82, 121-128.
- PAUL, V. J., ARTHUR, K. E., RITSON-WILLIAMS, R., ROSS, C. & SHARP, K. 2007. Chemical defenses: from compounds to communities. *The Biological Bulletin*, 213, 226-51.
- PAUL, V. J., RITSON-WILLIAMS, R. & SHARP, K. 2011. Marine chemical ecology in benthic environments. *Natural Product Reports*, 28, 345-387.

- PAULETTI, P. M., CINTRA, L. S., BRAGUINE, C. G., DA SILVA FILHO, A. A., SILVA, M. L. A. E., CUNHA, W. R. & JANUÁRIO, A. H. 2010a. Halogenated indole alkaloids from marine invertebrates. *Marine Drugs*, 8, 1526-1549.
- PAULETTI, P. M., CINTRA, L. S., BRAGUINE, C. G., FILHO, A. A., SILVA, M. L. A., CUNHA, W. R. & JANUÁRIO, A. H. 2010b. Halogenated indole alkaloids from marine invertebrates. *Marine Drugs*, 8, 1526-1549.
- PAWLIK, J. R. 1993. Marine invertebrate chemical defenses. *Chemical Reviews*, 93, 1911-1922.
- PAWLIK, J. R., LOH, T. L., MCMURRAY, S. E. & FINELLI, C. M. 2013. Sponge communities on Caribbean coral reefs are structured by factors that are top-down, not bottom-up. *PLoS One*, 8, e62573.
- PEREIRA, R., ANDRADE, P. & VALENTÃO, P. 2016. Chemical diversity and biological properties of secondary metabolites from sea hares of *Aplysia* genus. *Marine Drugs*, 14, 39.
- PETTIT, G. R. 1997. The Dolastatins. In: HERZ, W., KIRBY, G. W., MOORE, R. E., STEGLICH, W. & TAMM, C. (eds.) *Fortschritte der Chemie organischer Naturstoffe Progress in the Chemistry of Organic Natural Products*. Springer Vienna.
- PETTIT, G. R., KAMANO, Y., HERALD, C. L., TUINMAN, A. A., BOETTNER, F. E., KIZU, H., SCHMIDT, J. M., BACZYNSKYJ, L., TOMER, K. B. & BONTEMS, R. J. 1987. Antineoplastic Agents .136. The Isolation and Structure of a Remarkable Marine Animal Antineoplastic Constituent - Dolastatin 10. *Journal of the American Chemical Society*, 109, 6883-6885.

- PHILLIPS, B. F. 1969. The population ecology of the whelk *Dicathais aegrota* in Western Australia. *Australian Journal of Marine and Freshwater Research*, 20, 225-265.
- PHILLIPS, B. F. & CAMPBELL, N. A. 1974. Mortality and longevity in the whelk *Dicathais orbita* (Gmelin). *Marine and Freshwater Research*, 25, 25-33.
- POHNERT, G., STEINKE, M. & TOLLRIAN, R. 2007. Chemical cues, defence metabolites and the shaping of pelagic interspecific interactions. *Trends in Ecology & Evolution*, 22, 198-204.
- PONDER, W. 1998. Family Muricidae. In: BEESLEY, P. L., ROSS, G. J. B. & WELLS, A. (eds.) *Mollusca: the southern synthesis* Melbourne: CSIRO.
- POVEY, A. C., BADAWI, A. F., COOPER, D. P., HALL, C. N., HARRISON, K. L., JACKSON, P. E., LEES, N. P., O'CONNOR, P. J. & MARGISON, G. P. 2002. DNA alkylation and repair in the large bowel: animal and human studies. *The journal of Nutrition*, 132, 3518s-3521s.
- POWER, A. J., KEEGAN, B. F. & NOLAN, K. 2002. The seasonality and role of the neurotoxin tetramine in the salivary glands of the red whelk *Neptunea antiqua* (L.). *Toxicon*, 40, 419-425.
- PRZESLAWSKI, R., BENKENDORFF, K. & DAVIS, A. R. 2005. A quantitative survey of mycosporine-like amino acids (MAAS) in intertidal egg masses from temperate rocky shores. *Journal of Chemical Ecology*, 31, 2417-2438.
- RAMASAMY, M. S. & MURUGAN, A. 2005. Potential antimicrobial activity of marine molluscs from tuticorin, southeast coast of India against 40 biofilm bacteria. *Journal of Shellfish Research*, 24, 243(9).
- RAMON, M. & AMOR, M. J. 2001. Increasing imposex in populations of *Bolinus brandaris* (Gastropoda: Muricidae) in the northwestern Mediterranean. *Marine Environmental Research*, 52, 463-75.

- RAVEENDRAN, P., IKUSHIMA, Y. & WALLEN, S. L. 2005. Polar attributes of supercritical carbon dioxide. *Accounts of Chemical Research*, 38, 478-485.
- REVERCHON, E. & DE MARCO, I. 2006. Supercritical fluid extraction and fractionation of natural matter. *Journal of Supercritical Fluids*, 38, 146-166.
- REYNOLDS, L., GARDECKI, J. A., FRANKLAND, S. J. V., HORNG, M. L. & MARONCELLI, M. 1996. Dipole solvation in nondipolar solvents: Experimental studies of reorganization energies and solvation dynamics. *Journal of Physical Chemistry*, 100, 10337-10354.
- RICHARD, D. M., DAWES, M. A., MATHIAS, C. W., ACHESON, A., HILL-KAPTURCZAK, N. & DOUGHERTY, D. M. 2009. L-Tryptophan: basic metabolic functions, behavioral research and therapeutic indications. *International Journal of Tryptophan Research*, 2, 45-60.
- RODRIGUES, T., MOREIRA, R., GUEDES, R. C., ILEY, J. & LOPES, F. 2008. Unanticipated acyloxymethylation of sumatriptan indole nitrogen atom and its implication in prodrug design. *Archiv der Pharmazie*, 341, 344-350.
- ROGERS, C. N., NYS, R. & STEINBERG, P. D. 2002. Effects of algal diet on the performance and susceptibility to predation of the sea hare *Aplysia parvula*. *Marine Ecology Progress Series*, 236, 241-254.
- ROLLER, R. A., RICKETT, J. D. & STICKLE, W. B. 1995. The hypobranchial gland of the estuarine snail *Stramonita haemastoma canaiculata* (Gray) (Prosobranchia, Muricidae) - a light and electron-microscopic study. *American Malacological Bulletin*, 11, 177-190.
- ROMERO, M. S., GALLARDO, C. S. & BELLOLIO, G. 2004. Egg laying and embryonic-larval development in the snail *Thais (stramonita) chocolata* (Duclos, 1832) with observations on its evolutionary relationships within the Muricidae. *Marine Biology*, 145, 681-692.

- RONCI, M., RUDD, D., GUINAN, T., BENKENDORFF, K. & VOELCKER, N. H. 2012. Mass spectrometry imaging on porous silicon: investigating the distribution of bioactives in the marine mollusc tissues. *Analytical Chemistry*, 84, 8996-9001.
- ROSEGHINI, M., ERSPAMER, V., RAMORINO, L. & GUTIERREZ, J. E. 1970. Choline esters, their precursors and metabolites in the hypobranchial gland of prosobranchiate molluscs, *Concholepas concholepas* and *Thais chocolata*. *European Journal of Biochemistry FEBS*, 12, 468-73.
- ROSEGHINI, M., SEVERINI, C., ERSPAMER, G. F. & ERSPAMER, V. 1996. Choline esters and biogenic amines in the hypobranchial gland of 55 molluscan species of the neogastropod Muricoidea superfamily. *Toxicon*, 34, 33-55.
- RUDD, D. & BENKENDORFF, K. 2014. Supercritical CO<sub>2</sub> extraction of bioactive Tyrian purple precursors from the hypobranchial gland of a marine gastropod. *The Journal of Supercritical Fluids*, 94, 1-7.
- RUDD, D., BENKENDORFF, K. & VOELCKER, N. H. 2015a. Solvent separating secondary metabolites directly from biosynthetic tissue for surface-assisted laser desorption ionisation mass spectrometry. *Marine Drugs*, 13, 1410-1431.
- RUDD, D., RONCI, M., JOHNSTON, M. R., GUINAN, T., VOELCKER, N. H. & BENKENDORFF, K. 2015b. Mass spectrometry imaging reveals new biological roles for choline esters and Tyrian purple precursors in muricid molluscs. *Scientific Reports*, 5, 13408.
- SAITO, K., MITSUTANI, T., IMAI, T., MATSUSHITA, Y. & FUKUSHIMA, K. 2008. Discriminating the indistinguishable sapwood from heartwood in discolored ancient wood by direct molecular mapping of specific extractives

using time-of-flight secondary ion mass spectrometry. *Analytical chemistry*, 80, 1552-7.

SALCEDO, M., CUEVAS, C., ALONSO, J. L., OTERO, G., FAIRCLOTH, G., FERNANDEZ-SOUSA, J. M., AVILA, J. & WANDOSELL, F. 2007. The marine sphingolipid-derived compound ES 285 triggers an atypical cell death pathway. *Apoptosis*, 12, 395-409.

SANTOS, M. C., WAGNER, M., WU, B., SCHEIDER, J., OEHLMANN, J., CADORE, S. & BECKER, J. S. 2009. Biomonitoring of metal contamination in a marine prosobranch snail (*Nassarius reticulatus*) by imaging laser ablation inductively coupled plasma mass spectrometry (LA-ICP-MS). *Talanta*, 80, 428-433.

SCHAPIRA, M., ABAGYAN, R. & TOTROV, M. 2002. Structural model of nicotinic acetylcholine receptor isotypes bound to acetylcholine and nicotine. *BMC Structural Biology*, 2, 1.

SCHATZ, P. F. 2001. Indigo and Tyrian purple - In nature and in the lab. *Journal of Chemical Education*, 78, 1442-1443.

SCHOENIAN, I., SPITELLER, M., GHASTE, M., WIRTH, R., HERZ, H. & SPITELLER, D. 2011. Chemical basis of the synergism and antagonism in microbial communities in the nests of leaf-cutting ants. *Proceedings of the National Academy of Sciences of the United States of America*, 108, 1955-1960.

SCHONE, C., HOFER, H. & WALCH, A. 2013. MALDI imaging mass spectrometry in cancer research: combining proteomic profiling and histological evaluation. *Clin Biochem*, 46, 539-45.

- SCHWAMBORN, K. & CAPRIOLI, R. M. 2010. Molecular imaging by mass spectrometry — looking beyond classical histology. *Nat Rev Cancer*, 10, 639-646.
- SENER, P. D. & SIEVERS, E. L. 2012. The discovery and development of brentuximab vedotin for use in relapsed Hodgkin lymphoma and systemic anaplastic large cell lymphoma. *Nature Biotechnology*, 30, 631-7.
- SHARIATGORJI, M., SVENNINGSSON, P. & ANDREN, P. E. 2014. Mass spectrometry imaging, an emerging technology in neuropsychopharmacology. *Neuropsychopharmacology*, 39, 34-49.
- SHEN, Z., THOMAS, J. J., AVERBUJ, C., BROO, K. M., ENGELHARD, M., CROWELL, J. E., FINN, M. G. & SIUZDAK, G. 2001. Porous silicon as a versatile platform for laser desorption/ionization mass spectrometry. *Analytical Chemistry*, 73, 612-619.
- SHIOMI, K., ISHII, M., SHIMAKURA, K., NAGASHIMA, Y. & CHINO, M. 1998. Tigloylcholine: A new choline ester toxin from the hypobranchial gland of two species of muricid gastropods (*Thais clavigera* and *Thais bronni*). *Toxicon*, 36, 795-798.
- SIMMONS, T. L., COATES, R. C., CLARK, B. R., ENGENE, N., GONZALEZ, D., ESQUENAZI, E., DORRESTEIN, P. C. & GERWICK, W. H. 2008. Biosynthetic origin of natural products isolated from marine microorganism-invertebrate assemblages. *Proceedings of the National Academy of Sciences of the United States of America*, 105, 4587-4594.
- ŠKRÁŠKOVÁ, K. & HEEREN, R. M. A. 2013. A review of complementary separation methods and matrix assisted laser desorption ionization-mass spectrometry imaging: Lowering sample complexity. *Journal of Chromatography A*, 1319, 1-13.

- SOMERVILLE, M. J., MOLLO, E., CIMINO, G., RUNGPRON, W. & GARSON, M. J. 2006. Spongian diterpenes from Australian nudibranchs: an anatomically guided chemical study of *Glossodoris atromarginata*. *Journal of Natural Products*, 69, 1086-1088.
- SRILAKSHMI, G. 1991. The hypobranchial gland in *Morula Granulata* (Gastropoda: Prosobranchia). *Journal of the Marine Biological Association of the United Kingdom*, 71, 623-634.
- STERMAN, B. & STERMAN, J. 2012. *The Rarest Blue*, Connecticut, Lyons Press.
- STEWART, M. P. & BURIK, J. M. 2000. Chemical and biological applications of porous silicon technology. *Advanced Materials*, 12, 859-869.
- SUAREZ, Y., GONZALEZ, L., CUADRADO, A., BERCIANO, M., LAFARGA, M. & MUNOZ, A. 2003. Kahalalide F, a new marine-derived compound, induces oncosis in human prostate and breast cancer cells. *Molecular Cancer Therapeutics*, 2, 863-872.
- SUCIATI, LAMBERT, L. K. & GARSON, M. J. 2011. Structures and anatomical distribution of oxygenated diterpenes in the Australian nudibranch *Chromodoris reticulata*. *Australian Journal of Chemistry*, 64, 757-765.
- SVATOS, A. 2010. Mass spectrometric imaging of small molecules. *Trends in Biotechnology*, 28, 425-34.
- SWANSON, R. L., WILLIAMSON, J. E., DE NYS, R., KUMAR, N., BUCKNALL, M. P. & STEINBERG, P. D. 2004. Induction of settlement of larvae of the sea urchin *Holopneustes purpurascens* by histamine from a host alga. *The Biological Bulletin*, 206, 161-172.
- SZEKELY, T. & GAILLARD, A. 2007. Conserving biodiversity using patent law. *Nature Biotechnology*, 25, 1087-1088.

- TATA, A., FERNANDES, A. M., SANTOS, V. G., ALBERICI, R. M., ARALDI, D., PARADA, C. A., BRAGUINI, W., VERONEZ, L., SILVA BISSON, G., REIS, F. H., ALBERICI, L. C. & EBERLIN, M. N. 2012. Nanoassisted laser desorption-ionization-MS imaging of tumors. *Analytical Chemistry*, 84, 6341-5.
- TEICHERT, R. W., JIMENEZ, E. C. & OLIVERA, B. M. 2005. Alpha S-conotoxin RVIIIA: a structurally unique conotoxin that broadly targets nicotinic acetylcholine receptors. *Biochemistry*, 44, 7897-902.
- THOMAS, J. J., SHEN, Z., CROWELL, J. E., FINN, M. G. & SIUZDAK, G. 2001. Desorption/ionization on silicon (DIOS): A diverse mass spectrometry platform for protein characterization. *Proceedings of the National Academy of Sciences*, 98, 4932-4937.
- TRAUGER, S. A., GO, E. P., SHEN, Z., APON, J. V., COMPTON, B. J., BOUVIER, E. S., FINN, M. G. & SIUZDAK, G. 2004. High sensitivity and analyte capture with desorption/ionization mass spectrometry on silylated porous silicon. *Analytical Chemistry*, 76, 4484-9.
- TYLER, B. J., RANGARANJAN, S., MÖLLER, J., BEUMER, A. & ARLINGHAUS, H. F. 2006. TOF-SIMS imaging of chlorhexidine-digluconate transport in frozen hydrated biofilms of the fungus *Candida albicans*. *Applied Surface Science*, 252, 6712-6715.
- VAIDYANATHAN, S., FLETCHER, J. S., GOODACRE, R., LOCKYER, N. P., MICKLEFIELD, J. & VICKERMAN, J. C. 2008. Subsurface biomolecular imaging of *Streptomyces coelicolor* using secondary ion mass spectrometry. *Analytical Chemistry*, 80, 1942-51.
- VANCHA, A., GOVINDARAJU, S., PARSA, K., JASTI, M., GONZALEZ-GARCIA, M. & BALLESTERO, R. 2004. Use of polyethyleneimine polymer

in cell culture as attachment factor and lipofection enhancer. *BMC Biotechnology*, 4, 23.

VESTAL, M. L. & CAMPBELL, J. M. 2005. Tandem time-of-flight mass spectrometry. *In: BURLINGAME, A. L. (ed.) Methods in Enzymology*. Academic Press.

VIDOVÁ, V., NOVÁK, P., STROHALM, M., PÓL, J., HAVLÍČEK, V. R. & VOLNÝ, M. 2010. Laser desorption-ionization of lipid transfers: tissue mass spectrometry imaging without MALDI matrix. *Analytical Chemistry*, 82, 4994-4997.

VINE, K., LOCKE, J., RANSON, M., BENKENDORFF, K., PYNE, S. & BREMNER, J. 2007. In vitro cytotoxicity evaluation of some substituted isatin derivatives. . *Bioorganic & Medicinal Chemistry*, 15, 931-938.

VINE, K. L. 2002. *An investigation into the cytotoxic properties of isatin-derived compounds: potential use in targeted cancer therapy*. Doctor of Philosophy Doctoral, University of Wollongong.

WAGELE, H., BALLESTEROS, M. & AVILA, C. 2006. Defensive glandular structures in opisthobranch molluscs - From histology to ecology. *Oceanography and Marine Biology - an Annual Review, Vol 44*, 44, 197-276.

WAKIMOTO, T., KONDO, H., NII, H., KIMURA, K., EGAMI, Y., OKA, Y., YOSHIDA, M., KIDA, E., YE, Y. P., AKAHOSHI, S., ASAKAW, T., MATSUMURA, K., ISHIDA, H., NUKAYA, H., TSUJI, K., KAN, T. & ABE, I. 2011. Furan fatty acid as an anti-inflammatory component from the green-lipped mussel *Perna canaliculus*. *Proceedings of the National Academy of Sciences of the United States of America*, 108, 17533-17537.

WANG, S.-Q., CHENG, L.-S., LIU, Y., WANG, J.-Y. & JIANG, W. 2016. Indole-3-Carbinol (I3C) and its Major Derivatives: Their Pharmacokinetics and

- Important Roles in Hepatic Protection. *Current drug metabolism*, 17, 401-409.
- WATJEN, F., DREJER, J. & JENSEN, L. H. 1995. *Isatin derivatives, their preparation and use*. Denmark patent application 90123474.0.
- WATROUS, J., HENDRICKS, N., MEEHAN, M. & DORRESTEIN, P. C. 2010. Capturing bacterial metabolic exchange using thin film desorption electrospray ionization-imaging mass spectrometry. *Analytical Chemistry*, 82, 1598-600.
- WATROUS, J., ROACH, P., HEATH, B., ALEXANDROV, T., LASKIN, J. & DORRESTEIN, P. C. 2013. Metabolic profiling directly from the petri dish using nanospray desorption electrospray ionization imaging mass spectrometry. *Analytical Chemistry*, 85, 10385-10391.
- WATROUS, J. D. & DORRESTEIN, P. C. 2011. Imaging mass spectrometry in microbiology. *Nature Reviews Microbiology*, 9, 683-94.
- WEI, J., BURIK, J. M. & SIUZDAK, G. 1999. Desorption-ionization mass spectrometry on porous silicon. *Nature*, 399, 243-246.
- WEST, D. J., ANDREWS, E. B., BOWMAN, D., MCVEAN, A. R. & THORNDYKE, M. C. 1996. Toxins from some poisonous and venomous marine snails. *Comparative Biochemistry and Physiology Part C: Pharmacology, Toxicology and Endocrinology*, 113, 1-10.
- WESTLEY, C. 2008. *The distribution, biosynthetic origin and functional significance of Tyrian purple precursors in the Australian muricid *Dicathais orbita* (Neogastropoda: Muricidae)*. PhD Doctoral, Flinders University.
- WESTLEY, C. & BENKENDORFF, K. 2008. Sex-specific tyrian purple genesis: Precursor and pigment distribution in the reproductive system of the marine mollusc, *Dicathais orbita*. *Journal of Chemical Ecology*, 34, 44-56.

- WESTLEY, C. & BENKENDORFF, K. 2009a. The distribution of precursors and biosynthetic enzymes required for Tyrian purple genesis in the hypobranchial gland, gonoduct, and egg masses of *Dicathais orbita* (Gmelin, 1791) (Neogastropoda: Muricidae). *The Nautilus*, 123, 148-153.
- WESTLEY, C. B. & BENKENDORFF, K. 2009b. Histochemical correlations between egg capsule laminae and the female gonoduct reveal the process of capsule formation in the Muricidae (Neogastropoda: Mollusca). *Invertebrate Reproduction & Development*, 53, 59-59.
- WESTLEY, C. B., BENKENDORFF, K., MCIVER, C., R.K, L. L. & ABBOTT, C. A. 2013. Gastrointestinal and hepatotoxicity assessment of an anticancer extract from muricid molluscs. . *Evidence-Based Complementary and Alternative Medicine.*, 2013 Article ID 837370.
- WESTLEY, C. B., LEWIS, M. C. & BENKENDORFF, K. 2010a. Histomorphology of the female pallial gonoduct in *Dicathais orbita* (Neogastropoda, Muricidae): sperm passage, fertilization, and sperm storage potential. *Invertebrate Biology*, 129, 138-150.
- WESTLEY, C. B., LEWIS, M. C. & BENKENDORFF, K. 2010b. Histomorphology of the hypobranchial gland in *Dicathais orbita* (Gmelin, 1971) (Neogastropoda: Muricidae). *Journal of Molluscan Studies*, 76, 186-195.
- WESTLEY, C. B., MCIVER, C. M., ABBOTT, C. A., LE LEU, R. K. & BENKENDORFF, K. 2010c. Enhanced acute apoptotic response to azoxymethane-induced DNA damage in the rodent colonic epithelium by Tyrian purple precursors A potential colorectal cancer chemopreventative. *Cancer Biology & Therapy*, 9, 371-379.
- WESTLEY, C. B., VINE, K. L. & BENKENDORFF, K. 2006. A proposed functional role for indole derivatives in reproduction and defence of the

- Muricidae (Neogastropoda: Mollusca). *In*: MEIJER, L., GUYARD, N., SKALTSOUNIS, L. & EISENBRAND, G. (eds.) *Indirubin, the Red Shade of Indigo*. . Roscoff, France: "Life in Progress" Editions.
- WHITEHOUSE, M. W., MACRIDES, T. A., KALAFATIS, N., BETTS, W. H., HAYNES, D. R. & BROADBENT, J. 1997. Anti-inflammatory activity of a lipid fraction (lyprinol) from the NZ green-lipped mussel. *Inflammopharmacology*, 5, 237-46.
- WILLIAMS, D. H., STONE, M. J., HAUCK, P. R. & RAHMAN, S. K. 1989. Why are secondary metabolites (natural products) biosynthesized? *Journal of Natural Products*, 52, 1189-1208.
- WILLIAMS, E. A., CUMMINS, S. & DEGNAN, S. M. 2009. Settlement specifics: Effective induction of abalone settlement and metamorphosis corresponds to biomolecular composition of natural cues. *Communicative & Integrative Biology*, 2, 347-349.
- WILLIAMSON, P. T. F., VERHOEVEN, A., MILLER, K. W., MEIER, B. H. & WATTS, A. 2007. The conformation of acetylcholine at its target site in the membrane-embedded nicotinic acetylcholine receptor. *Proceedings of the National Academy of Sciences of the United States of America*, 104, 18031-18036.
- WISEMAN, H. & HALLIWELL, B. 1996. Damage to DNA by reactive oxygen and nitrogen species: role in inflammatory disease and progression to cancer. *Biochemical Journal*, 313, 17-29.
- WITSCHI, C. & DOELKER, E. 1997. Residual solvents in pharmaceutical products: Acceptable limits, influences on physicochemical properties, analytical methods and documented values. *European Journal of Pharmaceutics and Biopharmaceutics*, 43, 215-242.

- WOLYNIAK, C. J., BRENNAN, J. T., MURPHY, K. J. & SINCLAIR, A. J. 2005. Gas chromatography-chemical ionization-mass spectrometric fatty acid analysis of a commercial supercritical carbon dioxide lipid extract from New Zealand green-lipped mussel (*Perna canaliculus*). *Lipids*, 40, 355-360.
- WOOD, J. B., PENNOYER, K. E. & DERBY, C. D. 2008. Ink is a conspecific alarm cue in the Caribbean reef squid, *Sepioteuthis sepioidea*. *Journal of Experimental Marine Biology and Ecology*, 367, 11-16.
- WOODCOCK, S. H. & BENKENDORFF, K. 2008. The impact of diet on the growth and proximate composition of juvenile whelks, *Dicathais orbita* (Gastropoda: Mollusca). *Aquaculture*, 276, 162-170.
- YANES, O., WOO, H. K., NORTHERN, T. R., OPPENHEIMER, S. R., SHRIVER, L., APON, J., ESTRADA, M. N., POTCHOIBA, M. J., STEENWYK, R., MANCHESTER, M. & SIUZDAK, G. 2009. Nanostructure initiator mass spectrometry: tissue imaging and direct biofluid analysis. *Analytical Chemistry*, 81, 2969-2975.
- YANG, Y. L., XU, Y. Q., STRAIGHT, P. & DORRESTEIN, P. C. 2009. Translating metabolic exchange with imaging mass spectrometry. *Nature Chemical Biology*, 5, 885-887.
- YARNOLD, J. E., HAMILTON, B. R., WELSH, D. T., POOL, G. F., VENTER, D. J. & CARROLL, A. R. 2012. High resolution spatial mapping of brominated pyrrole-2-aminoimidazole alkaloids distributions in the marine sponge *Stylissa flabellata* via MALDI-mass spectrometry imaging. *Molecular BioSystems*, 8, 2249-2259.
- YAZBACK, R., LINDSAY, R., ABBOTT, C. A., BENKENDORFF, K. & HOWARTH, G. S. 2015. Combined effects of muricid extract and 5-

fluorouracil on intestinal toxicity in rats. *Cancer Biology and Therapy*, In review.

YONG-JIN WU 2010. New indole-containing medicinal compounds. *In: GRIBBLE, G. W. (ed.) Heterocyclic Scaffolds II: Reactions and Applications of Indoles*. Heidelberg, Germany: Springer.

ZATYLNÝ, C., MARVIN, L., GAGNON, J. & HENRY, J. 2002. Fertilization in *Sepia officinalis*: the first mollusk sperm-attracting peptide. *Biochemical and Biophysical Research Communications*, 296, 1186-93.

ZHONG, W., GALLIVAN, J. P., ZHANG, Y., LI, L., LESTER, H. A. & DOUGHERTY, D. A. 1998. From *ab initio* quantum mechanics to molecular neurobiology: A cation- $\pi$  binding site in the nicotinic receptor. *Proceedings of the National Academy of Sciences*, 95, 12088-12093.